Spark Assisted Compression Ignition, SACI

Persson, Håkan

2008

Spark Assisted Compression Ignition
SACI

Håkan Persson

Doctoral Thesis

Division of Combustion Engines
Department of Energy Sciences
Faculty of Engineering
Lund University

LUND UNIVERSITY

ISBN 978-91-628-7578-7
ISRN LUTMDN/TMHP--08/1063—SE
ISSN 0282-1990

Division of Combustion Engines
Department of Energy Sciences
Faculty of Engineering
Lund University
P.O. Box 118
SE-22100 Lund

Printed in Sweden by Media-Tryck, Lund, September 2008

List of papers

Paper I
The Effect of Intake Temperature on HCCI Operation Using Negative Valve Overlap
H. Persson, M. Agrell, J-O. Olsson, B. Johansson, H. Ström
SAE Technical paper 2004-01-0944
Presented at the SAE World Congress, March, 2004, Detroit, Michigan

Paper II
Cylinder-to-Cylinder and Cycle-to-Cycle Variations at HCCI Operation with Trapped Residuals
H. Persson, R. Pfeiffer, A. Hultqvist, B. Johansson, H. Ström
SAE Technical paper 2005-01-0130
Presented at the SAE World Congress, April 2005, Detroit, Michigan

Paper III
Investigation of Boundary Layer Behaviour in HCCI Combustion using Chemiluminescence Imaging
H. Persson, L. Hildingsson, A. Hultqvist, B. Johansson, J. Ruebel
SAE Technical paper 2005-01-3729
Presented at the SAE Powertrain & Fluid Systems Conference, October 2005, San Antonio, Texas
Approved for SAE Transactions 2005

Paper IV
Investigation of the Early Flame Development in Spark Assisted HCCI Combustion Using high Speed Chemiluminescence Imaging
H. Persson, A. Rémon, A Hultqvist, B. Johansson
SAE 2007-01-0212
Published at the SAE World Congress, April 2007, Detroit, Michigan

Paper V
The Effect of Swirl on Spark Assisted Compression Ignition (SACI)
H. Persson, A. Rémon, B. Johansson
JSAE 20077167, SAE 2007-01-1856
Published at the JSAE/SAE International Fuels and Lubricants meeting, July 2007, Kyoto, Japan

Paper VI
Study of Fuel Stratification on Spark Assisted Compression Ignition (SACI) Combustion with Ethanol Using High Speed Fuel PLIF
H. Persson, J. Sjöholm, E. Kristensson, B. Johansson, M. Richter, M. Aldén
SAE 2008-01-2401
Approved for publication at the SAE Fuels & Lubricants Meeting, Chicago 2008

Other publications

Optical Diagnostics of HCCI and Low-Temperature Diesel Using Simultaneous 2-D Plif of Oh and Formaldehyde
L. Hildingsson, H. Persson, B. Johansson, R. Collin, J. Nygren, M. Richter, M. Aldén, R. Hasegawa, H. Yanagihara
SAE Technical Paper 2004-01-2949
Presented at the SAE Powertrain & Fluid Systems Conference, October 2004, Tampa, Florida
Approved for SAE Transactions 2004

Optical Diagnostics of HCCI and UNIBUS Using 2-D PLIF of OH and Formaldehyde
L. Hildingsson, H. Persson, B. Johansson, R. Collin, J. Nygren, M. Richter, M. Aldén, R. Hasegawa, H. Yanagihara
SAE Technical Paper 2005-01-0175
Presented at the SAE World Congress, April 2005, Detroit, Michigan

Quantification of the Formaldehyde Emissions From Different HCCI Engines Running on a Range of Fuels
M. Lemel, A. Hultqvist, A. Vressner, H. Nordgren, H. Persson, B. Johansson
SAE Technical Paper 2005-01-3724
Presented at the SAE Powertrain & Fluid Systems Conference, October 2005, San Antonio, Texas
Approved for SAE Transactions 2005

Abstract

The strong focus on decreasing carbon dioxide emissions due to limited natural resources of fossil fuel as well as alarming climate changes drives the research and development of our prime mover, the combustion engine, faster then ever. The minimum requirement is a power source with increased efficiency while emitting ultra low levels of hazardous local and regional emissions. The concept of Homogeneous Charge Compression Ignition (HCCI) promises increased efficiency and low levels of NO_x, insignificant smoke but increased levels of CO and HC when utilized in the spark ignition (SI) engine. Since HCCI in the SI engine can only be utilized at part load and does not cover the entire operating range of the engine mode shifts are necessary. This is where spark assisted compression ignition (SACI) comes in. Using SACI combustion a controlled mode shift from SI to HCCI and vice versa can be achieved under certain conditions.

This thesis is based on experimental investigations of HCCI combustion mainly addressing the SI engine environment. Here HCCI combustion is achieved by trapping hot residuals through a negative valve overlap and thereby raising charge temperature during compression to auto ignition. When combined with spark assistance it is addressed as SACI combustion. SACI is shown to increase the possible operating region without switching to SI thus increasing the gain of HCCI combustion further. Further it is shown that HCCI combustion timing is affected using spark assistance under proper conditions. This enables a means of direct control of combustion timing. The usage of SACI combustion at low load can affect cycle to cycle variations related to residual gas status. By decreasing the cycle to cycle dependence a lower load can be achieved without misfire.

The effect of spark assistance in SACI combustion is investigated using high speed chemiluminescence, laser Doppler velocimetry (LDV) and heat release analysis for understanding the interaction between the heat release origin from the spark and the subsequent HCCI combustion. It is found to be turbulent flame propagation also at low load from low to high residual dilution that raises the temperature and initiates auto ignition. From LDV measurements a positive effect of increased turbulence is seen on the growing flame. The results are confirmed by experiments with intake valve deactivation changing the tumble flow to include swirl. The flame expansion speed increases with turbulence while the effect on the HCCI part is more modest. The effect on auto ignition is found to be more related to increased mixing.

In a combustion boundary layer investigation only small deviations are seen on HCCI combustion when increasing the swirl. On the other hand it is concluded that a thicker boundary layer with more thermal stratification is related to slower combustion.

Effects of fuel stratification in combination with SACI and residual dilution are investigated using Planar Laser Induced Fluorescence (PLIF) Charge homogeneity is affected both by different strategies of port injection as well as by combining port injection and direct injection. For increased stratification effects from fuel heat of vaporisation and reactions during the negative valve overlap are seen to counteract. Increased reactivity due to richer zones seems not as strong as reported for fuels exhibiting low temperature reactions.

Acknowledgements

Many people have contributed to this work. To be able to fit this text in such short space, only some can be mentioned, but I am grateful to you all.

First I would like to thank Volvo Car Corporation and the Centre of Competence for Combustion Processes (KCFP) for financing my project.

I would like to thank my supervisor and also head of the combustion engines division, Professor Bengt Johansson. Thank you for letting me start as a Ph.D. student with a interesting project, for having lots and lots and lots of good ideas and suggestions and for always making time for a discussion when needed. I would also like to show my appreciation to my co-supervisors Anders Hultqvist and Rolf Egnell for supervising me and together with Per Tunestål helping with vast knowledge and ideas as well as all sorts of problems. You have all had the door open when needed.

I would also like to show my appreciation to my office mates during my time at the division. Vittorio Manente, the fastest man in the lab. Magnus Andersson, for interesting discussions, help with my faulty language and for his interest in the environment and cars with insignificant size engines. Kent Ekholm, for teaching me a new language from the far north and for showing his entrepreneuring spirit. Uwe Horn for always being in a good mood, and being responsible for the language from the south. Petter Strandh, Ola Stenlåås, Olof Erlandsson, my room mates from the past, you have all been a great help both with Matlab related problems as well as during many interesting discussions. Andreas Vressner and Carl Wilhelmsson for being good friends and solving problems like how many turbochargers you can actually fit on a BMW. Leif Hildingsson, for being the optical expert, always keeping track of us so we did not forget to have a social life together, combined with good quality beer. Jari Hyvönen and Göran Haraldsson, for sharing their knowledge and good ideas. My former engine cell time sharer, as well as master thesis supervisor Jan-Ola Olsson for helpful hints and for helping me with engine management programming together with Per. Per, whose help has saved me from many nightmares in Delphi. Mats Agrell for being a part of the initial work when struggling with getting the mechanical parts into place and also produce results. Jochen Rübel and Alfredo Remón who conducted endless image processing from our experiments, both good friends spread over Europe. Ryo Hasegawa, my later engine cell time sharer who showed me the beautiful country of Japan. Sasa Trajkovic who helped me with the valve train demons together with Urban Carlson and Anders Höglund. Patrick who is continuing the SACI project with great enthusiasm. Clas-Göran Zander, Clément Chartier, Hans Aulin, Helena Persson, Magnus Lewander, Mehrzad Kaiadi, Noriyuki Takada, Thomas Johansson and Ulf Aronsson, be aware, you will turn in to the old PhD Students of the division sooner than you think.

Elias Kristensson and Johan Sjöholm from the combustion physics department, together we struggled long hours to get the engine, valve train, laser and data acquisition system to work, preferably simultaneously.

Bertil Andersson, Kjell Jonholm, Jan-Erik Nilsson and Tom Hademark for helping me whenever I broke something or when things should be built in the engine test rigs. Tommy Petersen for building electronic gadgets and helping me find errors in the

acquisition systems, Krister Olsson for his great formula interest and for keeping our computers alive so we can do anything at all. Jan-Erik Everitt for a fight off life and death against the evil and viscous soul of the emission measurement system. Maj-Lis Roos, Ingrid Elofsson and Gunvi Andersson for helping me with things I don't understand. You are all doing a marvellous job. The new guys, Öivind Andersson and Bert Berglund helping the division keeping up the steam, or is it diesel? All the people at the department for making the working atmosphere so inspiring that also on a rainy monday morning (it does happen in Lund) it was possible to go to work with a smile.

Last but not least I would like to thank the love of my life, Helena, and the rest of my family for putting up with me when working strange hours and being more than usual disorientated.

Nomenclature

ATAC	Active Thermo-Atmosphere Combustion
BDC	Bottom Dead Centre
BMEP	Brake Mean Effective Pressure
CAD	Crank Angle Degree
CA10	Crank angle for 10 % burned mass fraction
CA50	Crank angle for 50 % burned mass fraction
CA90	Crank angle for 90 % burned mass fraction
CI	Compression Ignition
CIHC	Compression Ignited Homogeneous Charge
CO	Carbon Monoxide
COV	Coefficient of Variation
CO_2	Carbon Dioxide
CPS	Cam Profile Switching
CR	Compression Ratio
DI	Direct Injection
EGR	Exhaust Gas Recirculation
FMEP	Friction Mean Effective Pressure
FuelMEP	Fuel Mean Effective Pressure
h	Heat Transfer Coefficient
HC	Hydrocarbon
HCCI	Homogenous Charge Compression Ignition
HR	Heat Release
HTR	High Temperature Reaction
$IMEP_{gross}$	Gross Indicated Mean Effective Pressure
$IMEP_{net}$	Net Indicated Mean Effective Pressure
ISHR	Initial Slow Heat Release
IVC	Inlet Valve Closing
IVO	Inlet Valve Opening
KCFP	Competence Centre Combustion Processes
LDV	Laser Doppler Velocimetry
LIF	Laser Induced Fluorescence
LTR	Low Temperature Reaction
m	Mass
MK	Modulated Kinetics
NO_x	Nitrogen Oxides ($NO + NO_2$)
NVO	Negative Valve Overlap
O_2	Oxygen
p	Pressure [Pa]
PFI	Port Fuel Injection
PIV	Particle Image Velocimetry
PLIF	Planar Laser Induced Fluorescence
PM	Particulate Matter
PMEP	Pumping Mean Effective Pressure
PPC	Partially Premixed Combustion
PPM	Parts Per Million
PRR	Pressure Rise Rate
PVO	Positive Valve Overlap
Q	Heat

QemisMEP	Emission Mean Effective Pressure (heat chemically bound in emissions)
QexhMEP	Exhaust Mean Effective Pressure (sensible exhaust energy)
Q_{HR}	Accumulated Heat Release
QhrMEP	Accumulated Heat Released Mean Effective Pressure
QhtMEP	Heat Transfer Mean Effective Pressure (heat transfer to cylinder walls)
Q_{LHV}	Lower Heating Value of Fuel
R	Correlation Coefficient
R^2	Coefficient of Determination (The square of the correlation coefficient)
RMS	Root Mean Square
RoHR	Rate of Heat Release
SACI	Spark Assisted Compression Ignition
SI	Spark Ignition
Sp	Mean Piston Speed
T	1) Temperature
	2) Torque
TDC	Top Dead Centre
U	1) Internal Energy
	2) Velocity
$u´$	Turbulence
UNIBUS	Uniform Bulky Combustion System
UV	Ultra Violet
V	Volume [m^3]
VVA	Variable Valve Actuation
VVT	Variable Valve Timing
w	Characteristic Velocity
W	Work
γ	Ratio of Specific Heats (C_P / C_V)
η_{BRAKE}	Brake Efficiency
η_{COMB}	Combustion Efficiency
η_{GE}	Gas exchange Efficiency
η_{MECH}	Mechanical Efficiency
η_{TERM}	Thermal Efficiency
λ	1) Relative Air / fuel Ratio
	2) Wave length

Table of content

1 Introduction

The last decades have shown a significant advancement in engine technology for the automotive market. The Spark Ignition (SI) engine has become a very clean engine with catalytic after-treatment and more complex engine management. The main emphasis has been on reducing local emissions such as Nitrogen Oxides (NO_x), Carbon monoxide (CO), Hydrocarbons (HC) and Particulate Matter (PM). With the world's increasing population the demand for transport and thus fuel is raised. Simultaneously, the seriousness of our global emissions of Carbon dioxide (CO_2) becomes more apparent, both in terms of usage of natural recourses and regarding the greenhouse effect. Shown below in Figure 1 is the global emission of carbon dioxide from fossil fuel from the sixties up until 2004. Although the slope changes with time for different continents the grand total still shows a continuous increase. From the sixties until now the total amount has tripled.

Along with the development of the SI engine the Compression Ignition (CI) engine has become accepted as a fuel efficient alternative also for passenger cars, far from the old smoky, noisy pre-chamber machines, now with advanced high pressure multi sequence fuel injections and particulate filters. All these advanced systems contribute to higher efficiency and lower emissions.

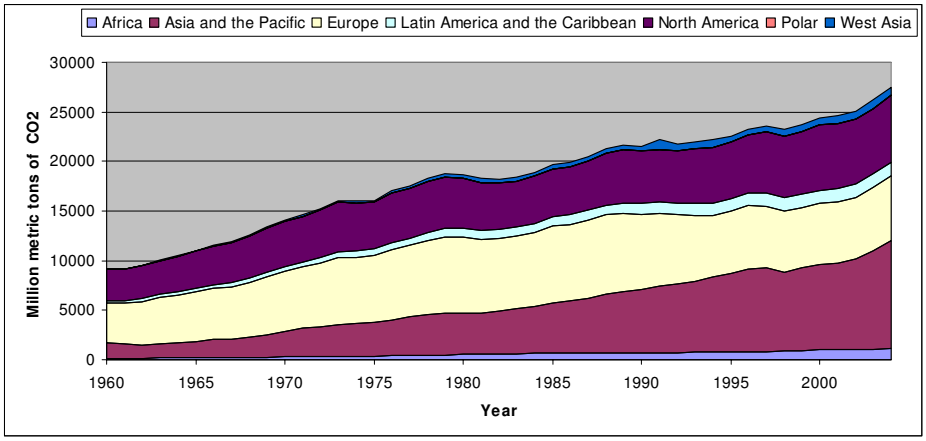

Figure 1. Annual global carbon dioxide emissions from fossil fuel 1960-2004 [1].

The environmental demands shift from only local to stringent demands on global CO_2 emission. Much of the improvement in fuel efficiency of both the SI and CI engines is counteracted by increased weight and size of the vehicles. This calls for further improvements of the combustion concepts to keep or increase the high CI efficiency, but with ultra low local emissions. This could be achieved by deploying Homogenous Charge Compression Ignition (HCCI) and Spark Assisted Compression Ignition (SACI). Hybrid engines combining the new combustion concepts and an electric motor could further improve fuel efficiency and reduce the complexity of the combustion system. HCCI combustion has also been demonstrated on a variety of non fossil fuels which would further reduce the addition of CO_2 in the atmosphere.

1.1 Objective

This work started as a continuation of earlier work regarding spark ignition combustion that mainly concerned fluid flow, valve timings and lean burn to reach better efficiency. The research in this work was conducted as a vertical project within the Competence Centre Combustion Processes (KCFP) at Lund University up until the end of 2005, when it was fully incorporated into KCFP.

Since HCCI combustion is branching into several different combustion strategies, some closer to diesel and some to SI, the main path of the project was confined to the SI engine environment. HCCI with trapped residuals can be achieved in an SI environment and this type of combustion was thus the target for this work. This combustion mode is generally seen as a mean to achieve better low and part load efficiency of the SI engine.

The aim of the project was to find out what operating regime was possible in a multi cylinder engine with SI specifications to be followed by further in-depth analysis of the load regime constraints and possibilities to affect these. Early in the project the attention was shifted towards spark assisted HCCI, or Spark Assisted Compression Ignition (SACI), which turned into the main focus of this thesis.

Metal engine experiments as well as optical experiments have been carried out during the course of the thesis work. However, the optical investigations started towards diesel HCCI [2-3], followed by traditional HCCI, then residual HCCI with SACI combustion.

1.2 Method

An experimental approach was chosen for this project. To get initial insight into the combustion behaviour, the experiments were started in a multi cylinder all metal engine. The main source of information is then in-cylinder pressure which is a global measurement of the in-cylinder conditions. This was then continued and complemented by experiments in a single cylinder optical engine, to better resolve and understand detailed combustion phenomena compared to the averaged information obtained from pressure measurements. The usage of an optically accessible engine enables non intrusive measurement techniques. To gain optical access some sacrifices have to be done on engine geometry and boundary conditions, the gain is however much greater than the drawbacks.

2 Combustion fundamentals

2.1 Working principle

All the internal combustion principles that are dealt with in depth in this work are of the four stroke type. Although different types of combustion the cycle is divided into the same four parts, repeated continuously as long as the engine runs. The four stroke principle is shown in Figure 2 for a Spark Ignition (SI) engine.

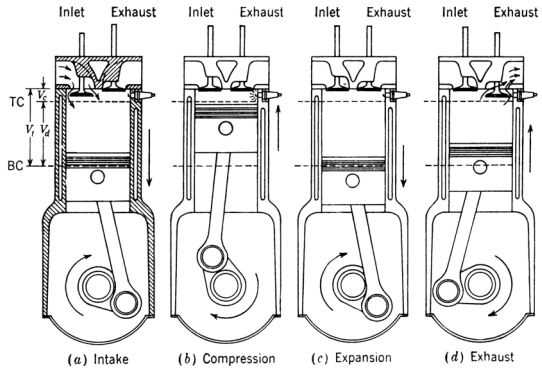

Figure 2. The four stroke principle for an SI-engine [4].

The cycle starts with the intake stroke when air is induced into the cylinder through the inlet ports as the piston is moving towards its lower position. If the engine is Port Fuel Injected (PFI) a mixture of fuel and air is inhaled. If the engine is Direct Injected (DI) fuel can be added at any desired time during the cycle.

When the piston passes Bottom Dead Centre (BDC) the inlet valves close and the compression stroke starts. During the compression stroke the piston performs work on the charge rasing the in-cylinder pressure and temperature. Close to the end of the stroke the charge is ignited.

For both the SI and the HCCI engine, fuel is added early so it is mixed with the air in the combustion chamber before combustion. In the SI case it is ignited by a spark plug and then a turbulent flame propagates from the spark plug throughout the combustion chamber. In the HCCI case multiple ignition sites start to oxidize almost simultaneously only due to the elevated temperature. For a Compression Ignition (CI) engine commonly called the diesel engine, fuel is injected close to top dead centre (TDC). The high Compression Ratio (CR) and thereby high temperature in combination with high injection pressure makes the fuel atomize and burn as it is being injected, first in a premixed phase and then continued by a diffusion flame. In all cases the charge is ignited and starts to burn around TDC in the compression stroke and then burns during a part of the expansion stroke, increasing the pressure and temperature. During the expansion stroke the charge performs work on the piston.

In the last stroke, the exhaust stroke, the burnt gases are evacuated from the cylinder through the exhaust ports as the piston moves towards TDC.

2.2 SI / CI

Almost all internal combustion engines of today are spark ignition (SI) or compression ignition (CI) engines. They exist as both two stroke and four stroke engines. The choice of engine depends on what demands are of most importance for the given application. Important parameters for choosing engine type involve initial cost, efficiency, environmental impact (efficiency, emissions), durability and power density.

For the really small engines, cost and weight are usually of most importance. Since the number of parts is smaller and the power density is higher the two-stroke engine is the common choice despite a lower efficiency and higher emission level.

For engines in the size normally found in passenger cars both SI and CI four-stroke engines are common. Here it is a slightly more difficult choice for the consumer. The SI engine is very clean with the three-way catalyst; however the efficiency is lower than for the CI engine. The CI engine also comes with a higher initial cost due to expensive components. Local legislations and taxes can, to a high extent, influence this choice. If the production of CO_2 is of greatest importance, then the CI engine with higher efficiency is the choice. If more local effects from for instance NO_x (NO, NO_2), PM and HC is seen as the most important, then the choice will be the SI engine. Historically the SI engine has had a higher power density and has been less noisy compared to CI; these differences are no longer as apparent and are therefore becoming less important.

When it comes to truck engines the common choice is the CI engine due to high efficiency combined with a long service life. However, truck size SI engines running on gaseous fuels, with the advantage that they produce relatively less CO_2 due to lower carbon content in the fuel, are increasing in numbers.

For the really big engines the choice is still CI but then often in the two-stroke appearance again. The large engines are running at low speed with enough time for gas exchange and have very high fuel efficiency.

2.3 Mean effective pressures

To analyze the performance of an engine and be able to compare it with others the engine fuel efficiency can be broken down into the performance of each process. Further, to compare engines of different sizes running at different speed normalized quantities are needed. This can be achieved by comparing the performance per cycle normalized by the displacement resulting in mean effective pressures [Pa]. Mean effective pressures are used to compare as well as to visualize the energy flow through the engine from the incoming fuel to the output power as shown in the Sankey diagram in Figure 3.

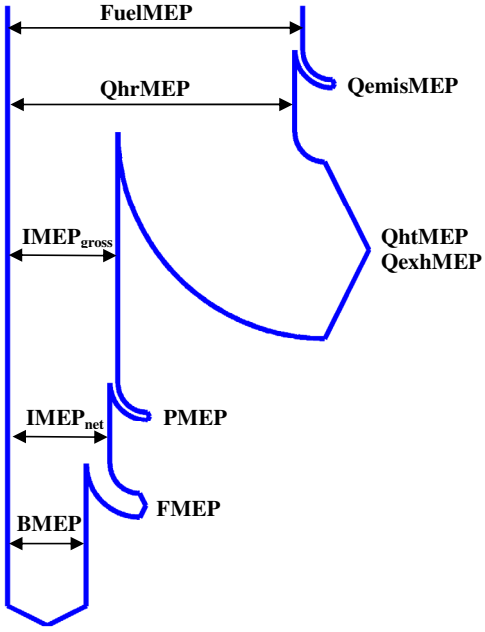

Figure 3. Sankey diagram of mean effective pressures.

Starting with the total amount of added energy from the supplied fuel gives the FuelMEP according to (2.1), where m_f is the added fuel mass per cycle, Q_{LHV} the lower heating value of the fuel and V_d the engine displacement.

$$FuelMEP = \frac{m_f \cdot Q_{LHV}}{V_d} \tag{2.1}$$

Subtracting the losses of chemically bonded and partially burned components in the exhausts (QemisMEP) gives QhrMEP as defined in (2.2). QhrMEP is the ratio between Q_{HR} which is the heat released during combustion and the displacement.

$$QhrMEP = \frac{Q_{HR}}{V_d} \tag{2.2}$$

Energy from the accumulated heat release that is not converted to work can be separated into two different losses. QhtMEP which is energy losses due to heat transfer to the cylinder walls and QexhMEP that is energy lost with the exhausts flow due to the elevated temperature.
The Indicated Mean Effective Pressure (IMEP) is the energy transformed into work (W_c) on the piston divided by the displacement. IMEP can be calculated in two ways depending on whether the entire cycle is considered (2.3) or if the gas exchange process is excluded (2.4). The difference between IMEP$_{gross}$ and IMEP$_{net}$ is called PMEP. PMEP reflects the pumping losses during the gas exchange process according to (2.5).

$$IMEP_{net} = \frac{W_c}{V_d} = \frac{\oint_{entirecycle} pdV}{V_d} \tag{2.3}$$

$$IMEP_{gross} = \frac{\oint_{closedcycle} pdV}{V_d} \tag{2.4}$$

$$PMEP = IMEP_{gross} - IMEP_{net} \tag{2.5}$$

The Brake Mean Effective Pressure (BMEP) is the engine work per cycle and displaced volume. BMEP is calculated from the torque of the engine according to (2.6) for a four stroke engine.

$$BMEP = \frac{4\pi T}{V_d} \tag{2.6}$$

The difference between $IMEP_{net}$ and BMEP is the Friction Mean Effective Pressure (FMEP) shown in (2.7). FMEP is the normalized engine friction.

$$FMEP = IMEP_{net} - BMEP \tag{2.7}$$

2.4 Efficiencies

Using the mean effective pressures defined in the previous section the efficiencies for the different processes can be calculated. The combustion efficiency η_{COMB} reflects how much of the fuel that is converted into heat according to (2.8).

$$\eta_{COMB} = \frac{QhrMEP}{FuelMEP} = 1 - \frac{QemisMEP}{FuelMEP} \tag{2.8}$$

The thermodynamic efficiency shown in (2.9) is the ratio between $IMEP_{gross}$ and QhrMEP reflecting the efficiency of converting released heat to indicated work.

$$\eta_{THERM} = \frac{IMEP_{gross}}{QhrMEP} = 1 - \frac{QhtMEP + QexhMEP}{QhrMEP} \tag{2.9}$$

The gas exchange efficiency, representing the engines ability to breathe, is defined by the ratio between the indicated work for the entire cycle and the closed cycle respectively i.e. with or without the gas exchange process (2.10).

$$\eta_{GE} = \frac{IMEP_{net}}{IMEP_{gross}} = 1 - \frac{PMEP}{IMEP_{gross}} \tag{2.10}$$

Finally the mechanical efficiency defined in (2.11) accounting for the friction by piston rings, bearings, auxiliary equipment and more.

$$\eta_{MECH} = \frac{BMEP}{IMEP_{net}} = 1 - \frac{FMEP}{IMEP_{net}} \tag{2.11}$$

The total efficiency of the engine can then be descried either by the ratio between BMEP and FuelMEP or by multiplying the efficiencies to obtain what is also called the brake efficiency according to (2.12).

$$\eta_{BRAKE} = \eta_{COMB} \cdot \eta_{THERM} \cdot \eta_{GE} \cdot \eta_{MECH} \tag{2.12}$$

3 HCCI

One possible solution to improve the trade-off between efficiency and emissions is the new third type of engine; homogeneous charge compression ignition (HCCI). It is however not a specific engine but a combustion concept, HCCI combustion. HCCI is known as a combustion concept that combines some of the features of both the SI and the CI engine. As the SI engine, the HCCI engine runs with a premixed charge of fuel and oxidizer and as the CI engine it runs un-throttled and is auto ignited due to the increased temperature by the compression.

The fuel is introduced into the cylinder either by PFI or by DI so early that it has time to mix with the air in the cylinder. When the temperature increases during compression to the point of auto ignition, the charge will ignite at multiple points where the temperature is slightly higher or where the mixture is slightly richer and more favorable for reactions to occur [5]. Since the combustion occurs almost simultaneously throughout the combustion chamber no global flame propagation occurs, the combustion rate is much higher than what is caused by ordinary turbulent flame growth deflagration. [6]. Instead the whole bulk oxidizes simultaneously placing chemical kinetics in control of the reaction rate [7] instead of the turbulent flame speed as for the SI engine.

Since there is no direct control of the position for start of combustion, the auto ignition timing will depend on; initial charge temperature, pressure history, and charge composition. This means that combustion timing must be controlled to first of all get ignition at all and secondly to achieve high efficiency. To be able to control combustion timing, some kind of monitoring of the combustion event is needed; this can be done in a number of ways. The most common way is by measurement of the in-cylinder pressure which gives direct information and also makes it possible to calculate burn rate and make heat release analysis [8]. Other methods as ion-sensing, measurement of torque and speed variations are being developed [9 - 11].

When having enough knowledge about the combustion event, auto ignition timing can be controlled in a number of ways. An engine run on two fuels with different auto ignition properties will have the potential to control timing over a variety of loads and speeds [12]. Other possible ways are using variable compression ratio or intake temperature control [13 - 16]. A fourth way is to trap hot burned gases in the cylinder to reach ignition temperature, this method will be described more thoroughly in Section 3.3.

3.1 Evolution

The interest for HCCI combustion has its roots in the late seventies when Onishi et al. presented the ATAC (Active Thermo-Atmosphere Combustion) concept for two stroke engines [17]. By exhaust throttling, enough hot exhausts were trapped to attain auto ignition at part load. By keeping some of the burned gases in the cylinder any un-burned hydrocarbons (HC) get a second chance to react and thereby the engine-out emissions decrease.

The first reported four stroke engine with HCCI combustion was presented in 1983 by Najt and Foster [18]. For the four stroke engine the goal is to both decrease emissions and to increase efficiency. The abbreviation HCCI first appeared in 1989 in a SAE

paper by R. H. Thring [19]. Numerous names are used for the same type of combustion. ATAC and HCCI are already mentioned. Najt and Foster used Compression Ignited Homogeneous Charge (CIHC) combustion. Premixed charge compression ignition (PCCI) is another one. Yet another name is controlled auto ignition (CAI) combustion, this is however usually used for a more specific type of HCCI combustion.

In one way the HCCI combustion concept can be said to be a re-invention of the old hot-bulb engines. Many similarities are described by Erlandsson in [20]; these are also supported in [21] where an old hot-bulb engine is evaluated and found to be running at HCCI-like conditions.

3.2 Branches

During later years the research on HCCI combustion has been intensified with the goal of getting a clean engine with low fuel consumption. What started as a concept with a port injected well mixed charge that was compressed to auto ignition has now started to branch into two main groups. The first one, here referred to as partially premixed combustion (PPC), is closely related to the diesel engine in the sense that the combustion timing is dependent on injection timing, but still the charge has time to mix enough so that lower emissions comparable to HCCI emissions are possible. To achieve enough mixing the ignition delay must be increased i.e. the injection event must be separated from start of combustion. One way of achieving this is by adding high amounts of Exhaust Gas Recirculation (EGR), thus increasing the specific heat and decreasing the charge temperature simultaneously. The PPC group can be further divided into subgroups depending on early or late injection strategies, two of them are described below.

A combustion system concept called Modulated Kinetics (MK) was presented by Kimura et. al. using high levels of EGR in combination with late injection and increased swirl [22]. The increased EGR content thus lowered oxygen dilution in combination with the increased ignition delay results in a lower combustion temperature with reduced NOx emissions as a consequence. The long ignition delay provoked by the high EGR content and late injection increases the mixing and suppresses increased soot as well as NOx production. To compensate for the late injection and lower combustion rate the swirl level is increased. Mixture formation occurred closer to the centre with increased swirl resulting in lower cooling losses to the combustion chamber walls.

Another concept called Uniform Bulky Combustion System (UNIBUS) features one early injection only undergoing Low Temperature Reactions (LTR) [23]. This is followed by a second injection that initiates the main heat release with the High Temperature Reactions (HTR). The fuel content from the first injection is kept as high as possible while maintaining only LTR, HTR from the second injection is found to have multiple HCCI like ignition sites. Ignition properties are moderated by boost pressure and EGR

The second HCCI branch more related to the SI engine uses hot residual gases to achieve auto ignition temperature. This type of combustion is often referred to as CAI combustion or residual HCCI combustion.

3.3 Residual HCCI

The SI engine experiences low part load efficiency and HCCI combustion is constrained when it comes to high load. This makes it attractive to run an SI engine with HCCI combustion at low and part load and switch back to SI when running high load. HCCI combustion can be achieved in an SI engine with only modest modifications of the engine. The compression ratio of an SI engine is low compared to the CI engine, so to achieve auto ignition under these conditions an increased charge temperature before compression is required. Increasing the compression ratio is only possible to some extent due to the risk of damaging engine knock when running in SI mode. By diluting the charge with hot burned residuals the initial charge temperature is raised enough to obtain auto ignition around TDC and thereby HCCI combustion. This is usually done in one of two ways described in the next two sub sections:

3.3.1 Exhaust re-breathing

By exhaust re-breathing, a large amount of residuals will be trapped in the cylinder when the compression stroke starts. This can be achieved in a number of ways. Four strategies are shown in Figure 4. A first approach is as follows, by closing the exhaust valve late in the induction stroke, exhausts are first exhaled out into the exhaust pipe and during the early induction stroke hot residuals are sucked back in. This is followed by late Intake Valve Opening (IVO) with short lift duration to get Inlet Valve Closing (IVC) at conventional timing.

Another approach (Figure 4, second graph) is to have a large Positive Valve Overlap (PVO) between exhaust valve closing (EVC) and IVO. Combined with a slightly longer exhaust duration this will partially push out the burned gases through the exhaust valve, but also through the intake. During the intake stroke both residuals and a fresh charge are inducted.

A third way (Figure 4, third graph) is by early EVC and IVO. This will exhale hot residuals into the intake manifold and then re-induce it together with a fresh charge during the intake stroke.

What all three have in common is that they all have either intake or exhaust valves fully open at TDC which will give constrains in both combustion chamber and piston crown design. In the third approach exhausts are sucked into the cold intake system so this can be expected to give the lowest rise in charge temperature and less possibility to reach auto ignition temperature. For the second approach a large positive valve overlap is used, this makes it slightly difficult to control the amount of residuals. To combine this technique with boosting is a clear challenge. The first of the three approaches is the one that will give the highest charge temperature and thereby a greater operating regime according to Lang et al. [24].

Yet a fourth re-breathing approach is shown at the bottom of Figure 4. Here the exhaust valve is opened a second time during the induction stroke, pulling back burned gases from the exhaust system. This strategy requires a more advanced valve train but on the other hand it is expected to result in a relatively high charge temperature since the residuals are temporarily stored in the high temperature un-cooled exhaust system. Since this strategy does not have high valve lift around TDC

in contrast to the previous strategies this is the only one that is applicable in many combustion systems.

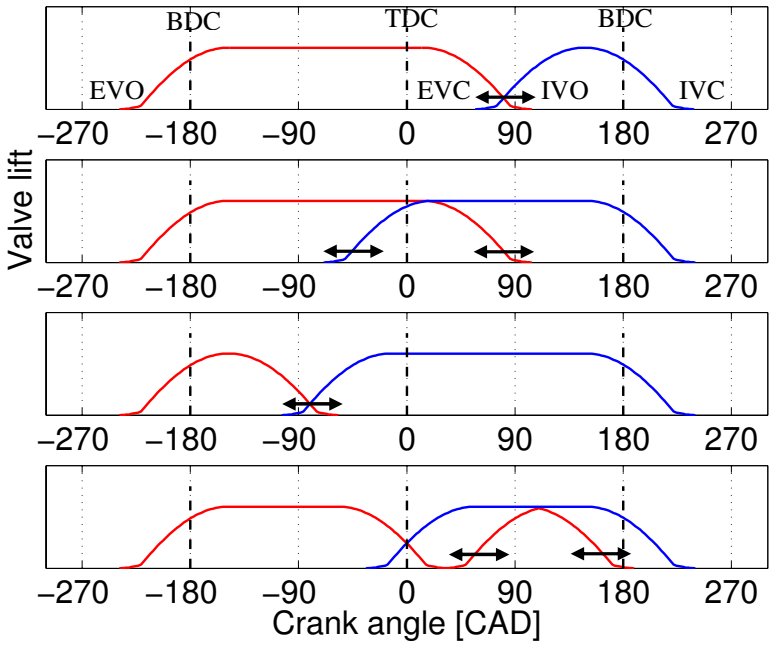

Figure 4. Schematic valve strategies for HCCI with Exhaust re-breathing techniques.

3.3.2 Negative valve overlap

Another way to achieve HCCI combustion under SI conditions is to use a negative valve overlap (NVO). The proposal for this strategy was first published by Willand et al. [25] in 1998. The first presented results of NVO HCCI combustion by Lavy et al. [26] followed in 2000. The difference compared to the re-breathing methods described above is that for NVO the needed burned gases never leave the cylinder, instead they are trapped in the combustion chamber. The differences in cam timing compared to that of the standard SI engine are shown in Figure 5.

Instead of using the standard cam lobe, a low lifting camshaft with short duration is used on both the intake and the exhaust side for HCCI operation. By closing the exhaust valves early a large amount of hot residuals are trapped in the cylinder and compressed during the rest of the exhaust stroke. The residuals are then expanded to ambient conditions when the intake valves are opened and a fresh charge is inhaled during the rest of the intake stroke. The residual diluted charge is then auto ignited at the end of the compression stroke and expansion work is achieved during the power stroke. Figure 6 shows mean pressure traces for three different loads run with NVO HCCI. When the NVO is increased the amount of trapped residuals increases, thus the amount of fresh charge is decreased together with a lowered possible maximum load.

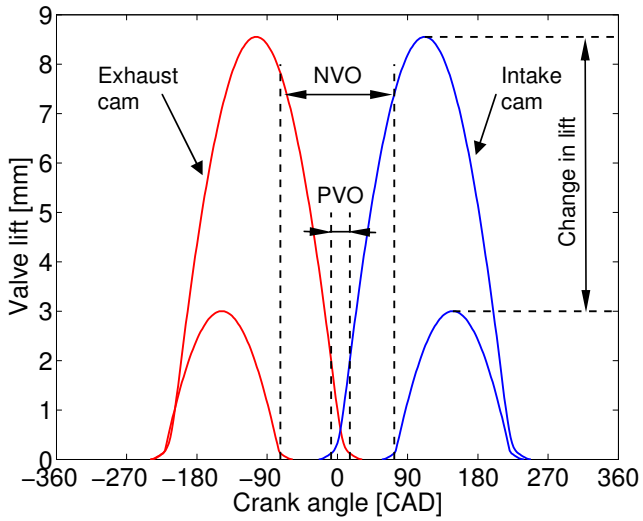

Figure 5. Cam profiles and timings for SI combustion and for HCCI with NVO. 0 CAD is gas exchange TDC.

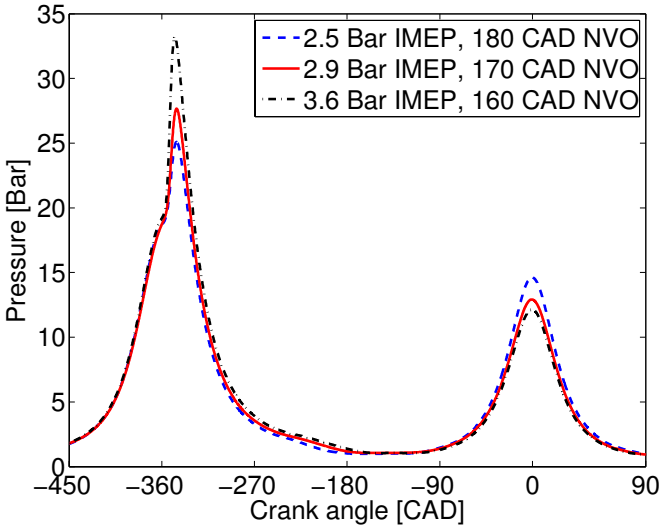

Figure 6. Pressure traces for different NVO and resulting different loads at stoichiometric conditions, 2000rpm. 0 CAD is gas exchange TDC.

Except for the pure residual trapping methods to reach HCCI in combination with SI combustion another method was presented by Yang et. al. [27] In this concept the geometrical CR is increased to approximately 15:1 and the duration of the intake camshaft is increased. With normal Inlet Valve Closing (IVC) settings a Positive Valve Overlap (PVO) is obtained, re-inducting burned gases and compressing with a high enough CR to get auto ignition. When the intake camshaft is phased to late Inlet Valve Closing (IVC), the engine is run in SI mode according to the Atkinson cycle with higher expansion ratio than compression ratio. One drawback with the concept is

the lower possible load due to late IVC; on the other hand efficiency should be high due to the Atkinson cycle, higher compression ratio and less residuals.

3.3.3 Operating strategies for NVO HCCI

Two main operating strategies can be discerned for NVO type of HCCI. Lean burn in the sense that the engine is run with enough residuals to auto ignite and then also diluted with as much air that is needed to keep NO_x emissions at single digit Parts Per Million (ppm) level. Still emissions of HC and CO must be dealt with by an oxidizing catalyst.

The second way is to run combustion at stoichiometric conditions, but still diluted with inert residual gases. When running close to stoichiometric the NOx level will be unacceptable at higher loads and a three-way catalyst must be employed. Since NVO HCCI is thought to be used in combination with SI the catalyst is already present and causes no additional cost. Running stoichiometric will on the other hand cause a slightly lower efficiency due to higher amounts of not fully oxidized fuel after combustion.

The reason for high NO_x when running stoichiometric is that in-cylinder variations in residual rates will cause locally higher combustion temperature with NO_x production.

To achieve the different valve strategies as described in sub chapter 3.3.1 and 3.3.2 the basic requirement that is needed is a Cam Profile Switching (CPS) mechanism going from standard SI camshaft durations and timings to a secondary profile with appropriate lift and duration. To get more leverage this is best used in a combination with a cam phasing mechanism on both the intake and exhaust side making it possible to change the amount of residuals for a given cam shaft profile. The best alternative in terms of combustion would of course be a fully flexible valve train making it possible to adjust timing, duration and lift as needed. This kind of systems [29, 30] are although well functioning however still confined to laboratory environments.

By combining NVO HCCI with spark assistance, the engine is run in what in this thesis is called Spark Assisted Compression Ignition (SACI) for increased combustion control. SACI is thoroughly described in the results section.

3.4 Efficiency comparison

3.4.1 SI/CI and HCCI

Both the SI and the CI engines performances have increased considerably during the last decades. Still there are issues that need to be addressed.

The SI engine is since the introduction of the three-way catalyst on the market in the 70s and the 80s a very clean engine. Since then the efficiency has also increased by the usage of variable valve timing (VVT), to some extent variable valve lift, increasing CR, DI and to some extent charge stratification. However, the SI engine still has much lower efficiency than the CI engine mainly due to lower compression ratio in combination with the need to run at stoichiometric conditions to have a working three-way catalyst. The need to run stoichiometric introduces the greatest disadvantage: for decreased load the throttling losses increases.

The CI engine has excellent efficiency running un-throttled with a higher compression ratio. However emissions are an issue, the high temperature in the diffusion combustion zones generates nitrogen oxides (NO_x) and in the local rich zones soot is formed. Since soot and NO_x are linked, early combustion timing will render high temperature and large amounts of NO_x; retarded timing will instead increase soot due to shorter residence time at high temperature, freezing further soot oxidation. Since the CI engine is run lean it is not possible to use a three way catalyst for reducing NOx, instead expensive active systems like selective catalytic reduction (SCR) catalysts or NOx-traps are needed and a particulate trap is needed for the soot. The usage of EGR can lower the amounts of NO_x enough to meet the nearest coming legislations, but it can't make it vanish. To lower the CI engine emissions further, active aftertreatment systems are needed.

HCCI combustion is typically run with a close to homogeneous mixture of fuel and oxidizer, thereby the levels of soot drop to practically zero. Since the fuel, at least in theory, oxidizes simultaneously throughout the combustion chamber, at lean conditions the peak temperature will stay below were NOx formation is significant.

The challenge with HCCI combustion is to keep track of combustion timing since it is not directly controlled. Also the operating regime for HCCI combustion is a challenge. To be able to reach auto ignition temperature at idle and simultaneously enable high load where the reaction rate rises fast if not diluting enough.

3.4.2 NVO HCCI

The HCCI approaches that are implemented in the SI engine enviroment e.g. the residual methods have generally lower efficiency than the basic HCCI concept. This can be understood by looking at the thermal efficiency of an ideal Otto cycle which can be written according to (3.1).

$$\eta_T = 1 - \frac{1}{CR^{\gamma-1}} \tag{3.1}$$

The equation shows the impact of CR on efficiency. Since compression ratio is lower for the SI and residual HCCI engine, efficiency is lower. This equation also includes the specific heat ratio, gamma ($\gamma = C_p / C_v$). The lower γ with increasing amounts of residuals also decreases the thermal efficiency.

To put HCCI with NVO in perspective regarding efficiency a comparison is done to data presented by Hyvönen et al. [28] Results from the present work both with HCCI and SI are compared to lean burn high CR HCCI, high CR SI and a standard SI engine. Both engines have a displacement of approximately 0.5 L per cylinder, the comparison is performed at 2000 rpm. The Engine denoted B6 in the figures bellow is from the present work whereas the one denoted L850 is from Hyvönen's work. The L850 has combustion control through fast thermal management, i.e. inlet temperature control.

3.4.2.1 NVO HCCI Combustion efficiency

Figure 7 show the combustion efficiency (η_{COMB}). SI with normal CR as well as NVO HCCI combustion features combustion efficiencies higher than 95 %. The high

combustion efficiency results from all of them being run close to stoichiometric conditions. For the high CR engines the low combustion efficiency results from increased crevices in the combustion chamber resulting in emissions of CO and various HC components. The lean conditions with low combustion temperature for the L850 HCCI engine further decrease the combustion efficiency.

3.4.2.2 Thermodynamic efficiency

When it comes to the thermodynamic efficiency (η_{THERM}) showed in Figure 8 both the SI engines show very similar and poor behaviour. Compared to the high CR engines this can be explained by the increased expansion ratio directly related to equation 3.1. However this does not explain the increase for the NVO HCCI engine run at the same compression ratio as in SI mode. When the engines are run in HCCI mode the combustion duration is much shorter, again increasing the expansion ratio. The faster HCCI combustion gives cycle appearance closer to the ideal Otto cycle. This is supported by the increased thermal efficiency for the lean burn CR 18:1 HCCI engine compared to SI at CR 18. The phenomenon is further enhanced for the L850 SI CR18:1 engine at higher load when it has to run with more retarded combustion to avoid damaging engine knock.

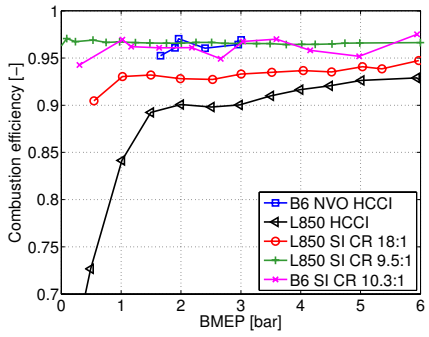

Figure 7. Combustion efficiency.

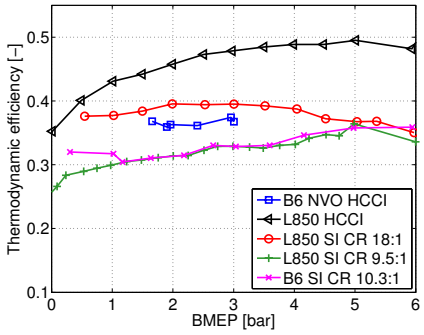

Figure 8. Thermodynamic efficiency.

3.4.2.3 Gas exchange efficiency

The gas exchange efficiency (η_{GE}) of the engines when run in SI mode with stoichiometric conditions clearly shows the pumping work due to throttling (Figure 9). The gas exchange efficiency is dropping fast with lowered load. When comparing the lean burn high CR HCCI engine with NVO HCCI slightly lower gas exchange efficiency can be seen for NVO. This can be explained by heat losses to the cylinder walls during the recompression in the NVO thus increased pumping losses. Also the lower valve lift with NVO HCCI is expected to render higher throttling losses.

3.4.2.4 Mechanical efficiency

The mechanical efficiency (η_{MECH}) of the engines is expected to show small deviation dependent on combustion mode. This is in agreement with what is shown in Figure 10. What deviates is the higher mechanical efficiency, thus lower FMEP for the L850 engine with lower CR. The decreased cylinder pressure with lower CR is expected to decrease the piston ring friction thus increase the mechanical efficiency. A very slight decrease in η_{MECH} can be seen for the high CR HCCI compared to the SI case. This can also be related to cylinder pressure. HCCI generally has shorter

combustion duration, thus higher peak pressure. It should be mentioned that the friction for the B6 engine is based on a single value obtained from the manufacturer and not from brake values in the lab due to dynamometer issues.

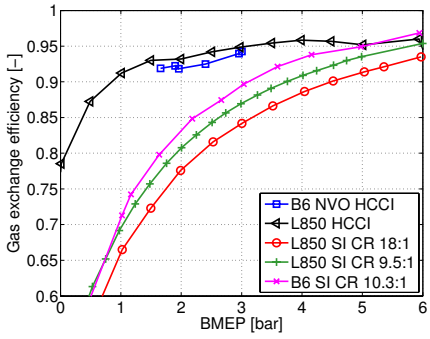

Figure 9. Gas exchange efficiency.

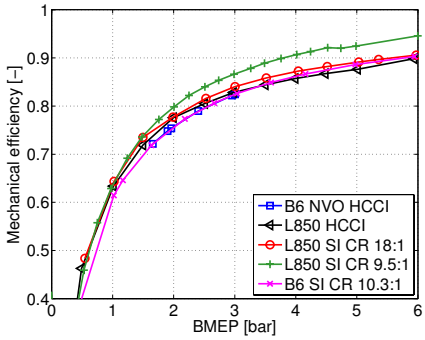

Figure 10. Mechanical efficiency.

3.4.2.5 Brake efficiency

Multiplying the η_{COMB}, η_{THERM}, η_{GE} and η_{MECH} results in the brake efficiency (η_{BRAKE}) as shown in Figure 11. The poor low load efficiency of the SI engines is clear. The main reasons as shown above is a combination of low thermodynamic and gas exchange efficiency. For the high CR SI engine the increased thermodynamic efficiency by higher expansion ratio elevates the brake efficiency. Even higher brake efficiency has the NVO HCCI with a combination of higher thermodynamic and gas exchange efficiency compared to the low CR SI engines. The clearly highest brake efficiency can be achieved by the high CR lean burn HCCI engine run with thermal management. The same results in terms of brake specific fuel consumption (bsfc) are shown in Figure 12. The great difference between HCCI and stoichiometric low CR SI combustion is again clear. It also shows the improvement by running high CR SI.

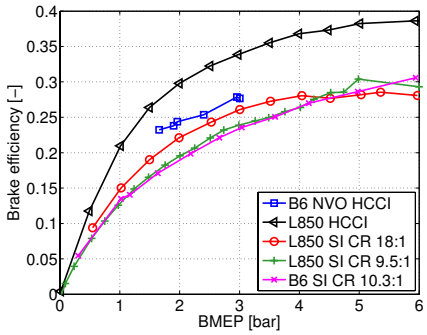

Figure 11. Brake efficiency.

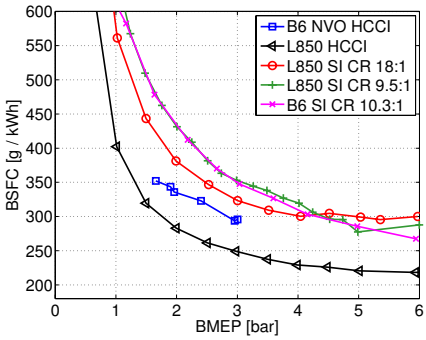

Figure 12. Brake specific fuel consumption.

4 Experimental apparatus

Two distinctively different engines in separate test beds have been used in this work. A multi cylinder all metal engine was used for load sweep, intake temperature sensitivity, cycle-to-cycle and cylinder to-cylinder investigations (Papers I and II). The single cylinder optical engine was used in three different configurations to understand more of the detailed and local phenomena during combustion.

4.1 Multi cylinder engine

4.1.1 Engine

The all metal test engine was a Volvo in-line six-cylinder engine with a total displacement of 2.9L. It was a production SI engine with four valves per cylinder and a pent-roof combustion chamber. Fuel was injected with a PFI system with separate injectors for each cylinder. Engine specifications can be found in Table 1. The engine was unchanged from its automotive application except for the modified camshafts. Camshafts comprising low lift and short duration were used to be able to trap hot residuals and attain auto ignition. The low lifting cams were obtained from Volvo Cars and they were a compromise between getting high enough lift and still keep the duration short enough so the negative valve overlap can be attained without compromising with the compression (IVC timing) and the expansion (EVO timing) stroke. An even higher lift with shorter duration would be desired but this would sharply increase the stress on the valve train with increased accelerations for the valves as well as increased contact pressure between the cam lobe and the valve tappet.

Table 1. Engine specifications, Volvo B6294

Displacement	2922 cm^3
Number of cylinders	6
Bore	83 mm
Stroke	90 mm
Combustion chamber	Pent-roof
Compression ratio	10.3:1
Valve lift	3 mm
Inlet / Exhaust valve duration	150 CAD
Possible negative valve overlap	100 - 220 CAD
EVO	160 – 100 CAD ATDC
IVC	160 – 100 CAD BTDC
Injection system	PFI
Fuel	RON 98

For the initial tests no cam phasing mechanism was available, instead the camshafts were manually adjusted. Later a cylinder head with cam phasing mechanisms on both intake and exhaust was installed, making it possible to change the NVO by 120 CAD between its end positions during operation. The camshafts were mounted so the NVO could be adjusted from 100 to 220 CAD. This enabled the engine to be started in SI mode still allowing the full HCCI operating regime. The engine was further equipped with a pulse width modulated (PWM) throttle for starting at close to stoichiometric

conditions in SI mode at low load. The engine in its test rig can be seen in Figure 13. All experiments were run on commercial RON 98 gasoline.

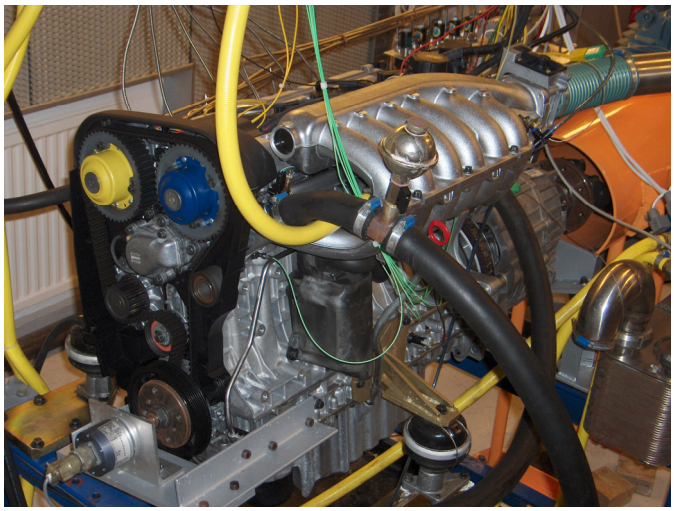

Figure 13. The Volvo B6294 installed in the test rig.

4.1.2 Test rig and measurement apparatus

All cylinders were monitored by uncooled Kistler 6053C60 in-cylinder pressure sensors, flush-mounted between the intake valves. The piezo-electric sensors were connected to Kistler 5011 charge amplifiers and the output signal sampled by a multiplexed 16 bit A/D converter. The position of the VVT on both intake and exhaust camshafts were controlled by a PCI slot 4 channel digital counter card. A crank angle encoder mounted on the engine crank shaft gave a resolution of 0.2 CAD of the cylinder pressure obtained from the A/D converter.

A slow 0.3 Hz logger was used for monitoring and saving exhaust and intake temperatures and pressure, coolant temperature, oil temperature, emissions, torque and fuel flow. Both exhaust temperature and emissions could be individually measured for each cylinder. Temperatures and emissions were collected approximately 100 mm downstream of the exhaust valves. Emissions could only be measured on one cylinder at the time and some cross-talk between the cylinders was unavoidable due to the exhaust pipe geometry. For the experiments not involving cylinder to cylinder deviations, emissions were measured further downstream to reflect the full engine emissions.

The emission analysis equipment consisted of a flame ionization detector (FID) for measuring HC, a chemiluminescence detector (CLD) for measuring NOx, a non dispersive infra red (NDIR) detector for measuring CO2 and CO and a paramagnetic detector for measuring O2. Smoke was not measured.

The engine was connected to a 355 kW AC dynamometer via a Volvo M90 gearbox. The gearbox was necessary due to a limited speed range of the dynamometer. The oversized dynamometer resulted in usage of a small portion of the torque range, especially when running low load HCCI. Brake specific values were thus not used

since the accuracy of the brake torque signal was expected to be limited; a further source of uncertainty is the friction losses due to the gearbox. Therefore, indicated quantities based on cylinder pressure were used for all evaluations.

Intake air temperature was controlled by moderating the mixing of a hot and a cold water flow to a water to air heat exchanger. This enabled control of the intake air temperature-between 15 and 50 degrees Celsius.

4.1.3 Program interface

The engine was controlled from a PC with a user interface in a Borland® Delphi™ environment. This program has been developed earlier within the division and has here been modified to include support for spark assistance as well as cam phasing and throttle control. The program collected pressure information obtained from the A/D converter, the position of the VVT obtained from the counter card and control signals feedback. The software also controlled injection timing and quantity as well as intake throttle. The program performed on-line heat release calculations and saved raw pressure files for post processing. The injection event as well as spark timing is sent to the engine via PIC-processors and optical fibres to minimise electric interference as well as effects from sudden delays from the operating system of the control programs host computer. The graphical user interface is shown in Figure 14

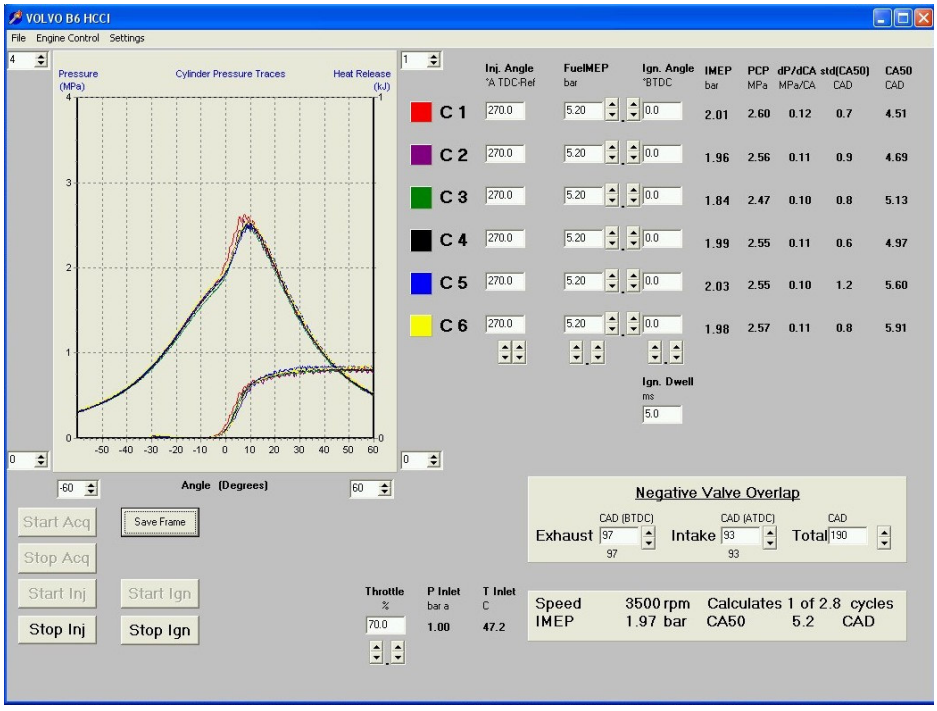

Figure 14. Graphical user interface of engine control program.

4.2 Optical single cylinder engine

4.2.1 Engine and optical access

The optical engine was based on a Volvo D5, which is a passenger car size five cylinder CI engine. The engine was used in three different configurations. Engine data are given in Table 2.

Table 2. Engine specifications, Volvo D5244 in optical configuration

Configuration	I	II	III
Displacement	0.48 L	0.48 L	0.48 L
Valves per cylinder	4	4	4
Bore	81 mm	81 mm	81 mm
Stroke	93.2 mm	93.2 mm	93.2 mm
Combustion chamber	Pancake	pent-roof	Pancake
Compression ratio	12:1	9:1	12:1
Valve train	Standard	Fully flexible	Fully flexible
Injection system	PFI / DI	PFI	PFI / DI
Fuel	50 % iso-octane 50 % n-heptane	40 % ethanol 60 % n-heptane	90 % ethanol 10 % acetone

The engine was operating on only one cylinder while the other four were motored. The motored pistons were drilled through and did neither compression nor expansion work. Additional mass was added to the motored pistons in the form of tungsten alloy weights to compensate for the increased mass of the working piston. The increased mass of the working piston is due to the Bowditch piston extension [32]. Using the piston extension enabled optical access to the combustion chamber from below through a 58 mm in diameter quartz window in the piston crown. In combination with a 45 degree UV enhanced mirror mounted on the cylinder block below the piston crown allowed stationary horizontal mounting of image recording systems in the vicinity of of the engine.

The piston rings in the piston extension had to be run unlubricated. If not, the lubricant would have contaminated the optical surfaces and fluorescence from the lubricant could interfere with measurements. Piston rings made of Rulon® J were used. These have a very low friction and are self lubricant. The downside is that they are temperature sensitive compared to traditional piston rings. An elevated temperature will result in excessive wear of the rings and thereby gradual degradation of the engine behaviour.

4.2.2 Configuration I

The first optical studies (Paper III) were conducted with the standard automotive CI cylinder head and cam shafts, although modified for single cylinder operation with modified cooling water and oil flow as well as deactivation of the valve train on cylinders 2 through 5. The cylinder head had four valves per cylinder with a port design inducing a swirling intake flow pattern. A butterfly valve in one of the intake ports enabled the swirl number of the engine to be moderated from approximately 2 to 2.6. A quartz ring, 25 mm thick, was mounted as an elongation of the cylinder liner for radial optical access to the upper part of the combustion chamber. As the piston quarts glass was flat, there was no bowl-in-piston as in the production engine, instead

a pancake shaped combustion chamber fully accessible through the quarts liner close to TDC. The engine in optical configuration is shown in Figure 15. The piston extension and the quarts liner can be seen in front of the camera to the right in the image. The engine had capability of both PFI and DI. The DI system was the original common rail system modified for single cylinder usage and featured a solenoid injector with a 5 hole nozzle and an umbrella angel of 140 degrees. The system was capable of injection pressures up to 1600 bar. In cylinder pressure was monitored by an AVL GU12S piezo electric transducer mounted in the glow plug hole.

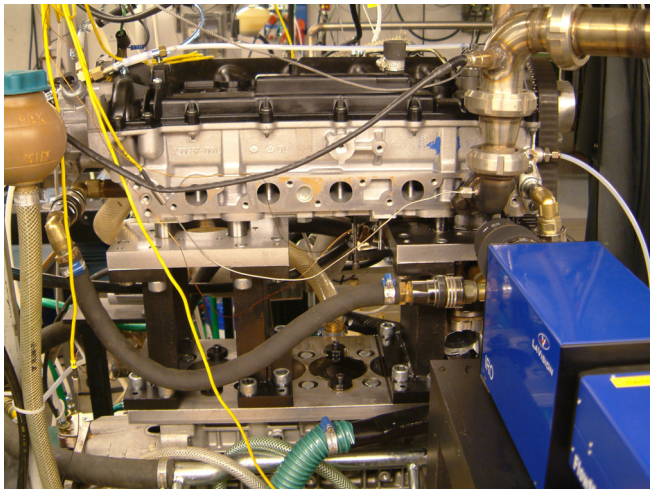

Figure 15. Optical Volvo D5 engine with pancake combustion chamber.

4.2.3 Configuration II

To enable spark assisted HCCI combustion a pent-roof 4 valve SI cylinder head replaced the CI head. The cylinder head originates from a Volvo B5254 engine and has been modified for single cylinder operation during an earlier project [33]. To permit a variable NVO the cam shafts were removed and replaced by a Cargine pneumatic fully flexible valve train. The features of the valve train are further described in chapter 4.2.5. The pneumatic actuators were mounted on top of the valves, acting directly on the valve stems, resulting in a compact setup.

Due to optical constraints and the pent-roof combustion chamber the CR was lowered to 9:1. The optical access through the cylinder liner was limited to two Ø 15 mm quartz windows in the pent-roof giving pass through optical access to the spark plug area. The cylinder head with the optical access and the pneumatic valve train is shown in Figure 16.

Since the cylinder head had three access points for measurement, the two windows and the spark plug hole, pressure was monitored with a Kistler 6117BFD16 combined spark plug and pressure sensor. The piezo electric pressure sensor was flush mounted in the spark plug, i.e. no ducts for the cylinder pressure to travel through. The spark plug had heat range 6 and an electrode gap of 0.8 mm. This is the setup used in Papers IV & V.

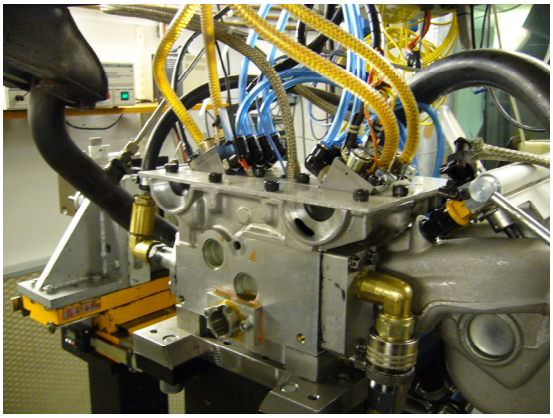

Figure 16. SI cylinder head with pneumatic valve train and optical access.

4.2.4 Configuration III

For Paper VI the engine was modified to feature PFI as well as DI, variable valve train and a spark plug. The engine with the VVA system mounted is shown in Figure 17. To enable DI, the CI cylinder head at hand was used again. The actuators for the variable valve train were fitted on an elevated plate connected to the valve stems with short push rods. The elevated position of the actuators had the consequence that no machining had to be done on the cylinder head and also allowed space for the CI injector to be mounted. By modifying the glow plug hole an 8 mm thread NGK ER8EH spark plug (Figure 18) could be fitted and fixated using a custom made isolator. The spark plug electrode gap had to be decreased to 0.6 mm to ensure breakthrough in the spark gap also at elevated pressure, rather than in the narrow glow plug tunnel. The ignition system was the same as described in 4.2.3. A Kistler 6053C60 un-cooled piezo-electric pressure transducer was fitted through a cooling channel and emerged between the intake and exhaust valves. Since the cylinder head cap had to be removed when the VVA system was mounted, new separate intake runners were built for the two intake ports, each equipped with a separately controlled PFI system. The DI system was the same as described in 4.2.2. Usage of the CI cylinder head meant that a quarts liner could be mounted again with excellent optical access. The combustion chamber was pancake shaped due to the flat piston crown.

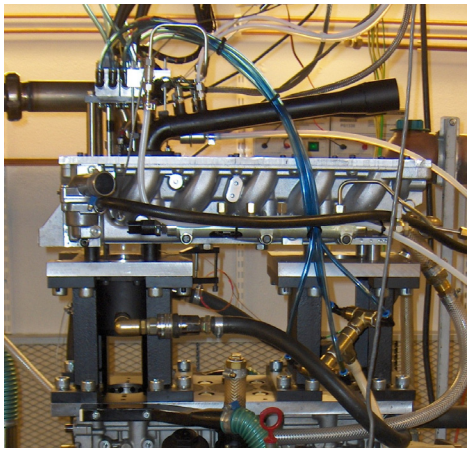

Figure 17. Single cylinder optical engine with VVA, DI, PFI and spark ignition

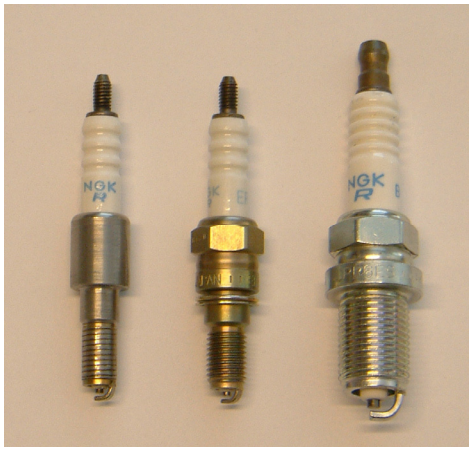

Figure 18. Right: Std. spark plug, Center: 8mm thread spark plug, Left: 8mm spark plug modified to fit in glow plug hole

4.2.5 Variable valve actuation

To allow operation with a variable NVO a VVA system was supplied by Cargine Engineering AB®. The system consists of four actuators controlling one valve each. The actuators are small enough to be fitted directly on top of the valve stem. However, in case of the CI cylinder head the actuators had to be lifted to allow room also for the injector. The system is working with pressurized air to achieve valve lift. Two solenoids in each actuator together jointly control valve timing, duration and lift by regulating the air pressure on the working piston. To achieve a stable and constant valve lift a pressurised hydraulic circuit is deployed. To get a smooth low noise valve seating the hydraulic system is also used to decelerate the valve. A small leak flow of oil through the actuator is sufficient to lubricate the remaining valve mechanism. No other oil supply is needed to the cylinder head since the camshafts are removed.

The solenoids and thus the valve control are managed with FPGA (Field Programmable Gate Array) similar to what was used by Trajkovic et al. in [29]. Since the FPGA runs independent of other activity of the host computer this was found a reliable system with the weakest link being the signal from the engine CAD encoder. Error of the CAD signal can result in an unexpected phasing between piston position and valve opening. In the lab, this clearly showed the benefit of compressibility of air compared to the stiff cam shaft operated valve train. From The GUI controlling the FPGA parameters, it was possible to control valve lift, duration, timing and deactivation for each valve separately as well as all together.

The lift profiles of the pneumatic valve train differ from that of a traditional cam shaft controlled system. Since the performance of the system is based on the air pressure to the actuators as well as the force of the valve springs, it is not dependent on engine speed. Most experiments were conducted at a speed of 1200 rpm of the engine. A valve lift height of approximately 8 mm was used with air pressure and spring forces resulting in an opening and closing ramp of approximately 25 CAD. The pressure of both the pneumatics and hydraulics was kept at 4 bars gauge (5 bar abs.). At Increased speed the valve lift profiles would then resemble a more traditional valve lift curve.

To change the shape of the lift, the air pressure can be moderated, but for the descent it is the spring properties that must be altered. Single cycle lift curves are presented in Figure 19. These lift curves were obtained from image processing of high speed videos of the valve movement when running the engine. Due to limitations in the optical access for the SI cylinder head, the opening and closing ramps are not shown. The actuators had built in optical sensor for detecting valve lift. However, the signal was highly nonlinear, with high sensitivity for detecting opening and closing events, but less for increased lift. Since the system was always run on an optical engine, valve timings were calibrated each day with the PIV camera described in 5.2.1 and the performance during experiments was monitored by the built in sensors to ensure constant conditions.

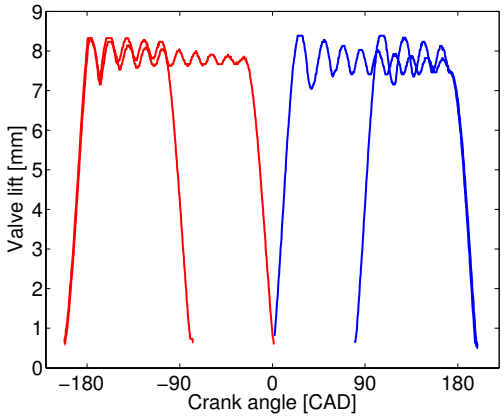

Figure 19. Valve lift curves for 0 and 160 CAD NVO captured at 1200 rpm with high speed camera. 0 CAD is gas exchange TDC.

4.2.6 Test rig and measurement apparatus

Data acquisition of the fast signals i.e. cylinder pressure and triggering signals to and from optical measurement devices was performed with a National Instruments card in a PC running the same type of in-house program as for the multi-cylinder engine. A 1 Hz logger system monitored and stored various pressures and temperatures and also emissions. The emissions were obtained from a Horiba MEXA 8120. The test bed was equipped with a cooled EGR system making it possible to run with high amounts of EGR. Also a 5kW heater was installed on the intake system allowing combustion timing control when not running with NVO. The engine speed was controlled with a 30 kW AC motor used as dynamometer with the ability to both motor and brake the engine.

5 Diagnostic techniques

5.1 In-cylinder pressure and HR-calculations

For knowledge of in-cylinder conditions, pressure traces are recorded with a resolution of 0.2 CAD regardless of engine speed. The pressure signal from the piezo electric sensor is converted to voltage and adjusted depending on transducer sensitivity. The signal level is floating so it must be pegged to absolute pressure. This is performed during the gas exchange period using the signal from an absolute pressure sensor in the intake manifold. From the in-cylinder pressure and calculated volume, engine performance in terms of gas exchange efficiency and load can be directly derived. By performing heat release (HR) calculations more details such as combustion timing (CA50) and combustion duration can be obtained.

The heat release analysis in this work was based on a single zone model. The model is based on the first law of thermodynamics for a control volume as shown in (5.1). The change in energy obtained from combustion equals the sum of internal energy, the work done by the system, heat transfer to the cylinder walls and energy losses by flow in and out of crevices.

$$dQ = dU + \partial W + dQ_{HT} + dQ_{Crevice} \tag{5.1}$$

Using the equation of state, assuming the cylinder content to be an ideal gas and that the trapped mass in the cylinder is kept constant, the change in energy per CAD or heat release per CAD is given by (5.2). V and p are cylinder volume and pressure, γ *is* C_p / C_v.

$$\frac{dQ}{d\theta} = \frac{\gamma}{\gamma - 1} p \frac{dV}{d\theta} + \frac{1}{\gamma - 1} V \frac{dp}{d\theta} + \frac{dQ_{HT}}{d\theta} + \frac{dQ_{Crevice}}{d\theta} \tag{5.2}$$

The heat transfer to the cylinder walls is estimated with a zero-dimensional model. The temperature of the gas (T_{gas}) is assumed to be homogeneous and the wall surface temperature (T_{wall}) constant. This statement does not resemble the actual behaviour in the cylinder. Also HCCI combustion with a homogeneous air fuel mixture show cycle to cycle fluctuations of the size and positions of the burning structures, rendering temperature heterogeneity. For an SI flame as well as for the diffusion flame of the CI engine the temperature variations are expected to be even higher, with an increased cycle to cycle deviation of the SI flame behaviour. However, the true state of the gas temperature distribution close to the walls is very hard to predict and the influence of heat transfer (h) is estimated according to (5.3). The wall area is the sum of cylinder head, piston crown and exposed cylinder liner area.

$$\frac{dQ_{HT}}{dt} = h \, Area_{\text{wall}} (T_{gas} - T_{wall}) \tag{5.3}$$

The heat transfer coefficient is modeled by the relationship introduced by Woschni [34]. This is based on a Nusselt-Reynolds relationship as shown in (5.4). C is a constant, depending on the specific engine, B is engine bore, p and T are in-cylinder pressure and temperature. w is a characteristic gas velocity.

$$h\left[W / m^2 K\right] = CB[m]^{-0.2} \, p[kPa]^{0.8} T[K]^{-0.55} \, w[m / s]^{0.8} \tag{5.4}$$

The characteristic velocity in (5.4) for the gas movement was defined according to (5.5). C_1 and C_2 are correlation coefficients that must be tuned for the individual engine the model is applied to. Sp is the mean piston speed and V_d displacement, V_r, P_r an T_r are reference volume, pressure and temperature reflecting in-cylinder conditions at IVC. P is the actual pressure and Pm is calculated motored pressure.

$$w = C_1 S_P + C_2 \left(\frac{V_d}{V_r} \right) \left(\frac{p - p_m}{p_r} \right) T_r \tag{5.5}$$

However for the HR calculation to be valid the initial conditions must be correct. The pressure levels are set according to intake pressure, constant mass is set depending on valve timings. What is left is residual fraction and thus the charge temperature and γ. For an engine running with normal SI or CI valve timings the residual fractions are low and the charge temperature can be estimated from the intake temperature with a small offset also depending on vaporisation of fuel. Differences in γ are also small. When running with a NVO the amount of residuals is higher. The charge will be a mix of the incoming fuel and air combined with the trapped hot residuals. The residuals increase the charge temperature and lowers γ. A rough estimation of the residual fraction can be calculated by using the fuel flow and the air fuel ratio to the engine, with certain assumptions. By assuming the fresh charge to have the same temperature and density in the cylinder as in the intake manifold, the rest of the displaced volume can be assumed to contain trapped residuals with a temperature corresponding to the exhaust temperature. From this, a charge temperature as well as γ at intake valve closing can be calculated. The actual residual fraction is difficult to predict with certainty since it is depending on the trapping efficiency as well as on the actual temperature of the residuals and the fresh charge which both are affected by heat transfer.

Since the estimation is rather rough, no analysis is done regarding in-cylinder temperature. However load (IMEP) and combustion timing (CA50) are more robust and reliable. IMEP is more sensitive to the phasing between pressure traces and calculated instant volume which is well determined.

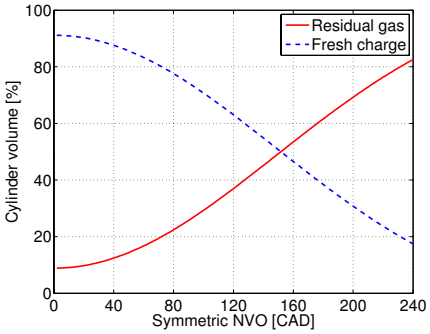

Figure 20. Geometrical estimation of residuals and fresh charge trapped in the cylinder as a function of NVO.

What is known for all measurements is fuel flow (fuel balance) and combustion efficiency (emissions) giving the total heat released. By small modifications of the estimated γ and charge temperature the corresponding heat release can be reached.

Another way of looking at the residual proportions is by only considering geometry and valve timings as shown in Figure 20. This is by no means a correct assumption since no fluid dynamics or properties are considered. Still it gives an idea of the residual fractions for increased NVO.

5.2 Chemiluminescence

Chemiluminescence imaging or flame photography has been used extensively in SI and CI engine research over the years. The method offers possibilities to make quantitative measurements such as flame location, propagation, size and front thickness. The link between recorded pressure and flame structures has been recognised [67] making it a very useful tool for further understanding of the combustion behaviour.

Chemiluminescence imaging is a line of sight method, meaning that the emitted light intensity received by the camera is integrated over the line of sight.

In the later years the measuring technique has also been implemented for HCCI combustion [6, 36]. Chemiluminescence is defined as the emission of light due to chemical reaction. It is commonly proposed that chemiluminescence from species like CH* OH* and C_2* produced in an excited state is a measure of global heat release in a flame [37]. If the physical quenching process is assumed to be faster than the chemical reactions producing the species, then chemiluminescence will be a measure of the species production rate and thus the heat release rate.

5.2.1 PIV system

Two sets of hardware have been used for chemiluminescence imaging. For the boundary layer investigation in Paper III a PIV system with higher spatial resolution but slower repetition was used. It was a LaVision Flowmaster system consisting of two double framing image intensified CCD cameras controlled by a programmable timing unit: The system was capable of taking four images with one CAD separation within the same cycle. The CCD resolution was 1024 x 1280 pixels and both cameras were equipped with Sigma EX 105 mm f 2.8 macro lenses. The triggering scheme for the system is shown in Figure 21. The exposure times are generally kept as short as possible to minimize the smearing of the images due to the fluid movement in combination with the ongoing combustion. By raising the intensification of the images, exposure time can be decreased. Unfortunately this also increases the noise level. A reasonable compromise was found with an exposure time of 100µs and still using the dynamic range of the camera for those operating conditions.

The camera's double exposure abilities were limited, the first image could be set arbitrary while the second has a fixed long exposure time related to the read-out time of the first. To get the same exposure time for both images the image intensifier was used as an electrical shutter. The camera triggering could not be separated, so to get four individual images with equal time separation the image intensifiers had to be run in double pulse mode with a time delay, dt, for intensifier two. This meant that image order was interlaced between the cameras. Camera one took Images one and three, and camera two took Images two and four.

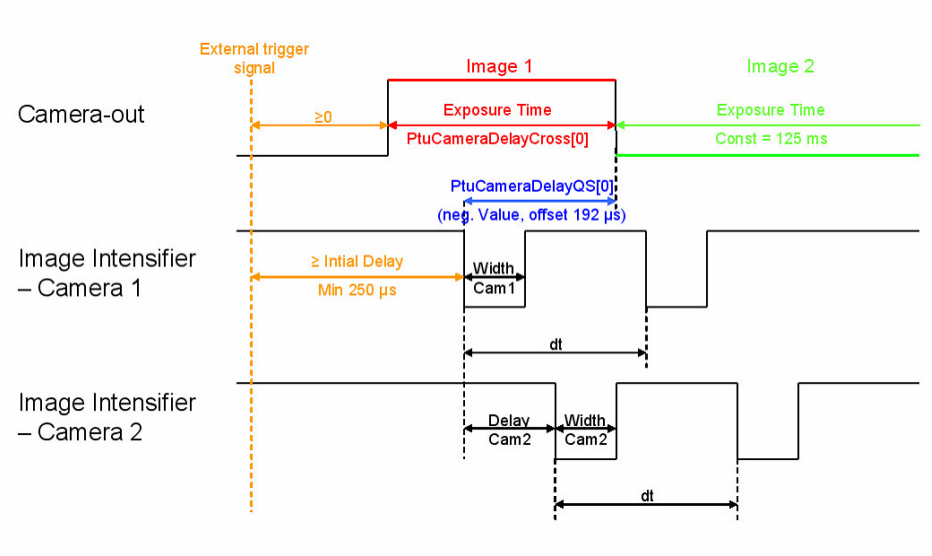

Figure 21. Triggering scheme for LaVision flowmaster system [38]

5.2.2 High speed video

For the chemiluminescence studies in Papers IV and V a Phantom high speed framing camera was used. The camera is capable of image acquisition at up to 190 kHz. At this framing rate the resolution is very limited, by decreasing the framing rate a higher spatial resolution can be achieved. The camera was run synchronised with the engine taking 2.5 images per CAD using a modified signal from the engine CAD encoder. This corresponds to 18000 Hz at 1200 rpm. At this framing rate, image resolution was limited to 304 x 304 pixels, giving a pixel size of 0.2 mm. The camera was used in combination with a Hamamatsu high speed gated image intensifier, this allowed short exposure times with less smearing of the images. For all cases an exposure time of 12 µs has been used. The lens used was a 105 mm f 2.8 macro lens. Apertures were kept in the range from 5.6 to 11 depending on operating conditions. The system showed an extremely low noise level in combination with a 12 bit dynamic range. In contrast to the previous hardware the image intensifier was here run continuously while the exposure times were controlled by the camera.

5.3 Schlieren

Another flame imaging method is the Schlieren technique. With the Schlieren technique parallel light is passed through the combustion chamber. The outgoing light is focused on the tip of a knife edge. The light passing the knife edge is imaged on a screen. The different refractive index between the hot reacting zone and the colder unburned gas will deflect portions of the flame where the density gradients are normal to the beam. Therefore the edge of the flame will appear as a darker region on the image since some of the light is being blocked by the knife edge. By slightly moving the knife edge the sensitivity of the method can be altered e.g. the amount of light blocked by the knife edge. A schematic of the setup in combination with LDV is shown in Figure 22. As the chemiluminescence method, Schlieren is also a line of sight measurement technique.

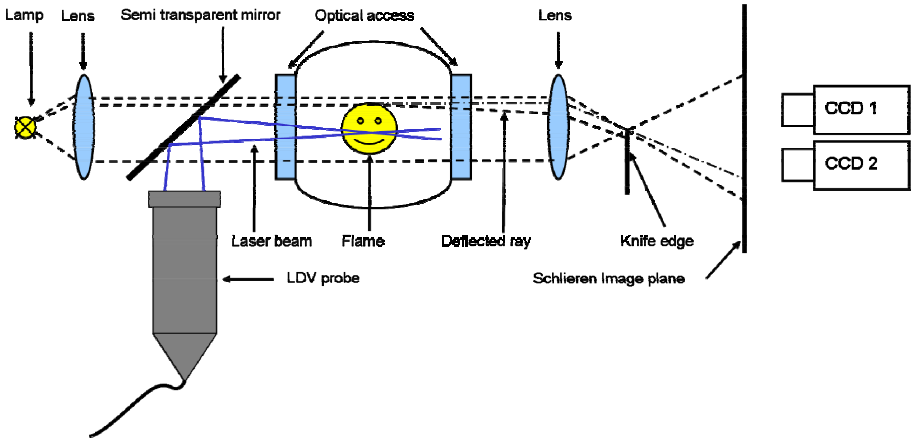

Figure 22. Simultaneous Schlieren – LDV setup.

During experiments a 100 W mercury lamp was used as a light source, a f 300 lens was used to get parallel light first passing the mirror for the simultaneous Laser Doppler Velocimetry (LDV) measurements, as described in the next section. The light then passes through the optical cylinder head. Another f 300 lens is used to focus the light on the knife edge. The images are then collected by back illumination on a screen by two image intensified CCD cameras from the PIV system described above.

5.4 Laser doppler velocimetry (LDV)

5.4.1 Principle

Laser Doppler Velocimetry (LDV) or Laser Doppler Anemometry (LDA) is a non intrusive optical method for measuring velocity of gases. It is a point measurement technique i.e. no spatial resolution is obtained, but a high temporal resolution is possible making it feasible to also do turbulence estimations.

The working principle of LDV can be explained by the fringe model. When two coherent laser beams intersect, they will interfere in the volume of the intersecting beam waists. This will produce approximately plane wave fronts or interference fringes as shown in Figure 23.

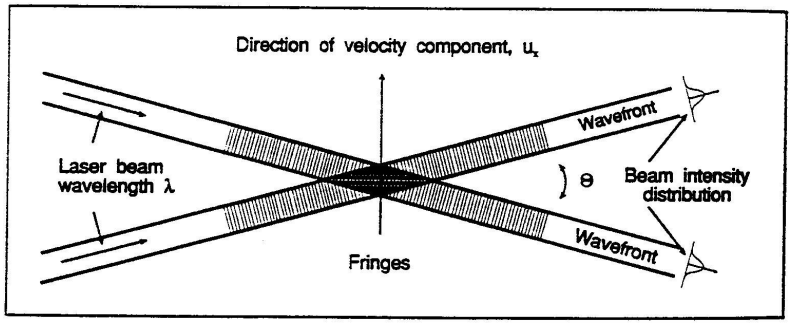

Figure 23. Laser beam crossing with interference fringes [39]

The distance between the fringes is decided by the laser wavelength and the angle between the incident beams according to (5.6) where κ is half the angle between the laser beams. As a particle passes through the measuring volume the intensity of light reflected from the particle will vary with a frequency v_D proportional to the particle velocity u normal to the fringes. Knowing the laser wavelength and the angle between the incident beams, the velocity component can be calculated from (5.7).

$$d_f = \frac{\lambda}{2\sin\kappa} \tag{5.6}$$

$$v_D = \frac{u}{d_f} = \frac{2u\sin\kappa}{\lambda} \tag{5.7}$$

To determine the direction of the velocity component a 40 MHz frequency shift is introduced to one of the two joined beams. The frequency shift causes the fringes in the measurement volume to move, thus the velocity and direction of a particle can be obtained by comparing to the known 40MHz frequency shift.

5.4.2 Seeding

To follow the fluid flow some kind of seeding particles have to be used. These must be small enough in size to ensure that they correctly follow and reflect the flow motion. At the same time they should scatter enough light to be detected. Further, it must be possible to add enough particle density to the working fluid without agglomeration of the seeding or sticking to the optical access surfaces. Lower particle density will directly lower the sampling rate and thus the data quality. Previous research by Johansson [40] with different seeding compounds has shown good results using a polystyrene-latex dispersion, which is also used here. The polystyrene-latex dispersion endures the elevated pressure and temperature during compression, but is rapidly consumed by the combustion. The downside of the extinction of the seeding is naturally that no measurements can be performed once combustion is started. On the other hand the optical access is kept clean enabling long measurements with stable conditions. Lastly, the usage of the polystyrene-latex dispersion posed no risk of excessive engine wear like some dry powder seeding as TiO_2 and SiO_2.

5.4.3 Practise

The particle dispersion had a mean size of 0.46μm and was added upstream of the intake manifold by a set of 24 Hudson Up-Draft nebulizers. To minimize soiling of the optics, the seeding equipment was only activated when the engine was fired.

The fluid flow was measured by a 2-component Dantec-fibre flow LDV system. The system features a model 2040 5 W Ar-ion laser from Spectra-Physics. The laser beam is led into a transmitter, through a bragg-cell that splits the beam into two. One of the beams is frequency shifted by 40 MHz. The two beams pass a colour separator to enable three pairs of laser beams, 512, 488 and 476 nm. With the three pairs it is possible to extract three individual velocity components. Here only two are used: 488 nm (blue) and 512 nm (green), thus giving possibility of two dimensional velocity information when measuring in the same volume. The laser beams are transferred with fibre optics to the measurement probe mounted on the engine. The probe is equipped with a beam expander and a beam translator. With the beam translator the beam separation can be moderated, changing the angle of the incident beams after the focusing lens and thus the fringe spacing. An f 310 lens is used to focus the beams to

a measurement volume near the spark plug through the optical access to the combustion chamber pent-roof. The size of the measurement volume diameter was approximately 50 µm in diameter and the length 700 µm. The backscattered light from the seeding particles is collected through the f 310 lens and transferred back through a fibre. The signal is separated into the blue and green and converted into an electric signal by two Photo Multiplier (PM) tubes. This signal is digitized and analysed with Fast Fourier Transformation (FFT) by Burst Spectrum Analysers (BSA) to obtain valid velocity data. The BSAs are run with an external frequency generator giving a fixed mean data rate of close to 150 kHz.

The LDV measurements are run synchronised with both Schlieren image acquisition and in-cylinder pressure recording. The LDV-Schlieren setup is schematically shown in Figure 22. The two component laser beams was reflected on a semi transparent mirror before entering the combustion chamber. The mirror was coated to reflect the green and blue laser light while still transmitting the broadband light from the mercury lamp for the Schlieren measurements.

5.4.4 Velocity and turbulence

Stationary flow velocities can be separated by Reynolds decomposition into the mean velocity ($\bar{U}$) and the instant fluctuations, $u(t)$, as shown in (5.8).

$$U(t) = \overline{U} + u(t) \tag{5.8}$$

The turbulence (u') is defined by the Root Mean Square (RMS) of the instant velocity fluctuations according to (5.9). For steady flows the turbulence intensity is usually derived by dividing the RMS value with the mean velocity. In engine research the RMS value is used without the mean velocity and turbulence is discussed with the unit [m/s] since the mean flow in a reciprocating engine is not constant.

$$u' = \lim_{\tau\to\infty}\left(\frac{1}{\tau}\int^{t+\tau} u^2(t)dt\right)^{1/2} = \lim_{\tau\to\infty}\left(\frac{1}{\tau}\int^{t+\tau}\left(U^2(t) - \overline{U}^2\right)dt\right)^{1/2} \tag{5.9}$$

In the definition in (5.8) above the mean velocity is time independent which is hardly appropriate in an internal combustion engine. Instead a slowly fluctuating mean velocity can be used defined the same way as the stationary mean velocity except that the time interval (τ) is not infinite. This allows low frequency changes of the mean velocity, following the gas flow pattern (5.10).

$$\overline{U}(t) = \frac{1}{\tau}\int^{t+\tau} U(t)dt \tag{5.10}$$

The ensemble average velocity and turbulence can be obtained if calculating the mean and the fluctuating velocities from different engine cycles, but at the same crank angle, thus compensating for the engine flow pattern. Better yet is if the amount of velocity measurement per cycle are high enough for within cycle evaluation. Then the mean velocity, $\bar{U}(\theta,i)$, can be calculated using a moving average as shown in (5.11). θ is the current CAD, α the window width and i the cycle number. (5.12) describes the corresponding turbulence definition.

$$\overline{U}(\theta,i) = \frac{1}{N}\sum_{\alpha=\theta-\frac{\Delta\theta}{2}}^{\alpha=\theta+\frac{\Delta\theta}{2}} U(\alpha,i) \tag{5.11}$$

$$u'(\theta,i)=\left[\frac{1}{N}\sum_{\beta=\theta-\frac{\Delta\theta}{2}}^{\beta=\theta+\frac{\Delta\theta}{2}}\left(U(\beta,i)^2-\overline{U}(\beta,i)^2\right)\right]^{1/2} \tag{5.12}$$

The differences between the ensemble average mean velocity and the in cycle mean velocity is illustrated for four consecutive cycles in Figure 24. As can be seen the usage of ensemble average does not take into account the single cycle deviations in the mean flow for the turbulence calculations. In this work the method of using a moving window for cycle resolved measurements has been applied.

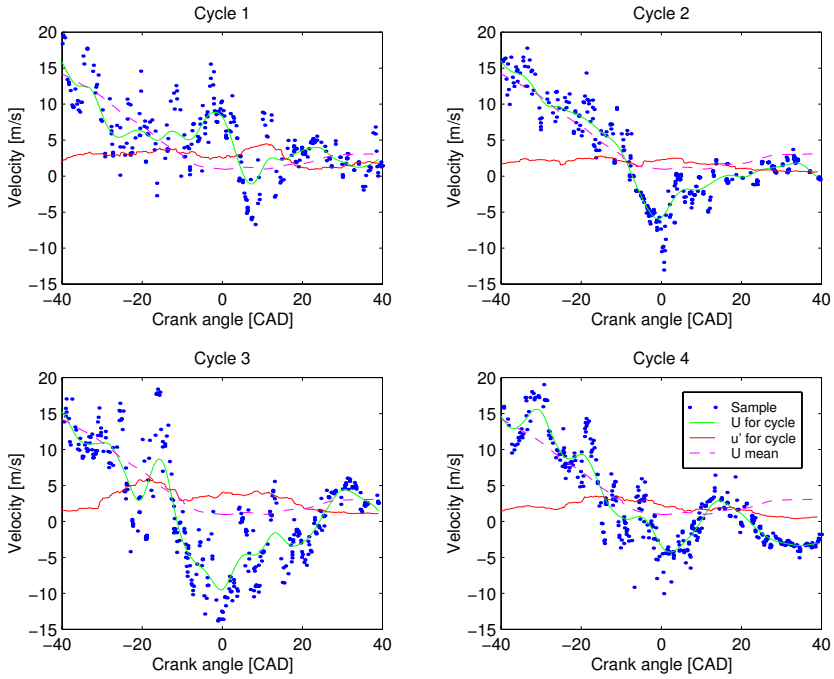

Figure 24. Sample velocities, cycle resolved mean velocity (U for cycle), ensemble averaged mean velocity(U mean) and cycle resolved turbulence(u´ for cycle) [41].

5.5 Planar laser induced fluorescence (PLIF)

5.5.1 Principle

Laser Induced Fluorescence (LIF) is an inelastic scattering process. Molecules or atoms are excited to a higher state due to the absorption of photons from a laser. When transitioning again to the ground state the light emission, the fluorescence can be measured. When used in two dimensional measurements the technique is usually called PLIF. The measurement technique is well suited to study the presence of various species and intermediates. While the method works well for finding different species and to study their distributions, making quantitive measurements is more difficult. The LIF signal is both pressure and temperature dependent; to make absolute measurements requires calibration against a known concentration at the correct

temperature and pressure. Further, absorption causing beam attenuation must also be accounted for. A more complete description of the LIF theory and relevant issues can be found in [42]. The number of variables that influence the LIF signal in a HCCI engine is extensive. The variation in in-cylinder temperature will vary due to a mixture of residuals and fresh gas, DI with lower temperature due to heat of vaporisation and cycle to cycle variations changing the residual state. Since the signal is pressure dependent the LIF calibration must be repeated depending on where in the cycle to measure. Lastly fluctuations in the measurement system have to be accounted for.

5.5.2 Fuel tracer

In this work PLIF was used for fuel visualisation. Ethanol which is non fluorescent was used as fuel with ten percent acetone (CH_3COCH_3) as a fuel tracer. A wavelength of 266 nm was used for excitation of the acetone tracer. Subsequent fluorescence occurs between 350 and 550 nm. The usage of a non fluorescent fuel has the benefit that the acetone LIF signal easily can be distinguished compared to the strong signal from multi component fuels. When looking at the fuel oxidation by LIF it must however be emphasised that it is the consumption of the exact tracer molecule that is shown, other species may still be reacting. The tracer should therefore have as similar behaviour as the fuel as possible.

5.5.3 Setup

A custom made multi-YAG laser cluster was used to make high speed fuel PLIF measurements. The system enables several images to be recorded with short separation within the same cycle. The laser sheet was directed through the quarts cylinder liner approximately 5mm from the fire deck. The arc was slightly diverged before the engine to compensate for the focusing effect of the cylinder liner, thereby a significant part of the optically accessible combustion chamber was covered. The fluorescence signal from the acetone was imaged perpendicularly to the sheet down through the quartz window in the piston and via a 45 degree UV enhanced mirror in the piston extension using a UV sensitive high-speed framing camera.

A more thorough specification of the measurement system and the requirements for the fuel tracer can be found in Paper VI.

6 Results

The following chapter contains a summary of the results from the papers as well as additional complementary information. The intention is to order the results according to topic. Since some issues have been addressed in more than one paper the results sections do not fully follow in the same order as the papers.

The fist section, “Operating conditions”, handles the operating regimes obtained in Papers I & II as well as some additional results. Section 6.2 addresses spark timing when running SACI combustion and is related to results in the first two papers.
In Section 6.3, “Intake temperature and combustion phasing”, the main results from Paper I is summarized both with pure HCCI as well as with SACI combustion. In this paper SACI is still denoted spark assisted HCCI. Section 6.4, Cycle-to-cycle and cylinder-to-cylinder dependence, handles the results from Paper II regarding mainly cycle to cycle deviations with NVO HCCI and the effect of SACI combustion. The results from optical investigations start with Section 6.5, “Boundary layer and near wall effects”, which summarises the results from Paper III. These results are obtained with pure HCCI combustion, no SACI is utilised. Section 6.6, “Flame expansion with residuals”, covers Paper IV looking at the early flame development in SACI combustion by chemiluminescence imaging. Paper V is addressed in Section 6.7, “Increased turbulence by swirl”. This chapter is a direct continuation of the previous one combining chemiluminescence imaging with fluid velocity measurements for SACI combustion. Section 6.8, “Stratification”, summarizes the results from Paper VI. Here different ways of achieving stratification with SACI combustion are investigated.

6.1 Operating conditions

The operating range for NVO HCCI combustion is limited in speed and load for a number of reasons. The speed and load range for the initial trials with NVO HCCI published in Paper I is shown in
Figure 25. The fundamental restrictions of the speed-load range are mainly related to temperature and pressure rise rates (PRR). Running higher load means less dilution by residuals, thus faster reaction rate. The maximum allowed PRR in these experiments was set to 5 bar / CAD. The purpose of the PRR limit is mainly noise reduction and thus the appropriate level is somewhat arbitrary and depends on other factors such as vehicle design. Peak pressure is not an issue in this application since the engine is naturally aspirated and has a rather low CR. When running at higher speed the main issue goes from PRR to also include gas exchange. The volumetric efficiency decreases with increased speed making it difficult to attain enough fresh charge with the low lift, short duration cam shaft and still maintain combustion. Low load is on the other hand restricted by insufficient temperature for auto ignition. It is clear that it is possible to run at lower load as speed is increased, mainly due to lower heat losses and higher combustion chamber wall temperatures. The effect is illustrated in Figure 26 by Zhao et al. where the exhaust temperature for a given residual rate is plotted for different speeds [43]. A substantial decrease in available temperature is shown for lower speeds. The calculated temperature at CA10 is also included to illustrate the requirement in auto ignition temperature.

To attain auto ignition at lower speed and load spark assisted HCCI combustion is used. Where appropriate the abbreviation SACI, Spark Assisted Compression Ignition is used for this combustion mode.

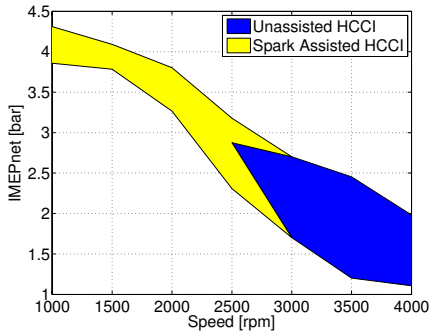

Figure 25. Load regime with fixed camshafts

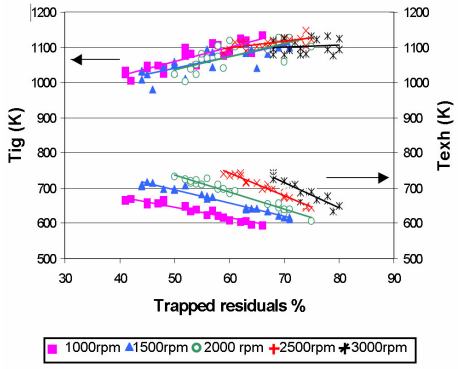

Figure 26. Exhaust temperature and calculated temperature for CA10 as a function of residual rate [43].

The different load limitations are clearly shown in Figure 27 relating to Paper II. Here the engine is equipped with variable valve timing (VVT) The PID-controlled cam phasing mechanisms control both intake and exhaust valves. The phasers make it possible to change the NVO by 120 CAD during operation. The engine is started with smallest possible NVO to achieve throttled SI combustion. By increasing the NVO pumping losses decrease as residuals are increased until HCCI combustion can be achieved with ambient intake pressure. A much broader but still limited operating regime is achieved. If running with a symmetrical NVO, higher negative overlap will cause IVC to occur well into the compression stroke, lowering the effective compression ratio. By phasing the exhaust valve further than the intake valve a higher yet asymmetrical NVO is achieved, trapping more residuals. By doing so the operating regime was increased as seen in Figure 28.

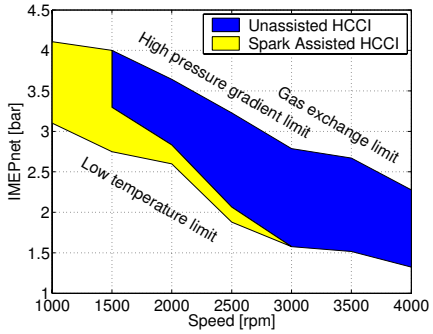

Figure 27. Load regime with VVT

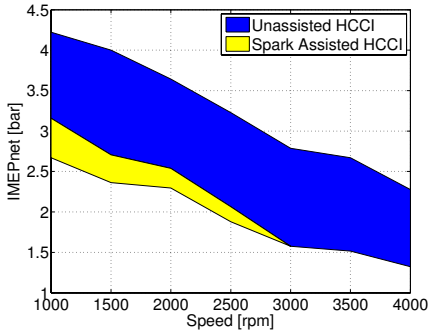

Figure 28. Load regime with VVT and asymmetric NVO

Already for the operating regime shown in Figure 27 a small offset was used to avoid lower effective compression ratio. The difference in valve timing and PMEP is illustrated in Figure 29 and Figure 30. All cases except the 1000 rpm cases are run within the unassisted regime. The offset from symmetric valve overlap is increased for lower speed although the total overlap decreases slightly. As the volumetric

efficiency goes up with lower speed due to the short duration, low lifting camshaft, a higher NVO is needed to trap the same percent of residuals. On the other hand at lower speed the possible loads are higher, again decreasing the NVO. So in general the lower speed cases are at a lower total NVO.

Operating ranges for HCCI with NVO have been reported by various authors. In 2002 both Zhao et al. [43] and Allen et al. [44] presented load regions with similarities to what is shown in Figure 28 in the sense that the fundamental limitations are the same. Both investigations are performed at stoichiometric conditions and show reduction in NO_x emissions up to 97 – 99 % while increasing the fuel economy by up to more than 30 %. Although a significant improvement in efficiency a low improvement is shown for the NEDC drive cycle by Zhao. The operating regime in HCCI mode simply covers too few of the operating points from the test cycle.

To increase the low load potential DI during the NVO has been suggested by Willand [25] and later performed by Urushihara [46] and Koopmans [47]. By fuel injection during the recompression in the NVO fuel reformation occurred which increased the reactivity of the charge as well as increased the temperature. By adopting fuel injection during the NVO advanced combustion phasing as well as increased lean capability is shown. For greater amounts of fuel in the NVO significant expansion work could be detected leading to lower efficiency due to decreased thermal efficiency with the low CR of the NVO. The injection strategy is only applicable when operating at lean conditions with excess air during the recompression and is not applicable if running stoichiometric.

Cairns et al. combined stoichiometric operation at higher loads utilising the 3-way catalyst with low load lean operation and DI in the recompression. To further increase the high load, boosting as well as cold EGR was utilized increasing the volumetric efficiency [45].

As the engine speed is decreased, IVC has to be retarded to keep effective compression ratio at a constant level. The main reason for this is thought to be due to lower flow velocity in the intake changing the gas dynamics. The pumping losses shown in Figure 30 also indicate that the difference from symmetric overlap is not the only parameter affecting these. However the changes in gas dynamics with engine speed seems to have a large effect. By using asymmetric NVO with earlier EVC the PMEP can be expected to increase due to a shorter expansion than compression for the recompression. In Figure 29 and Figure 30 an increase in PMEP is shown when increasing the offset from symmetric NVO. Since the engine speed is also changed the significance of the effect can not be fully isolated. The again increased PMEP at high speed with higher mass flow through the engine is thought to be related to the limited breathing capabilities of the low lifting valves. Heat losses to the cylinder walls during the NVO should also change the ideal proportions between EVC and IVO; this is however not dealt with in this work. The effect on combustion timing by asymmetrical NVO is illustrated in Figure 31 for an NVO of 185 CAD. Here the combination of the increased hot residuals and simultaneous increase in effective compression ratio dramatically affects the combustion timing.

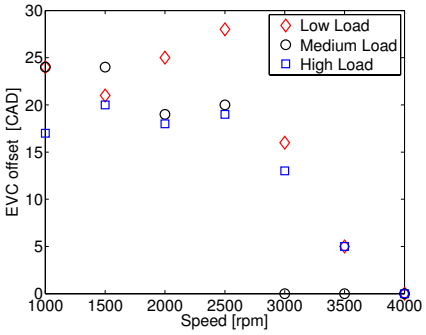

Figure 29. Offset from symmetric NVO by increased phasing of exhaust valve timing as a function of speed.

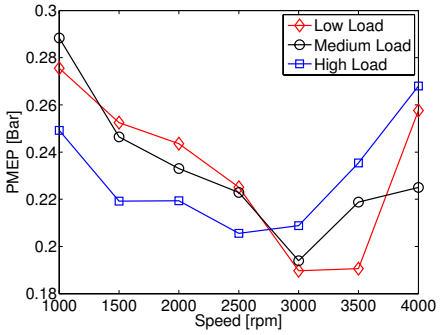

Figure 30. PMEP as a function of speed for the different NVO.

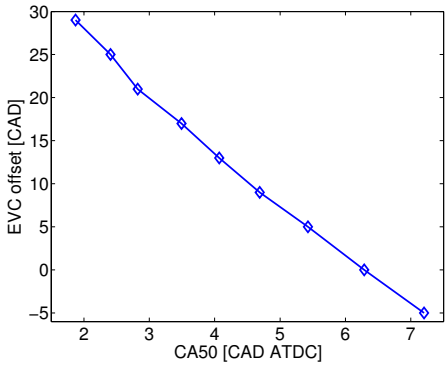

Figure 31. Effect of combustion timing by increasing offset from symmetrical NVO by relatively earlier EVC, total NVO kept to 185 CAD. ~2.3 bar IMEP

The usage of spark assistance is needed if the transition from SI to HCCI is to be done over several cycles by gradually changing valve timings. Figure 32 shows a manual transition at 4 bar $IMEP_{net}$, 1000 rpm for cylinder 1 of the Volvo B6. Since the throttle, VVT settings and spark are set manually it takes some time to do the transition; therefore the figure only shows every 50th cycle. The cam phasing mechanism is limited in operating range giving an NVO adjustable from 100 to 220 CAD for the used setup. The engine is run in SI mode with lowest possible NVO and late spark timing to avoid knocking. This operating condition for SI is far from optimal and is only used to heat the engine before making a transition to HCCI. The transition is made by increasing the NVO and adjusting the spark timing. Since the volumetric efficiency decreases with increased NVO only small changes of the throttle position are needed. As the residuals are increased the flame speed goes down; to keep combustion timing the spark is set off earlier. With even more residuals the charge seems to auto ignite during the SI combustion and combustion timing is again advanced with a resulting retarded spark timing until full HCCI is reached and the spark can be turned off.

Gradually increasing the NVO to enter an intermediate region between SI and HCCI may not be without problems. If λ, intake pressure and combustion timing are not controlled very thoroughly, high pressure gradients and knocking behaviour can occur. This is especially important at the lower overlaps where the engine is run

throttled with too little dilution to slow down combustion rate if early auto ignition is achieved. At low speed the transition is easy, even manually. When passing above 1500 rpm, problems start to occur with random cycles with too high pressure gradients in combination with high cycle to cycle variations. These problems are to some extent related to the lack of closed loop control of engine parameters and thereby combustion timing. Transition problems are also reported by Hyvönen et al. [48], problems with both knock and cycle to cycle behaviour were observed. This was however run at slightly different conditions; high CR making it more difficult to get sufficient spark breakthrough, low turbulence combustion chamber slowing down flame speed and air diluted instead of residual diluted combustion.

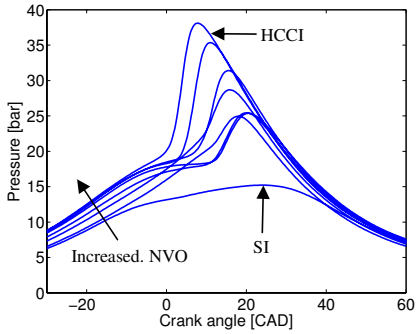

Figure 32. Transition from low NVO SI to high NVO HCCI at 1000rpm, 4 bar $IMEP_{net}$

To avoid problems with intermediate regions the mode shift can be made from one cycle to the next either by using an active valve train (AVT) as shown by Koopmans et al. [49], or by using a CPS system [50]. For the later strategy to work the amount of residuals needed for the given operating point in HCCI must be known to avoid misfire or high reaction rate. The throttle response in combination with the CPS systems is of importance to get proper conditions for the subsequent cycle following a mode change. A smother transition is shown stretching for several cycles by utilising an AVT system. In [51] the usage of sequential profile switching with CPS system is suggested as one way to prevent misfire or torque variations due to different stages in the cycle for the various cylinders. This way a cylinder individual mode shift would be possible further lowering the variation in engine torque.

6.2 Spark timing

When running SACI it is not only possible to force auto ignition but it is also possible to phase combustion timing by altering the spark timing. Figure 33 shows a spark timing sweep connected to the operating regime shown in Figure 27. All points are run at the border of the region between SACI and pure HCCI except the point at 1000 rpm that is only spark assisted. The difference in combustion timing when advancing spark timing is evident for the lower speeds.

At higher speeds the engine is run at lower load. Since the engine is run slightly lean the negative correlation between residuals and load is not necessarily perfect. To keep combustion timing at higher speed λ is moderated slightly.
For higher speed and lower load, combustion timing is advanced, this due to increased amount of residuals and lower heat losses in combination with a seemingly higher effective compression ratio. To keep combustion timing optimal for efficiency, λ increases with lower load in combination with increased speed.

At a speed of 3000 rpm and a load of 1.7 bar $IMEP_{net}$ no effect of the spark can be seen. Here it seems as the flammability limit is reached and any flame propagation is quenched. At 2500 rpm no change in timing can be seen from Figure 33, but still it is possible to sustain SACI at even lower load than HCCI. This could be due to cycle to cycle oscillations which are dealt with more in depth in Section 6.4.

Since Figure 33 only deals with engine average timing it is of interest to see the distribution of all cylinders. Figure 34 shows the behaviour for an operating point at 1500 rpm, 3.4 bar $IMEP_{net}$. The spread in timing is quite small although cylinder 6 is slightly late. The changes in combustion timing by advancing the spark is more than enough to be able to do cylinder individual balancing at the lower speeds.

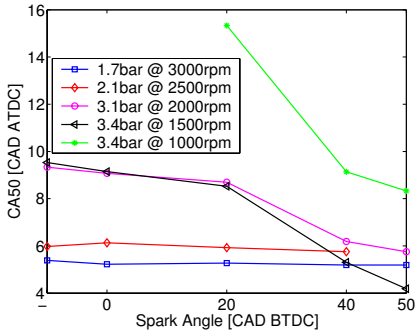

Figure 33. Influence on CA50 for unassisted HCCI and for spark assisted HCCI with advanced spark timing, engine average.

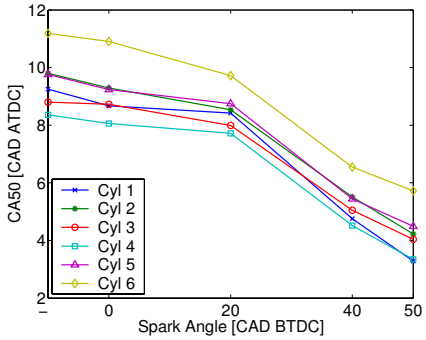

Figure 34. Influence on CA50, from unassisted HCCI to spark assisted HCCI with advanced spark timing, at ~3.4 bar IMEP at 1500 rpm.

The RoHR for cylinder six from the spark sweep at 1500 rpm is shown in Figure 35. With advanced spark timing the earlier combustion phasing is evident. As the spark timing is advanced the RoHR changes with a slow heat release seen appearing earlier and increasing with spark timing. The slow heat release is then followed by an advanced higher RoHR more characteristic for HCCI combustion.

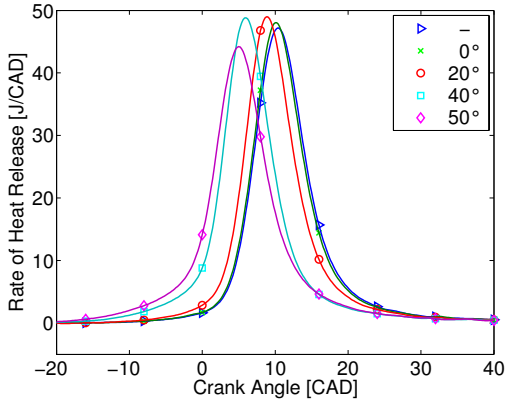

Figure 35. Rate of heat release in J/CAD from unassisted HCCI to spark assisted HCCI with advanced spark timing. cylinder 6 at ~3.4 bar IMEP, 1500 rpm.

6.3 Intake temperature and combustion phasing

Usually HCCI combustion has problems with excessive reaction rates if running with a lambda (λ) lower than approximately 2 [53] without dilution with burnt gases. With NVO the amount of residuals is high enough to enable stoichiometric conditions without excessive reaction rate. If the engine is run at stoichiometric conditions the engine load will be directly controlled by the NVO and the combustion timing by the trapped residual temperature. The only feasible way to control combustion timing is then by changing the inlet cam phasing, The CAD for inlet valve closing will control the effective compression ratio and thereby the point of auto ignition. Since changing IVC will affect the volumetric efficiency this has to be done in interaction with exhaust valve timings to keep the desired load.

If running lean, combustion timing can be controlled by simply moderating the exhaust valve phasing, increasing or decreasing charge dilution and temperature. As long as limiting NO_x levels are not exceeded.

One undesired effect of the increased amount of residuals is the lower γ of the residuals. This lowers the temperature after compression and thereby counteracts the initial elevated temperature gained with the hot residuals. The effect of γ is however small compared to what is gained due to initial residual temperature.

Small changes in intake temperature have shown to have great impact to combustion timing for HCCI combustion. Yet changing the inlet conditions for an engine running in HCCI mode with trapped residuals has less impact. The low impact of intake temperature on combustion timing is a result of the high amount of residuals. If the charge is homogeneously mixed, the higher amount of trapped hot residuals will decrease the impact of intake temperature due to a lower fraction of the charge being fresh air. This means that for lower loads, differences in intake temperature will have less impact on charge temperature.

When changing the intake temperature from 15 to 50 degrees centigrade, a difference of 35° C, the combustion timing only changes by approximately 3 CAD as shown in Figure 36. The behaviour is the same whether the engine is run spark assisted or not as shown for an average of cylinder 1 and 4 in Figure 37. The spark is however only used here to prevent misfire and is set at TDC. The difference in total timing between spark assisted and unassisted is thought to be due to cycle to cycle behaviour. Very late burning cycles are prevented by the spark so the averaged cycles shown in Figure 36 and Figure 37 that are spark assisted give slightly earlier timing.

The points compared have the same load and negative overlap, but as a result of the change in temperature the equivalence ratio differs somewhat due to different air density.

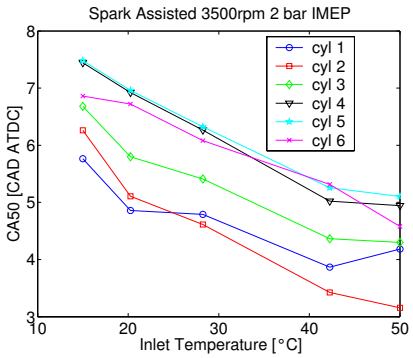

Figure 36 Combustion timing for cylinder 1 through 6 when varying intake temperature by 35˚C

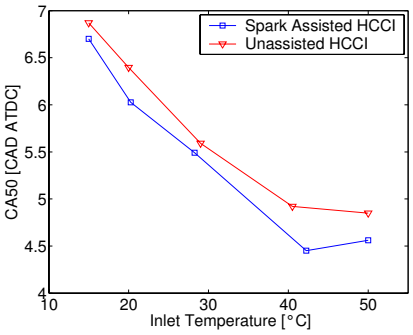

Figure 37 Combustion timing for spark assisted and unassisted HCCI as a function of intake temperature

The effect of intake temperature on emissions is illustrated in Figure 38. Here indicated specific NO_x is shown to decrease with lower intake temperature. This is mainly related to the later timing and lower maximum temperature. The overall NOx level is also very low. It seem as the emission level is affected by the usage of the spark. The spark is phased very late in the cycle and, as shown earlier only has moderate influence on the mean combustion timing; still there is an increase in NO_x with SACI combustion.

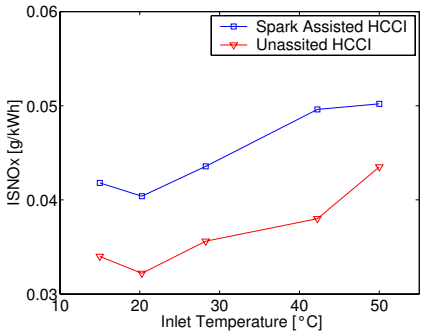

Figure 38. Indicated specific emissions when altering inlet temperature for both spark assisted and unassisted HCCI at 3500 rpm, 2 bar IMEP.

It can be assumed that trapped residuals by NVO HCCI results in a more stratified charge compared to preheated HCCI with EGR mixed with air in the intake system. If the charge is stratified, local areas with high residual rates could reach auto ignition temperature although the average temperature is too low. Ignition could then be expected to take place in the layer between the hot, almost inert, residuals and the colder fresh induced mix of fuel and air. This would then decrease the impact of intake temperature even further. On the other hand, more air/fuel to residual stratification can lead to different combustion behaviour with effects on burn rates, temperature and thus emissions.

6.4 Cycle-to-cycle and cylinder-to-cylinder dependence

The effect of cylinder-to-cylinder deviations and also the cycle-to-cycle coupling and variations are important issues because these effects limit the obtainable working region. The engine relies on trapped hot residuals to attain auto ignition temperature.

Due to the hot residuals the combustion in one cycle can affect the next in a much more extensive way than an SI or HCCI engine run with little or no residual gas.

For HCCI combustion with trapped residuals at low temperature conditions, periodic behavior has been observed [52] i.e. a late burning cycle due to low charge temperature generates high temperature residuals which elevates the charge temperature for the next cycle resulting in early combustion timing generating low charge temperature and so on. One way of analysing this phenomenon is to use calculate a correlation coefficient, as shown in (6.1), between two consecutive cycles. The correlation coefficient (R) is a linear correlation coefficient between two parameters. In this case it is between CA50 of cycle i and CA50 of cycle j. If R = 0 then no correlation is found. If R = -1 then a perfect inverted linear correlation is found which implies that a high value is followed by a low etc.

$$R(i,j) = \frac{C(i,j)}{\sqrt{C(i,i) \times C(j,j)}} \tag{6.1}$$

Figure 39 shows the correlation for the whole sweep in speed along the boundary between SACI and pure HCCI as shown in Figure 27. Between 2000 and 3500rpm some negative correlation can be seen. Especially at 3000rpm the negative correlation for Cylinders 2, 4 and 5 is very high. These cylinders also have relatively high COVimep. Cylinder 3 has, on the other hand, also high COVimep, but a low R, so a high COV does not have to imply a high correlation, but vice versa!

A correlation investigation is also done with an increased cycle separation for a vector containing 100 consecutive measured cycles; this is shown in Figure 40. The figure shows cylinder 5 for the measuring point at 3000rpm with an R of approximately -0.8, which is a strong negative correlation. Here an auto correlation is done for an offset of up to 55 cycles. It is obvious that the largest correlation is for a separation of one cycle, which is the same as shown in Figure 39. For an increased offset in cycles the correlation effect is dampened out, still with an increased negative correlation for every second cycle. Although the combustion timing fluctuates back and forth from one cycle to the next some slower variations in combustion timing due to parameters such as wall temperatures will decrease the correlation. Still a higher correlation is recognized again for a higher cycle separation. This is an indication of a disruption in the cycle-to-cycle behaviour, i.e. the periodic behaviour ceases and starts again, in a repetitive way. It should be noted though, that the correlation for higher cycle separation is overall low.

One reason for the self-extinction of the periodic phenomenon is that when the changes in combustion timing gets so high that partial misfire occurs, the very late combustion timing will no longer increase the charge temperature for the next cycle. Instead the next cycle will also burn late. Here the phenomenon can be extinct or start again in counter phase to the earlier behaviour. If the amplitude gets even higher it will not be self stabilizing, instead of a very late combustion, misfire will occur. If misfire occurs no residuals are present for the next cycle to initiate combustion again.

A cross-correlation between the different cylinders for an increased number of cycles separation is conducted, also looking at CA50. The correlation from one cylinder to another cylinder in the next cycle is negligible. No communications between the cylinders have been observed in terms of combustion timing variation.

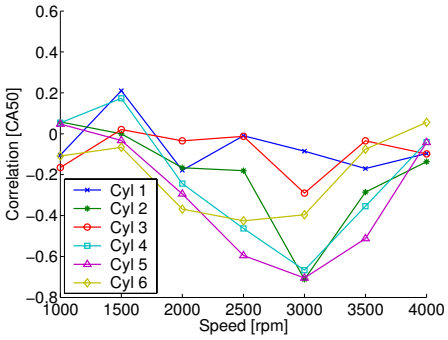

Figure 39. Correlation between cycle n and cycle n+1

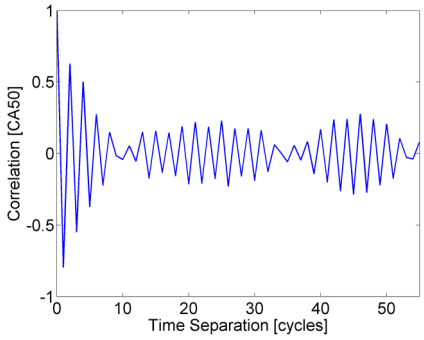

Figure 40. Correlation between cycle n and cycle n+k, k= 1:55

By running SACI it is possible to lower the load compared to what is possible with pure HCCI, but the increased residual rate will eventually limit the usage of spark assistance. When the load is decreased the exhaust temperature and thus the residual temperature goes down, although the amount of residuals is increased. To reach even lower load the effect from the spark needs to increase. To a certain extent it can be compensated for by advancing the spark timing. However, too advanced spark timing will again increase the cycle to cycle variations. The conditions in the vicinity of the spark plug deteriorate due to lower turbulence, gas composition and low temperature. Increased combustion stability and increased low load capability by spark assistance is supported in later work by Xie et al. [54].

At lowest possible load with SACI combustion the correlation R is again investigated. The correlation is shown in Figure 41. The oscillations are increased compared to the higher load shown in Figure 39 for pure HCCI. The oscillation for single cylinders also increases with speed. This is expected as the influence from the spark should be higher at lower speed since the load is higher and thus the residual fraction is lower.
In both correlations the case at 1000 rpm is run in SACI mode. Here it goes from no oscillation tendencies at the higher load case to a clear negative correlation for the lowest possible load. In this case it is cylinder 4 and 6 that oscillate and set the low load limit.

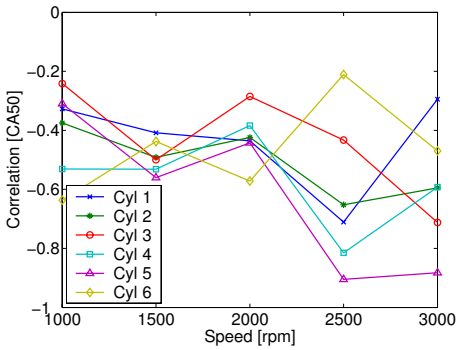

Figure 41. Correlation coefficient [R] for spark assisted HCCI at low load.

6.5 Boundary layer and near wall effects

Up until here most of the discussion has been about the problems with low load characteristics. High load is limited by steep pressure derivatives. Stratification of temperature has been indicated to be one possible way of extending the burn duration in HCCI and thus enable higher load without excessive pressure rise rates. Changing the boundary layer thickness has a direct influence on the thermal stratification inside the cylinder and could be a possible way of affecting the burn duration.

The intention is to thoroughly investigate the combustion boundary layer. It should be noted that this work is conducted under lean conditions without residuals with a CI cylinder head to achieve adequate optical access.

The boundary layer is defined as the area enclosed between the high reacting zone and the less reacting outer part near the combustion chamber surface. It is characterized by a steep decrease in local temperatures due to the comparably low wall temperature.
The main intention is to see how the boundary layer behaves when changing the operating conditions in terms of speed (turbulence), load (equivalence ratio), swirl (mixing) and injection strategy (homogeneity). The boundary layer behaviour is then correlated to the combustion process calculated from heat release data.

For each operating point the chemiluminescence measurement interval reaches from - 10 to 16 CAD ATDC with a resolution of one CAD. For each CAD, 50 images are collected and used both for single cycle analysis and for ensemble averaging. Since only single images can be acquired per cycle, all boundary layer calculations are based on the average of 50 images.

A base case is used as reference. This is run at 2 bar $IMEP_{net}$, PFI and open swirl valve at 1200 rpm. Four different sweeps are made, changing one parameter at a time: load, speed, injection strategy and swirl as shown in Table 3. For all cases combustion timing is kept at 3 CAD ATDC +/- 0.5 CAD.

Table 3. Operation strategies

sweep	swirl valve	inj. strategy	load	speed
			1.0 bar 1.5 bar	700 RPM 900 RPM
base case	0% (open)	PFI	2.0 bar	1200 RPM
	25 %	DI -180°	2.5 bar	1500 RPM
	50 %	DI -130°	3.0 bar	
	75 %	DI -90°		
	100 % (fully closed)	DI -50°		
		DI -30°		

The correlation between rate of heat release and chemiluminescence intensity is of great importance for accepting the proposition that chemiluminescence intensity is a measure of global heat release for HCCI combustion. Although this proposition is commonly accepted and has been reported earlier [36] it is first verified before further conclusions are drawn. Figure 42 shows both the rate of heat release and the corresponding chemiluminescence intensity. A deeper analysis shows a very high correlation as can be seen in Figure 43 where the averaged intensity is compared with heat release rate showing a coefficient of determination, R^2, of 98,69 %. R^2 is the

square of the correlation coefficient and denotes the strength of the linear relation between chemiluminescence intensity and RoHR or, x and y as shown in (6.2).

$$R^2 = \frac{\left[\sum_{i=1}^{n}(x_i - \bar{x})\cdot(y_i - \bar{y})\right]^2}{\sum_{i=1}^{n}(x_i - \bar{x})^2 \cdot \sum_{i=1}^{n}(y_i - \bar{y})^2} \qquad (6.2)$$

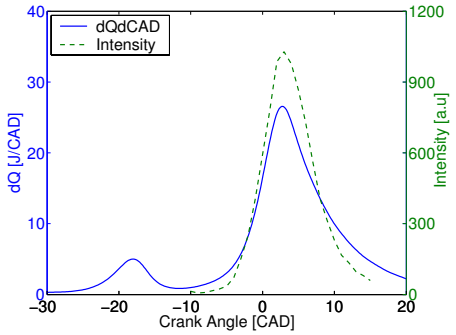

Figure 42. Rate of heat release and maximum chemiluminescence intensity for the base case

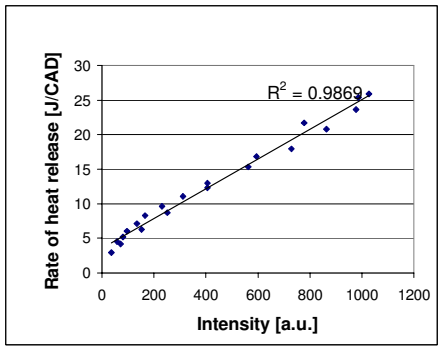

Figure 43. Variation of image average maximum intensity versus rate of heat release for the base case.

The steep temperature gradient in the boundary layer is indicated by a fast decrease in chemiluminescence intensity towards the combustion chamber surface. Therefore chemiluminescence imaging can be used to calculate the boundary layer behaviour.
For these calculations the boundary layer is defined as the area from 15 to 85 % of maximum intensity at each crank angle. These intensities are calculated from the mean images of 50 cycles taken through the quartz liner. One such image is shown in Figure 44.

Since the boundary layer calculations are based on averaged information it is of great interest to have a look at the cycle to cycle variations. Figure 46 shows the variation coefficient for single images of the base case. What is obvious is the high cycle to cycle variation at the start of main combustion, especially where the boundary layer is situated. Comparing to the rate of heat release in Figure 42 it can be seen that for increasing burn rate the variations from cycle to cycle decrease rapidly, becoming low during the main combustion. For late crank angles the cycle to cycle variations increase slightly again, now mainly at the area of the main combustion while the boundary layer shows less variations.

The change in combustion duration for the different sweeps can be seen in Figure 45. For later injection, increased load and increased speed, the burn duration goes down. Yet for the swirl case no effect in any direction can be seen. Since both later direct injection and higher load will give zones of richer mixture these are expected to burn faster. For increased engine speed heat losses are expected to decrease, thus enhancing the burn rate. Here constant burn duration in CAD means shorter burn duration in time. For the 1500 rpm case an even faster burn duration is seen, decreased also in CAD.

The closing of one of the intake ports changes the swirl number from 2 to 2.6 for fully closed port and should then also increase the turbulence. Geometry generated turbulence by modifying the piston crown has shown longer burn duration in earlier studies [61, 62]. A later simulation suggested that the main reason for the increased burn duration was due to changes in heat transfer and thermal stratification in the piston bowl [63, 64]. However no such behaviour can be seen for turbulence generated by the intake flow in a pancake shaped combustion chamber. The pancake combustion chamber simply doesn't allow the same conditions for temperature stratification as the bowl. Another reason for not seeing any change in burn duration can be that at low speed the generated turbulence variation is too small. Also the effect of turbulence should increase for increased fuel stratification, with more fuel rich zones. If the PFI charge is well mixed this effect should be small, so the effect of increased swirl should have greater impact on DI HCCI.

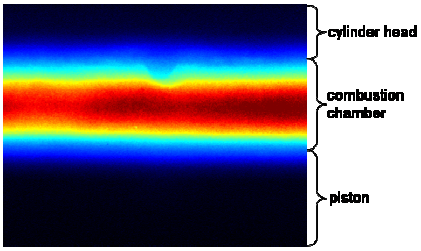

Figure 44. Averaged horizontal view of combustion through the quartz liner with the injector clearly visible in the center

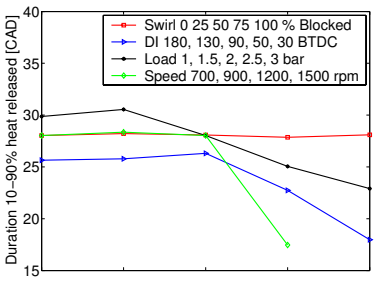

Figure 45. 10 to 90 percent burnt duration for the different sweeps. Different conditions from left to right side of the figure.

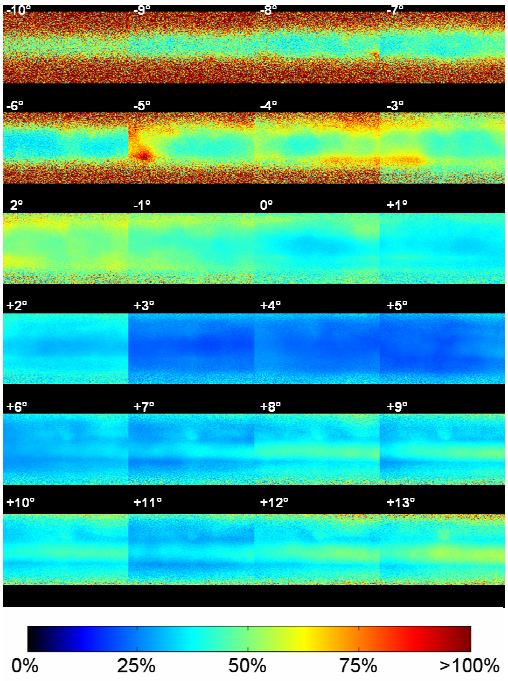

Figure 46. Coefficient of variation of chemiluminescence intensity for single images at each CAD (ATDC) for one of the base cases.

Although it is not possible to see a difference in burn duration due to turbulence the boundary layer thickness is still affected. Figure 47 shows the change in boundary layer thickness over crank angle for increasingly blocked intake port. During the early combustion the boundary layer thickness actually decreases with increased swirl, and then in the later part it instead increases. The over all increase in boundary layer thickness for very early CADs can be disregarded since the overall signal level is very low and no clear conclusions can be drawn.

What can be seen though is a constant increase in boundary layer thickness during combustion. A thicker boundary layer is slightly unexpected since the reacting core is expected to increase the temperature closer to the walls and increase the reaction rate of the inner part of the boundary layer. This is actually also the case. During combustion the chemiluminescence intensity increases closer to the combustion chamber walls above the 15 % level set as the lower level for the boundary layer calculation. The intensity level of the core is not uniform so although the reaction rate increases from the centre towards the piston and fire deck the chemiluminescence intensity still does not reach above the upper level for the boundary layer definition, thus the boundary layer is seen to increase during combustion.

For the DI sweep and late injection, for the load sweep at high load and for the speed sweep at high speed all show shorter burn duration and a corresponding thinner boundary layer. A correlation between boundary layer thickness and the burn duration can be found.

For increasing speed a slight decrease in boundary layer thickness can be seen, from 700 to 1500 rpm, shown in Figure 48. For the 1500 rpm case a strange phenomenon can be seen during the late combustion. A sharp increase in boundary layer thickness seams to occur. This is however not completely true. Figure 49 shows the intensity distribution from the cylinder head to the piston crown for different CADs for the 1500 rpm case. It shows a plateau at an intensity level close to what is used to define the boundary layer. This can be explained by the later combustion moving closer to the piston as the boundary zone is heated simultaneously as the core of the charge is already partially oxidized with a decreasing reaction rate. The effect is even more pronounced when doing tests with high levels of EGR as shown in Figure 50.

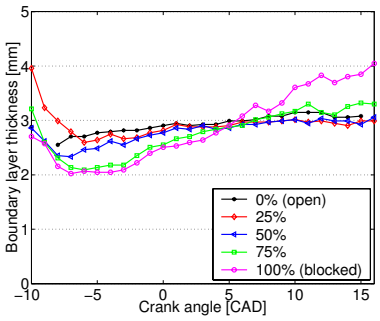

Figure 47. Boundary layer thickness for swirl sweep.

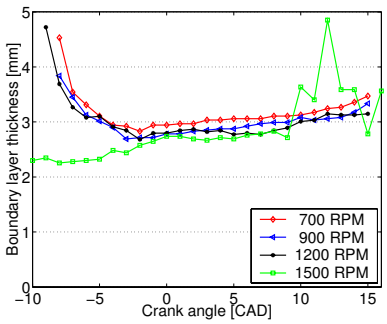

Figure 48. Boundary layer thickness for speed sweep.

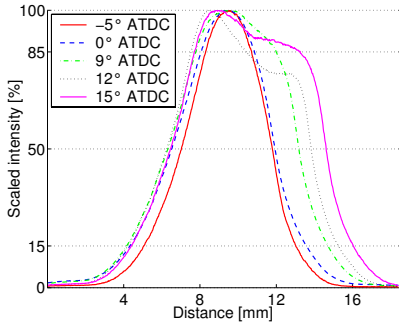

Figure 49. Scaled intensity profile for 1500rpm case from speed sweep at different CADs. Cylinder head located at ~4 mm and piston at ~13 at TDC.

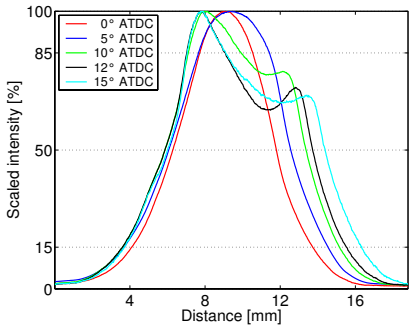

Figure 50. Scaled intensity profile for 50 % EGR at different CADs. Cylinder head located at ~4 mm and piston at ~13 at TDC.

6.6 Flame expansion with residuals

The first published results of a stabilising effect on NVO HCCI combustion with spark assistance were published by Koopmans et al [55]. Later experiments have shown possibility to also affect combustion timing [56, 57]. The influence of spark assistance has been shown here in both Papers I and II where it was used to enhance the low load capability. Urushihara et al showed the potential of also increasing the high load limit [58], the combustion mode is here referred to as spark-ignited compression ignition (SI-CI) combustion.

The mechanism behind SACI combustion at lower loads has been discussed since the total dilution by residuals and air means operation past the limit to where it is possible to use flame propagation in a traditional SI engine. In [59] it was suggested that local hot spots were formed rather than flame propagation. Hyvönen et al showed combustion behaviour similar to what was found for advanced spark timing at high NVO shown in Figure 35 when doing sweeps from SI to HCCI in an all metal engine. Hyvönen defined the initial slow heat release (ISHR) according to (6.3). This was done with the intention of separating the HCCI combustion from the slower reactions related to the spark discharge. Q_{max} is the total accumulated HR while $Q_{threshold}$ is the amount of HR when reactions are considered to shift from ISHR to the faster RoHR characteristic for HCCI combustion.

$$ISHR = \frac{Q_{threshold}}{Q_{\max}} \cdot 100\,[\%] \qquad (6.3)$$

In this work the ISHR is calculated from pressure information using the 2nd derivative of the RoHR. The calculated threshold therefore indicates the point where the combustion speed changes the most. This is done by fitting a moving first order polynomial of finite length to the derivative of RoHR. Using the polynomial fit noise can be excluded to get more reliable results. Figure 51 shows the result for a single cycle with SACI combustion at an NVO of 160 CAD. In this case the calculated threshold will give an estimate of 30 % ISHR.

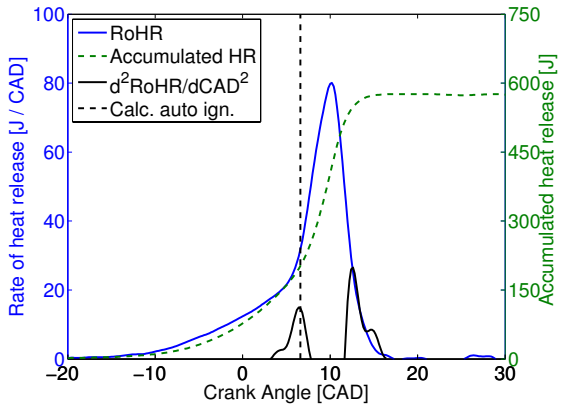

Figure 51. accumulated HR, RoHR and calculated break point using second derivative of RoHR for SACI combustion.

To increase the knowledge of the double mode combustion, optical experiments were conducted. The effect of spark assistance by simultaneous pressure measurement and high speed imaging of the natural chemiluminescence from combustion is studied. A mean flame expansion speed, u_f, is calculated for the ISHR from the two dimensional chemiluminescence images according to (6.4). The area, A, of the flame is calculated for each image, thus the area growth per time step can be calculated. Division by the flame perimeter length, L, allows calculation of a mean speed. Using the actual circumference has the drawback that the length will depend on how well it is resolved. Instead the assumption of the flame growing as a sphere is used according to Heywood [4], or in this two dimensional case as a circle. Thus the perimeter is calculated from a circle with the area of the actual flame. With this information the mean expansion speed, u_f, can be calculated and used to interpret the influence on the flame when changing the in-cylinder conditions. It should be noted that the mean expansion speed of the flame front does not take into account temperature and volume, hence density changes between the burnt and unburned zones and is therefore higher then the actual flame speed.

$$u_f = \frac{dA/dt}{L} \qquad 6.4$$

When increasing the NVO, thus increasing the residual dilution the flame expansion speed decreases as shown in Figure 52. It can be seen that the flame expansion speed for an NVO of 200 CAD close to TDC reaches almost 2/3 of that of the case with 40 CAD NVO. The residuals have two different effects on the flame in this case. As the charge is stoichiometric, the residuals acts as an inert dilution lowering the heating value per unit mass and thereby the adiabatic flame temperature. On the other hand, the residuals are used to raise the initial charge temperature thus lowering the heat transfer from the flame to the surrounding fluid. The increased temperature of the unburned gas will increase the laminar flame speed. [60]. Generally flame development shows a slight negative dependence on pressure, this will act to lower flame speed for increased NVO when the engine is less throttled.

The results in Figure 52 are based on approximately 20 single cycles. Looking at the case of 200 CAD NVO in Figure 53 shows the cycle to cycle variation for the flame

expansion. This illustrates the downside of introducing SI combustion in an HCCI system with the intention of fast and stable combustion. However, despite the cycle to cycle variation in the SI flame behaviour, spark assistance has in the previous section shown stabilising effects on cycle to cycle variations related to the residuals. Furthermore, despite the variations in flame expansion shown in Figure 53 the combustion stability is still excellent with COV_{imep} below 1.4 %. One explanation for this could be cycle to cycle variations in trapped residual fraction. Lower amount of residuals means faster flame expansion, but lower average charge temperature, thus increased amount of heat released from the SI combustion to keep combustion timing and load.

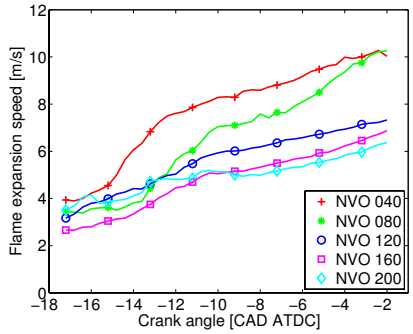

Figure 52. Mean flame expansion speed as a function of CAD for increased NVO.

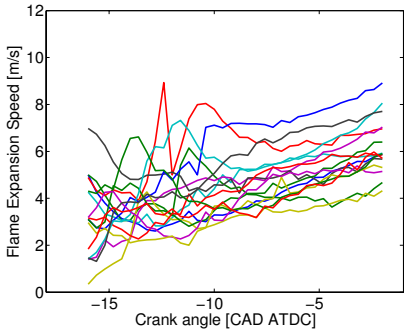

Figure 53. Single cycle flame expansion speeds as a function of CAD at a NVO of 200 CAD.

By increasing the NVO to 215 CAD and thereby also further raising the amount of residuals the engine is run at 2.4 bar $IMEP_{net}$ at stoichiometric conditions. At this load the charge temperature rise due to the residuals is not enough to reach auto ignition without spark assistance. By making a sweep in spark timing it is possible to analyse the interaction between the SI and the subsequent HCCI combustion is possible to analyse. The flame expansion can be viewed in Figure 54. Compared to the previous sweep in NVO the ignition delay is here increased when the load is lowered. As the spark timing is advanced the ignition delay is further increased. In this case ignition delay is discussed in terms of the separation in CAD from spark discharge until a flame can be detected by the camera. As the spark timing is advanced the in cylinder conditions in the vicinity of the spark plug deteriorate with respect to flame propagation; both temperature and turbulence are lowered. In case of very early spark timing the turbulence levels and temperature conditions are thought to prohibit flame propagation. One more unknown factor is how well the fresh charge of fuel and air is mixed with the trapped residuals. If the main tumble flow in the cylinder consists of a slightly stratified charge it is possible that the mixture at the spark plug position changes in both equivalence ratio and temperature during the compression, affecting the ignitability of the charge. Still by advancing the spark timing the flame expansion is also advanced and closer to TDC similar mean expansion speeds are reached. The response in combustion timing is illustrated in Figure 55. CA50 is advanced more than 7 CAD when changing spark timing from - 30 to - 55 CAD ATDC. The calculated threshold for the ISHR calculations follows in a similar way, thus the auto ignition timing is also advanced. This is achieved while maintaining combustion stability until a spark timing is advanced further to - 60 CAD ATDC where eventually misfire occurs.

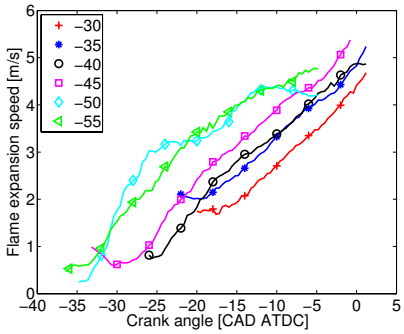

Figure 54. Mean flame expansion speed for advanced spark timing at 215 CAD NVO.

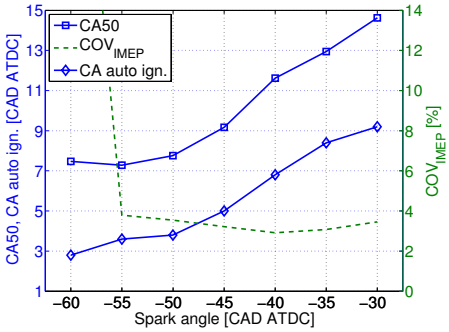

Figure 55. Combustion timing, calculated auto ignition timing and COV_{imep}.

An increased amount of ISHR is expected to be needed to advance auto ignition, this is also the case for the spark timing sweep discussed above. With residual HCCI this is further enhanced since the exhaust temperature is lowered with earlier end of combustion thus lower charge temperature. These effects are slightly counteracted by the early heat release from the flame that increases the compression work and thus increases the temperature at TDC. For combustion timings close to TDC the opposite trend could be seen in the optical engine, earlier combustion timing showed less ISHR. The early combustion phasing means lower residual temperature, on the other hand the combustion chamber wall temperatures are increasing. Since the optical engine is run at cold conditions not to stress the optical components the heat losses are expected to be higher and the residual temperature lower and therefore having less effect of charge temperature for the consecutive cycle. Further, with early end of combustion the expansion ratio is not expected to change much for further advancement of combustion, therefore the effect on exhaust and residual temperature is lower.

Figure 56 and Figure 57 both show selected frames from single cycle high speed chemiluminescence videos. In both cases the plasma from spark ignition can be seen followed by flame propagation and the subsequent auto ignition closer to the perimeter of the visible part of the combustion chamber. When the spark timing is advanced from - 19 to - 21 CAD ATDC it can be seen that the amount of fuel consumed before auto-ignition is significantly lowered. By looking at the images for these individual cycles the first sign of auto-ignition in Figure 56 is after 20% heat released by the flame compared to less than 4 % in Figure 57 with earlier spark timing. Even further advancement of the spark can then actually result in full HCCI with early auto ignition. To control combustion timing residual rate or valve strategy must then be utilized. Later phasing will again demand SACI combustion. In these two single cycle sequences, each image is scaled from zero to maximum intensity to be able to see the early flame with lower intensity. In order not to lose information of RoHR from intensity the calculated amount of HR from pressure information is added above each image.

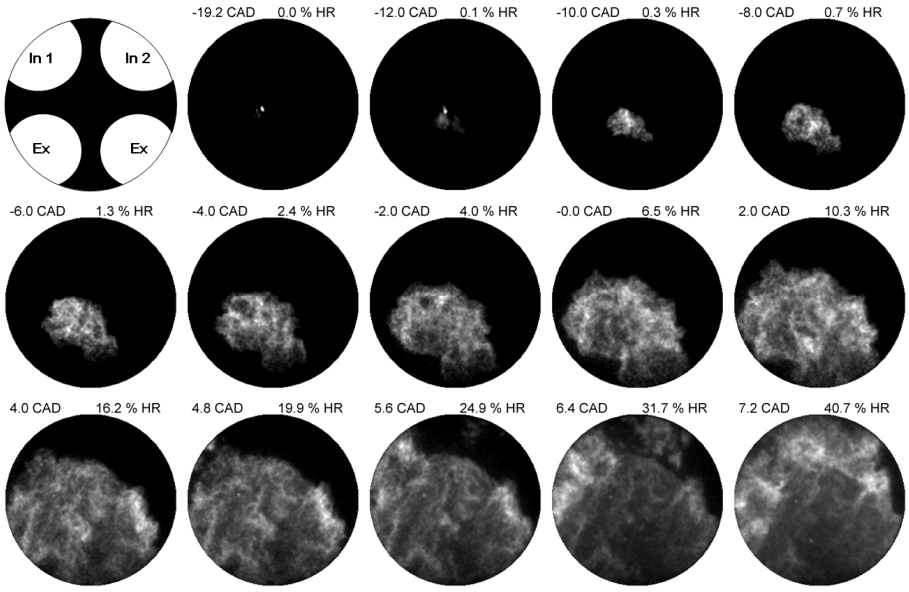

Figure 56. SACI combustion, 200 CAD NVO, spark timing - 19 CAD ATDC. First image show valve locations.

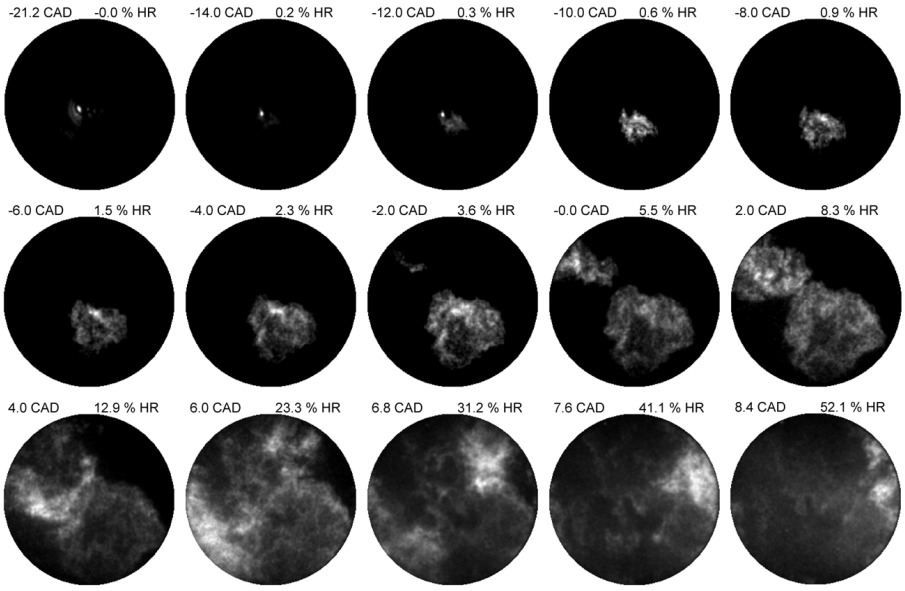

Figure 57. SACI combustion, 200 CAD NVO, spark timing – 21 CAD ATDC

For the ISHR calculations a threshold is calculated to separate the two modes of SACI combustion, the slow reactions that were seen to be related to SI flame propagation and the higher reaction rates related to HCCI combustion. To further see the differences between the modes the visible area showing chemiluminescence is plotted as a function of CAD in Figure 58. The smooth S-shape of the SI combustion is distinctively different to the SACI combustion showing a slower growth of the flame followed by the faster auto ignition. Also for the pure HCCI case an ISHR can be

seen. Since the chemical kinetics are temperature dependent the auto ignition is expected to be slower. When running HCCI some cycles showed a very stratified auto ignition and combustion with a flame front like behaviour. Similar calculations as for the early flame was conducted but now with the reaction front approximated to a straight line instead of a circle. The resulting front spreading speed is shown for three individual cycles in Figure 59. Directly after ignition a continuous slow reaction rate can be detected by a constant low spreading speed. For Cycle 2 the speed is well above what could be seen with SACI combustion, but for Cycle 3 the phenomena is present for a duration of approximately 10 CAD with speeds resembling that of flame expansion. One suggestion is that Cycle 3 exhibits surface ignition resulting in actual flame propagation. It can be concluded that the ISHR calculations can be biased by slow reaction not originating from the spark plug. As the reaction rate increases spreading speeds of up to110 m/s can be noted.

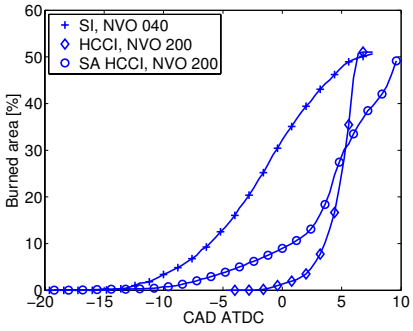

Figure 58. Reacting area as a function of CAD.

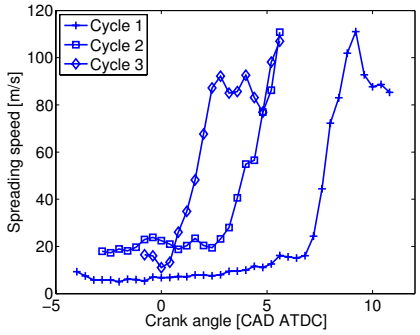

Figure 59. Combustion front spreading speed

6.7 Increased turbulence by swirl

To increase the tolerance for dilution with SACI combustion the effect of increased turbulence is investigated. For the SI engine the flame speed is highly dependent on the turbulence level. By increasing turbulence the lean tolerance is increased, or for a given equivalence ratio the burn duration can be decreased. For HCCI combustion the effect is not as evident. Generally HCCI combustion is assumed to be kinetically controlled, thus the effect of turbulence should be small. The results from Paper III, discussed in Section 6.5 show no significant change in burn duration when the swirl level is changed in a fixed geometry (pancake). Early HCCI research showed slower combustion when using combustion chambers witch enhanced turbulence [61, 62] However the turbulence effect was not possible to separate from the geometry effect due to different combustion chambers. Aceves et al showed, using CFD and multizone chemical kinetics models, that the longer burn duration could be explained by increased wall heat transfer, mainly due to the different geometries [63, 64]. Later optical experiments with resembling geometries also show increased combustion duration for the supposed higher turbulence combustion chamber [65]. Simultaneous Large Eddy Simulations (LES) support the slower combustion and relates it to temperature stratifications due to heat transfer from optical components with higher surface temperatures, possibly in combination with stratification of residual gases [71]. It is shown by the LES simulations that the later combustion chambers have very small deviations in turbulence generation. Higher surface temperatures of optical parts on the combustion chamber walls giving temperature stratification in combination with large squish regions resulting in quenching are found to be the main sources of

the slower combustion. Subsequent metal engine experiments with modified squish and piston material supports the LES conclusions [66] .

Prior SI combustion studies with the combustion chamber used in this work have shown great improvement in lean burn capability with maintained combustion stability at lean conditions [33]. This has been accomplished by both inlet valve deactivation and late IVC. The deactivated inlet valve changed the tumbling in-cylinder flow to include a swirling motion with increased turbulence intensity and thus faster burn rate. The increased turbulence close to compression TDC can be seen by comparing Figure 60 with normal valve strategy and Figure 61 with inlet valve deactivation. Here the valve strategy is enabled using a pneumatic valve train compared to traditional camshaft for the previous experiment.

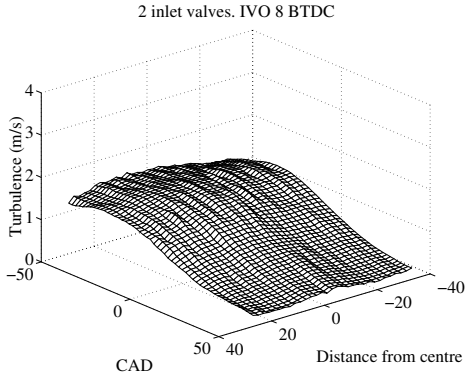

Figure 60. Turbulence for two valve strategy [33].

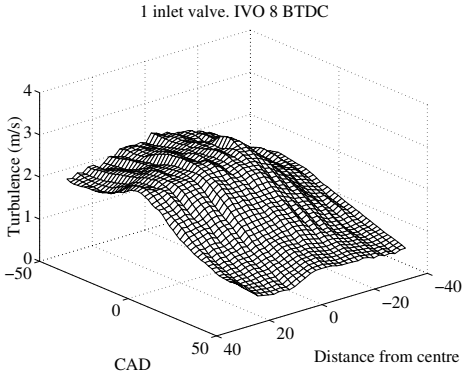

Figure 61 Turbulence for inlet valve deactivation [33].

Prior studies in a truck size SI engine have shown a strong correlation between turbulence in the vicinity of the spark plug and the timing of the early HR. This was performed with the engine running in skip fire mode therefore the influence of burnt gases could be excluded. Correlation coefficients between the position of 0.5 % HR and the turbulence of up to approximately 0.7 were reported for lean conditions [40].

In the present study the influence of turbulence is studied by measuring the fluid flow at different positions approximately 1 mm upstream of the mean flow from the spark gap as shown in Figure 62. The engine is run un-throttled at a NVO of 200 CAD under stoichiometric conditions. To interpret the relation between turbulence and early HR a linear correlation coefficient is used according to (6.1).

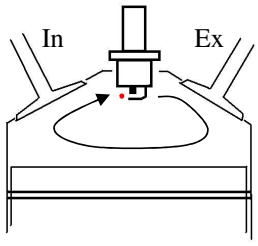

Figure 62. Schematic of position for LDV measurements with main flow direction around spark plug.

The spark plug is mounted with the side electrode at the exhaust side making it possible to measure the fluid motion more undisturbed, this can be seen by looking at Figure 63. The mean fluid velocity from the intake to the exhaust side due to the bulk tumble motion is greater than 4 m/s at 40 CAD BTDC and then decays as the piston slows down closer to TDC. The same trend is visible upwards in the vertical direction just below the spark plug as shown in Figure 64. One can also see the maintained turbulence levels as the main flow velocity decays. Spark timing is set to -19 CAD ATDC. Velocity and turbulence information is only presented until 5 CAD after ignition, since the seeded polystyrene latex is burned and for later CADs the amount of data is limited.

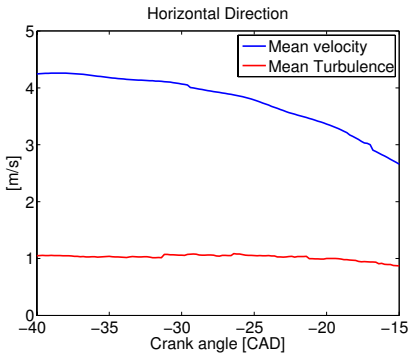

Figure 63. Horizontal mean velocity towards the exhaust side and mean turbulence.

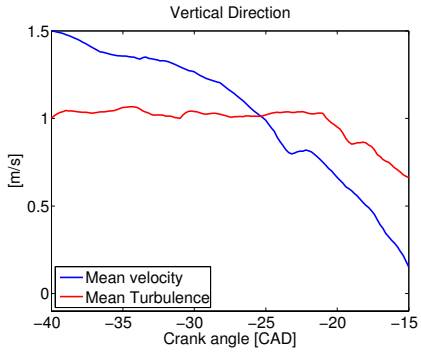

Figure 64. Vertical upwards mean velocity and corresponding mean turbulence.

The nature of the correlation is presented in Figure 65. This is at the crank angle of spark discharge shown by the black dashed line in Figure 66 for the measurement slightly offset from the spark plug compared to a perfect tumble flow (x = -2 mm). When fitting a second order polynomial to the turbulence scatter an earlier position of CA 1 % burned is seen for increased turbulence levels. The correlation coefficient at this position is 0.39. Although a low correlation the behaviour is consistent if looking at both different crank angles and measurement points as seen in Figure 66. At even higher turbulence levels the effect is the opposite and the flame growth is delayed (Figure 65). This effect is however not as pronounced for all measurement points. The retarded flame growth for very high turbulence levels can be due to increased heat losses when the early flame is too heavily wrinkled with high area to volume ratio, also the whole flame kernel can be forced against the spark plug with excessive heat losses as a result.

It can be concluded that the turbulence level plays an important role for the early flame propagation in SACI combustion. The correlation is much lower compared to the correlation found for an SI engine without residuals. The lower correlation can be explained by the high residual content rendering dilution as well as variations in charge homogeneities and cycle to cycle deviations in temperature. The turbulence effect on flame propagation is however still significant and further shows that it is actual flame propagation followed by auto ignition.

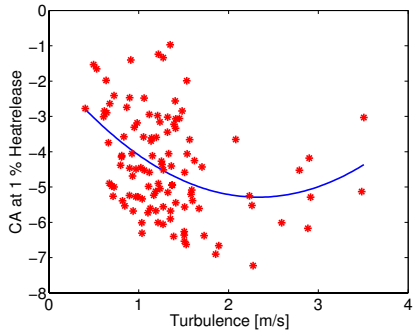

Figure 65. Correlation between CA at 1 % heat released and turbulence at -20 CAD ATDC, corr. coeff = 0.39.

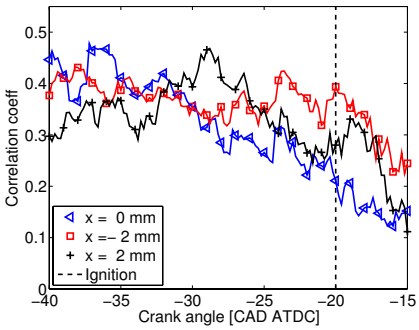

Figure 66. Correlation coefficient of relation between timing of CA 1 % heat released and turbulence w.r.t. CAD.

To further quantify the effect on HRR by turbulence, imaging of the early flame development was preformed. The initial intention was to use the Schlieren technique since it is suitable for usage in combination with LDV. The laser beams from the LDV measurements do not interfere with the Schlieren image as shown in Figure 22. Unfortunately the increased amount of residuals and the following increase in temperature for NVO HCCI lowers the Schlieren image quality. Disturbing temperature gradients between the residuals and the fresh gas are introduced simultaneously as the temperature difference between the diluted flame and the surrounding fluid is decreased. Instead chemiluminescence measurements are performed. Figure 67 and Figure 68 show images taken through the pent-roof quartz windows with the two techniques; note that the Schlieren image is taken with a lower residual rate. Since chemiluminescence imaging does not require pass through optical access, images are instead acquired through the piston glass from below enabling a larger optical access although not simultaneous LDV and chemiluminescence measurements.

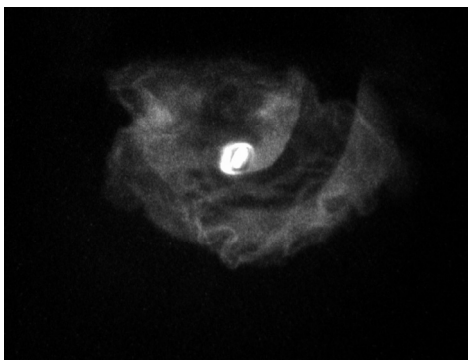

Figure 67. Chemiluminescence imaging of initial flame growth around the spark plug at SACI combustion, 200 CAD NVO

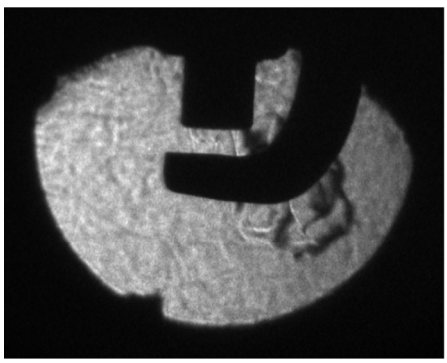

Figure 68. Schlieren imaging of the initial flame growth around the spark plug at SI conditions, 40 CAD NVO

To clarify the fluid flow effect on the early flame high speed chemiluminescence videos are captured for the case using both intake ports, called the reference case. The intake valves are then deactivated one at a time and finally the test is concluded by

recording a second reference case as a proof of stable operating conditions. The corresponding calculated mean flame expansion speeds are presented in Figure 69. The increased turbulence by valve deactivation causes the flame expansion speed to increase to almost the same levels as seen for an NVO of only 40 CAD. Since the laminar flame speed is highly dependent on equivalence ratio it could be suggested that valve deactivation would decrease the volumetric efficiency thus reduce lambda which in turn would increase the laminar flame speed. But the intake flow rate at the selected operating conditions is relatively low and the increased flow resistance only caused a drop in lambda from 1.01 to 0.99 for the same fuel flow rate.

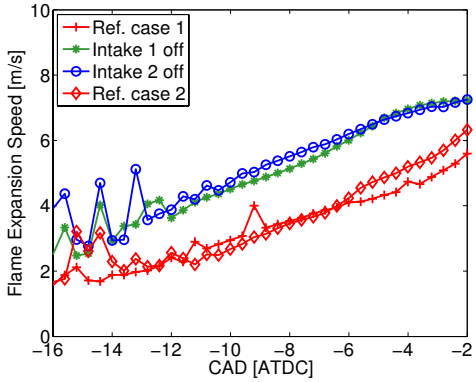

Figure 69. Mean flame expansion speed for different valve strategies at a NVO of 202 CAD, stoichiometric conditions.

Since the SI flame is used to trigger auto ignition it is of utmost interest to see how the increased turbulence and faster flame propagation affects the subsequent HCCI combustion. Figure 70 shows increased combustion stability when the conditions for flame propagation are improved by increased turbulence. Less encouraging are the results on CA50 presented in Figure 71; as the turbulence is increased combustion seems to be slightly retarded. The faster flame expansion will increase the temperature earlier in the cycle which should advance ignition timing.

The timing for the breakpoint of the calculated ISHR is inconclusive but can be said to be slightly retarded when increasing the turbulence as shown in Figure 72, although the amount of ISHR is increased as shown in Figure 73. The latter is supported by the increased mean expansion speed seen in Figure 69. For increased turbulence flame propagation starts earlier and at a given CAD the amount of HR is higher compared to the case with low turbulence. The conclusion is then that for the cases with higher turbulence more heat must be added to reach auto ignition. Although the calculated auto ignition occurs almost at the same CAD, the burn duration of the HCCI combustion as show in Figure 74 is increased The HCCI burn duration is defined here as the crank angle interval from calculated auto ignition to CA90. Since the larger part of the charge is reacting in HCCI mode, the longer HCCI combustion duration will also delay CA50. It should further be noted that the HCCI combustion duration is prolonged although the amount of fuel burnt in HCCI mode is less for the high turbulence cases.

The reason for the delay in auto ignition with increased swirl and thus turbulence is thought to be due to the increased mixing between the residual gases and fresh charge lowering the mean temperature of the charge and thereby delaying auto ignition. The stratification between residuals and fresh charge has been reported to have a significant effect [67].

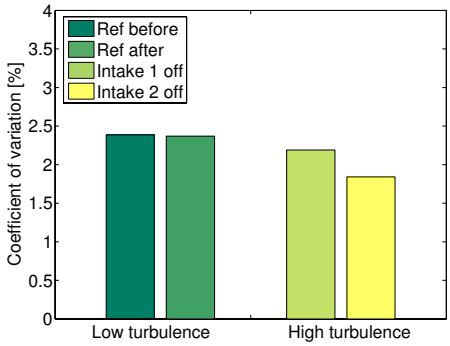

Figure 70. Coefficient of variation when changing turbulence by valve deactivation.

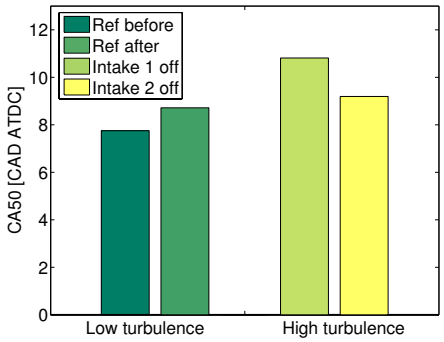

Figure 71. Combustion timing when changing turbulence by valve deactivation.

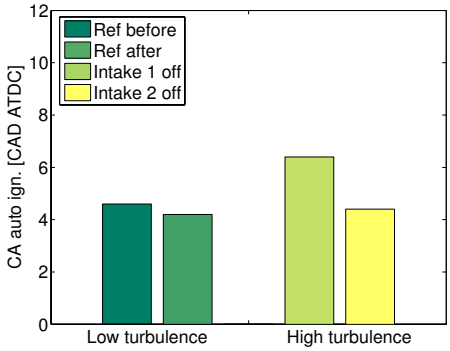

Figure 72. Calculated CAD for auto ignition.

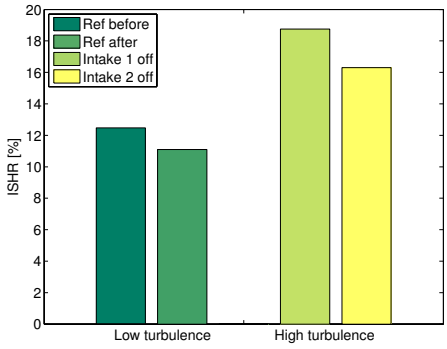

Figure 73. Calculated amount of ISHR when changing turbulence by valve deactivation.

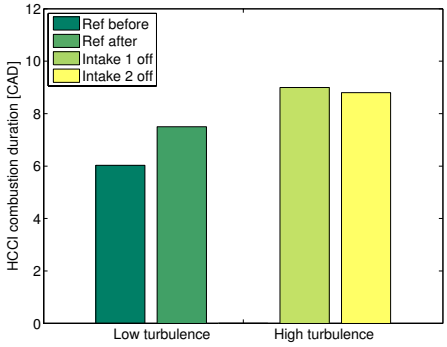

Figure 74. Calculated HCCI combustion duration when changing turbulence by valve deactivation.

The increased turbulence will increase the fluid to wall interaction which in turn leads to increased heat transfer with lowered in-cylinder temperature and thus lower reaction rate. This can be seen as especially important for this particular optical engine since it is run with rather low coolant temperature and the effect of coolant

temperature is strong [70]. On the other hand temperature stratification which can be expected to be stronger for lower turbulence has been reported to slow down reaction rate [68, 69]. The strongest temperature inhomogeneities in an NVO HCCI engines are expected to be between hot residuals and colder fresh charge. When running stoichiometric the residuals can be seen as inert and therefore non-reacting whereas the richer zones are expected to be colder. Therefore the effect of temperature stratifications will be lower compared to a lean burn HCCI engine with temperature stratifications.

6.8 Stratification

To further expand the operating regime for HCCI, fuel stratification has been suggested. Effects such as longer burn duration and thus slower RoHR have been reported for fuels that exhibit LTR [72 - 75]. This enables higher possible load in HCCI mode due to a staged auto ignition with a resulting lower RoHR. Dec et al reported a significant effect of fuel stratification with fuels exhibiting LTR reactions whereas the effect on single stage ignition fuels was more modest [76]. For fuels exhibiting single stage ignition, fuel stratification has been used to increase low load combustion efficiency by reducing over-lean zones [78].

In this work different ways of achieving fuel stratification are tested. The focus is on how stratification affects combustion and then especially the interaction between the flame development and auto ignition of an engine run in SACI mode. This is performed with a fuel exhibiting single stage ignition which is the common behaviour of the high octane fuels when used in the SI engine environment.

Fuel PLIF is a useful technique for investigating fuel distribution as well as ignition behaviour [77]. Earlier studies have been conducted for HCCI combustion with lean burn and preheating to reach auto ignition temperatures [78]. Acetone has successfully been used as a fuel tracer in combination with ethanol as fuel in earlier work by Seyfried et al [79]. Ethanol is used as fuel also in this work due to tracer performance in combination with the fact that ethanol is advancing as a non-fossil fuel on the automotive market.

The success in achieving fuel stratification is observed by PLIF imaging. The captured PLIF images are studied by numerically calculating a homogeneity index. This process requires each evaluated image to be digitalized and the charge is considered homogeneous if the pixels containing no signal are randomly distributed throughout this digitized image. To evaluate this, the number of shifts between no signal and signal is calculated when traversing the image in rows and columns. For comparison to the digitized image, a homogeneous image is generated, with the same surface fraction covered with signal as the original image. The number of shifts from the digitized image is then divided by the number of shifts found in the randomly generated one, giving the homogeneity index for the original image. By using this approach, an image with a homogeneous, random spatial distribution of the fuel will result in a high index value (close to unity), whereas a non-homogeneous distribution will result in a low value. An example of the result is given in Figure 75, showing both the digitized image (to the left) and the corresponding randomly generated image (to the right). Indicated below both images is the number of shifts, providing a

measure of the homogeneity (also indicated) of the charge distribution. More details about the homogeneity calculations can be found in Paper VI and in [80, 81].

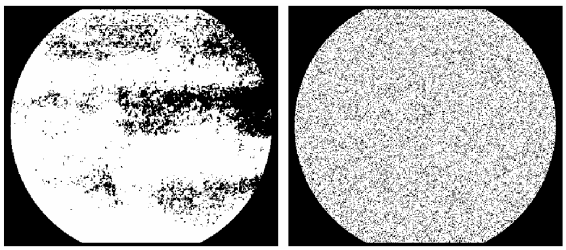

Figure 75. Example of the homogeneity index procedure.

The PLIF images are a measure of the input variable stratification, or heterogeneity and the output is the combustion performance monitored by cylinder pressure. Both PLIF and HR can give a mean value for the in-cylinder conditions, however the PLIF signal is based on the visible centre part of the combustion chamber that is covered by the laser arc, i.e. approximately 50 % of the total area. This can distort interpretation of the results if the fuel is unevenly distributed between the visible and the outer parts of the combustion chamber.

6.8.1 Port fuel injection

A previous study [74] showed a large scale stratification effect of the fuel using PLIF imaging, but no significant effects on combustion timing or RoHR. In that study a tumble flow combustion chamber was used in combination with fuels exhibiting both single and two stage ignition. Here, a swirling combustion system is used. Hence more communication is expected between the flows of the two intake ports. Since the mixing time for the fuel rich and the pure air flow is long, the charge is expected to either reach the same homogeneity as that of PFI in both ports or have more small scale heterogeneity. This differs compared to the large scale stratification effect that can be achieved when using a tumble flow.

Tests are conducted with fuel injection in both intake ports and then with deactivation of one injector and increased injection duration of the other to keep the same fuel mass to the engine. The engine is run at a load of approximately 2.7 bar IMEPnet and lambda 1.4 with residual dilution to come close to auto ignition. Spark timing is kept at -40 CAD ATDC.

Figure 76 shows the homogeneity indices for the three different PFI strategies that are analyzed. The homogeneity values represent the conditions for the early SI flame in the combustion chamber. The figure also contains the 95% confidence levels for the mean values. The injection strategy that uses both ports can be seen to give a more homogeneous fuel distribution compared to the cases where all the fuel is delivered through one port.

Combustion timing in terms of CA50 is kept unchanged without the need to moderate residual rate. Start of combustion in terms of CA10 remains unchanged while end of combustion is significantly retarded as shown in Figure 77 for a less homogeneous charge. The single point injection cases have much longer burn duration.

A slightly increased amount of fuel was injected for the double port injection. The increased fuel mass is expected to increase reaction rate and thus, decrease combustion duration. However the effect of the load change is not expected to be as great as the changes seen for a less homogeneous charge with single port injection. Also the longer burn duration is in agreement with the increased stratification shown by the homogeneity calculations. An explanation to the unchanged timing for start of combustion can be the usage of spark assistance. The local deviation in equivalence ratio at the spark plug position rather than richer conditions will keep the average flame development unaffected of the stratification.

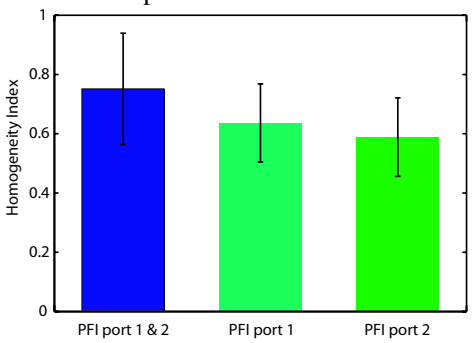

Figure 76. Homogeneity index for different PFI strategies. The bars indicate the 95% confidence interval for the mean values.

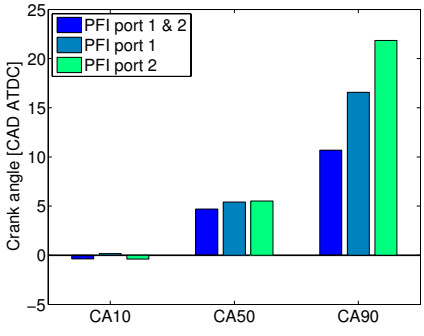

Figure 77. Combustion timing for PFI SACI combustion with port fuel stratification.

6.8.2 Combined PFI and DI

By applying DI in combination with PFI the level of stratification can be enhanced. The combined injection strategy is visualized in Figure 78. To the left the combustion chamber is shown from below. The centre mounted fuel injector is situated in such a way that one of the fuel sprays passes in the vicinity of the spark plug as seen to the right in the corresponding PLIF image. The homogenous fluorescence from the port injected fuel can be seen in the background. The intention was to create charge stratification simultaneously with a more fuel rich zone created by the tail of the fuel spray around the spark plug. To decrease the drag of the spray in the vicinity of the spark plug the injection pressure was decreased and set to 130 bars.

The result of the homogeneity calculations for combined PFI and DI at 70 CAD BTDC is shown in Figure 79. The calculations are performed at 40 CAD BTDC, which coincides with the spark timing. As the amount of DI is increased an even stronger decrease in the homogeneity index could be expected, however a large part of the fuel is transported outside the visible part of the combustion chamber.

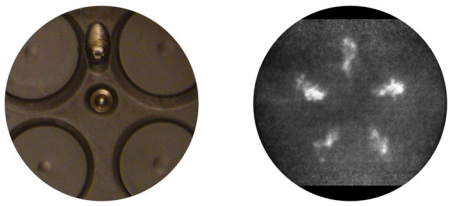

Figure 78. Optical access through piston extension and PLIF image of combined PFI and DI.

This combustion system is a compromise between the need for optical access and the possibility to utilize DI, PFI, spark ignition and a variable valve train while using certain combustion chamber geometry. For this setup the optical access was excellent, the compromise in combustion chamber and injector specifications proved less optimal regarding the location of the fuel stratifications.

As the amount of DI is increased the combustion timing stays almost constant as shown in Figure 80. For the cases with a DI ratio of 30, and 60 % a clear decrease can be seen in RoHR as well as in accumulated HR. This is thought to be due to high stratification in the combustion chamber perimeter with possible wall wetting as well as over rich mixtures resulting in partial burn. This high stratification in the outer rim will then result in too lean conditions at the spark plug position. The early RoHR for these cases show an absence of ISHR. Since the spark is thought to have less effect two main reasons remain for explaining the maintained combustion timing.

- Increased fuel stratification provoking advanced auto ignition at multiple sites.
- Increased charge temperature for the high stratification case due to partial burn, leaving reactive species in the cylinder during the NVO.

The presence of reactive species is supported by pressure data showing increased expansion work during the NVO for the high DI ratio. The incomplete combustion during the NVO results in both an increased temperature during the compression stroke as well as remaining radicals that will affect ignition. Further advancement of combustion timing can be inhibited by the heat of vaporisation of the injected fuel that unfortunately can be expected to lower the temperature especially of the fuel richer zones. This is also described in the work of Thirouard et. al. [74]. Since the heat of vaporisation is high for ethanol compared to regular fuels such as gasoline the effect is expected to be strong in this work.

The cooling effect due to the heat of vaporisation is further supported when looking at single cycle PLIF images of combustion. Fuel rich zones are not the first to react, instead they can be seen to stay unaffected when reactions occur in the leaner zones where the temperature is higher or rather in the mixing region between the lean and the colder rich zones.

While the combustion timing maintains at the same CAD the combustion duration in terms of CA10 – CA90 increases slightly with increasing stratification. The trend in combustion duration with increasing stratification is contradicted by the PFI point. However, the PFI point is run at a slightly lower load thus giving longer burn duration. The change in RoHR is insignificant until the DI proportion is increased to the point of partial burn which is also visible from the COV_{imep}.

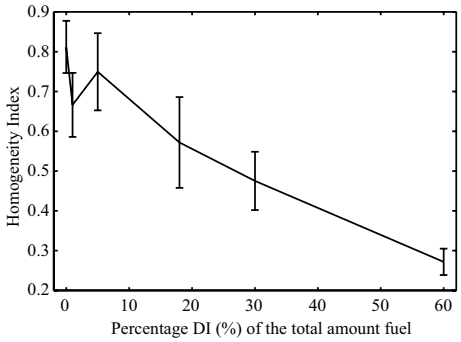

Figure 79. Homogeneity index as a function of DI duration. The bars indicate the 95% confidence intervals for the mean values.

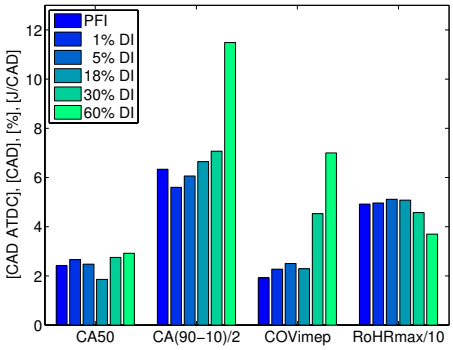

Figure 80. Combustion timing CA50 [CAD ATDC], combustion duration CA(90 – 10)/2 [CAD], combustion stability COV_{IMEP} [%] and RoHRmax/10 [J / CAD] for different percentages of DI.

Single cycle PLIF images chosen to be representative can be seen in Figure 81 for increased amount of DI. As the proportion of DI increases the flame growth can be seen to be reduced while auto ignition advances. Furthermore the auto ignition sites can be seen to increase in numbers. The development of individual cycles shows the presence of fuel richer zones that exist while combustion occurs in the surroundings.

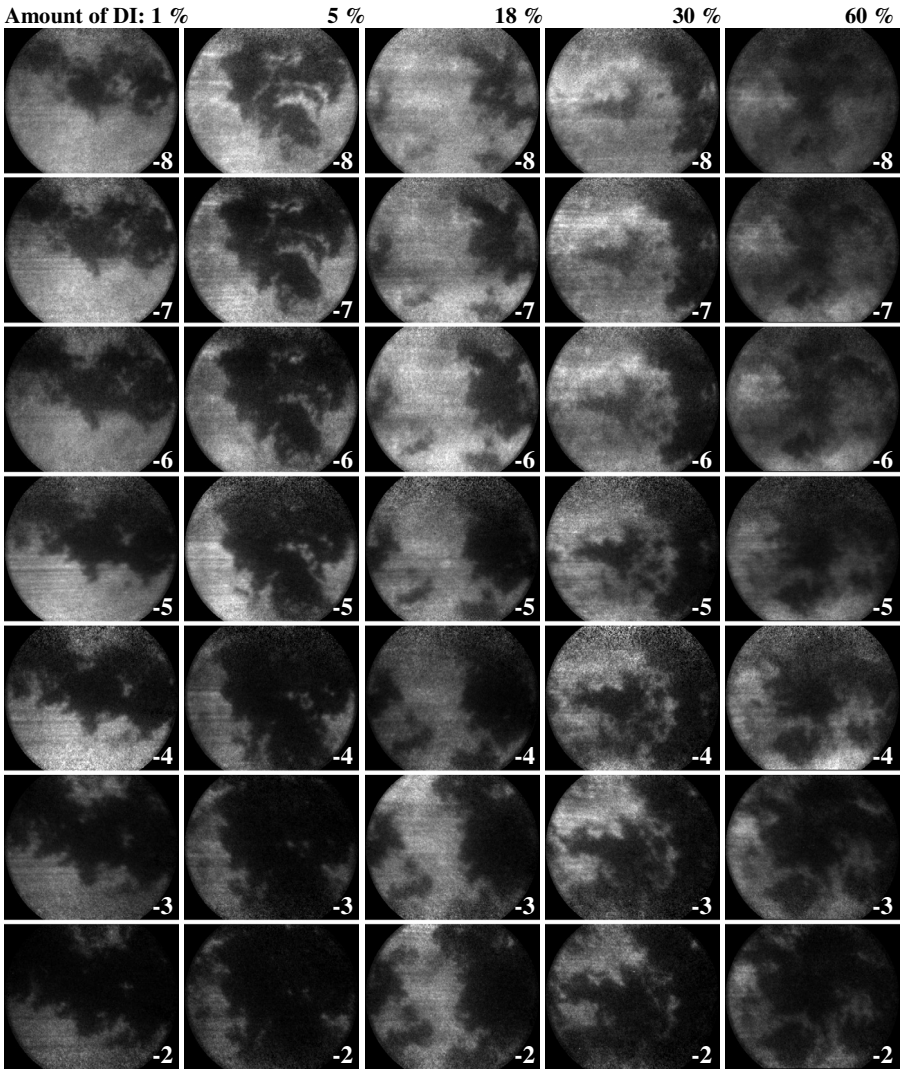

Figure 81. PLIF images taken between -8 and -2 CAD ATDC Each column is taken in one cycle for a specific DI duration. The DI duration is from the left to the right 1, 5, 18, 30 and 60 %. The DI timing is -70 CAD ATDC. In each column the gray scale is set between minimum and maximum values.

7 Summary

The focus of current HCCI research is divided into two main paths directed towards either the SI or the CI engine. In this work the focus has been from the SI perspective, how to gain as much as possible with limited changes of the base engine. This is where HCCI with NVO comes in. A limited load speed range in HCCI mode is shown by utilising camshafts with low lift and short duration. The modification of the engine is limited, cam phasing is available on the production engine. Engines capable of cam profile switching have been in the automotive market for some time. To maximize the gain in efficiency by NVO HCCI the operating regime must be increased to include as much as possible of the total operating range of the engine, not only the regulated drive cycles. SACI combustion is one way of reaching further towards this goal.

The low load limit is caused by insufficient temperature to reach auto ignition. The sensitivity to intake temperature is investigated at the low load limit showing a rather low sensitivity to changes mainly due to the low volumetric efficiency with high residual dilution. Unstable combustion at low load is confirmed to show a repetitively pattern due to cycle by cycle dependence of the residual state. Further it is shown that the usage of spark assistance can stabilise and advance combustion and thus lower the load at some conditions. While it is still necessary to lower the possible load with HCCI towards idle a gain in engine total efficiency can be achieved if the efficiency of the HCCI part can be further raised. When comparing the efficiency of the NVO HCCI engine to a high CR HCCI engine as well as to conventional SI combustion the part load efficiency for the residual diluted HCCI engine is much higher than that of the SI engine but the lean burn high CR engine still has even higher efficiency. The NVO HCCI engine is found to be suffering of mainly lower thermal efficiency due to the low CR. The usage of higher compression ratio would also lower the necessary amount of residuals, further increasing the efficiency. Increased CR goes hand in hand with current development of SI engines in combination with introduction of DI. The usage of DI for the SI engine also enables further increase of the HCCI operating regime by injection and fuel reformation during the NVO as well as possibilities of fuel stratification.

For further incentive of switching from SI to HCCI, also the high load boundary must be addressed. One way of decreasing the excessive reaction rate with low dilution is using temperature stratification. The positive effect of temperature stratification is confirmed here by a thicker combustion boundary layer correlating to longer combustion durations. However an active thermal stratification within the fluid is needed, the combustion boundary layer related to chamber wall interaction is not attractive since it will increase heat transfer thus increase heat losses.

The relation between ISHR and HCCI is investigated optically for SACI combustion to increase the knowledge of what happens when high residual dilution is used in combination with spark assistance. Reports of effects on combustion up to lambda 3 have been reported [48], here the lowest load run with spark assistance is slightly above 2 bar $IMEP_{net}$. Using the definition of ISHR on pressure information in combination with high speed chemiluminescence imaging it can be concluded that flame propagations occurs also in the highly diluted cases. Further, advancing spark timing will both advance flame propagation and auto ignition timing. A very stratified slow auto ignition appearance suggests stratification of both species and temperature.

The known influence of turbulence on SI combustion inspired turbulence modification by swirl introduction. A significant improvement could be seen for the SI part of SACI combustion while the subsequent auto ignition was slightly delayed and HCCI combustion duration was increased. To fully understand how homogeneity of residuals and fresh charge as well as the temperature distribution changes with the flow pattern and thus affects auto ignition requires either modelling or laser based measurements looking at temperature distributions [82] as well as location of specific species.

The main reasons why SACI combustion is possible in combination with high residual dilution are found to be:

- The increased temperature of the surrounding gas increasing the dilution capability with less heat losses.
- Lower demands on flame propagation speed due to the subsequent fast HCCI combustion
- Lower actual dilution compared to SI due to increased charge temperature thus lower gas density

Charge stratification was investigated with the motive of improving the auto ignition properties as well as the conditions for spark assistance with SACI combustion. The swirling DI combustion chamber that was a trade of between optical access and the possibility of combining DI and spark ignition proved less favourable for SACI combustion. While the conditions for SACI combustion deteriorate with increased stratification the combustion timing is maintained due to two reasons. Lower combustion efficiency increases the reactivity in the NVO creating reactive species and increases the charge temperature. Zones more prone to auto ignite are created with the stratification; this later effect is however inhibited by the high heat of vaporisation of the fuel. Thus it is not the fuel richest zones that react first, rather the mixing layer between the hotter residuals and the fuel rich zones.

The engine used in the final experiments was capable of flexible valve timings, PFI, DI as well as spark ignition making it capable of SI, DI, SACI, PPC and HCCI if had the geometric CR been slightly increased. To expect that the production engines will be capable of multi mode combustion depending on desired load and available fuel is perhaps not reasonable in the near future, although the multi fuel capability is already common on the market. However, the CR of the SI engines is going up to increase efficiency simultaneously as it is reduced for the CI engines to increase maximum load. The SI engines are going towards advanced DI injection systems with lean burn and piston shapes to support the spray. Larger CI engines are emerging with lost motion valve trains. Although far apart the differences are decreasing between the two.

8 References

1. UNEP (2006). The GEO Data Portal. United Nations Environment Programme. http://geodata.grid.unep.ch
2. L. Hildingsson, H. Persson, B. Johansson, R. Collin, J. Nygren, M. Richter, M. Aldén, R. Hasegawa, H. Yanagihara: “Optical Diagnostics of HCCI and Low-Temperature Diesel Using Simultaneous 2-D Plif of Oh and Formaldehyde”, SAE Paper 2004-01-2949
3. L. Hildingsson, H. Persson, B. Johansson, R. Collin, J. Nygren, M. Richter, M. Aldén, R. Hasegawa, H. Yanagihara: “Optical Diagnostics of HCCI and UNIBUS Using 2-D PLIF of OH and Formaldehyde”, SAE Paper 2005-01-0175
4. J. Heywood: ”Internal Combustion Engine Fundamentals”, MacGraw-Hill ISBN 0-07-100499-8, 1988
5. M. Richter, J. Engström, A. Franke, M. Aldén, A. Hultqvist, B. Johansson: ”The Influence of Charge Inhomogeneity on the HCCI Combustion Process”, SAE Paper 2000-01-2868
6. A.Hultqvist, M. Christensen, B. Johansson, M. Richter, J. Nygren, J. Hult, M. Aldén: ”The HCCI Combustion Process in a Single Cycle-High-Speed Fuel Tracer LIF and Chemiluminescence Imaging”, SAE Paper 2002-01-0424
7. M. Christensen, B. Johansson, P. Amnéus, F. Mauss: ”Supercharged Homogeneous Charge Compression Ignition”, SAE Paper 980787
8. G. M. Rassweiler, L. Withrow: ”Motion Pictures of Engine Flames Correlated With Pressure Cards”, SAE Paper 380139
9. P. Strandh, M. Christensen, J. Bengtsson, R. Johansson, A. Vressner, P. Tunestål, B. Johansson: ”Ion Current Sensing for HCCI Combustion Feedback” SAE Paper 2003-01-3216
10. A.Vressner, A. Hultqvist, P. Tunestål, B. Johansson, R. Hassegava:” Fuel Effects on Ion Current in an HCCI Engine” SAE Paper 2005-01-2093
11. H. Hamedovic, F. Raichle, J. Breuninger, W. Fischer, W. Dieterle, M. Klenk, J. F. Böhme: IMEP-Estimation and In-Cylinder Pressure Reconstruction for Multicylinder SI-Engine by Combined Processing of Engine Speed and One Cylinder Pressure”, SAE Paper 2005-01-0053
12. J-O. Olsson, P. Tunestål, B. Johansson: ”Closed-Loop Control of an HCCI Engine”, SAE Paper 2001-01-1031
13. M. Christensen, A. Hultqvist, B. Johansson: ”Demonstrating the Multi Fuel Capability of a Homogeneous Charge Compression Ignition Engine with Variable Compression Ratio”, SAE Paper 1999-01-3679
14. G. Haraldsson, P. Tunestål, B. Johansson, J. Hyvönen: ”HCCI Combustion Phasing with Closed-Loop Combustion Control Using Variable Compression Ratio in a Multi Cylinder Engine”, JSAE Paper 20030126, SAE Paper 2003-01-1830
15. J. Martinez-Frias, S. Aceves, D. Flowers, R. Smith, R. Dibble: ”HCCI Engine Control by Thermal Management”, SAE Paper 2000-01-2869
16. G. Haraldsson, P. Tunestål, B. Johansson, J. Hyvönen: ”HCCI Closed-Loop Combustion Control Using Fast Thermal Management”, SAE Paper 2004-01-0943
17. S. Onishi, S. Hong Jo, K. Shoda, P. Do Jo, S. Kato: ”Active Thermo-Atmosphere Combustion (ATAC) – a New Combustion Process for Internal Combustion Engines”, SAE Paper 790501

18. P. Najt, D. E. Foster: ”Compression-Ignited Homogeneous Charge Combustion”, SAE Paper 830264
19. R. H. Thring: ”Homogeneous-Charge Compression-Ignition (HCCI) engines”, SAE Paper 892068
20. O. Erlandsson: ”Early Swedish Hot-Bulb Engines - Efficiency and Performance Compared to Contemporary Gasoline and Diesel Engines”, SAE Paper 2002-01-0115
21. P. Håkansson: ”Study of Performance and Exhaust Emissions from 2-stroke Hot Bulb Engine”, Master Thesis, Dept. of Energy Sciences, Lund Institute of Technology, Sweden 2004
22. S. Kimura, O. Aoki, H. Ogawa, S. Muranaka, Y. Enomoto: “New Combustion Concept for Ultra-Clean and High-Efficiency Small DI Diesel Engines”, SAE Paper 1999-01-3681
23. R. Hassegawa, H Yanagihara: “HCCI Combustion in DI Diesel Engine”, SAE Paper 2003-01-0745
24. O. Lang, W. Salber, J. Hahn, S. Pischinger, K. Hortmann, C. Bücker: ”Thermodynamical and Mechanical Approach Towards a Variable Valve Train for the Controlled Auto Ignition Combustion Process”, SAE paper 2005-01-0762
25. J. Willand, R-G. Nieberding, G. Vent, C. Enderle: ”The knocking Syndrome – Its Cure and its Potential”, SAE Paper 982483
26. J. Lavy, J-C. Dabadie, C. Angelberger, P. Duret, J. Willand, A. Juretzka, J. Schäflein, T. Ma, Y. Lendresse, A. Satre, C. Schulz, H. Krämer, H. Zhao, L. Damiano: ”Innovative Ultra-low NOx Controlled Auto-Ignition Combustion Process for Gasoline Engines: the 4-SPACE Projekt
27. J. Yang, T. Culp, T. Kenney: ”Development of a Gasoline Engine System Using HCCI Technology – The Concept and the Test Results”, SAE Paper 2002-01-2832
28. J. Hyvönen, C. Wilhelmsson, B. Johansson: ”The effect of displacement on air-diluted multi-cylinder HCCI engine performance”, SAE paper 2006-01-0205
29. S. Trajkovic, A. Milosavljevic, P. Tunestal, B. Johansson: ”FPGA Controlled Pneumatic Variable Valve Actuation”, SAE Paper 2006-01-0041
30. D. Law, J. Allen, D. Kemp, G. Kirkpatrick, T. Copland: ”Controlled Combustion in An Ic-Engine With a Fully Variable Valve Train”, SAE Paper 2001-01-0251
31. J. Hyvönen, G. Haraldsson, B. Johansson: ”Balancing Cylinder-to-Cylinder Variations in a Multi-Cylinder VCR-HCCI Engine”, SAE Paper 2004-01-1897
32. F. Bowditch: ”A new tool for Combustion Research A Quartz Piston Engine”, SAE Paper 610002
33. B. Johansson, F. Söderberg: “The Effect of Valve Strategy on In-Cylinder Flow and Combustion”, SAE Paper 960582
34. G. Woschni: ”A Universally Applicable Equation for the Instantaneous Heat Transfer Coefficient in the Internal Combustion Engine”, SAE Paper 670931
35. G. Rassweiler, L. Withrow: ”Motion Pictures of Engine Flames Correlated with Pressure Cards”, SAE Paper 380139
36. A. Hultqvist, M. Christensen, B. Johansson, A. Franke, M. Richter, M. Aldén: ”A Study of the Homogeneous Charge Compression Ignition Combustion Process by Chemiluminescence Imaging”, SAE Paper 1999-01-3680

37. H. N. Najm, ”On the Adequacy of Certain Experimental Observables as Measurements of Flame Burning Rate”, Combustion and Flame, 113:312-332, 1998
38. J. Rübel: ”Homogeneity and Near-wall Combustion Behaviour in a HCCI Engine”, Master Thesis Dept. of Energy Sciences, Lund Institute of Technology, Sweden 2005
39. Dantec Elektronik: Users guide to 57N20/57N35 BSA enhanced
40. B. Johansson: ”On Cycle to Cycle Variations in Spark Ignition Engines –The Effect of Fluid Flow and Gas Composition in the Vicinity of the Spark plug on Early Combustion”, Doctoral Thesis, Lund 1995, ISRN LUTMDN/TMVK- -1010-SE
41. B. Johansson: “Förbränningsmotorer”, textbook on Combustion Engines for students attending the Mechanical Engineering program at Lund Institute of Technology, Lund University
42. A. C. Eckbreth: “Laser Diagnostics for Combustion Temperature and Species”, Gordon and Breach Publishers, Amsterdam, second edition 1996
43. H. Zhao, J. Li, T. Ma, N. Ladommatos: “Performance and Analysis of a 4-Stroke Multi-Cylinder Gasoline Engine with CAI Combustion”, SAE Paper 2002-01-0420
44. J. Allen, D. Law: “Variable Valve Actuated Controlled Auto-Ignition: Speed Load Maps and Strategic Regimes of Operation” SAE Paper 2002-02-0422
45. A. Cairns, H. Blaxill: “Lean Boost and External Exhaust Gas Recirculation for High Load Controlled Auto-Ignition”, SAE Paper 2005-01-3744
46. T. Urushihara, K. Hiraya, A. Kakuhou, T. Itoh: “Expansion of Hcci Operating Region By the Combination of Direct Fuel Injection, Negative Valve Overlap and Internal Fuel Reformation”, SAE Paper 2003-01-0749
47. L. Koopmans, R. Ogink, I. Denbratt: “Direct Gasoline Injection in the Negative Valve Overlap of a Homogeneous Charge Compression Ignition Engine”, SAE Paper 2003-01-1854
48. J. Hyvönen, G. Haraldsson, B. Johansson: “Operating Conditions Using Spark Assisted HCCI Combustion During Combustion Mode Transfer to SI in a Multi-Cylinder VCR-HCCI Engine”, SAE Paper 2005-01-0109
49. L. Koopmans, H. Ström, S. Lundgren, O. Backlund, I. Denbratt: ”Demonstrating a SI-HCCI-SI Mode Change on a Volvo 5-Cylinder Electronic Valve control Engine”, SAE Paper 2003-01-0753
50. N. Milovanovic, D. Blundell, S. Gedge, J. Turner: ”Cam Profile Switching (CPS) and Phasing Strategy vs Fully Variable Valve Train (FVVT) Strategy for Transitions between Spark Ignition and Controlled Auto Ignition Modes”, SAE Paper 2005-01-0766
51. A. Cairns, H. Blaxill: “The Effects of Two-Stage Cam Profile Switching and External EGR on SI-CAI Combustion Transitions”, SAE Paper 2007-01-0187
52. L. Koopmans, O. Backlund, I. Denbratt: ”Cycle to Cycle Variations: Their influence on Cycle Resolved Gas Temperature and Unburned Hydrocarbons from a Camless Gasoline Compression Ignition Engine”, SAE Paper 2002-01-0110
53. M. Christensen: “HCCI Combustion – Engine Operation and Emission Characteristics”, Doctoral Thesis, Lund 2002, ISBN 91-628-5424-0
54. H. Xie, L. Yang, J. Qin, R. Gao, H. G. Zhu, B. Q. He, H. Zhao: “The Effect of Spark Ignition on the CAI Combustion Operation”, SAE Paper 2005-01-3738

55. L. Koopmans, I. Denbratt: ”A Four Stroke Camless Engine, Operated in Homogenous Charge Compression Ignition Mode with Commercial Gasoline”, SAE Paper 2001-01-3610
56. A. Fuhrhapter, W. F. Piock, G. K. Fraidl: ”CSI – Controlled Auto-ignition – The Best Solution for the Fuel Consumption – Versus Emission Trade-Off?”, SAE Paper 2003-01-0754
57. N. Kalian, R. Standing, H. Zhao: “Effects of Ignition Timing on CAI Combustion in a Multi-Cylinder DI Gasoline Engine” SAE Paper 2005-01-3720
58. T. Urushihara, K. Yamaguchi, K. Yoshizawa, T. Itoh: ”A Study of a Gasoline-fueled Compression Ignition Engine ~ Expansion of HCCI Operation Range Using SI combustion as a Trigger of Compression Ignition”, SAE Paper 2005-01-0180
59. P. G. Aleiferis, A. G. Charalambides, Y. Hardalupas, A. M. K. P. Taylor, Y. Urata: ”Autoignition Initiation and Development of n-heptane HCCI Combustion assisted by Inlet Air Heating, internal EGR or Spark Discharge: An Optical Investigation”, SAE Paper 2006-01-3273
60. G. E. Andrews, D. Bradley: “The Burning Velocity of Methane-Air Mixtures“, Combustion & Flame, 19: 275-288 (1972)
61. M. Christensen, A. Hultqvist, B. Johansson: “The Effect of Combustion Chamber Geometry on HCCI Operation”, SAE Paper 2002-01-0425
62. M. Christensen, A. Hultqvist, B. Johansson: “The Effect of in-Cylinder Flow and Turbulence on HCCI Operation”, SAE Paper 2002-01-2864
63. S. M. Aceves, D. L. Flowers, J. Martinez-Frias, F. Espinosa-Losa, M. Christensen, B. Johansson, R.P. Hessel; “Analysis of the Effect of Geometry Generated Turbulence on HCCI Combustion by Multi-Zone Modeling”, SAE 2005-01-2134
64. R. P. Hessel, S. M: Aceves, D. L. Flowers: “A Comparison on the Effect of Combustion Chamber Surface Area and In-Cylinder Turbulence on the Evolution of Gas Temperature Distribution from IVC to SOC: A Numerical and Fundamental Study”, SAE Paper 2006-01-0869
65. A. Vressner, A. Hultqvist, B. Johansson: ”Study on Combustion Chamber Geometry Effects in an HCCI Engine using High-Speed Cycle-Resolved Chemiluminescence Imaging”, SAE Paper 2007-01-0217
66. A. Vressner, R. Egnell, B. Johansson: ”Combustion Chamber Geometry Effects on the Performance of an Ethanol Fueled HCCI Engine”, SAE Paper 2008-01-1656
67. A. Babajimopoulos, G. A. Lavoie, D. N. Assanis: “Modeling HCCI Combustion With High Levels of Resiudal Gas Fraction – A Comparison of Two VVA Strategies”, SAE Paper 2003-01-3220
68. J. E. Dec, W. Hwang, M. Sjöberg: “An Investigation of Thermal Stratification in HCCI Engines Using Chemiluminescence Imaging”, SAE Paper 2006-01-1518
69. M. Nagamine, A. Kakuho, Y. Amenomori, T. Urushihara, T Itoh: “In-Cylinder Temperature Distribution Measurement and Its Application to HCCI Combustion”, SAE Paper 2006-01-1202
70. N. Milovanovic, D. Blundell, R. Pearson, J. Turner R. Chen: “Enlarging the Operational Range of a Gasoline HCCI Engine By Controlling the Coolant Temperature” SAE Paper 2005-01-0157

71. R. X. Yu, X. S. Bai, A. Vressner, A. Hultqvist, B. Johansson, J. Olofsson, H. Seyfried, J. Sjöholm, M. Richter, M. Aldén: “Effect of Turbulence on HCCI Combustion”, SAE Paper 2007-01-0183
72. K. Kumano, N. Iida: “Analysis of the Effect of Charge Inhomogeneity on HCCI Combustion by Chemiluminescence Measurement”, SAE Paper 2004-01-1902
73. M. Sjöberg, J. E. Dec: “Smoothing HCCI Heat-Release Rates Using Partial Fuel Stratification with Two-Stage Ignition Fuels”, SAE Paper 2006-01-0629
74. B. Thirouard, J. Cherel, V. Knop: “Investigation of Mixture Quality Effect on CAI Combustion”, SAE Paper 2005-01-0141
75. A. W. Berntsson, I. Denbratt: “HCCI Combustion Using Charge Stratification for Combustion Control”, SAE Paper 2007-01-0210
76. J. E. Dec, M. Sjöberg: “Isolating the Effects of Fuel Chemistry on Combustion Phasing in an HCCI Engine and the Potential of Fuel Stratification for Ignition Control”, SAE Paper 2004-01-1900
77. M. Richter, J. Engström, A. Franke, M. Aldén, A. Hultqvist, B. Johansson: ”The influence of charge inhomogeneity on the HCCI combustion process”, SAE Paper 2000-01-2868
78. W. Hwang, J. E. Dec, M. Sjöberg: “Fuel Stratification for Low-Load HCCI Combustion: Performance & Fuel-PLIF Measurements”, SAE Paper 2007-01-4130
79. H. Seyfried, J. Olofsson, J. Sjöholm, M. Richter, M. Aldén, A. Vressner, A. Hultqvist, B. Johansson ”High Speed PLIF Imaging for Investigation of Turbulence Effects on Heat Release Rates in HCCI Combustion”, SAE Paper 2007-01-0213
80. R. Collin, J. Nygren, M. Richter, M. Aldén, L. Hildingsson, B. Johansson: “The Effect of Fuel Volatility on HCCI using Simultaneous Formaldehyde and OH PLIF”, SAE Paper 2004-01-2948
81. M. Richter, R. Collin, J. Nygren, M. Aldén, L. Hildingsson, B. Johansson: “Studies of the Combustion Process with Simultaneous Formaldehyde and OH PLIF in a Direct-Injected HCCI Enging”, JSME International Journal, vol. 18, 701-707 (2005)
82. R. Hasegawa, I. Sakata, H. Yanagihara, B. Johansson, A. Omrane, M. Aldén: ” Two-dimensional gas-phase temperature measurements using phosphor thermometry” Appl. Phys B 88, 2007, p 291 - 296

9 Summary of papers

9.1 Paper I

The Effect of Intake Temperature on HCCI Operation Using Negative Valve Overlap
H. Persson, M. Agrell, J-O. Olsson, B. Johansson, H. Ström
SAE Technical paper 2004-01-0944
Presented at the SAE World Congress, March, 2004, Detroit, Michigan

In this first paper a naturally aspirated SI engine is converted to HCCI operation by means of camshafts comprising low lift and short duration. This enables a negative valve overlap and thereby trapping of hot residuals in order to reach auto ignition. A limited operating region is defined stretching from 1 to 4 bar IMEP and 650 to 4000 rpm. The operating regime is possible with the help of spark assistance. Limiting factors such as temperature and pressure rise rates are recognized.

The effect of intake temperature is studied in detail showing a much smaller effect compared to what is seen for traditional HCCI combustion. The high amount of trapped residuals reduces the amount of induced air and fuel. This makes the engine less and less sensitive for intake temperature as residuals are increased. The behavior is seen for all cylinders but with variation in combustion timing.
Further, engine out emissions of NO_x two orders of magnitudes lower than similar SI conditions in combination with 20 % lower indicated specific fuel consumption are observed.

Experiments were carried out by the author together with M. Agrell, The author post processed data and wrote the paper.

9.2 Paper II

Cylinder-to-Cylinder and Cycle-to-Cycle Variations at HCCI Operation with Trapped Residuals
H. Persson, R. Pfeiffer, A. Hultqvist, B. Johansson, H. Ström
SAE Technical paper 2005-01-0130
Presented at the SAE World Congress, April 2005, Detroit, Michigan

This paper can be seen as a continuation of the first. By variable valve timing a broader operating regime is possible for HCCI combustion with trapped residuals. Still reaching lower load is a major concern. Cycle-to-cycle variations for individual cylinders are found to be limiting lower loads. At some points oscillation phenomena related to the trapped residual temperature can cause misfire. At speeds below 3000 rpm it is possible to use spark assistance and further lower the load suppressing oscillations until the low load boarder when oscillation phenomena rapidly increase again. Possibility to phase combustion timing by means of spark timing is shown and makes it possible to adjust cylinder individual combustion timing. Early spark timing shows an initial slower heat release indicating initial SI combustion although highly residual diluted conditions.

The author did the experiments, evaluated the data and wrote the paper.

9.3 Paper III

Investigation of Boundary Layer Behaviour in HCCI Combustion using Chemiluminescence Imaging
H. Persson, L. Hildingsson, A. Hultqvist, B. Johansson, J. Ruebel
SAE Technical paper 2005-01-3729
Presented at the SAE Powertrain & Fluid Systems Conference, October 2005, San Antonio, Texas

This third paper is an optical study with the intention to learn more about how the combustion boundary layer affects the combustion burn rate, possibly enabling higher load. The research tool is chemiluminescence imaging which is shown to agree well with RoHR. A boundary layer is defined as a percentage of the maximum and minimum average intensity and found to be in the range of 2 to 4 mm by the definition used. Only small variations in boundary layer are observed but a thinner boundary layer is seen to correspond to a higher burn rate. During combustion the boundary layer is seen to move closer to the walls as the temperature is increasing. For increased swirl thus increased turbulence the boundary layer changes being thinner at first and thicker towards the end of combustion whereas no change in combustion duration is seen.

Experiments and post processing were carried out by the author and J. Rübel. The paper was written by the author.

9.4 Paper IV

Investigation of the Early Flame Development in Spark Assisted HCCI Combustion Using high Speed Chemiluminescence Imaging
H. Persson, A. Rémon, A Hultqvist, B. Johansson
SAE 2007-01-0212
Presented at the SAE World Congress, April 2007, Detroit, Michigan

In this work the influence of spark assistance on HCCI combustion is studied in a single cylinder engine with optical access. Combustion is monitored by in-cylinder pressure and simultaneous high speed chemiluminescence imaging. It is seen that even for large NVO and thus high residual fractions it is a growing turbulent SI flame that interacts with, and governs the subsequent HCCI combustion. By advancing the spark timing it is possible to phase the combustion timing even when the major part of the released heat is from HCCI combustion. The flame expansion speed decreases for higher NVO, but prevails also for high residual fractions. A higher spark advance is found to compensate for the slower flame expansion up to a point.
The auto-ignition process is found to be stratified for both spark assisted HCCI and pure HCCI. For pure HCCI the initial front spreading velocity is found to be of the same order of magnitude as the expansion speed of the SI flame.
Calculations to estimate the crank angle of auto-ignition are performed based on cylinder pressure information providing good statistics on how the proportion of SI to HCCI behaves for different operating conditions.

Experiments and post processing were carried out by the author and A. Rémon. The paper was written by the author.

9.5 Paper V

The Effect of Swirl on Spark Assisted Compression Ignition (SACI)
H. Persson, A. Rémon, B. Johansson
JSAE 20077167, SAE 2007-01-1856
Presented at the JSAE/SAE International Fuels and Lubricants meeting, July 2007, Kyoto, Japan

This is a direct continuation of the previous paper. By intake valve deactivation the flow pattern is altered from tumble to also include swirl resulting in increased turbulence. Synchronized simultaneous pressure and high speed chemiluminescence measurements are conducted making it possible to reproduce fully resolved cycles from the onset of the spark throughout the entire combustion event. From the chemiluminescence images changes in flame expansion speeds are evaluated. The effect on combustion in terms of auto ignition timing, combustion duration and the amount of heat released in the different combustion modes is investigated using heat release analysis. LDV measurements are conducted to support the turbulence effects on SACI combustion.

The flame expansion speed is found to increase also at high residual rates with increased turbulence. This is important since it could enhance the region where SACI combustion can be achieved. For the subsequent HCCI combustion auto ignition is seen to be slightly delayed and the burn duration is increased. More heat release from the flame is needed to reach auto ignition with increased turbulence. Combustion stability is improved with better conditions for flame propagation which implies that further spark advance will enable lower loads.

Experiments and post processing were carried out by the author and A. Rémon. The paper was written by the author.

9.6 Paper VI

Study of Fuel Stratification on Spark Assisted Compression Ignition (SACI) Combustion with Ethanol Using High Speed Fuel PLIF
H. Persson, J. Sjöholm, E. Kristensson, B. Johansson, M. Richter, M. Aldén
Submitted to the SAE Fuels & Lubricants Meeting, Chicago 2008

The effect of fuel stratification is investigated by means of port fuel injection in combination with direct injection for SACI combustion with NVO

A high speed multi-YAG laser system and a framing camera are used to capture planar laser induced fluorescence (PLIF) images of the fuel distribution. Charge homogeneity in terms of fuel distribution is investigated using a homogeneity index calculated from PLIF images.

It is shown that charge stratification can be achieved using port fuel injection in a swirling combustion system. For the combined port fuel and direct injection strategy a strong stratification is shown, although combustion phasing remains constant, a slight increase in combustion duration can be seen. For increased stratification with direct injection in a base of port injected fuel an increased number of ignition sites can occur. However, it is not the most fuel rich regions that ignite first. Instead ignition

occurs in the mixing zone between the rich and the leaner regions. Earlier ignition due to more reactive zones is inhibited by the heat of vaporization for higher amounts of DI.

Experiments, post processing as well as the paper writing were performed by the author, J. Sjöholm and E. Kristensson.

2004-01-0944

The Effect of Intake Temperature on HCCI Operation Using Negative Valve Overlap

Håkan Persson, Mats Agrell, Jan-Ola Olsson and Bengt Johansson
Lund Institute of Technology

Hans Ström
Volvo Car Corp.

ABSTRACT

A naturally aspirated in-line six-cylinder 2.9-litre Volvo engine is operated in Homogeneous Charge Compression Ignition (HCCI) mode, using camshafts with low lift and short duration generating negative valve overlap. This implementation requires only minor modifications of the standard SI engine and allows SI operation outside the operating range of HCCI. Standard port fuel injection is used and pistons and cylinder head are unchanged from the automotive application. A heat exchanger is utilized to heat or cool the intake air, not as a means of combustion control but in order to simulate realistic variations in ambient temperature. The combustion is monitored in real time using cylinder pressure sensors.

HCCI through negative valve overlap is recognized as one of the possible implementation strategies of HCCI closest to production. However, for a practical application the intake temperature will vary both geographically and from time to time. It is therefore very important to gain knowledge of how this variation affects the combustion process.

The operating range in HCCI mode for this specific engine stretches from 650 rpm to 4000 rpm and from 1 bar IMEP to 4 bar IMEP. The emissions of NO_x are approximately two orders of magnitude lower in HCCI mode compared to SI mode. The emissions of CO are slightly lower while the emissions of HC are slightly higher for HCCI operation. When run in HCCI mode the engine's efficiency is improved throughout the operating range by as much as 10 percentage units compared to SI operation. The effect of inlet air temperature variation on HCCI combustion through negative valve overlap is insignificant when the engine runs well inside of the HCCI operating range. The effect is however prominent when the engine is operated close to the border of the operating range.

INTRODUCTION

Homogeneous Charge Compression Ignition (HCCI) is a hybrid of the ordinary Spark Ignition (SI) and the Compression Ignition (CI) engine. Similar to the SI engine the HCCI engine is port fuel injected creating a more or less homogeneous mixture. During compression the temperature increases to the point of auto-ignition. As in the CI engine the mixture burns without the help of an ignition system, the challenge for HCCI compared to the SI and CI engines is that ignition timing is dependent on the in-cylinder temperature and is not directly controlled.

The first studies of this type of combustion were performed on 2-stroke engines [1,2]. The primary purpose with HCCI for 2-stroke engines is to reduce the hydrocarbon (HC) emissions at part load operation.

Najt and Foster showed in 1983 that it is possible to achieve HCCI in a four stroke engine [3]. More recent studies of HCCI have been focused on reducing emissions and improving efficiency in 4-stroke engines [4-7].

Due to auto ignition of a homogeneous mixture no flame propagation is present and instead the whole bulk will begin to oxidize almost simultaneously. It is commonly accepted that the onset of combustion is controlled by chemical kinetics [8,9]: As the mixture is compressed the temperature and pressure increase. Temperature and pressure history, together with the concentration of O_2, different fuel contents and combustion products govern how combustion is initiated. As a consequence the combustion timing will be influenced by air-fuel ratio (AFR), inlet temperature, compression ratio, residual gases and EGR.

A feasible way to improve low load efficiency for cars currently running with SI engines would be to use an engine that can run in HCCI mode at part load and

switch to SI at high load. Mode shift from SI to HCCI and vice versa is demonstrated by Koopmans et al.[10].

To obtain auto ignition of a high-octane fuel such as ordinary gasoline at relatively low compression ratio the temperature must be raised [11]. In this work the temperature is raised by trapping residual gases in the cylinder by early exhaust valve closing and late inlet valve opening as shown by Li et. al. [12] and Koopmans et. al. [13].

In this work HCCI is studied as a means to increase the part load efficiency of the SI engine, which struggles with poor part load efficiency due to throttling and heat losses. Special consideration is taken to effects on the combustion related to changes in the intake temperature.

EXPERIMENTAL SETUP

ENGINE

The engine used in this work is an in-line six-cylinder 2.9L Volvo engine. It is a naturally aspirated production engine with double overhead camshafts and multi point port fuel injection. The standard camshafts are replaced by a set comprising low lift and short duration. The camshafts are equipped with encoding discs for easy and accurate setting of the valve timing. The engine is equipped with an air heat exchanger installed upstream from the throttle. The heat exchanger can be operated with either hot or cold tap water making it possible to either heat or cool the intake air. All experiments in this work are run using a regular commercial, unleaded gasoline with an octane number (RON) of 98. Further engine specifications can be seen in table 1.

Table 1. Engine data.

Bore	83 mm
Stroke	90 mm
Displaced Volume	2922 cm^3
Compression ratio	10.3:1
Lift	3 mm
Inlet/Exhaust Valve Duration	150 CAD

The engine is controlled by an in-house developed management system with the ability to set ignition timing, dwell, injection timing, injection duration, throttling and inlet air temperature to desired values.

The dynamometer is an A/C motor that can be set to a desired speed. Due to an oversized dynamometer the engine brake torque is not reliable at low loads. The accuracy of the dynamometer is simply too low for part load HCCI operation. Therefore comparisons are made using indicated quantities.

MEASUREMENT EQUIPMENT

The in-cylinder pressure is monitored separately for each cylinder using Kistler 6053C60 pressure transducers. However, only two calibrated transducers are available, these are placed in cylinder 1 and 4. To see any differences in wall temperature they are placed so one is at the end of the cylinder bank and one approximately in the middle. For the other four cylinders only approximate information of in-cylinder conditions are available. The exhaust temperature is measured individually for each cylinder approximately 10 cm downstream of the exhaust ports, using type K thermocouples. The oil temperature, cooling water temperature and intake air temperature are also measured. The emission analysis equipment consists of a flame ionization detector (FID) for measuring HC, a chemiluminecence detector (CLD) for measuring nitrogen oxides (NO_x), a non dispersive infra red (NDIR) detector for measuring carbon dioxide (CO_2) and carbon monoxide (CO) and a paramagnetic detector for measuring oxygen (O_2). The AFR is measured with an Etas LA3 lambda meter with a Bosch broadband lambda probe. Fuel consumption is measured with a Sartorius LP6200S scale where the fuel cannister is placed. The brake torque is obtained using a load cell, but is not very accurate at low load.

DATA AQUISITION

For each operating point various data is saved. The in-cylinder pressure for all cylinders is saved for 100 consecutive cycles with a resolution of 1 CAD. This is done using a 16 bit multiplexed A/D converter with simultaneous sample and hold, which is connected to a PC. For all other signals, e.g. torque, exhaust temperatures, fuel flow, AFR, oil and water temperatures e.t.c., approximately 20 values are saved during a 2 minute period. This is done using a Hewlett-Packard logger connected to a PC. All crank angle resolved signals are synchronized using a Leine & Linde incremental encoder.

METHOD

The engine used in this work has a compression ratio typical for SI engines and hence a compression temperature too low for auto ignition of normal gasoline. To attain HCCI operation the compression temperature needs to be raised to the point of auto-ignition and in this work this is accomplished by using large negative valve overlap thus trapping hot residuals. Overlap from 140 to 200 CAD is used. Considering trapped volume normalized by displacement volume this would be in between 40 to 70 %, this is an indication of how much residuals can be kept within the cylinder. In this calculation tuning effects and flow characteristics have not been taken into account. Phasing the camshafts during operation is not an option so the engine's operating range is investigated separately for each

negative overlap. Varying the negative overlap is done by stopping the engine and manually phasing the camshafts.

During tests where the effect of the inlet air temperature is investigated the inlet air heat exchanger is used. The desired temperature is set in the engine management system that controls the flow of hot and cold tap water to the secondary side of the heat exchanger.

RESULTS AND DISCUSSION

HCCI OPERATING REGIMES

To get the engine running in HCCI mode the amount of residuals must be sufficient to obtain auto ignition. At low speed, high load HCCI is achieved by starting the engine in SI mode and then advancing the timing until the engine runs in spark assisted HCCI mode. At higher speed the first cycle is still spark ignited without residual gas however in the next cycle the cylinder contains enough trapped hot residuals so the engine runs directly in spark assisted HCCI. At even higher speed the engine runs smoothly without ignition, however it isn't possible to start without spark ignition since no hot residuals are present.

The engine load is altered by changing various parameters: Increasing the negative valve overlap increases the amount of trapped residuals. Thereby the amount of fresh air that enters the cylinder decreases, which results in a lower load and slower reaction rate. Altering the air fuel ratio directly affects the amount of fuel and thereby controls the engine load. If the emissions of NO_x are low the engine can be run on lean mixtures, otherwise it has to be run using the three way catalyst at stoichiometric mixture. A third way of altering the engine load is by throttling; this is the least desirable option since this increases the pumping work.

At low speed the engine is run at • 1 to get within the limits for ignition, whereas at higher speed the engine runs with a leaner mixture. Above 3000rpm it runs with approximately • 1.3. At high speed the mixture is enriched to increase the load, but an excessive reaction rate makes it difficult.

The tests are initiated at a symmetric negative overlap of 140 CAD and are then increased in steps of 10 degrees up to 200 CAD negative valve overlap. For each overlap, attempts to run in HCCI are made at speeds from 650 to 4000rpm. Figure 1 describes the attainable operating regime and the limit to where it is possible to run without spark assistance. At higher speed the reason for spark assistance is mainly to prevent misfire, at very low speed the spark is fired early resulting in a slow heat release and temperature increase until the temperature reaches auto ignition temperature. At high speed the spark is fired at TDC. An early spark at higher speed when the amount of residuals is high can result in wery early combustion timing with pressure rise that can damage the engine. All points are run with an intake temperature of 50°C.

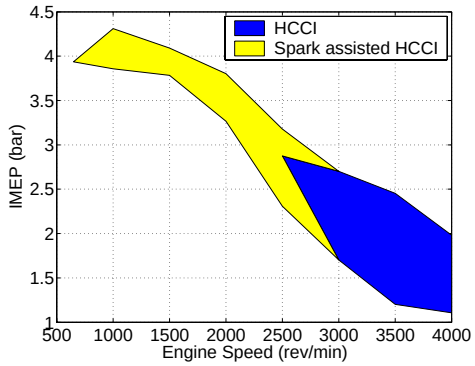

Figure 1. Operating regime and limit between HCCI and spark assisted HCCI.

The HCCI operating regime is limited by several factors. The combustion must be slowed down to avoid damaging in-cylinder pressure and pressure derivatives; this is done by diluting the mixture compared to the ordinary SI engine. In this case by trapping hot residuals in the cylinder. The short intake duration gives the HCCI engine a disadvantage at very high loads. Therefore HCCI operation is not very useful at high speed where the engine usually is run at high load. In this study measurements are made up to 4000rpm. It is most likely possible to obtain HCCI at higher speed, but already at 4000 rpm the indicated load is very low and comparable to the friction work.

The lower load limit is set by high cycle-to-cycle variations and misfire. Passing the limit for spark assisted HCCI may result in misfire, if the mixture is highly diluted it will not ignite at all. As a result the next cycle will not have any residual gas but some of the fuel will still be present in the cylinder. The result is very fast combustion also known as knock.

The reason for misfire in the low load region is basically that the residual gas is too cold for the mixture to self ignite when it is diluted, especially at low speed.

At higher load the problem is the opposite, high load is restricted by the fast reaction rate

INTAKE AIR TEMPERATURE VARIATION

The effect of changes in the intake temperature is studied to simulate realistic variations in ambient

temperature. The effects on combustion stability and emissions are specially studied. Several points are tested by changing the intake temperature in the span from 15 to 50°C, tests are made both with spark assisted HCCI and without spark assistance.

The intention is to study the effect of intake temperature at a given load. The points compared have the same load and negative overlap, but as a result of the change in temperature the AFR differs somewhat due to different air density. All points are run with a lean air/fuel mixture with lambda from 1.20 to 1.33. The readings of COV_{imep}, COV_{pmax} and CA50 are all an average from cylinders 1 and 4.

3500 rpm, 2bar IMEP

This point is run both with and with out spark assistance at a speed of 3500rpm and a load of 2.0 bar IMEP and 200 CAD negative overlap. Ignition angle is set to TDC when spark assisted. As expected the combustion timing is later for points that run with low intake temperature compared to high, but the difference is only a few CAD. Figure 2 shows the Rate of heat release (ROHR) and the pressure trace for spark assisted HCCI when the temperature is decreased from 50 to 15ºC. The plot shows three of the five measuring points taken, 50, 30 and 15 degrees. This makes it easier to separate the points and still shows the accurate course of events. The measuring point at 15ºC is at 2% lower load, this helps explaining the greater difference between 30 and 15ºC compared to 50 and 30ºC. The changes between cylinder 1 and 4 and the changes between HCCI and spark assisted HCCI was small in ROHR.

With an inlet air temperature of roughly 50°C the crank angle of 50 % burned mass (CA50) occurs at 4.5 CAD ATDC. By lowering the temperature, CA50 increases to 6.7 CAD ATDC. There is no great difference in CA50 between spark assisted HCCI and unassisted. The behaviour is similar when lowering the inlet temperature, which is shown in Figure 3. CA50 for each cylinder for spark assisted HCCI is shown in Figure 4. Here it can be seen that cylinder 1 and 4 with sufficient accuracy shows the behaviour of all cylinders. This has been the case for all measuring points.

When lowering the intake temperature the combustion stability also deteriorates, COV_{imep} and COV_{pmax} increase as shown in Figure 5. Figure 6 shows this for the unassisted HCCI points. The difference between spark assisted and unassisted HCCI is not very prominent. The overall magnitude of COV is also low.

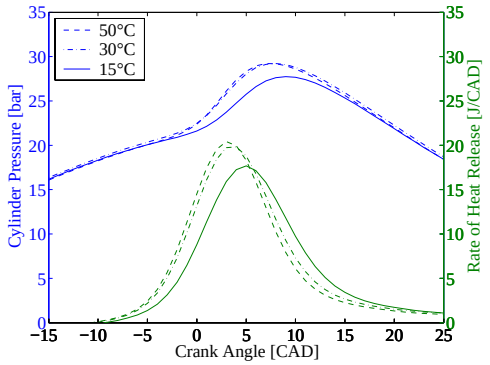

Figure 2. Pressure traces and ROHR for cylinder 1 with different intake temperature at 3500 rpm, 2 bar IMEP for spark assisted HCCI.

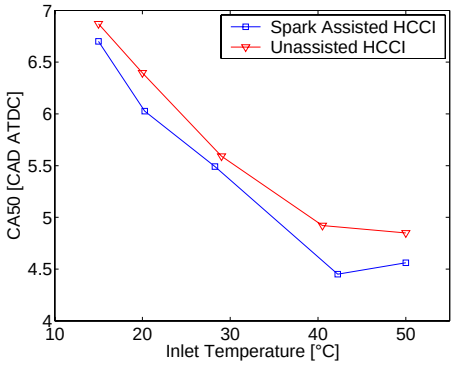

Figure 3. CA50 for both spark assisted and unassisted HCCI between 15 and 50°C at 3500 rpm, 2 bar IMEP.

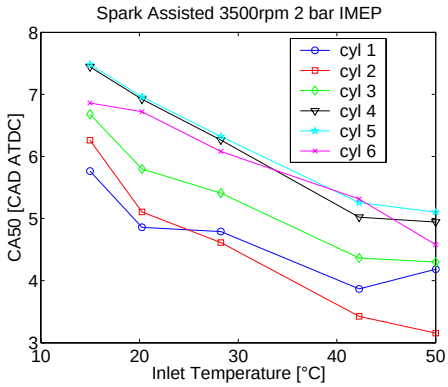

Figure 4. CA50 for all 6 cylinders between 15 and 50°C at 3500 rpm, 2 bar IMEP for spark assisted HCCI

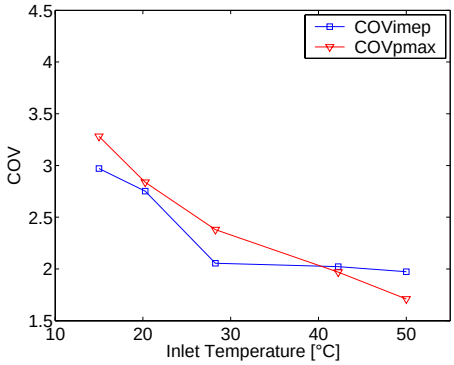

Figure 5. Decrease of the COV as a function of intake temperature for spark assisted HCCI at 3500 rpm, 2 bar IMEP.

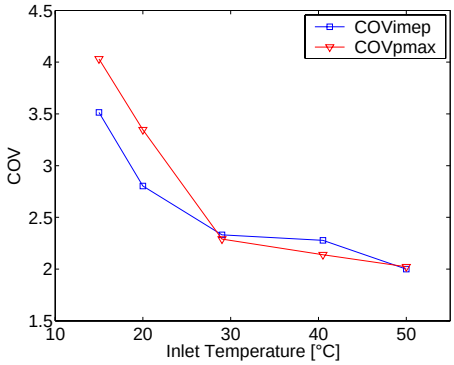

Figure 6. Decrease of the COV as a function of inlet temperature for unassisted HCCI at 3500 rpm, 2 bar IMEP.

A further comparison between spark assisted and unassisted HCCI is made at this load. The indicated specific fuel consumption (ISFC) for the various points is revealed in Figure 7. Due to the deteriorated combustion stability ISFC is expected to rise when the inlet temperature is lowered, which is the case with spark assisted operation while unassisted operation does not change much from the high temperature operation point. The changes are however very small.

An indication that the combustion temperature is a bit low is the indicated specific emissions, especially indicated specific HC (ISHC) that increases some when lowering the inlet temperature, also indicated specific CO (ISCO) increases while indicated specific NOx ($ISNO_x$) decreases due to lower temperature. This is shown in Figures 8 through 10.

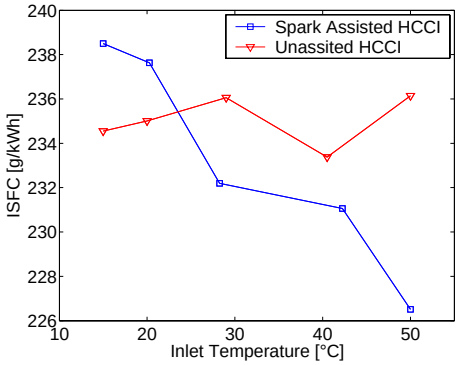

Figure 7. ISFC for 10 and 50°C inlet temperature for both spark assisted and unassisted HCCI at 3500 rpm, 2 bar IMEP.

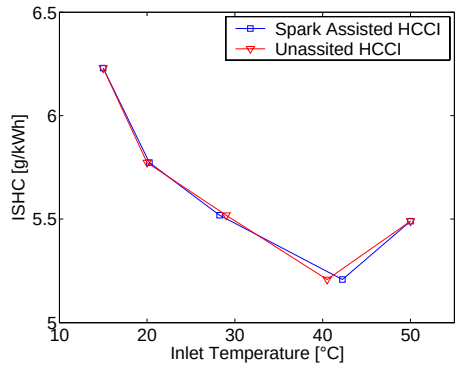

Figure 8. ISHC as function of inlet temperature at 3500 rpm, 2 bar IMEP.

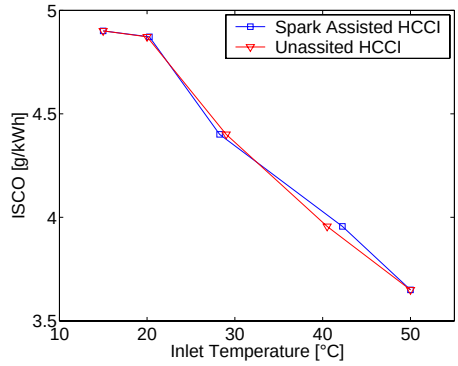

Figure 9. ISCO as function of inlet temperature at 3500 rpm, 2 bar IMEP.

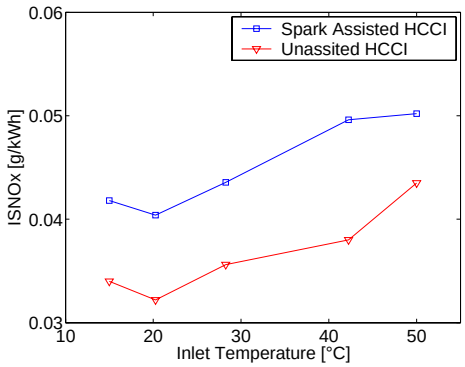

Figure 10. Specific emissions when altering inlet temperature for both spark assisted and unassisted HCCI at 3500 rpm, 2 bar IMEP.

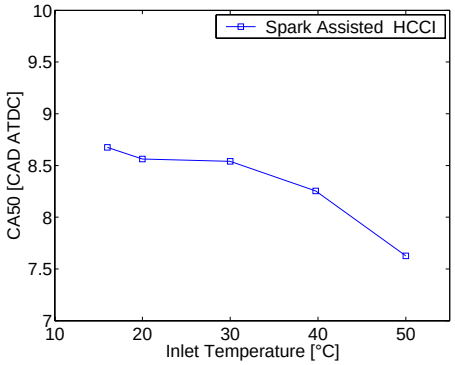

Figure 11. CA50 as a function of intake temperature for spark assisted HCCI operation at 3000 rpm, 2.6 bar IMEP.

8.6.2 3000 rpm, 2.6 bar IMEP

When running unassisted HCCI at 3000rpm, 2.6 bar IMEP with wide open throttle (WOT) and a 200 CAD negative valve overlap the 35° decrease in the ambient temperature can be enough for misfire if the load is to be kept constant without enriching the mixture. Of course a richer mixture keeps the engine going but it also causes higher amounts of NO_x, another problem is the fast reaction rate. For this reason there is a limit to how rich the mixture can be even if the emissions are disregarded. Figure 11 shows the later combustion timing for spark assisted HCCI with lowered intake temperature. For Unassisted HCCI at 50 degrees intake temperature CA50 was about 8.5.

It is clearly shown in Figure 14 that the combustion stability is severely affected when lowering the inlet temperature also for the spark assisted mode. At this point when operating unassisted, some cylinders misfired and stopped when lowering the intake temperature, this is an indication that small cylinder to cylinder variations are much more influential close to the border of the load region. Figure 12 shows the later combustion and the lower ROHR with lower intake temperature for spark assisted HCCI. Figure 13 shows the same spark assisted points for 50 and 15 degrees inlet temperature, but also the single point without spark assistance run at 50 degrees intake temperature. Although this point is run at slightly higher load, it still has later timing and lower ROHR than spark assisted HCCI. This indicates that the spark can stabilize and govern the conditions for HCCI combustion. In Figure 14 the increase in COV_{imep} and COV_{pmax} is shown for spark assisted HCCI. The specific emissions for spark assisted HCCI are revealed in Figure 15, although the combustion stability is affected, the influence on the emissions is not very prominent.

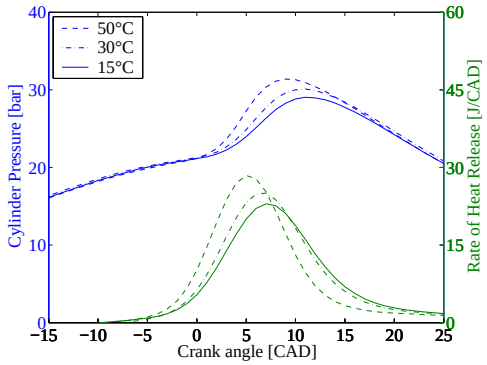

Figure 12. Pressure traces and ROHR for cylinder 1 with different intake temperature at 3000 rpm, 2.6 bar IMEP for spark assisted HCCI

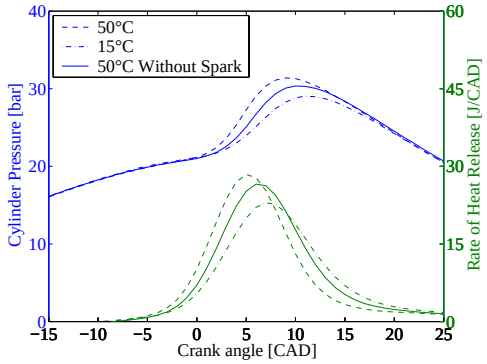

Figure 13. Pressure traces and ROHR for cylinder 1 with different intake temperature at 3000 rpm, 2.6 bar IMEP, showing later timing without spark assistance

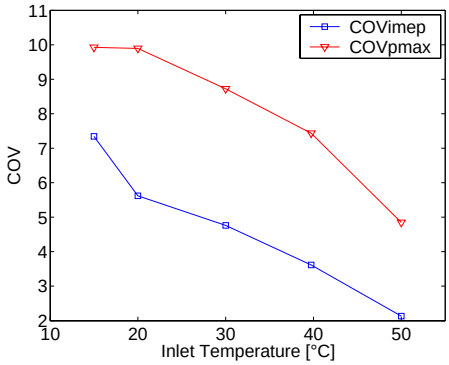

Figure 14. Increase of the COV as a function of lowered temperature for spark assisted HCCI at 3000rpm, 2.6 bar IMEP.

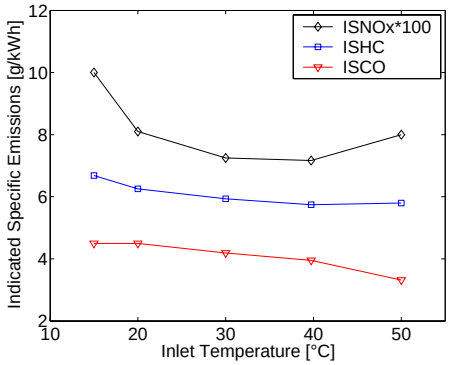

Figure 15. Specific emissions when altering inlet temperature for spark assisted HCCI at 3000rpm, 2.6 bar IMEP.

8.6.3 4000 rpm, 1.6 bar IMEP

At 4000 rpm the engine runs smoothly both with and without ignition and the effect of the inlet temperature decrease is small due to the higher amount of residuals, partially because of lower volumetric efficiency despite a decrease of the negative overlap to 190 degrees. CA50 is approximately between 5 and 5.5 ATDC as shown in Figure 16. Figures 17 and 18 show pressure traces and ROHR for spark assisted and unassisted HCCI. For both cases the ROHR decreases for lower intake temperature, but the differences are very small. As also can be seen in figure 16 the changes between spark assisted and unassisted HCCI are more or less insignificant, this is also the case when comparing ROHR for spark assisted and unassisted HCCI.

Both COVimep and COVpmax are low and never exceed 3%, this is shown in Figure 19. Compared to COV at 3500 and 3000rpm shown in Figure 5, 6 and 14 no similar increase in COV can be seen when lowering the inlet temperature at 4000rpm, this can be explained by the high amount of hot residuals that raises the temperature well above the critical temperature. The emissions shown in figure 20 and 21 are also relatively constant when the intake temperature is changed.

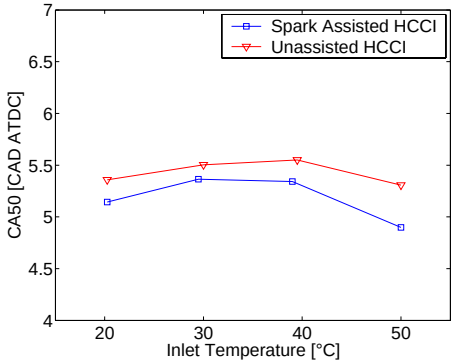

Figure 16. CA50 as a function of intake temperature for both spark assisted and unassisted HCCI operation at 4000 rpm, 1.6 bar IMEP.

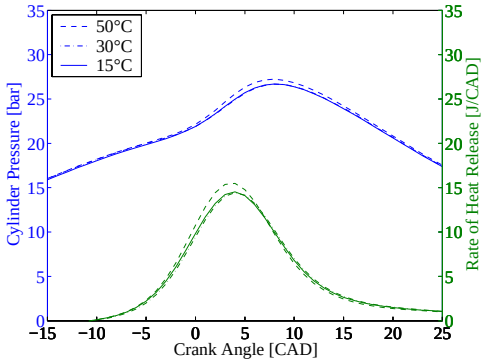

Figure 17. Pressure traces and ROHR for cylinder 1 with different intake temperature at 4000 rpm, 1.6 bar IMEP, for spark assisted HCCI

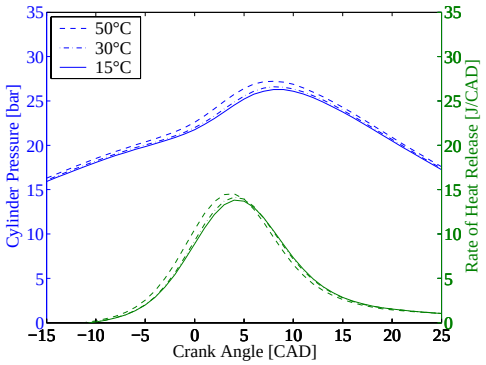

Figure 18. Pressure traces and ROHR for cylinder 1 with different intake temperature at 4000 rpm, 1.6 bar IMEP, without spark assistance

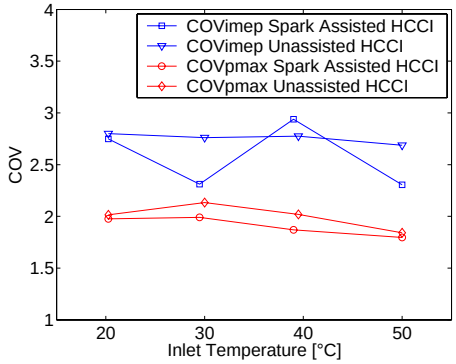

Figure 19. COV as a function of intake temperature for both spark assisted and unassisted HCCI operation at 4000 rpm, 1.6 bar IMEP.

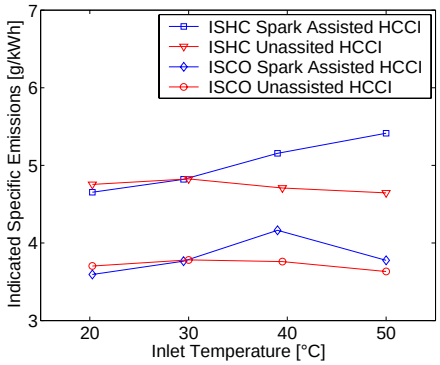

Figure 20. ISHC and ISCO as a function of intake temperature for both spark assisted and unassisted HCCI operation at 4000rpm, 1.6 bar IMEP.

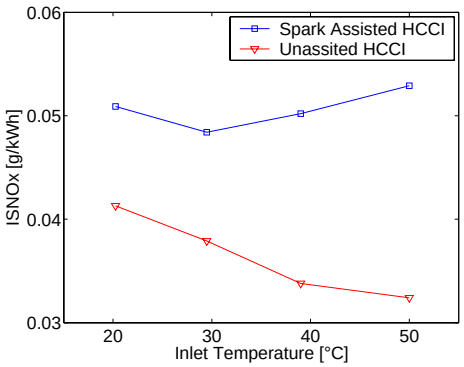

Figure 21. NOx as a function of intake temperature for both spark assisted and unassisted HCCI operation at 4000rpm, 1.6 bar IMEP.

Indicated efficiency

The indicated efficiency is shown in Figures 22 and 23 for both Spark assisted and unassisted HCCI. The difference is not very prominent between the different Speed/load points or between spark assisted and unassisted HCCI. What can be seen here is the later timing at lower speed, the most important reason for this is the lower amount of hot residuals at lower speed. The overall indicated efficiency is between 34 and 37 %.

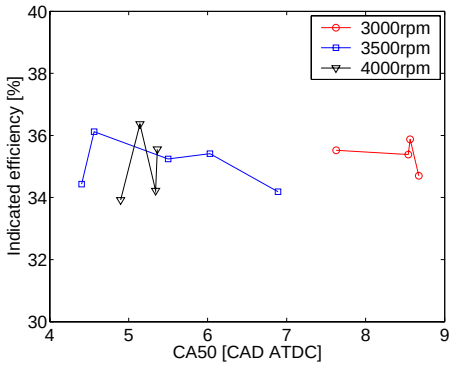

Figure 22. Indicated efficiency for spark assisted HCCI at 3000rpm 2.6 bar IMEP, 3500rpm 2 bar IMEP and 4000rpm 1.6 bar IMEP

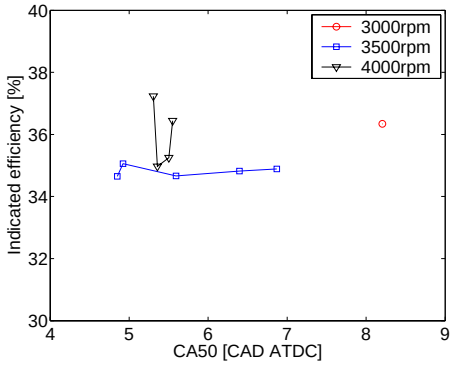

Figure 23. Indicated efficiency for unassisted HCCI at 3000rpm 2.6 bar IMEP, 3500rpm 2 bar IMEP and 4000rpm 1.6 bar IMEP

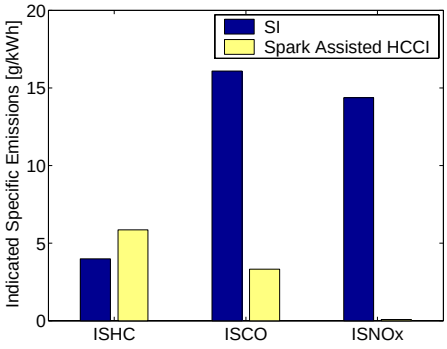

Figure 25. Specific emissions as comparison between SI and HCCI operation at 3000rpm, 2.6 bar IMEP.

Comparison with SI-Operation

To be able to relate the magnitude of the emissions, the COV and the ISFC, a comparison is made for a single point at a speed of 3000rpm, 2.6 bar IMEP between SI and HCCI operation. In SI-operation the engine is run at λ 1 with an intake temperature of 20°C, the emissions are measured engine out. For HCCI the engine is run spark assisted with spark timing at TDC. It is run on a lean mixture at λ 1.3, with an intake temperature of 50°C. Figure 24 shows a comparison of COV_{imep} and COV_{Pmax} for SI versus HCCI operation. It can be seen that both COVIMEP and COV_{Pmax} are of the same order of magnitude for SI and HCCI. A comparison of engine out emissions is shown in Figure 25. As could be expected the emission of ISHC is somewhat higher for HCCI operation due to lower in cylinder temperature. The low combustion temperature for HCCI also results in ISNOx emissions less than a hundredth compared to SI-operation. The lower ISCO for HCCI operation is mainly due to the lean combustion.

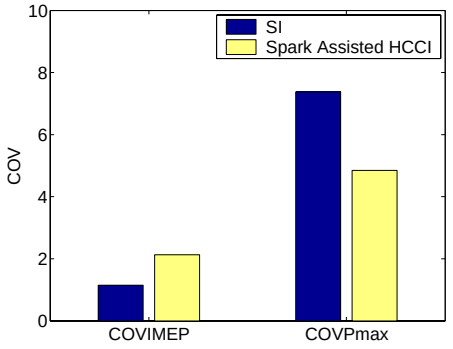

Figure 24. COVIMEP and COVPmax as comparison between SI and HCCI operation at 3000rpm, 2.6 bar IMEP.

At 3000 rpm and 2.6 bar IMEP the ISFC for HCCI is 230 g/kWh, for SI operation it is 290 g/kWh. The benefit in terms of ISFC from HCCI at this point of operation is more than 20 % compared to SI. For all HCCI operating points above 2000rpm the ISFC is more than 15 % lower compared to SI, mainly due to less heat and pumping losses for HCCI operation. This can be seen in Figure 26 in terms of MEP. FuelMEP described by Olsson et. al. [14], is the normalized heat of fuel supplied from the fuel system in one cycle, defined by Equation 1.

$$FuelMEP \equiv \sum \frac{\dot{m}_{FUEL} \cdot Q_{LHV,FUEL}}{n/120 \cdot V_{DISP}} \qquad \text{(Eq.1)}$$

QMEP is a similar normalization of the total accumulated heat release per cycle., IMEP gross (IMEPg) refers to compression/expansion only whereas IMEP net (IMEPn) refers to the full cycle.

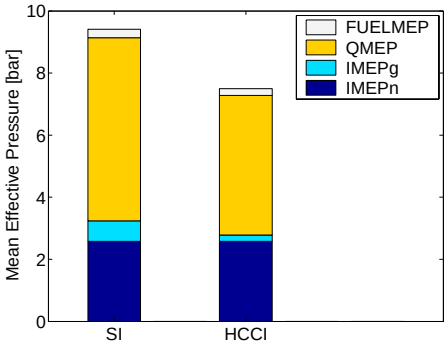

Figure 26. MEP at 3000rpm, left column SI and right column HCCI. For both columns bars are placed behind each other, all starting at zero.

CONCLUSIONS

The ambient conditions are important for ordinary HCCI combustion but when running on gasoline with large amounts of residuals to achieve auto ignition the sensitivity is lower. When running spark assisted the sensitivity to ambient conditions drops even further. Still a too low intake temperature can result in a misfire with high emissions as a result. At the limit to misfire the COV_{imep} and COV_{pmax} are very high which is unacceptable in a practical application. By keeping the amount of residuals high enough and thereby raising the temperature the COV and the risk of misfire is kept low. If high residual fraction is not an option due to high load demand, a small increase of the inlet temperature lowers COV and stabilises the combustion with as well as without ignition.

The low impact of the intake temperature is due to the high amount of hot residuals with much higher temperature than the intake air so the intake temperature does not affect the charge temperature at IVC in the same magnitude as it does for HCCI with higher compression ratios and low fractions of trapped residuals. This is also shown by the later timing for lower speed despite higher load.

The small changes in combustion timing well inside the operating regime, when changing the intake temperature is a big advantage in terms of engine control. It means that one parameter less has to be controlled. The combustion can be maintained without advanced control mechanisms.

For the objective of broadening the operating regime of HCCI by negative valve overlap the inlet air temperature does not have to be controlled, but if kept high, the heated air can have the same effect as a little more valve overlap in terms of charge temperature, it should not decrease the maximum load for HCCI with negative valve overlap but only extend the low-load capability.

Future work

The use of spark assistance for HCCI broadens the operational regime, but further study is necessary to fully understand how it affects the onset of HCCI combustion.

REFERENCES

1. S. Onishi, S. Hong Jo, K. Shoda, P Do Jo, S Kato: ”Active Thermo-Atmosphere Combustion (ATAC) – A New Combustion Process for Internal Combustion Engines”, SAE Paper 790501
2. N. Lida: ”Combustion Analysis of Methanol-Fueled Active Thermo-Atmosphere Combustion (ATAC) Engine Using a Spectroscopic Observation”, SAE Paper 940684
3. P. Najt, D. E. Foster: ”Compression-Ignited Homogeneous Charge Combustion”,SAE Paper 830264
4. M. Christensen, P. Einewall, B. Johansson: “Homogeneous Charge Compression Ignition (HCCI) Using Isooctane, Ethanol and Natural Gas – A Comparison to Spark Ignition Operation”, SAE Paper 972874
5. A. Hultqvist, M. Christensen, B. Johansson, A. Franke, M. Richter, M. Aldén: “A study of the Homogeneous Charge Compression Ignition Combustion Process by Chemiluminescence Imaging”, SAE Paper 1999-01-3680
6. J-O. Olsson, O. Erlandsson, B. Johansson: ”Experiments and Simulations of a Six-Cylinder Homogeneous Charge Compression Ignition (HCCI) Engine”, SAE Paper 2000-01-2867
7. J-O. Olsson, P. Tunestål, G. Haraldsson, B. Johansson: ”A Turbo Charged Dual Fuel HCCI Engine”, SAE Paper 2001-01-1896
8. S. Aceves, J. Martinez-Frias, D. Flowers, J Smith: “A Decoupled Model of Detailed Fluid Mechanics Followed by Detailed Chemical Kinetics for Prediction of Iso-Octane HCCI Combustion”, SAE Paper 2001-01-3612
9. M. Christensen, B. Johansson, P. Amnéus, F. Mauss: “Supercharged Homogeneous Charge Compression Ignition”, SAE Paper 980787
10. L. Koopmans, H. Ström, S. Lundgren, O. Backlund, I. Denbratt: “Demonstrating a SI-HCCI-SI Mode Change on a Volvo 5-Cylinder Electronic Valve Control Engine”, SAE Paper 2003-01-0753
11. H. Zhao, Z. Peng, J. Williams, N. Ladommatos: “Understanding the effects of Recycled Burnt Gases on the Controlled Autoignition (CAI) Combustion in Four Stroke Gasoline Engines”, SAE Paper2001-01-3607
12. J. Li, H. Zhao, N. Ladomatos: “Reserch and Development of Controlled Auto-Ignition (CAI) Combustion in a 4-Stroke Multi-Cylinder Gasoline Engine”, SAE Paper 2001-01-3608
13. L. Koopmans, I. Denbratt: ”A Four Stroke Camless Engine, Operated in Homogeneous Charge Compression Ignition Mode with Commercial Gasoline”, SAE Paper 2001-01-3610
14. J-O. Olsson, P. Tunestål, J. Ulfvik, B. Johansson: ”The Effect of Cooled EGR on Emissions and Performance of a Turbocharged HCCI Engine”, SAE Paper 2003-01-0743

DEFINITIONS, ACRONYMS, ABBREVIATIONS

AFR	Air-Fuel Ratio
ATDC	After Top Dead Center
CAD	Crank Angle Degree
CA50	Crank Angle Degree of 50 % burned mass
CI	Compression Ignition
CO	Carbon monoxide
CO_2	Carbon dioxide
COV	Coefficient Of Variation
FuelMEP	Fuel Mean Effective Pressure
HCCI	Homogeneous Charge Compression Ignition
IMEP	Indicated Mean Effective Pressure
IMEPg	Gross Indicated Mean Effective Pressure
IMEPn	Net Indicated Mean Effective Pressure
IVC	Inlet Valve Closing
ISCO	Indicated Specific Carbon Monoxide
ISFC	Indicated Specific Fuel Consumption
ISHC	Indicated Specific HydroCarbons
$ISNO_x$	Indicated Specific Nitrogen Oxides
NO_x	Nitrogen Oxides
O_2	Oxygen
PID	Proportional, Integral, Derivative
QMEP	Heat Release Mean Effective Pressure
ROHR	Rate of Heat Release
SI	Spark Ignition
TDC	Top Dead Center
WOT	Wide Open Throttle

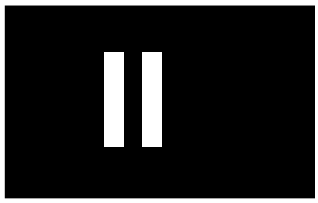

2005-01-0130

Cylinder-to-Cylinder and Cycle-to-Cycle Variations at HCCI Operation with Trapped Residuals

H. Persson, R. Pfeiffer, A. Hultqvist, B. Johansson
Lund Institute of Technology

H. Ström
Volvo Car Corporation

ABSTRACT

A naturally aspirated in-line six-cylinder 2.9-litre Volvo engine is operated in Homogeneous Charge Compression Ignition (HCCI) mode, using camshafts with low lift and short duration generating negative valve overlap. Standard port fuel injection is used and pistons and cylinder head are unchanged from the automotive application.

HCCI through negative valve overlap is recognized as one of the possible implementation strategies of HCCI closest to production. It is important to gain knowledge of the constraints and limits on the possible operating region. In this work, the emphasis is on investigating how cycle-to-cycle and cylinder-to-cylinder deviations limit the operating region, how these effects change in different parts of the operating region and how they can be controlled.

At low load the cycle-to-cycle phenomena cause periodic behavior in combustion timing; together with cylinder deviations this is found responsible for decreasing the operating regime. Increasing the operating region by spark assistance is demonstrated and also the possibility to phase combustion timing by advance of the spark timing.

The combustion is monitored in real time using cylinder pressure sensors. Emissions are measured individually for each cylinder. Results are discussed in terms of Coefficient Of Variation (COV), auto correlation coefficient (R), Crank Angle 50% burned (CA50) and emissions in terms of Indicated Specific Carbon Monoxides (ISCO), Hydro Carbons (ISHC) and Nitrogen Oxides (ISNOx).

INTRODUCTION

Homogeneous Charge Compression Ignition (HCCI) can be seen as a combination of the ordinary Spark Ignition (SI) and the Compression Ignition (CI) engines. Similar to the SI engine, the HCCI engine is port fuel injected creating a close to homogeneous mixture. During compression the temperature increases to the point of auto-ignition. As in the CI engine, the mixture is ignited without the help of an ignition system. The challenge for HCCI compared to the SI and CI engines is that ignition timing is dependent on the in-cylinder temperature and is not directly controlled.

The early studies of HCCI combustion were made on two-stroke engines in an effort to reduce the hydrocarbon (HC) emissions at part load operation [1]. Later, in 1983, Najt and Foster showed that it was possible to attain HCCI combustion in 4-stroke engines [2]. Studies have reported low NOx emissions and high efficiency compared to the SI-engine[3]. More recent studies have been focused on emissions and improving efficiency in 4-stroke engines [4-6]. HCCI with negative valve overlap, trapping hot residuals to attain auto ignition, was first presented by Willand et al. [7]. Both experiments and simulations have been presented, also different valve strategies and mode shifts from SI to HCCI and back have been reported [8-12].

In HCCI combustion a homogeneous mixture is compressed until the point of auto ignition; this inhibits flame propagation and instead the whole bulk ignites at the same time. It is commonly accepted that the onset of HCCI combustion is controlled by chemical kinetics [13,14]. Consequently, the combustion timing will be influenced by Air-Fuel Ratio (AFR), inlet temperature, Compression Ratio (CR) and residual gases.

HCCI combustion with trapped residuals is seen as a means to achieve higher efficiency at part load compared to throttled SI-operation.

Cycle-to-cycle phenomena in SI and HCCI combustion differ; in the SI engine they are mainly due to variations in the early flame propagation [15,16]. In an HCCI engine running with trapped residuals there is a strong coupling from cycle-to-cycle [17].

The effect of cylinder-to-cylinder deviations and also the cycle-to-cycle coupling and variations are important issues because these effects limit the obtainable operating region [18]. In this paper, the effects are studied in an engine with low compression ratio that relies on trapped hot residuals to attain auto ignition temperature. Due to the hot residuals the combustion in one cycle can affect the next in a much more extensive way than an HCCI engine run with little or no residual gas.

In earlier work by the author, effects of spark assistance have been shown [19], therefore the possibility of stabilizing the combustion in terms of cylinder-to-cylinder and cycle-to-cycle variations and to extend the obtainable operating region by spark assistance is studied, especially at low speed and load.

EXPERIMENTAL SETUP

ENGINE

The test engine is an in-line six-cylinder engine with a total displacement of 2.9L (Table 1). To achieve HCCI combustion, auto ignition temperature must be reached. The cams are phased so the Exhaust Valve Closes (EVC) early in the exhaust stroke trapping hot residuals. This is followed by late Intake Valve Opening (IVO) generating a negative valve overlap. To accomplish this cams comprising low lift and short duration are used. At Inlet Valve Closure (IVC), a raised charge temperature is achieved, and the charge is diluted with residuals. The engine is equipped with cam phasing mechanisms, making it possible to phase both intake and exhaust cams during engine operation. This makes it possible to make mode switches from SI to HCCI by increasing the negative valve overlap, thus increasing the amount of residuals, and vice versa from HCCI to SI. A too high negative valve overlap will however not only increase the amount of residuals. It will also predate on the compression stroke since IVC will take place well after Bottom Dead Center (BDC) and the effective compression ratio will decrease.

Table 1. Engine data.

Displacement	2922 cm^3
Number of cylinders	6
Bore	83 mm
Stroke	90 mm
Compression ratio	10.3:1
Valve lift	3 mm
Inlet/Exhaust valve duration	150 CAD
Possible negative valve overlap	100-220 CAD
Fuel	RON 98
Water temperature	95°C
Inlet temperature	50°C

All six fuel injectors used are calibrated and differ less than 3 % in injected fuel mass. This deviation is accounted for in the engine management program. The ignition system is the standard system from the production engine with one ignition coil for each spark plug.

The engine is controlled by an in-house developed management system with the ability to set ignition timing, dwell, injection timing, injection duration, cam timing and inlet air temperature to desired values.

MEASUREMENT EQUIPMENT

The in-cylinder pressure is monitored separately for each cylinder using Kistler 6053C60 pressure transducers. The exhaust temperature is measured individually for each cylinder approximately 10 cm downstream of the exhaust ports, using type K thermocouples. The emission analysis equipment consists of a Flame Ionization Detector (FID) for measuring HC, a ChemiLuminescence Detector (CLD) for measuring Nitrogen Oxides (NO_x), a Non Dispersive Infra Red (NDIR) detector for measuring carbon dioxide (CO_2) and carbon monoxide (CO) and a paramagnetic detector for measuring oxygen (O_2). Smoke was not measured. Emissions are measured individually, although not simultaneously, for each cylinder close to the thermocouples as shown in Figure 1. Fuel consumption is measured by a fuel balance.

Figure 1. The Volvo test engine with emission measurements separate for each cylinder.

For each operating point various data are saved. The in-cylinder pressure for all cylinders is saved for 100 consecutive cycles with a resolution of 0.2 Crank Angle Degrees (CAD). This is done using a 16 bit multiplexed A/D converter with simultaneous sample and hold, connected to the control computer for on-line heat release calculations. All other signals, e.g. torque, temperatures, fuel flow, AFR, oil and water temperatures etc. are saved with an approximate frequency of 0.3 Hz with a Hewlett-Packard logger.

RESULTS AND DISCUSSION

The operating regime for this engine is quite narrow in terms of load as shown in Figure 2, however the effects in terms of cylinder-to-cylinder and cycle-to-cycle variations can still be studied. The effects are mainly studied at the border of the operating regime, to see what limits operation at different speeds and loads. The intention is to run with a symmetric valve overlap with gas exchange TDC as the symmetry line. A negative valve overlap from 145 to 205 CAD is used for HCCI operation. For the points run with a large negative overlap the exhaust cam is phased somewhat further than the intake cam, in order to reduce the impact on the compression stroke.

First, both a close to maximum and minimum load sweep is made and studied in detail, later in the text referred to as high and low load case. Then the possibility of stabilizing HCCI combustion with spark assistance at the lower load is examined. For measurement of cycle-to-cycle variations a coefficient of variation (COV) is used which is defined as the standard deviation divided by the mean value. This is done both for fluctuations in maximum pressure (P_{max}) and for net Indicated Mean Effective Pressure (IMEP).

An auto correlation coefficient[1] (R) is also used, earlier used for detecting periodic behavior on HCCI combustion [13]. This correlation coefficient is used to see if there is a pattern for the variations, here applied to Crank Angle 50% burned (CA50). If early combustion timing is followed by late timing in the next cycle and so on, there is a strong negative correlation. The use of CA50 for the correlation gives almost identical results as using P_{max} for detecting the cycle-to-cycle behavior. The cycle-to-cycle behavior is investigated extensively further on in a separate section.

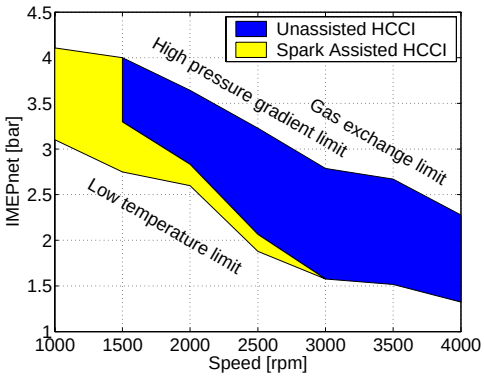

Figure 2. Operating regime for both spark assisted HCCI and unassisted HCCI.

1 See definition in the appendix

SPEED SWEEP

If one takes a look at the difference in load from cylinder to cylinder for a sweep in engine speed at both high and low load (Figure 3), it can be seen that the difference in load is small for each measuring point. It should be noted that the points at 1000 rpm are run with spark assistance.

The difference in IMEP is between 0.1 and 0.3 bar, from cylinder to cylinder. For all speeds, cylinder 5 has a slightly higher load while cylinder 3 runs at a slightly lower load. When looking at the motored peak pressure, cylinder 3 has a slightly lower pressure while cylinder 5 has slightly higher pressure than cylinder average. This could be due to a small difference in compression ratio or due to differences in the dynamics in the intake and exhaust ducts having individual impact on the cylinders.

The high load cases are limited by high rate of pressure rise; the limit has been set to five bar / CAD. In general it is the cylinders with earliest CA50 that limit the load. At high speed, a very early combustion is also limiting the load. This is due to a higher charge temperature caused by an increased amount of residuals and lower heat losses. At higher speed the volumetric efficiency decreases; increasing the amount of residuals. In these cases some cycles will sporadically ignite very early with high rate of pressure rise as a result. A later combustion phasing by decreasing the residual fraction is possible only to a small extent due to misfire.

At low speed an increased amount of hot residuals is needed to raise the charge temperature, thereby expanding the low load capabilities. In order to increase the residuals without affecting the compression stroke, the cam duration needs to be decreased below 150 CAD whilst maintaining the maximum lift.

Figure 4 and Figure 5 show the average CA50 for the two cases. The earlier timing at high speed for the low load case is due to a slightly richer AFR. There is a difference in combustion timing, and a slightly higher cylinder-to-cylinder variation for the low load case, but not a very significant difference, having in mind that no cylinder balancing is conducted. For the low load case there is a greater variation in CA50 at 2500 rpm, this is due to leaner conditions (lambda shown in Figure 9). The opposite is the case for the measuring point at 1500 rpm in the high load case in Figure 4; this point is run slightly richer.

At low speed and load the end cylinders have the latest timing, this can be explained by lower wall temperature. The effect is however not as prominent for cylinder 1 as for cylinder 6. The wall temperature difference due to cylinder placement decreases with increased engine speed and at higher speed no clear effects can be seen. Heat losses to the cylinder walls decrease with increased speed.

Lower heat losses combined with a higher charge temperature due to increased amount of residuals give an earlier timing and ability to run at lower load at high speed.

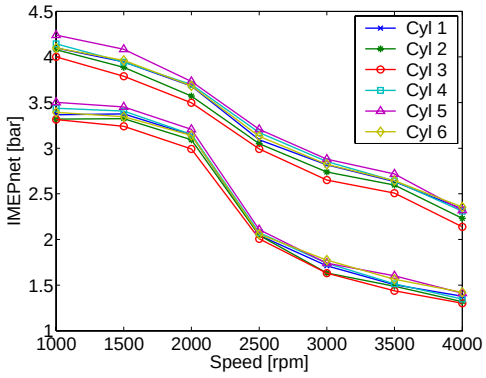

Figure 3. $IMEP_{net}$ for both high and low load HCCI.

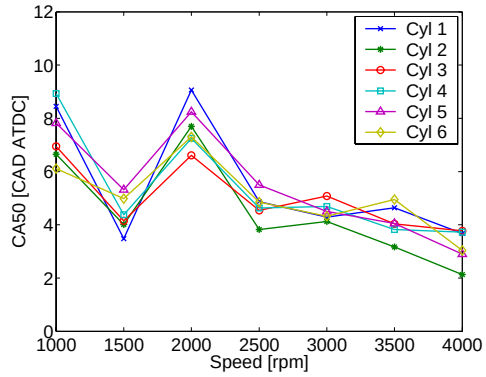

Figure 4. CA50 for high load speed sweep.

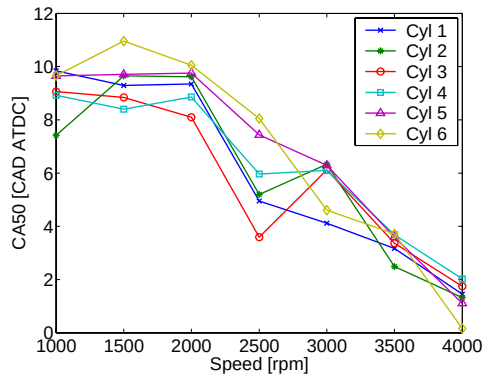

Figure 5. CA50 for low load speed sweep.

When looking at COV for the low load speed sweep in Figure 6, it shows that the absolute values in terms of COV_{imep} are low. COV_{imep} increases with speed from 1500 to 4000 rpm by approximately a factor 2 to 3 but stays at acceptable levels. It is important however to remember that the load at 4000 rpm is less than half the load at 1500rpm, which could explain the increase in COV_{imep}. The variation from cylinder to cylinder is prominent which is expected close to the limit of misfire.

COV_{pmax} shown in Figure 7 decreases with increased speed and its relative variation from cylinder to cylinder is smaller compared to that of COV_{imep}. For increased speed the load is lower and also the peak pressure. The ratio between the peak pressure and the peak pressure for a motored cycle also decreases. This will lower the impact of pressure deviations at higher speed on COV_{pmax}. At the spark assisted point at 1000 rpm the levels are at the limit of what can be accepted. At high speed, the variations are negligible. At lowest speed and minimum load it is the end cylinders 1 and 6 that have the highest COV, mainly due to lower wall temperatures.

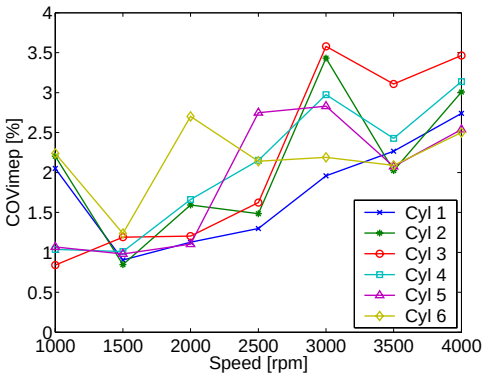

Figure 6. COV_{imep} for low load speed sweep.

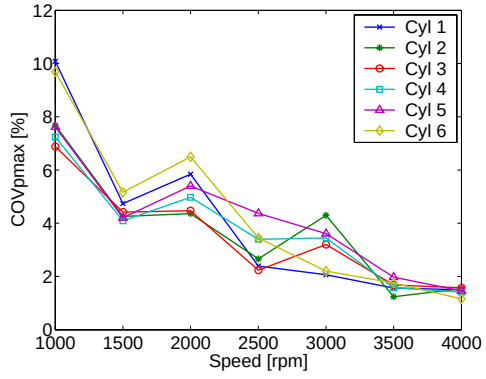

Figure 7. COV_{pmax} for low load speed sweep.

A glance at the emissions shows similar trends for all cylinders (Figure 8). $ISNO_x$ rises by a factor 10 at lower speed. There are several reasons for this. First, the residual fraction for a given overlap decreases at lower speed. Second, the measuring points at low speed are run at higher load and this decreases the residual fraction even more. Third, the points at low speed are run closer to stoichiometric conditions; this is shown in Figure 9. All this together results in a fast reaction rate causing excessive combustion temperature at lower speeds. The reason for not running leaner at low speed is that at this compression ratio and with this cam configuration it is not possible without misfire, unless running spark assisted like the 1000 rpm point. Therefore lambda is not kept constant across the speed range. Also at 1000rpm it would be desirable to run even leaner to lower the NO_x levels.

ISCO and ISHC show very similar trends for each cylinder. ISCO is increased at higher speed due to higher dilution in terms of both AFR and residuals.

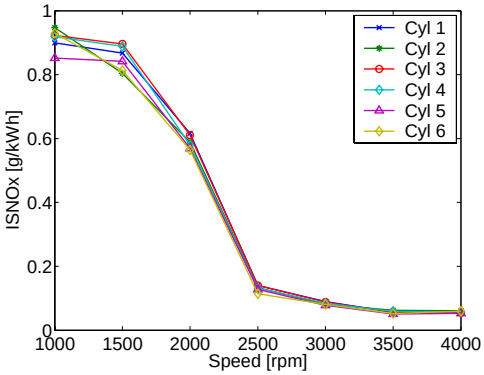

Figure 8. $ISNO_x$ for low load speed sweep.

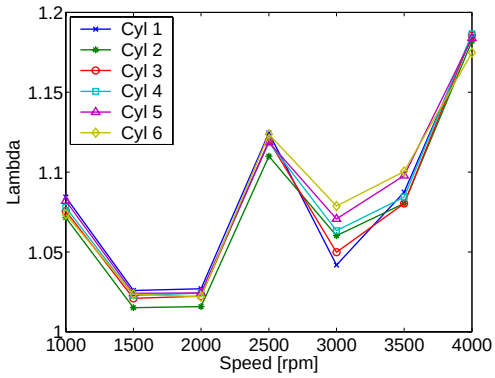

Figure 9. Lambda for low load speed sweep.

Cycle to cycle phenomena

When the temperature conditions for auto ignition is just barely reached for HCCI with trapped residuals, periodic behavior has been observed, i.e. a late burning cycle due to low charge temperature generates high charge temperature for the next cycle resulting in early combustion timing generating low charge temperature and so on. One way of observing this phenomenon is to look at the correlation (R) for CA50 between two consecutive cycles. Figure 10 shows a point at 3000 rpm run under cold conditions. Here a strong negative correlation can be seen for four of the six cylinders. It should be noted that the end cylinders that could be expected to run with the lowest wall temperature have the lowest correlation. On a single measuring point, this could be explained by pressure pulses or a temperature distribution in the intake or exhaust pipes having different impact on the residual fraction for different cylinders, thus on the charge temperature. However, as shown later on, the low correlation is consistent at higher speeds for the end cylinders, especially for cylinder 1. In fact cylinder 1 and 6 run with early combustion timing at 3000 rpm indicating higher charge temperature or wall temperature (Figure 5). No clear explanation has been found for this phenomenon. At lower speed, cylinder 6 has a later combustion timing and a higher correlation than engine average, but the correlation is still low.

To see if the correlation was consistent at this measurement point, several measurements were made at the same operating conditions with approximately 2 minutes between each measurement. The result is shown in Figure 11. Although the absolute levels fluctuate for each cylinder, still the behavior is fairly consistent with low correlation for cylinders 1 and 6.

Figure 12 shows R for the whole speed sweep at low load. Between 2000 and 3500 rpm some correlation can be seen. Especially at 3000 rpm there is a strong negative correlation for cylinder 2, 4 and 5, these cylinders also have high COV_{imep} as seen in Figure 6. Cylinder 3 has on the other hand also high COV_{imep}, but a small R, so a high COV does not necessarily have to imply a high negative cycle to cycle correlation (R), but vice versa.

A correlation investigation is also done with an increased offset in cycles for an array containing the 100 consecutive measured cycles; this is shown in Figure 13. The figure shows cylinder 5 for the measuring point at 3000 rpm with an R of approximately –0.8, which is a strong negative correlation. Here an auto correlation is done for an offset of up to 55 cycles (cycle n vs. cycle n+k, k=1:55). It is obvious that the largest correlation is for an offset of one cycle, which is the same as shown with the correlation coefficient R. For an increased offset in cycles the correlation effect is dampened out. Although the combustion timing fluctuates back and forth from one cycle to the next some slower variations in combustion timing due to for example changes in wall temperatures will decrease the correlation.

Still a higher correlation is recognized again for higher offsets. This is an indication of a disruption in the cycle-to-cycle behavior, i.e. the periodic behavior ceases and starts again, and can then be in counter phase to the earlier periodic behavior. It should be noted though, that the correlation for higher time separation is overall low.

The reason for the self-extinction of the periodic phenomena is that when the changes in combustion timing get high enough, the very late combustion timing will no longer increase the charge temperature for the next cycle. Instead the next cycle will also burn late. Here the phenomena can be extinct or start again in counter phase to the earlier behavior. If the amplitude gets even higher it will not be self stabilizing; instead of a very late combustion, misfire will occur.

A cross-correlation for CA50 between the different cylinders for an increased time separation in cycles is conducted. The correlation from one cylinder to another cylinder in the next cycle is negligible. No communications between the cylinders have been observed in terms of combustion timing.

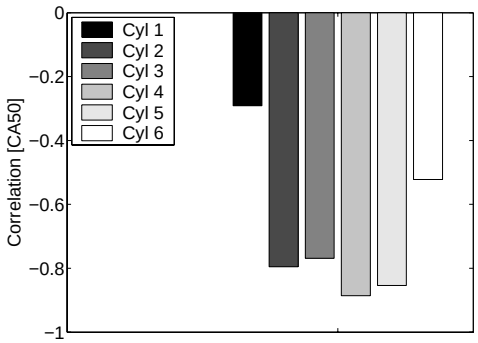

Figure 10. Correlation coefficient for unassisted HCCI at low temperature conditions, 3000 rpm.

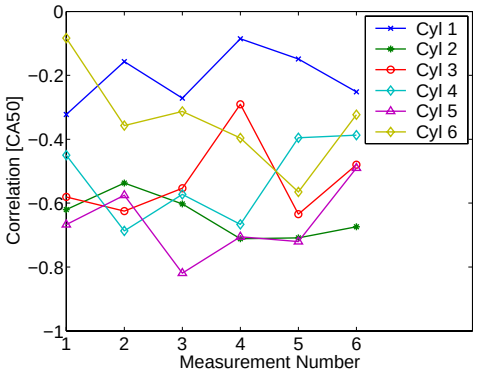

Figure 11. Consistency of the Correlation Coefficient for the same measuring point at 6 repeated measurements.

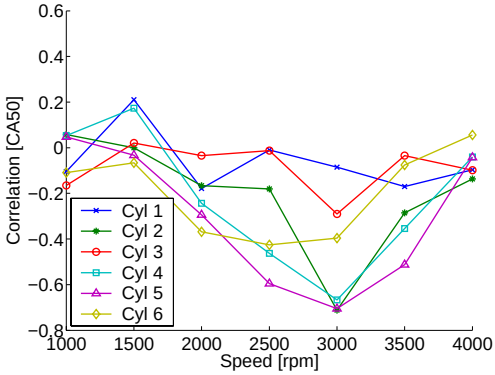

Figure 12. Correlation coefficient for speed sweep at low load.

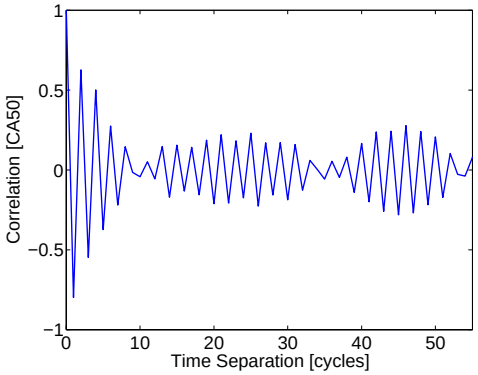

Figure 13. Correlation for CA50 with different time separation in cycles: Cycle n vs. cycle n+k, k=1:55, for cylinder 5 at 3000 rpm.

EFFECTS OF SPARK ASSISTANCE

At lower speed heat losses increase; therefore the lower load limit is at a higher IMEP. Under some conditions, the operating region can be extended by spark assistance. The spark-assisted area of the load regime is shown in Figure 2. Effects of spark assistance have been observed up to 3000 rpm. On the borderline between where ordinary HCCI combustion and spark assisted HCCI takes place the temperature after compression is at the limit for reaching auto ignition.

Figure 14 shows the influence on CA50 by going from unassisted HCCI to spark assisted HCCI with advanced spark timing. Unassisted HCCI is to the left in the figure and advanced timing to the right. This sweep is done for different speeds at the limit for unassisted HCCI. The line for 1000 rpm is spark assisted only.

The effect is more prominent at lower speed, which is also at higher load. For the sweep at 2500 and 3000 rpm there is no obvious change in CA50; however, at 2500 rpm, the load could be lowered further with a spark timing of 40 CAD BTDC. Without spark assistance, the combustion timing was retarded with random early burning cycles followed by misfire. Of course the lack of trapped residuals then hinder the charge from reaching auto ignition temperature again.

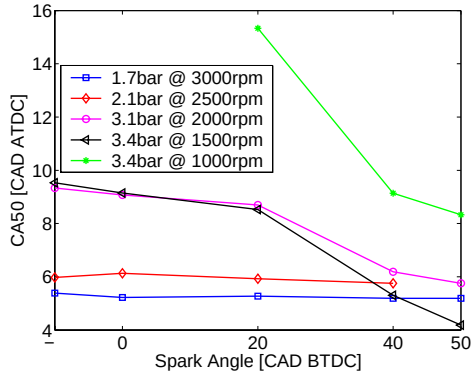

Figure 14. Influence on CA50 for unassisted HCCI and for spark assisted HCCI with advanced spark timing, engine average.

Sweep at 1500 rpm

At 1500 rpm, which is at the lower speed limit for unassisted HCCI due to increasing heat losses at lower speed, a load sweep is performed to investigate how the lower load affects combustion timing and stability. It should be noted that for the higher load cases it should be possible to run below 1500 rpm without spark assistance. However the sweep in engine speed is done in increments of 500 rpm and at 1000 rpm heat losses increase and the amount of residuals trapped for a given negative overlap decreases. A further increase in negative valve overlap will intrude on the compression stroke and thereby also lower the compression temperature. Figure 15 shows the load sweep at 1500 rpm, where the lowest load is spark assisted. It is no surprise that combustion timing is retarded as the load is lowered since wall temperatures and charge temperatures decrease. The point just below 3.8 bar IMEP has considerably higher variation in CA50; this is due to a drop in cooling water temperature, generating lower wall temperature, with the strongest effect on the end cylinder, number 6. For all test cases run on the border of the operating regime a sudden drop in cooling water temperature has a severe impact.

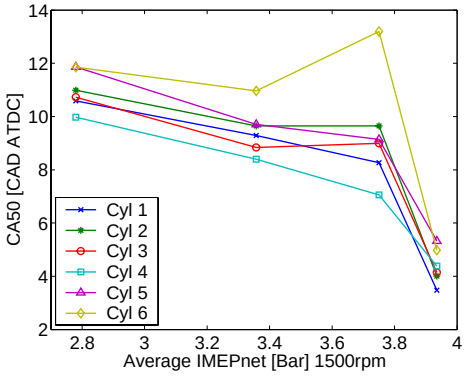

Figure 15. Spread in CA50 for all six cylinders for a load sweep at an engine average in IMEPnet at 1500 rpm.

At the low limit in both speed and load for unassisted HCCI which is the second lowest load point in Figure 15, a spark timing sweep is performed and compared with the unassisted case; this is shown in terms of CA50 in Figure 16. A very strong influence can be seen on all cylinders but still cylinder 6 has the latest combustion timing due to colder conditions. Figure 17 shows the average rate of heat release in J / CAD for the spark timing sweep for cylinder 6. For earlier spark timing the initial rate of heat release is extended and slower than for the unassisted case. This is an indication of some early flame propagation. Later on, the increase in rate of heat release is very similar for all cases indicating HCCI combustion for all cases. The main difference is in combustion timing.

For the cases with spark at 50 CAD BTDC a slightly slower rate of heat release is noted, this can be explained by some late burning cycles that seem unaffected by the spark and therefore run in ordinary HCCI mode, shown in Figure 18. This can be explained by too early spark timing when the charge doesn't have proper conditions for spark assistance. Turbulence levels, pressure and temperature conditions at the spark plug position are not yet sufficient.

It is interesting to see how the advanced combustion timing affects both performance and emissions; Figure 19 shows indicated emissions for the spark timing sweep. ISNOx increases somewhat with early spark timing (earlier than 20 CAD BTDC); this could be expected if any kind of flame propagation occurs. An early combustion itself can of course also increase the temperature and the ISNOx. A small decrease can be seen with a spark set off at top dead center (TDC). The effect on ISHC is only minor, but a small decrease is observed. ISCO is however strongly effected and almost doubled, but this could be as a result of running closer to stoichiometric conditions for early spark angles. Lambda and combustion efficiency are shown in Figure 20. There are no strong effects on combustion efficiency. Figure 21 shows a lower IMEP for very early spark timing. COVimep increases but is still at very moderate levels. COVpmax is slightly decreased up to the earliest spark timing where it rapidly increases and shows a stronger variation in between the cylinders. This is shown in Figure 22 and Figure 23. The increase of COV for very early spark timing is an indication of improper conditions for spark assistance. This was implied earlier regarding Figure 18 that shows the cylinder pressure traces with spark timing at 50 CAD BTDC for cylinder 6.

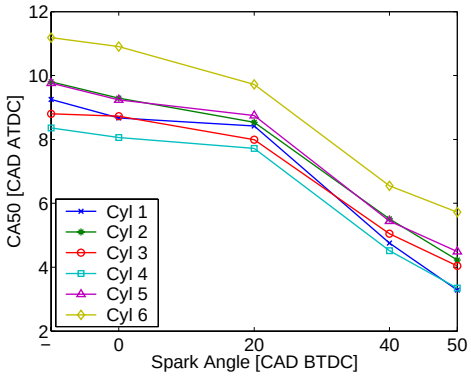

Figure 16. Influence on CA50, from unassisted HCCI to spark assisted HCCI with advanced spark timing, at ~3,4 bar IMEP at 1500 rpm.

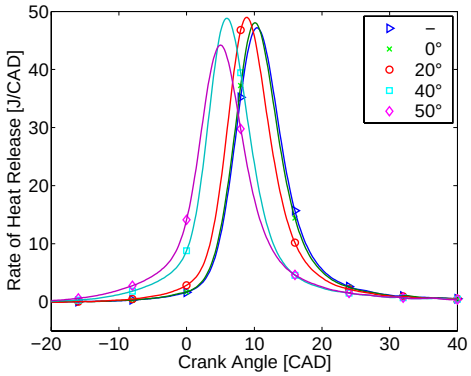

Figure 17. Rate of heat release in J/CAD from unassisted HCCI to spark assisted HCCI with advanced spark timing. cylinder 6 at ~3,4 bar IMEP, 1500 rpm.

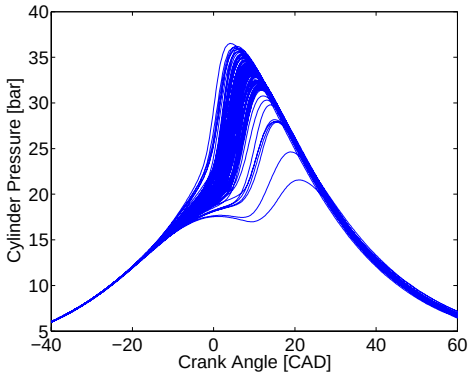

Figure 18. Pressure trace for 100 consecutive cycles for spark assisted HCCI with spark timing at 50 CAD BTDC, cylinder 6 at ~3,4 bar IMEP, 1500 rpm.

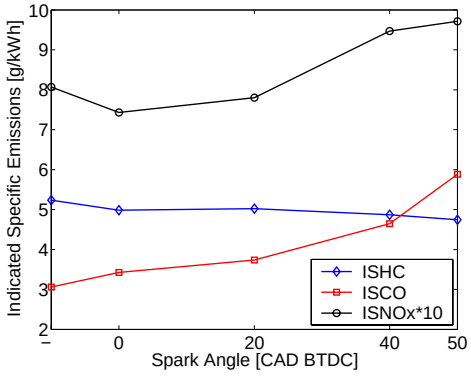

Figure 19. Indicated specific emissions for HCCI with and without spark assistance for cylinder 6 at ~3,4 bar IMEP, 1500 rpm.

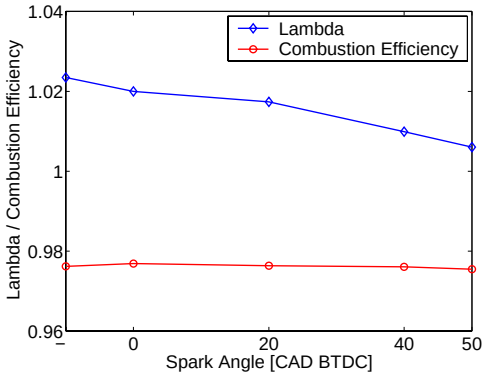

Figure 20. Lambda and combustion efficiency for HCCI with and without spark assistance for cylinder 6 at ~3,4 bar IMEP, 1500 rpm.

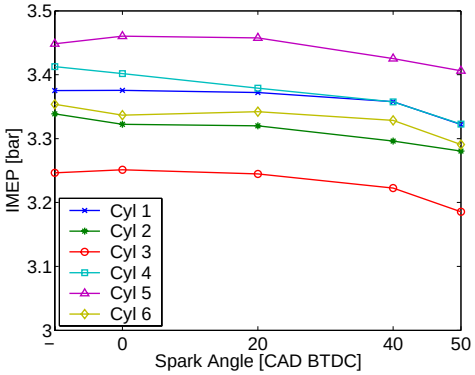

Figure 21. $IMEP_{net}$ from unassisted HCCI to spark assisted HCCI with advanced spark timing at 1500 rpm.

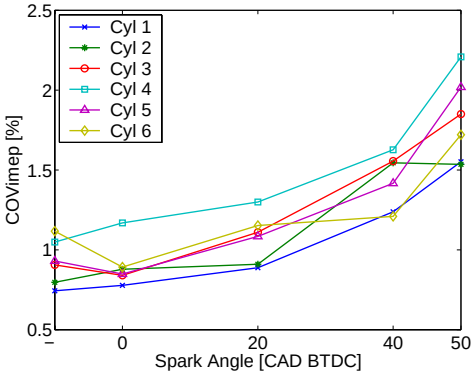

Figure 22. COV_{imep} for HCCI with and without spark assistance for ~3,4 bar IMEP at 1500 rpm.

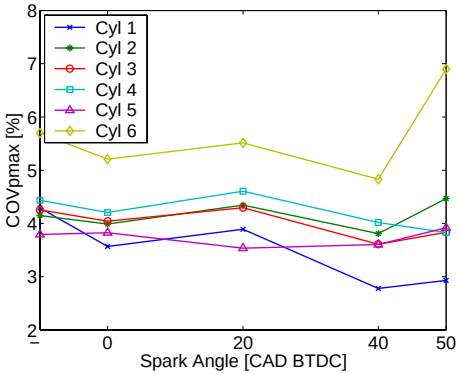

Figure 23. COV_{pmax} for HCCI with and without spark assistance for ~3,4 bar IMEP at 1500 rpm.

Sweep at 1000 rpm

Another spark timing sweep is done at 1000 rpm, which is past the point where it is possible to run without spark assistance. The sweep is done from 20 to 50 CAD BTDC. Later spark timing than 20 CAD BTDC was not possible due to misfire from random cylinders from time to time, due to cold in-cylinder conditions. Figure 24 shows a great advance in CA50 when the spark angle is changed from 20 to 40 CAD BTDC; When the spark angle is further advanced from 40 to 50 CAD BTDC the effect is weaker. Cylinder number 2 has the best response at this point compared to the measuring point at 1500 rpm (Figure 16) where no such effect can be seen for cylinder number 2. The deviations for different measuring points are not easily explained but one reason could be different amounts of residuals giving variations in charge temperature for different cylinders.

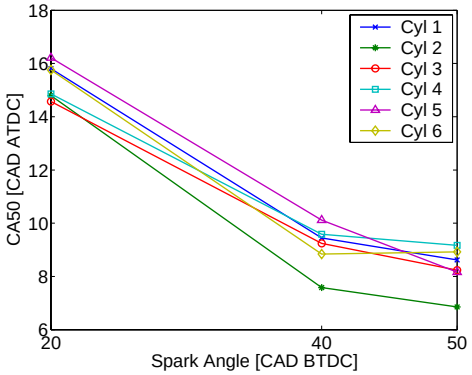

Figure 24. Spark timing sweep for spark assisted HCCI, ~3.4 bar IMEP at 1000 rpm.

The great effect on combustion timing suggests that cylinder individual spark timing could be used to eliminate cylinder-to-cylinder differences in timing. The possibility to run some cylinders without spark assistance for a couple of cycles suggests that a large part of the combustion is in HCCI mode. This is supported by the case with a spark set off at 40 CAD BTDC, generating conditions for HCCI combustion with a fast reaction rate. Accumulated heat release and rate of heat release is shown in Figure 25 and Figure 26. For the case with late spark timing the reaction rate is slower due to later combustion timing. Also for the case with very early spark timing the rate of heat release is lower suggesting more effect of spark assistance, and some initial SI combustion.

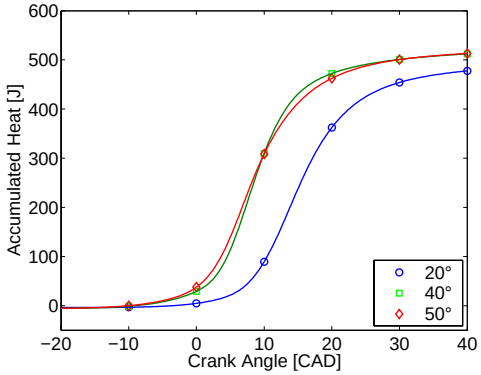

Figure 25. Accumulated heat release with increased spark timing for spark assisted HCCI, cylinder 6, ~3.4bar IMEP at 1000rpm.

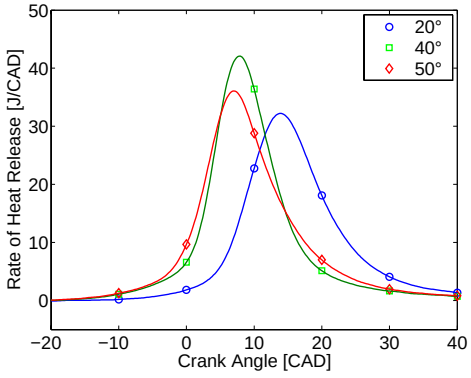

Figure 26. Rate of heat release in J/CAD with increased spark timing for spark assisted HCCI, cylinder 6, ~3,4 bar IMEP at 1000 rpm.

There is an increase in load for advanced spark timing, mainly due to the very late combustion at late spark timing which cases lower efficiency; this is shown in Figure 27. The deviation from cylinder to cylinder in terms of load is below 6 %. An early spark doesn't only improve efficiency, but it also lowers COV_{pmax} and COV_{imep} (Figure 28 and Figure 29). From these observations it can be established that an optimal ignition angle exists. With more measuring points it can be determined more exactly, but from the measured points an ignition angle of 40 CAD BTDC seems to be the optimum. The high levels in COV for spark timing at 50 CAD BTDC is an indication of some cylinders not responding to the early spark, contributing to the slow reaction rate. Figure 30 shows the indicated emissions for the sweep at 1000 rpm. Both ISCO and ISHC are lower with a spark set of at 40 CAD BTDC, mainly due to more stable combustion while $ISNO_x$ increases slightly for early spark timing, possibly due to some flame propagation. The overall high level of $ISNO_x$ is due to a close to stoichiometric mixture, although diluted with residuals.

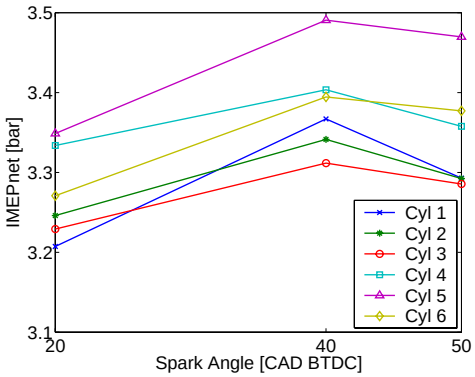

Figure 27. Increased IMEP with increased spark timing for spark assisted HCCI at 1000 rpm.

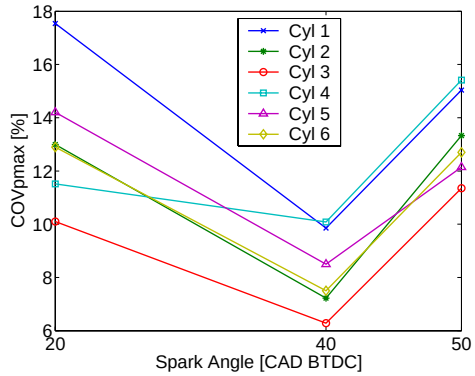

Figure 28. COV_{pmax} with increased spark timing for spark assisted HCCI, ~3.4 bar IMEP at 1000 rpm.

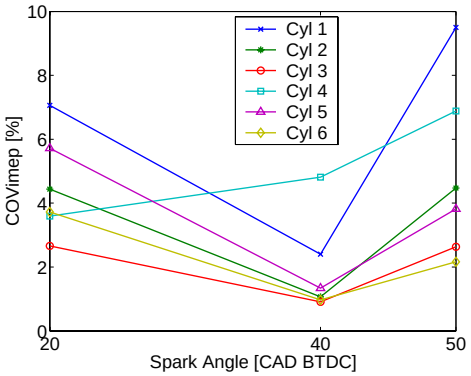

Figure 29. COV_{imep} with increased spark timing for spark assisted HCCI, 3.4 bar IMEP at 1000 rpm.

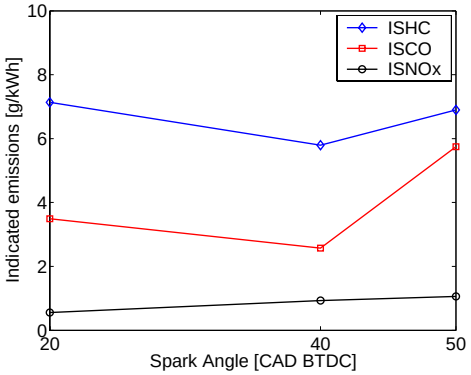

Figure 30. Indicated specific emissions with increased spark timing for spark assisted HCCI, ~3.4 bar IMEP at 1000 rpm.

Correlation Coefficient for Spark assistance

The correlation coefficient (R) has earlier been used to determine HCCI combustion at cold conditions close to the border of misfire. The question is what happens when running spark assisted HCCI at lowest possible load. When the spark is eliminated, the engine will run for a few cycles on some cylinders, but not on all. The cylinders that will keep on going are random for different speeds. Figure 31 shows the correlation coefficient for the spark assisted cases shown also in Figure 2 as the points run at lowest load. Some correlation can be seen for all cases. All cases are run with a spark timing in-between 35 to 45 CAD BTDC.

A distinct difference can be seen from 2000 to 2500rpm. At 2500 and above, R shows much higher negative correlation especially for cylinder 5. Cylinder 5 experiences very large changes in combustion timing and without the spark this cylinder would most likely be the first one to misfire. When running at higher speed and lower load the residual fraction is increased and thus the effect of spark assistance decreases which partially explains the greater difference in R from cylinder to cylinder. At the speed sweep at low load that is show in Figure 12 for unassisted HCCI, an increased negative correlation is observed at the same speeds as in Figure 31. For spark assisted HCCI the correlation is fairly consistent for the points that show impact in timing by spark assistance. At 1000 rpm cylinder 6 has a much higher correlation. Here the in-cylinder temperature is almost too low also for spark assistance. When increasing the spark timing the correlation decreases especially at low speed where the overall impact of spark assistance is higher.

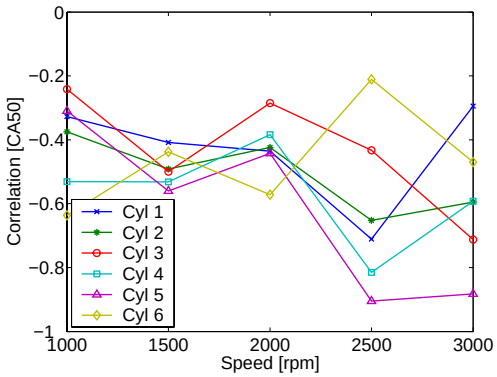

Figure 31. Correlation coefficient [R] for spark assisted HCCI at low load.

CONCLUSIONS

High load HCCI is mainly restricted by the rate of heat release, due to lowered amount of residuals at higher load if the engine is not run with boost pressure. At high speed the reaction rate is high even at low load compared to low speed with lower fractions of residuals.

Low load is restricted by cylinder-to-cylinder differences. Which cylinders are most affected differs at different speeds. One important phenomenon is that some cylinders will have a cycle-to-cycle behavior, which causes combustion timing to go back and forth to the point of misfire. An increased negative correlation for some speeds indicates that it is more than temperature that governs this phenomenon.

At low speed and load the changes in wall temperature for the end cylinders become prominent, but at higher speed no such effects are seen.

No communication from cylinder to cylinder has been detected that affects combustion timing.

The low load regime can be expanded by applying spark assistance. Up to a certain residual fraction, positive effects have been observed up to 3000 rpm.

The introduction of spark assistance makes it possible to advance HCCI combustion timing to a certain extent and to increase efficiency at points where it is not possible to run unassisted HCCI.

Using cylinder individual spark timing could balance combustion timing for all cylinders when running spark assisted.

A somewhat slower start of heat release can be seen for high spark advance that indicates some flame propagation. Also the correlation in CA50 from one cycle to the next is held back by spark assistance, although some cycles respond poorly to spark assistance for very early spark timing.

The correlation coefficient can be an indication for the success of applying spark assistance.

REFERENCES

1. S. Onishi, S. Hong Jo, K. Shoda, P Do Jo, S Kato: ”Active Thermo-Atmosphere Combustion (ATAC) – A New Combustion Process for Internal Combustion Engines”, SAE Paper 790501
2. P. Najt, D. E. Foster: ”Compression-Ignited Homogeneous Charge Combustion”,SAE Paper 830264
3. M. Christensen, P. Einewall, B. Johansson: ”Homogeneous Charge Compression Ignition (HCCI) Using Isooctane, Ethanol and Natural Gas – A Comparison to Spark Ignition Operation”, SAE Paper 972874
4. A. Hultqvist, M. Christensen, B. Johansson, A. Franke, M. Richter, M. Aldén: “A study of the Homogeneous Charge Compression Ignition Combustion Process by Chemiluminescence Imaging”, SAE Paper 1999-01-3680
5. J-O. Olsson, O. Erlandsson, B. Johansson: ”Experiments and Simulations of a Six-Cylinder Homogeneous Charge Compression Ignition (HCCI) Engine”, SAE Paper 2000-01-2867
6. J-O. Olsson, P. Tunestål, G. Haraldsson, B. Johansson: ”A Turbo Charged Dual Fuel HCCI Engine”, SAE Paper 2001-01-1896
7. J. Willand, R-G. Nieberding, G. Vent, C. Enderle: ”The Knocking Syndrome – Its Cure and Its Potential”, SAE Paper 982483
8. H. Zhau, J. Li, T. Ma, N. Ladommatos:” Performance and Analysis of a 4-stroke Multi-Cylinder Gasoline Engine with CAI Combustion”, SAE paper 2002-01-0420
9. J. Allen, D. Law:” Variable Valve Actuated Controlled Auto-Ignition: Speed Load Maps and Strategic Regimes of Operation”, SAE paper 2002-01-0422
10. R. J. Osborne, G. Li, S. M. Sapsford, J. Stokes, T. H. Lake, M. R. Heikail:”Evaluation of HCCI for Future Gasoline Powertrains” SAE paper 2003-01-0750
11. L. Koopmans, H. Ström, S. Lundgren, O. Backlund, I. Denbratt: “Demonstrating a SI-HCCI-SI Mode Change on a Volvo 5-Cylinder Electronic Valve Control Engine”, SAE Paper 2003-01-0753
12. J. Hyvönen, G. Haraldsson, B. Johansson: ”Operating conditions using spark assisted HCCI combustion during combustion mode transfer to SI in a Multi-Cylinder VCR-HCCI engine”, SAE Paper 2005-01-0109
13. M. Christensen, B. Johansson, P. Amnéus, F. Mauss: “Supercharged Homogeneous Charge Compression Ignition”, SAE Paper 980787
14. S. Aceves, J. Martinez-Frias, D. Flowers, J Smith: “A Decoupled Model of Detailed Fluid Mechanics Followed by Detailed Chemical Kinetics for Prediction of Iso-Octane HCCI Combustion”, SAE Paper 2001-01-3612
15. J. B. Heywood: “Internal Combustion Engine Fundamentals” Mc Graw-Hill, New York, 1988
16. B. Johansson: “On Cycle to Cycle Variations in Spark Ignition Engines –The Effects of Fluid Flow and Gas Composition in the Vicinity of the Spark Plug on Early Combustion” Doctoral Thesis, Lund Institute of Technology, Lund 1995
17. L. Koopmans, O. Backlund, I. Denbratt: ”Cycle to Cycle Variations: Their influence on Cycle Resolved Gas Temperature and Unburned Hydrocarbons from a Camless Gasoline Compression Ignition Engine”, SAE Paper 2002-01-0110
18. J. Hyvönen, G. Haraldsson, B. Johansson: ”Balancing cylinder to cylinder variations in a Multi-Cylinder VCR_HCCI engine”, SAE Paper 2004-01-1897
19. H. Persson, M. Agrell, J-O. Olsson, B. Johansson, H. Ström: “The Effect of Intake Temperature on HCCI Operation Using Negative Valve Overlap” SAE Paper 2004-01-0944

CONTACT

Håkan Persson, MSc M. E.
E-mail: hakan.persson@vok.lth.se

ACRONYMS

AFR	Air Fuel Ratio
BDC	Bottom Dead Center
BTDC	Before Top Dead Center
CI	Compression Ignition
COV	Coefficient Of Variation
CR	Compression Ratio
EVC	Exhaust Valve Close
EVO	Exhaust Valve Open
HCCI	Homogeneous Charge Compression Ignition
IMEP	Indicated Mean Effective Pressure
IVC	Inlet Valve Close
IVO	Inlet Valve Open
ISCO	Indicated Specific Carbon Monoxide
ISHC	Indicated Specific Hydro Carbons
$ISNO_x$	Indicated Specific Nitrogen Oxides
J	Joule
R	Linear Correlation Coefficient
SI	Spark Ignition
TDC	Top Dead Center

APPENDIX

The Correlation Coefficient (R) is a linear correlation coefficient between two parameters (i,j). In this paper its between CA50 in cycle i to CA50 in cycle j. C is the covariance

$$R(i,j) = \frac{C(i,j)}{\sqrt{C(i,i) \times C(j,j)}}$$

The correlation coefficient can vary from –1 to 1, if R = 0 then no correlation is found. If R = -1 then a perfect inverted linear correlation is found which implies that a high value is followed by a low etc, in this case that a late timing is followed by an early one.

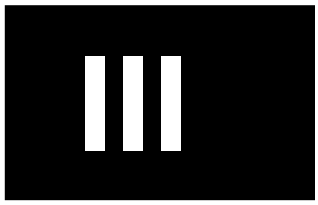

2005-01-3729

Investigation of Boundary Layer Behaviour in HCCI Combustion using Chemiluminescence Imaging

H. Persson, L. Hildingsson, A. Hultqvist, B. Johansson
Lund Institute of Technology

J. Ruebel
University of Karlsruhe

ABSTRACT

A five-cylinder diesel engine, converted to a single cylinder operated optical engine is run in Homogeneous Charge Compression Ignition (HCCI) mode. A blend of iso-octane and n-heptane is used as fuel.

An experimental study of the horizontal boundary layer between the main combustion and the non-reacting surface of the combustion chamber is conducted as a function of speed, load, swirl and injection strategy. The combustion behaviour is monitored by chemiluminescence measurements.

For all cases an interval from -10 to 16 crank angles after top dead center (CAD ATDC) in steps of one CAD are studied. One image-intensified camera observes the boundary layer up close from the side through a quartz cylinder liner while a second camera has a more global view from below to see more large scale structure of the combustion.

The averaged chemiluminescence intensity from the HCCI combustion is seen to scale well with the rate of heat release. A boundary layer is defined and studied in detail between the main combustion volume and the piston crown surface as a function of crank angle. The boundary layer is found to be in the range from 2 to 4 mm for all cases by the definition used; however, the location for the measurements becomes more and more important as combustion becomes more inhomogeneous. To get accurate calculations, the level of noise must also be considered and definitions of boundary layer thickness should not be made at to low chemiluminescence intensity.

INTRODUCTION

Homogenous Charge Compression Ignition (HCCI) is known as a combustion concept that combines some of the features of both the spark ignition (SI) and the compression ignition (CI) engine. As the SI engine, it runs with a premixed charge of fuel and oxidizer, and as the CI engine, it runs un-throttled. The main benefits of HCCI combustion are: high efficiency similar to the diesel engine, low emissions of NO_x due to low combustion temperature and also, no smoke. The challenge for HCCI combustion compared to SI and CI engines is that ignition timing depends on the in-cylinder temperature and is not directly controlled.

The early studies of HCCI combustion were made on two-stroke engines in an effort to reduce the hydrocarbon (HC) emissions at part load operation [1]. Later, in 1983, Najt and Foster showed that it was possible to attain HCCI combustion in 4-stroke engines [2]. Studies have reported low NOx emissions and high efficiency compared to the SI-engine [3]. More recent studies have been performed on both combustion stability and control [4-7]. In HCCI combustion, the premixed charge is compressed until the point of auto ignition. The more or less homogeneous charge starts to react almost simultaneously throughout the combustion chamber. However, some in-homogeneity in the combustion can be observed, and also a boundary layer exists between the strongly reacting charge in the main part of the combustion chamber compared to close to the cylinder head and piston crown where little or no reaction takes place.

One way to characterize the combustion behaviour closer is to make chemiluminescence measurements. Earlier experiments and simulations have been conducted in this area for HCCI combustion [8-10].

The intention of this study is to thoroughly investigate the combustion boundary layer. The boundary layer is defined as the area enclosed between the high reacting zone and the low reacting outer part near the combustion chamber surface. It is characterized by a steep decrease in local temperatures due to the comparably low wall temperature. Stratification of temperature has been indicated to be one possible way of extending the burn duration in HCCI and thus enable higher load without excessive pressure derivatives.

Changing the boundary layer thickness has direct influence on the thermal stratification inside the cylinder and is supposed to be a possible way of affecting the burn duration.

The main intention is to see how the boundary layer behaves when changing the operating conditions in terms of speed (turbulence), load (equivalence ratio), swirl (mixing), injection strategy (homogeneity). A correlation from the boundary layer behaviour to the impact of this on the combustion process as such is also done.

EXPERIMENTAL

ENGINE SETUP

The engine used is based on a five-cylinder Volvo diesel. The engine is modified for single cylinder operation, which gives a displacement of 0.5 liters with optical access. Engine specifications are given in Table 1 and the experimental setup can be seen in Figure 1.

Displacement	0.48 l
Valves per cylinder	4
Bore	81 mm
Stroke	93.15 mm
Compression ratio	12:1
Fuel	50/50 iso-octane/n-heptane

Table 1. Engine Data

The operating cylinder is equipped with a Bowditch piston extension. A quartz window, with a diameter of 58 mm in the elongated piston gives optical access to the combustion chamber from below. As the glass is flat, there is no bowl-in-piston as in the production engine, resulting in a pancake combustion chamber.

A quartz ring is mounted as an elongation of the cylinder liner for horizontal optical access to the upper part of the combustion chamber. The quartz liner has a height of 25 mm which gives full access to the disk shaped combustion chamber close to top dead center (TDC).

The in-cylinder pressure is monitored using an un-cooled AVL GU12S pressure transducer with a resolution of 0.2 crank angles (CAD). The pressure transducer is placed in the glow plug hole. Fuel is supplied either by port injection (PFI) or by direct injection (DI) by a five-hole nozzle, at 1000 bar. The fuel used for all measurements consists of 50% iso-octane and 50% n-heptane. Fuel consumption is measured by a fuel balance. An electrical intake heater is utilized to control combustion timing. The emission analysis equipment consists of a flame ionization detector (FID) for measuring HC, a chemiluminescence detector (CLD) for measuring nitrogen oxides (NO_x), a non dispersive infra red (NDIR) detector for measuring carbon dioxide (CO_2) and carbon monoxide (CO) and a paramagnetic detector for measuring oxygen (O_2). Smoke is not measured.

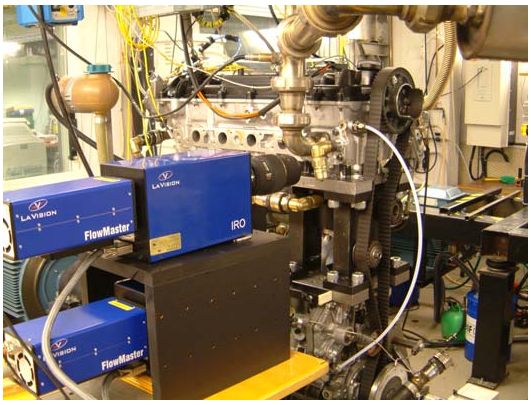

Figure 1. Experimental setup with the upper camera looking through the quartz liner and the lower camera through the piston extension from below.

CAMERA SETUP

For the chemiluminescence measurements a LA-Vision camera system was used. It consists of two CCD cameras with image intensifiers connected to a control computer. Both cameras are configured to take images simultaneously. The upper camera is mounted so it has focus in the center of the combustion chamber, giving a horizontal view through the quartz liner. The lower camera views the combustion from below through the quartz window in the piston with help of a 45° mirror placed in the piston extension.

The CCD chip resolution is 1280 x 1024 pixels. An intensifier gate time of 100 µs is used for all measurements. Both cameras are equipped with 105 mm f 2.8 macro lenses. The lens used for the boundary layer measurement is set to an aperture of f 4 and will give a depth of view of approximately 0.4 mm. When having the optics in the same height as the clearance volume, both the piston and cylinder head will block some of the light from the lens. This will create a so called optical boundary layer in the range of 8 mm vertically from both the cylinder head and piston crown. As a result, the intensity will be slightly under-estimated closer to the piston and cylinder head surfaces.

For this study only natural light is observed, no filters are used.

MEASURING PROCEDURE

For each operating point the measurement interval reaches from –10 to 16 CAD ATDC with a resolution of one CAD. For each CAD, 50 images are collected and used as well for single cycle information as for averaged. Since only one image per cycle can be acquired, all boundary layer calculations are based on the average of 50 images. The cylinder pressure is measured simultaneously making it possible to connect single cycle images to the corresponding pressure traces. All cases are run with a constant combustion timing with crank angle for 50% burned fuel mass (CA50) at approximately 3 CAD ATDC. CA50 is kept constant within +/- 0.5 CAD by moderating the intake temperature. After each measurement sweep, motored pressure traces are saved and used to verify proper operating conditions for the engine.

A base case is used as reference. This is run at 2 bar IMEPnet (entire cycle), PFI and unblocked swirl valve at 1200 rpm. Four different sweeps are made, changing one parameter at the time: load, speed, injection strategy and swirl as shown in Table 2.

sweep	swirl valve	inj. strategy	load	speed
			1.0 bar	700 RPM
			1.5 bar	900 RPM
base case	0% (open)	PFI	2.0 bar	1200 RPM
	25 %	DI -180°	2.5 bar	1500 RPM
	50 %	DI -130°	3.0 bar	
	75 %	DI -90°		
	100 % (fully blocked)	DI -50°		
		DI -30°		

Table 2. Measurement conditions.

BOUNDARY LAYER DEFINITION

The boundary layer is defined as the area enclosed between the high reacting zone and the low reacting outer part near the combustion chamber surface. The steep temperature gradient in the boundary layer is indicated by a high decrease in chemiluminescence intensity towards the combustion chamber surface. Therefore chemiluminescence imaging can be used to calculate the boundary layer behaviour. For these calculations the boundary layer is defined as the area from 15 to 85 % of maximum intensity at each crank angle. These intensities are calculated from the mean images of 50 cycles taken through the quartz liner. One such image is shown in Figure 2. By averaging these images in the horizontal direction a one-dimensional intensity is obtained. From this information the average boundary layer is obtained. For the camera system, an optical boundary effect was mentioned giving less intensity at the walls. Since the measurements are comparative, and the effect is the same in all cases, no attempts to exclude the phenomena are needed.

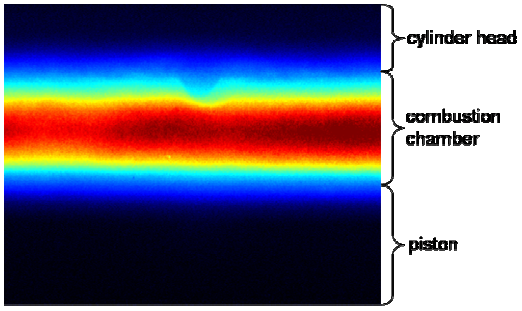

Figure 2 Averaged horizontal view of combustion through the quartz liner with injector clearly visible in the center. Image taken at point of CA50 at 3 CAD ATDC.

RESULTS

The correlation between rate of heat release and chemiluminescence intensity is of great interest for accepting the proposition that chemiluminescence intensity is a measure of global heat release in a flame. Although this proposition is commonly accepted and has been approved in previous studies [9], it is checked again with the current data to assure the measurement quality.

The maximum chemiluminescence intensity at each crank angle scales well against the rate of heat release as can be seen in Figure 3 for the reference case.

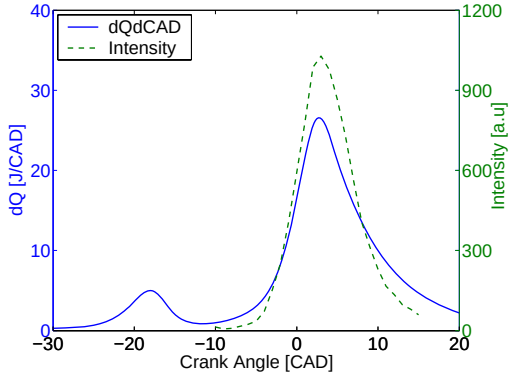

Figure 3. Rate of heat release and maximum chemiluminescence intensity for the base case.

The dotted curve in Figure 3 shows maximum intensity of natural light, starting at 10 CAD BTDC. The solid line shows the rate of heat release. As can be seen it is a two stage combustion with low temperature reactions (LTR) due to the n-heptane, followed by high temperature reactions (HTR). As the pre reactions have a low reaction rate and emit light partially in the ultra violet (UV) region, the LTR can only be faintly seen. Therefore the signal to noise ratio (SNR) in this area is too low, and because of that this region is not investigated.

For further statistical analyses of the correlation between rate of heat release and intensity, the average intensities of the measurements at each crank angle are matched with the corresponding values of the instant rate of heat release, giving the scatter plot shown in Figure 4. The intensity in this figure is calculated from the images taken from below through the piston crown.

A trend line of linear regression is also fitted to the scatter plot, showing a strong linear relationship between the rate of heat release and intensity. To quantify this relationship, the coefficient of determination R^2 is calculated. This coefficient is further explained in the appendix. For this case an R^2-value of 98.56% is calculated referring to a very strong linear relationship between the rate of heat release and average intensity. In Figure 5 this is calculated from the side images used for boundary layer calculations. Here it is seen that the horizontal averaged maximum intensity also shows very good linear correlation with R^2 of 98.69%.

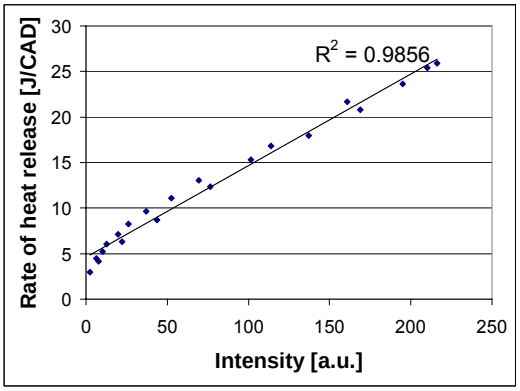

Figure 4. Variation of image average intensity versus rate of heat release and linear trend line for the base case, calculated from the intensity measured through the piston crown.

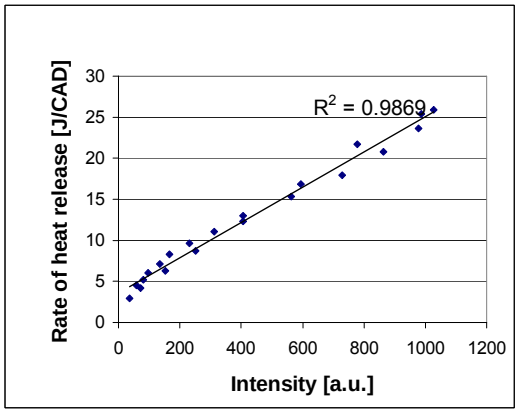

Figure 5. Variation of image average maximum intensity versus rate of heat release and linear trend line for the base case, calculated from the intensity measured horizontal through the glass liner.

Figure 3 shows the maximum chemiluminescence intensity at each CAD, this can be compared to the one-dimensional intensity distribution in Figure 6. Figure 6 shows the distribution with the cylinder head up front in the figure (~3.5mm) and the piston side in the back (~12 mm, at TDC). The plot goes from –10 to 14 CAD ATDC. As can be seen in both Figure 3 and Figure 6, the intensity does not begin to increase until just before top dead center. Because of the low signal at early CAD:s giving low SNR also for the average images, the boundary layer calculations are not very good until just before –5 CAD ATDC. The images collected for the boundary layer calculations are focused in the center of the combustion chamber from the exhaust side of the engine. The width of the images is about 28 mm and in height they stretch both slightly up over the combustion chamber and down on the piston. An image is shown in Figure 2 of this view; also the tip of the direct injector can be seen. The results shown further on are based on the boundary layer between the piston and the main combustion volume. At the upper boundary layer, the noise level was higher and therefore the lower one was chosen for evaluation.

The boundary layer calculations are as mentioned above based on horizontal averaging of the mean images. Using single points instead of average values will introduce so much noise that it is impossible to interpret data from the different cases; this is visible by the naked eye looking at Figure 2. Tests were conducted using different length and location of the averaging, all giving similar differences between the sweeps, although not exactly the same thickness. Using a longer averaging distance makes the obtained thickness more relevant for comparison between the different sweeps. Therefore the whole image width of 28 mm is chosen.

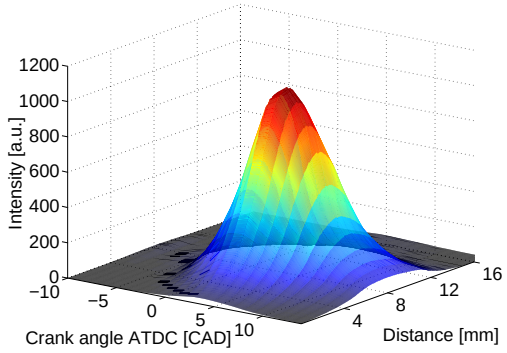

Figure 6. Averaged one-dimensional intensity from –10 to 14 CAD ATDC. Cylinder head located at approximately 3.5 mm and piston crown at 12 mm (at TDC).

Since only one image can be taken for an individual cycle it again makes sense to use an average image at each CAD for the boundary layer calculations. Yet to get some information about the changes from cycle to cycle Figure 7 shows a variation coefficient based on the standard deviation from the single images at each CAD divided by the mean intensity at each CAD for the base case. The figure shows each crank angle from the side view camera as shown for a mean intensity image in Figure 2. What is obvious is the high cycle to cycle variation at the start of main combustion, especially where the boundary layer is situated. Comparing to the rate of heat release in Figure 3, it can be seen that for increasing burn rate the variations from cycle to cycle decrease rapidly, becoming low during the main combustion. For late crank angles the cycle to cycle variations increase slightly again, now mainly at the area of the main combustion while the boundary layer shows less variations.

To get an overview of the results from the different sweeps, the duration of 10 to 90 percent burnt is showed in Figure 8. The swirl case (squares), starting to the left with fully open swirl valve, then 25% blocked, 50%, 75% and finally fully blocked, changing the swirl number from 2 to 2.6. The DI case (triangles) with injection at 180, 130, 90, 50 and 30 CAD BTDC. The load case (stars) stretches from 1 bar IMEPnet to 1.5, 2, 2,5 and 3 bar IMEP. Finally, the speed sweep (diamonds) reaches from 700rpm in the left of the figure, then 900, 1200 and 1500 rpm.

For the swirl case, no change in burn duration is observed. Pressure data only shows an average of the in-cylinder conditions so even if combustion is affected by the swirl sweep, it cannot be seen from the burn duration.

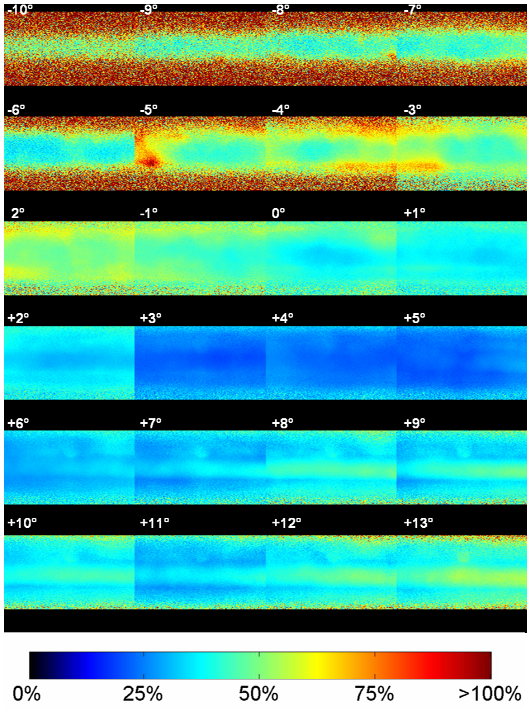

Figure 7. Variation coefficient for single images at each CAD (ATDC) for one of the base cases.

For the DI case, the burn duration is overall faster, most likely due to a more inhomogeneous charge. This is even more obvious at later injection timing when combustion duration gets shorter due to rich zones burning faster. At this point NOx is starting to form from parts of a ppm for early injection timing to a level close to 10 ppm for late injection.

In the load sweep the load was changed by altering the amount of fuel injected into the inlet port. Thereby the air/fuel ratio varied from 6.5 for low load to 4.0 for 3.0 bar IMEP. The lowest points of the load sweep have, as could be expected, the longest burn duration also compared to the other sweeps. For higher loads the richer mixture burns faster with a steeper rate of heat release and shorter burn duration.

For the speed sweep the burn duration changes dramatically when going from 1200 to 1500 rpm. At lower speed than 1200 rpm no prominent change can be seen. Increasing speed will both increase turbulence and decrease heat losses. Earlier results have shown longer combustion duration for HCCI due to increased turbulence [11]. Here the turbulence effect is lower than the effect of a hotter charge due to less heat losses.

Also the exhaust backpressure increased resulting in more trapped residuals, which also increases temperature and thus burn rate.

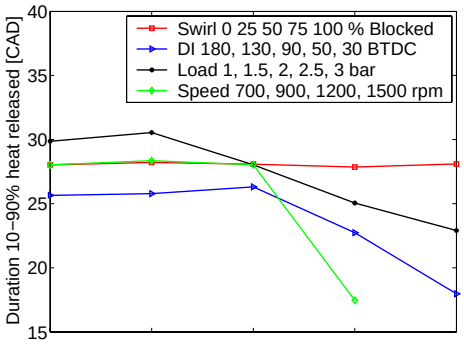

Figure 8. 10 to 90 percent burnt duration for the different sweeps. Different conditions from left to right side of the figure.

Since the engine piston has to run without oil lubrication the piston rings made out of rylon wear out quite fast. To ensure that the operating conditions are kept the same throughout the measurement campaign, new base cases have been taken during the measurements. The different base cases are shown in Figure 9. The sweeps were taken in the order that follows: First the swirl base case (diamonds), then the complete swirl sweep. Next was the DI case, for this case the injection system was modified and no base case was taken. Then the speed sweep was taken, after this a new base case was collected, the speed/load case (triangles) followed by the complete load sweep. This was followed by a final base case (squares). For all three cases the intake temperature and the corresponding motored peak pressure was in a narrow range.

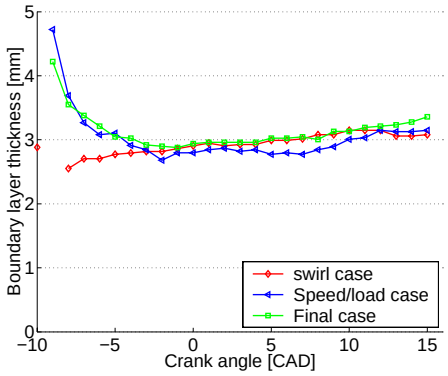

Figure 9. Boundary layer thickness for the three base cases.

SWIRL SWEEP

The swirl sweep consists of five measurements with increasingly blocked swirl valve, giving a swirl number from 2 to 2.6. The fully open swirl valve is the default setting used in all the other sweeps. So the “0% (open)” measurement is the reference case and one of the base cases discussed earlier. The intensity plots for this sweep can be seen in Figure 10 and the corresponding boundary layer thickness in Figure 11.

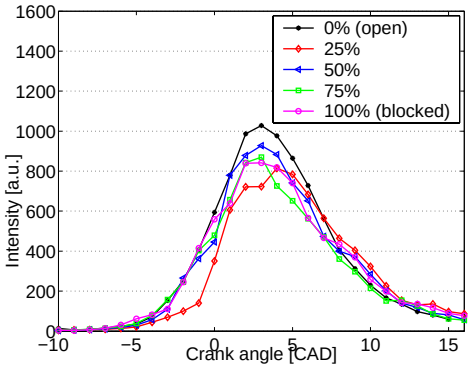

Figure 10. Maximum intensity for swirl sweep.

The intensity plots show no significant differences. The peak intensities seem to be only slightly lower with increasingly blocked swirl valve and it is unclear if the blocking is the reason. Furthermore, the case with 25% blocked intake appears to have slightly later timing.

The change in swirl and thereby turbulence caused by blocking one of the inlet ports appears to have no direct influence on HCCI combustion. Besides the just described low intensity differences, this statement is also approved by the minor changes in inlet temperature that is needed to keep constant combustion phasing. Furthermore, the burn duration displayed in Figure 8 is nearly constant for all measurements of the swirl sweep. A reason for this behaviour lies in the nature of HCCI combustion. It is generally accepted among researchers that the HCCI combustion process is controlled by chemical kinetics. This means that turbulent mixing does not affect the chemical reactions and heat release process during the main combustion because the local chemistry is an order of magnitude faster than turbulence effects. However, this explanation is only valid if no mass stratification exists, as this has been shown to increase the role of turbulence on combustion [12]. As PFI was used for the swirl sweep, no mass stratification is expected. The influence of mass stratification is investigated later in the DI sweep.

Regarding the boundary layer thickness for the swirl sweep in Figure 11, some obvious differences can be observed. The reference case with open swirl valve has a nearly constant thickness of about 3 mm. But with increasingly blocked valve a growing shifting of the thickness during combustion is visible leading to a thinner boundary layer in the first part and a thicker one in the last part of combustion. The intersection point where all cases have nearly the same boundary layer thickness is around 5 CAD ATDC.

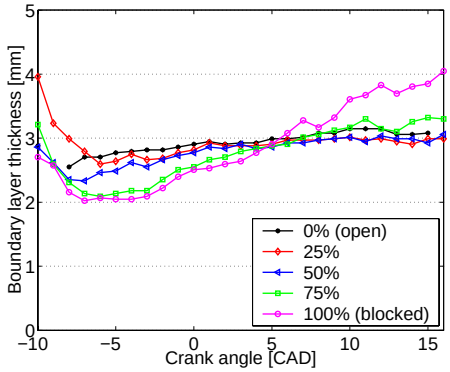

Figure 11. Boundary layer thickness for swirl sweep.

A recent paper by Aceves et al. [13] has indicated that geometry generated turbulence generates a thicker boundary layer and hence more thermal stratification resulting in a longer burn duration. The results of the measurements conducted in this swirl sweep do not allow the same conclusion for turbulence generated by blocking one inlet port. The increase in turbulence only leads to a thicker boundary layer towards the end of combustion. From -5 to +5 CAD ATDC the effect is just the other way around, meaning the boundary layer is thinner with more turbulence

The thinner boundary layer at increasing swirl seems to be a direct result of the increase in flow velocity, as all other parameters like burn duration and inlet temperature are nearly constant.

DIRECT INJECTION SWEEP

The direct injection sweep shows little difference in boundary layer thickness between the different cases as can be seen in Figure 12. For early injection timing from 180 to 90 CAD BTDC, nearly no changes in the boundary layer thickness are found. But for later injection the boundary layer seems to become thinner. The burn duration for the DI sweep in Figure 8 shows the same trend. For early injection it is nearly constant, but for later injection at 50 and 30 CAD BTDC the burn duration is much shorter. This similarity in behaviour brings out the assumption that there is a relationship between the boundary layer thickness and the burn duration.

Figure 13 gives an indication of the homogeneity for the different cases. The figure shows averaged images from both the lower camera through the piston extension and from the camera taking the horizontal images for boundary layer calculations. It can be seen that later injection leads to a less homogeneous combustion which also affects the horizontal intensity distribution of the side view image. While the side view of the 180 CAD case looks like all other sweeps with PFI, the cases with later injection timing show most of the combustion intensity in the right side of the side view image. To avoid unknown influences on the boundary layer calculation, the range for horizontal averaging for this sweep was reduced and set to the right half of the image where higher intensity levels are measured. The boundary layer thickness of the quite homogenous 180 CAD case that has been calculated in this way has the same level as other PFI cases. This indicates that this necessary adjustment in the calculation routine does not affect the comparability. However, it must be kept in mind that there may be some local differences in boundary layer thickness for the more inhomogeneous cases.

The intensities that are displayed in Figure 14 are analogous to the boundary layer calculation based on the adjustments described above. They show no significant differences. Only the 90 CAD case has generally lower intensity levels but without explainable reason.

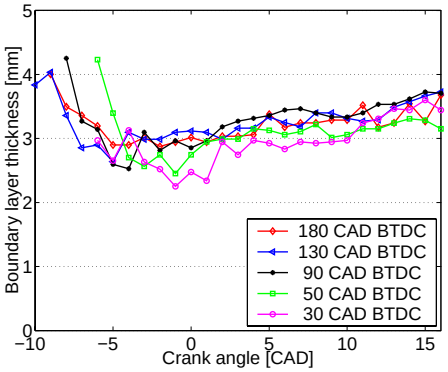

Figure 12. Boundary layer thickness for DI sweep.

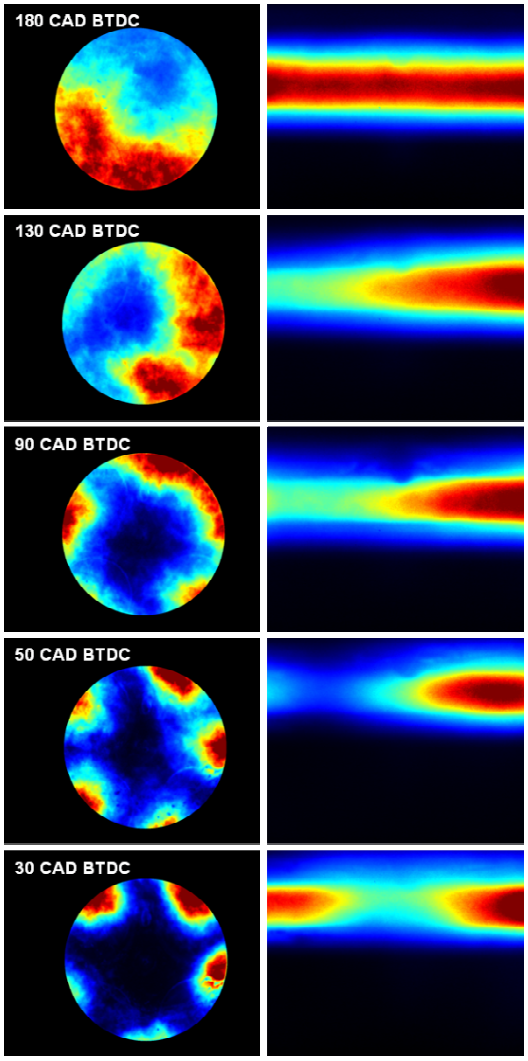

Figure 13. Comparison for DI with different injection timing, all taken at the point of CA50. Left images view from below, Right images side view used for boundary layer calculations.

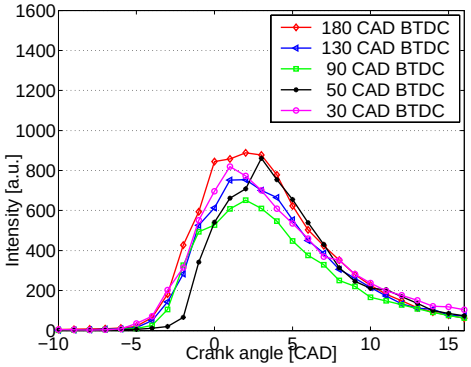

Figure 14. Maximum intensity for DI sweep.

LOAD SWEEP

For the load sweep, the reference case is included as the load at 2 bar IMEP. The combustion phasing was kept constant by controlling the inlet air temperature. Running higher loads was not possible because of limitations given by the optical access and inlet air temperature.

The calculated boundary layer thickness displayed in Figure 15 shows only minor differences. At lower loads, from 1.0 to 2.0 bar, the boundary layer thickness has nearly the same behaviour, which is slightly increasing with proceeding combustion. The apparently thicker boundary layer for the 1.0 bar case before TDC is probably not realistic as the intensity level and thus the SNR begins to rise later for this case. The high load case (3.0 bar IMEP) shows a different behaviour with a thinner boundary layer during the first half of combustion followed by a strong increase after 5 CAD ATDC. To exclude the possibility of a measurement error, this case was repeated, but the results only got verified by the second measurement.

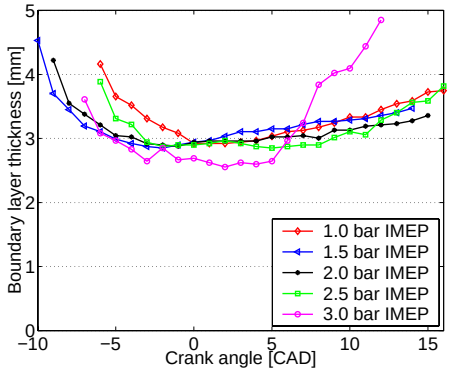

Figure 15. Boundary layer thickness for load sweep.

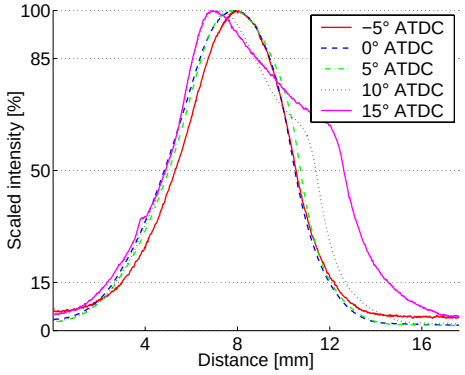

Figure 16. Scaled intensity for 3 bar case from load sweep at different CAD:s.

The phenomena can be explained by looking at Figure 16 displaying scaled intensities for different CAD:s for the 3 bar load case. On the intensity axis the 15% and 85% borders of the boundary layer definition are marked. The cylinder head is located at approximately 3 mm and the piston at approximately 12 mm moving even further for later crank angles. The maximum intensity for later CAD:s lies closer to the cylinder head and not in the middle of the combustion chamber. From the maximum towards the piston, the intensity first drops slowly to about 70% of the maximum before the same steep decrease as usual starts. During the first slow decrease, the intensity falls already below the 85% border and the area is per definition considered as part of the boundary layer. But as a steep temperature and thus intensity gradient is an essential characteristic for the boundary layer, the used boundary layer definition may not be accurate in this part of the sweep. Furthermore Figure 16 shows that the whole boundary layer moves closer to the cylinder head during combustion; if comparing at -5 and 15 CAD (solid lines) it is most obvious. This is probably due to the increased temperature during combustion.

The thinner boundary layer in the first part of combustion of the 3.0 bar case in combination with the lower burn duration shown in Figure 8 corresponds well to the assumption which has been established for the DI sweep. A shorter burn duration and thus faster combustion seems to lead again to a thinner boundary layer. In the other direction the relationship is not so definite. Although the burn duration is slightly longer for lower load, no significant difference can be seen in the boundary layer thickness. Perhaps the effect is neutralized in some way by the high inlet air temperature that is required to keep constant combustion phasing.

The faster burn rate and shorter duration for higher loads is also supported by the maximum intensity plots for the side view shown in Figure 17. It is clearly noticeable that higher load leads to higher intensity during the main combustion and to a steeper increase after ignition.

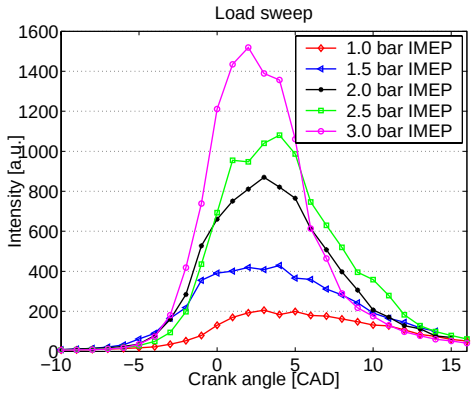

Figure 17. Maximum intensity for load sweep.

SPEED SWEEP

The speed sweep is run from 700 rpm up to 1500 rpm. The point at 1200 rpm is the speed/load reference case. In Figure 18 a slight decrease in boundary layer thickness can be seen for increasing speed, from 700 to 1500 rpm. The case at 1500 rpm has the smallest boundary layer; this can also be supported by the shorter burn duration shown in Figure 8. As the increase of engine speed comes along with strong increase of turbulence and flow velocity, this is probably the reason for the thinner boundary layer. From the start of the main combustion to the end all four cases show an increase in boundary layer thickness of about 0.5 mm each. The boundary layer for the case at 1500 rpm shows some inconsistency at the end of combustion, this is investigated and the reason shown in Figure 19 is the same as for the high load case. The threshold for the boundary layer calculations is above a plateau in the intensity towards the piston. For this case as well as for that shown in Figure 16 the upper boundary layer seems to move closer to the cylinder head during combustion.

The seemingly different behaviour of the 1500 rpm case before the main combustion allows no further conclusion. As explained before the results of the boundary layer calculation before ignition are not accurate because of a too low signal level. The 1500 rpm has the same bad SNR in this part of the measurement range, so that the seemingly better results here are probably just a matter of coincidence.

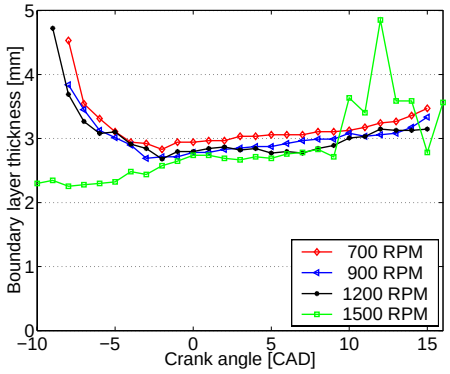

Figure 18. Boundary layer thickness for speed sweep.

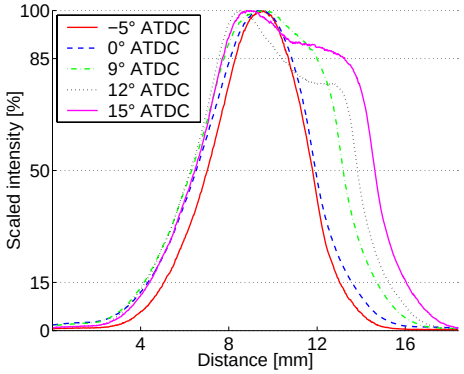

Figure 19. Scaled intensity for 1500rpm case from speed sweep at different CAD:s.

When looking at the maximum intensities in Figure 20 it shows that the combustion is slower at low speed giving less intensity but slightly longer duration. It should however be remembered that the intensifier gating time was kept constant in time, this has been compensated for afterwards by multiplying the intensities with the base case speed divided by the different speeds.

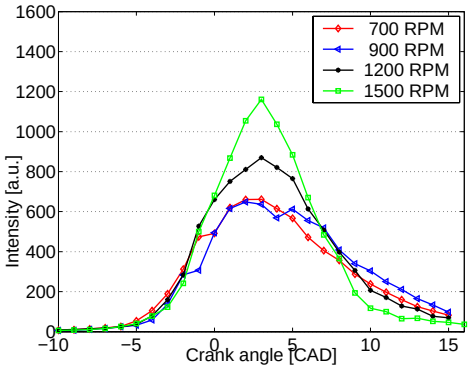

Figure 20. Maximum intensity for speed sweep with corrected intensities due to the difference in speed.

DISCUSSION

For all the cases studied, the boundary layer thickness is in the same order of magnitude. For the DI sweep a late injection, for the load sweep a high load and for the speed sweep a high speed all show shorter burn duration and a corresponding thinner boundary layer. A strong correlation between boundary layer thickness and the burn duration can be concluded. An explanation for this effect could be that shorter burn duration leads to a higher peak heat release and thus higher temporary temperatures which move the boundary layer closer to the wall, making it thinner. The boundary layer as such is shown to move closer to the wall during combustion. For the swirl case no change in combustion duration occurs; still the boundary layer behaviour changes. It does not however change in the same way as the other cases; instead it tilts more with a thinner boundary layer for the early combustion and then it gets thicker towards the end.

The average intensity is shown to have a strong linear correlation to the rate of heat release. Also the averaged maximum intensity seems to scale well with the rate of heat release according to Figure 3. The latter results also show this with increased maximum intensity for increased load, changes in burn durations in the same direction corresponding to those calculated from the pressure trace.

For all four sweeps it can be seen that the boundary layer gets slightly thicker at the end of combustion. Combustion occurs closer and closer to the wall as the in-cylinder temperature and the wall temperature increase during the combustion process, but still the heat release rate close to the piston doesn't increase to that of the core in the combustion chamber. Thereby the boundary layer gets thicker during the combustion.

In another publication [9] it has been seen that in the late combustion the intensity is higher close to the piston and to the cylinder head while the intensity is lower in the middle. In this study some similarity to this is shown for the highest load case (Figure 16) and for the highest speed case (Figure 19) where a plateau in the intensity can be seen at the late part of combustion. A reason for only seeing the phenomena for these cases can be that since it is an optical engine it is run with an although constant yet low cooling water temperature, so combustion is perhaps not as completed as in a hotter steel engine. This is supported by fairly high emissions of HC and CO.

CONCLUSIONS

A number of conclusions can be drawn from this experimental study:

- Chemiluminescence can be used as a tool for detecting combustion boundary layer behaviour in HCCI combustion.
- The averaged chemiluminescence intensity measured through the quartz liner and the averaged maximum intensity measured through the quartz liner both scale linearly against rate of heat release with high accuracy.
- Increasing swirl or speed (turbulence) leads to a thinner boundary layer.
- A thinner boundary layer correlates to faster burn duration.
- The boundary layer thickness is in the same order of magnitude for all cases and differs from 2 to 4 mm by the definition used.
- The boundary layer gets thicker towards the end of combustion.
- Changes in engine load and to some extent burn duration can be seen from the averaged maximum intensity.
- The entire boundary layer seems to move closer to the walls during the combustion.
- For more in-homogeneous cases, the location of the boundary layer measurements can affect the measured boundary layer thickness.

ACKNOWLEDGMENTS

The authors would especially like to thank the technicians at the division for making the engine and the measuring systems work and keep running.

REFERENCES

1. S. Onishi, S. Hong Jo, K. Shoda, P Do Jo, S Kato: ”Active Thermo-Atmosphere Combustion (ATAC) – A New Combustion Process for Internal Combustion Engines”, SAE Paper 790501
2. P. Najt, D. E. Foster: ”Compression-Ignited Homogeneous Charge Combustion”, SAE Paper 830264
3. M. Christensen, P. Einewall, B. Johansson: ”Homogeneous Charge Compression Ignition (HCCI) Using Isooctane, Ethanol and Natural Gas – A Comparison to Spark Ignition Operation”, SAE Paper 972874
4. J. Hyvönen, G. Haraldsson, B. Johansson: ”Balancing cylinder to cylinder variations in a Multi-Cylinder VCR_HCCI engine”, SAE Paper 2004-01-1897
5. H. Persson, R. Pfeiffer, A. Hultqvist, B. Johansson, H. Ström; “Cylinder-to-Cylinder and Cycle-to-Cycle Variations at HCCI Operation with Trapped Residuals”, SAE paper 2005-01-0130
6. J-O. Olsson, P. Tunestål, B. Johansson; “Closed-Loop Control of an HCCI Engine”, SAE Paper 2001-01-1031
7. G. Haraldsson, J. Hyvönen, P. Tunestål, B. Johansson; ”HCCI Closed-Loop Combustion Control Using Fast Thermal Management”, SAE Paper 2004-01-0943
8. S.B. Fiveland, D.N. Assanis; “Development of a Two-Zone HCCI Combustion Model Accounting for Boundary Layer Effects” SAE Paper 2001-01-1028
9. A. Hultqvist, M. Christensen, B. Johansson, A. Franke, M. Richter, M. Aldén; “A study of the Homogeneous Charge Compression Ignition Combustion Process by Chemiluminescence Imaging”, SAE Paper 1999-01-3680
10. A. Hultqvist, M. Christensen, M. Richter, J. Engström, A. Franke, B. Johansson; “Near-Wall Combustion in a Homogeneous Charge Compression Ignition (HCCI) Engine” International Symposium on Internal Combustion Diagnostics, pp 83-90, Baden-Baden, 2000
11. M. Christensen, B. Johansson, A. Hultqvist; “The Effect of Combustion Chamber Geometry on HCCI Operation” SAE Paper 2002-01-0425
12. Y.Z. Zhang, E.H. Kung, D.C. Harworth; “A PDF Method for Multidimensional Modeling of HCCI Engine Combustion: Effects of Turbulence/Chemistry Interactions on Ignition Timing and Emissions” Proceedings of the International Multidimensional Engine Modeling User’s Group Meeting, Detroit, 2004
13. S.M. Aceves, D.L. Flowers, J. Martinez-Frias, F. Espinosa-Losa, M. Christensen, B. Johansson, R.P. Hessel; “Analysis of the Effect of Geometry Generated Turbulence on HCCI Combustion by Multi-Zone Modeling”, SAE 2005-01-2134

Coresponding author:
Håkan Persson

Address
Lund Institute of Technology
Dept. of Heat and Power Engineering
Div. of Combustion Engines
P.O. Box 118
221 00 Lund
Sweden

E-mail
hakan.persson@vok.lth.se

ACRONYMS

ATDC	After Top Dead Center
BTDC	Before Top Dead Center
CAD	Crank Angle Degree
CI	Compression Ignition
CO	Carbon monoxide
DI	Direct Injection
HC	Hydrocarbons
HCCI	Homogeneous Charge Compression
IMEP	İndïcated Mean Effective Pressure
IMEPnet	Entire cycle, including pump loop
LTR	Low Temperature Reaction
HTR	High temperature Reaction
PFI	Port Fuel Injection
SI	Spark Ignition
SNR	Signal to Noise Ratio

APPENDIX

A linear regression is used to point out the correlation between the rate of heat release and intensity. To quantify this relationship the coefficient of determination R^2 is calculated by the following expression:

$$R^2 = \frac{\left[\sum_{i=1}^{n}(x_i - \bar{x})\cdot(y_i - \bar{y})\right]^2}{\sum_{i=1}^{n}(x_i - \bar{x})^2 \cdot \sum_{i=1}^{n}(y_i - \bar{y})^2}$$

where n is the number of pairs of data, x_i and y_i the actual value for the i-th CAD, $\bar{x}$ and $\bar{y}$ the mean values. The coefficient of determination is the square of the correlation coefficient and denotes the strength of the linear association between x and y.

IV

2007-01-0212

Investigation of the Early Flame Development in Spark Assisted HCCI Combustion Using High Speed Chemiluminescence Imaging

H. Persson, A. Hultqvist, B. Johansson
Lund University

A. Remón
Simon Bolivar University

ABSTRACT

Auto-ignition with SI-compression ratio can be achieved by replacing some of the fresh charge by hot residuals. In this work an engine is run with a negative valve overlap (NVO) trapping hot residuals. By increasing the NVO, thus raising the initial charge temperature it is possible to investigate the intermediate zone between SI and HCCI as the amount of residuals is increased. Recent research has shown the potential of using spark assistance to aid gasoline HCCI combustion at some operating conditions, and even extend the operating regime into regions where unsupported HCCI combustion is impossible.

In this work the influence of the spark is studied in a single cylinder operated engine with optical access. Combustion is monitored by in-cylinder pressure and simultaneous high speed chemiluminescence imaging. It is seen that even for large NVO and thus high residual fractions it is a growing SI flame that interacts with, and governs the subsequent HCCI combustion. Using the spark timing it is possible to phase the combustion timing even when the major part of the released heat is from HCCI combustion. The flame expansion speed is decreases for higher NVO, but prevails also for high residual fractions. A higher spark advance is found to compensate for the slower flame expansion up to a point.

The auto-ignition process is found to be stratified for both spark assisted HCCI as well as for pure HCCI. For pure HCCI the initial front spreading velocity is found to be in the same order of magnitude as for the expansion speed of the SI flame.

Calculations to estimate the crank angle of auto-ignition are performed based on cylinder pressure information providing good statistics on how the proportion of SI to HCCI behaves for different operating conditions.

INTRODUCTION

Homogeneous charge compression ignition (HCCI) research is branching into two main paths. Diesel HCCI with partially premixed combustion (PPC) and gasoline HCCI with different strategies of residual usage to reach auto-ignition temperature, also often referred to as CAI combustion. In the latter concept the idea is to run the engine in SI mode when high output power is required and in HCCI mode at low and part load to keep up efficiency. The proposal for using negative valve overlap (NVO) to reach HCCI combustion in an SI engine environment was first published by Willand et al. in 1998 [1]. The first presented results of NVO HCCI combustion by Lavy et al [2] followed in 2000. Cycle to cycle mode switches from SI to HCCI and vice versa have been demonstrated on multi cylinder engines [3] showing the possibility of such a concept. The first reports of combustion stability effects by usage of a spark with NVO HCCI were published by Koopmans et al [4]. Later experiments have shown possibility to also affect combustion timing [5] and to suppress oscillating behaviour in combustion timing at low temperature conditions [6]. In [7] the usage of spark assistance was used as a means to increase the high load limit

This implies that the usage of spark assisted HCCI or spark assisted compression ignition (SACI) which is different term to describe the interaction between SI and HCCI combustion could help expand the usable operating regime for NVO HCCI as well as assist during mode switching events. However more knowledge is needed on the nature of the spark effect since HCCI combustion is normally run highly diluted with air or residuals, an environment that a normal SI flame would not endure. Therefore, the effect of spark assistance is investigated by simultaneous pressure and high speed chemiluminescence imaging. The behaviour of the combustion initiation is observed by changing three different main parameters.

1. NVO. By going from low NVO (0 CAD) to high (200 CAD) the initial charge temperature is increased. As a side effect the fresh charge of fuel and air is diluted when the NVO is increased.

2. Spark timing. The spark timing is advanced when operating at high NVO and low load.

3. Load. A load sweep is conducted with SACI combustion at high NVO, affecting both the residual fractions and temperature.

To bring the investigation into perspective a comparison with full HCCI operation and NVO is also conducted.

EXPERIMENTAL APPARATUS

ENGINE SETUP

The engine used in this investigation is based on a Volvo D5, which is a passenger car size, five cylinder compression ignition (CI) engine. The engine has been converted to single cylinder operation with a Bowditch [8] piston extension. The remaining four pistons are motored and are equipped with counter weights to compensate for the extra weight of the piston elongation on the operated piston. A 58 mm diameter quartz glass is fitted in the piston extension resulting in a flat piston crown. The optical access is approximately 51 % of the total combustion chamber area. Also small vertical windows are mounted in the pent-roof giving see-through access to the vicinity of the sparkplug. The combustion chamber is of SI type with a high pent-roof, four valve design. The engine is port fuel injected (PFI). More engine specifications can be found in Table 1.

Table 1

Displacement	0.48 Liters
Valves per cylinder	4
Bore	81 mm
Stroke	93.15 mm
Combustion chamber	Pent-roof
Compression ratio	9:1
Valve timings	Fully flexible
Fueling	PFI
Speed	1200 rpm

The Engine is fitted with a pneumatic valve train system supplied by Cargine [10]. It features fully flexible valve lift, duration and timing, individual for each valve. The valve actuators mounted on the cylinder head are shown in Figure 1. In this work a 0 to 215 CAD symmetrical NVO is used. Intake closing and exhaust opening have been fixed at -160 and 160 CAD ATDC respectively. For all cases a lift height of approximately 8 mm is used with an opening and closing ramp of approximately 25 CAD at 1200 rpm, only EVC and IVO timings are moderated. Valve lift profiles for 0 and 160 CAD NVO are illustrated in Figure 2. For both SI and HCCI conditions, maximum valve lift has been kept constant at 8 mm.

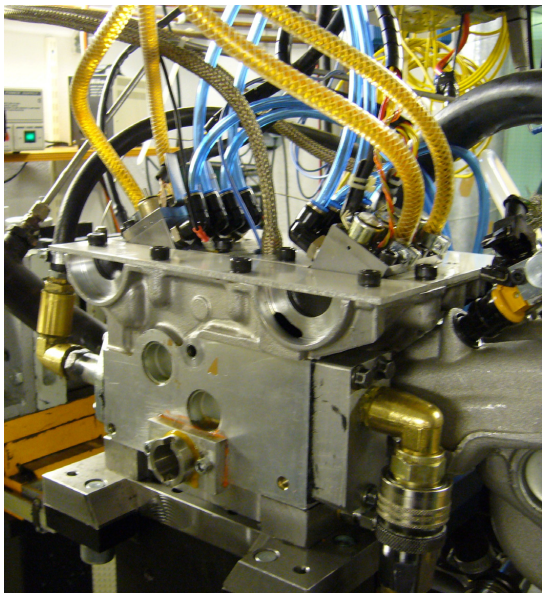

Figure 1. Cylinder head fitted with pneumatic valve actuators.

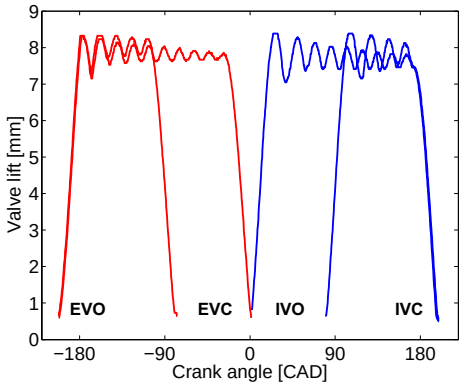

Figure 2. Valve lift curves for 0 and 160 CAD NVO. 0 CAD is gas exchange TDC

MEASUREMENT SYSTEM

Pressure is monitored with a Kistler 6117B combined sparkplug and pressure sensor with a sample rate of 5 per CAD. The piezo electric pressure sensor is flash mounted in the sparkplug. Emissions are monitored using a Horiba MEXA 8120, measuring NO_x, CO, HC, CO_2 and O_2.

Combustion is observed using chemiluminescence imaging from below through the piston crown with a Phantom high speed framing camera running synchronised with the engine, taking 2.5 images per CAD. This corresponds to 18000 Hz at 1200 rpm. At this framing rate, image resolution is limited to 304 x 304 pixels, giving a pixel size of 0.2 mm. The camera is used in combination with a Hamamatsu high speed gated image intensifier, this allows short exposure times with less smearing of the images. For all cases an exposure time of 12 µs has been used. The lens used is a 105 mm f 2.8 macro lens. Apertures have been kept in the range from 5.6 to 11 depending on operating conditions.

In general both the spark plasma and the main bulk combustion are very bright whereas the early combustion has very low chemiluminescence intensity. Apertures and gains have been balanced to see the early combustion, still not saturating the camera during high rate of heat release (RoHR).

FUEL

Due to optical constraints the engine is run with a slightly lower than normal compression ratio (CR = 9:1) and a cooling water temperature of 70° C. Therefore a fuel blend with lower octane number than normal has to be used. A blend of 40 % ethanol and 60 % n-heptane (mass percentage) is used. The choice of ethanol instead of iso-octane is due to that the former seems to cancel the low temperature reactions (LTR) normally associated with n-heptane. The LTR usually occur around 20 CAD BTDC and could smear any early reactions originating from the spark plug. No LTR were observed for these operating conditions, even during tests with 10 % ethanol and 90 % n-heptane.

MEASUREMENT PROCEDURE

Before any measurements are started the engine is run long enough for water and oil temperatures to stabilize. Valve timings are calibrated. After each measurement sweep, motored pressure traces are acquired for analysis and also to make sure that the setup is unchanged, the reason being that the piston rings are made of rulon with a limited lifetime.

For each operating point in the sweeps simultaneous pressure and image acquisition is conducted. The early flame development in SI combustion is known to show cycle to cycle behaviour [9] depending on mainly turbulence intensity, and charge in-homogeneities, therefore 20 chemiluminescence cycles are captured at each point to ensure valid comparisons between the different measurement points. When one chemiluminescence cycle has been acquired the images are sent from the camera to the computer, due to limited memory capacity. This is time consuming so, to be able to get images in synchronization with pressure information 1000 consecutive pressure cycles are saved simultaneously as images are acquired.

HEAT RELEASE ANALYSIS

Heat release analysis is conducted from the sampled in-cylinder pressure using a single zone model. The heat release model is based on the first law of thermodynamics for a control volume, using the equation of state, assuming constant mass. Heat transfer is estimated by the relationships introduced by Woschni [11]. More about the specific model can be read in [9].

IMAGE PROCESSING

The images obtained with the high speed camera have an extremely low noise level. This makes it possible to calculate the perimeter of a burning structure from the intensity image with good accuracy (Figure 3). Thus the flame area can also be obtained.

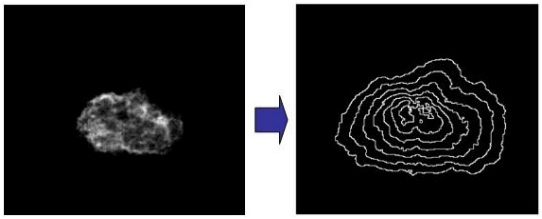

Figure 3. Left: Early flame originating from the spark plug at a NVO of 40 CAD. Right: Obtained perimeters for growing flames, image showing every fifth calculated flame (2 CAD separation).

The objective is to calculate the mean expansion speed of the flame. By applying Equation 1, using the differential area between two images and calculating the time step, then dividing it by the flame perimeter length (L), a mean expansion speed for the flame is obtained. However, using the flame perimeter as shown in Figure 3 for length, the resulting speed will depend on how well the perimeter is resolved e.g. a higher resolution camera will give a lower speed due to more highly resolved structures.

Instead the mean expansion speed is calculated according to Heywood [12] with the assumption that the flame is growing as a sphere, although it is here calculated in two dimensions, thus a circle. Therefore the perimeter of each flame image is calculated as the perimeter of a circle with the same area as the projected area of the flame. As the flame grows the assumption of the flame growing as a sphere becomes less valid, however the combustion chamber height is small compared to the bore. This means that the assumption of a two dimensional growth of the flame is valid, kept in mind that the chemiluminescence is integrated over depth.

Since dA/dt is obtained by numerical differentiation based on two consecutive flame images the perimeter length is calculated as the mean area between two time steps. Since the flame area grows exponentially with

time this assumption will slightly overestimate the expansion speed. This effect is very small though because of the short time between samples (55μs furthermore the time step is the same for all comparisons within this work.

Equation 1. Mean expansion speed.

$$u_f = \frac{dA/dt}{L} \qquad L = \text{Perimeter length}$$

For HCCI combustion a front spreading velocity is calculated for stratified cases when combustion moves from one side to the other of the visible part of the combustion chamber as shown by Hultqvist et al. [10]. This is then considered as a straight reacting front with the total reacting structure area summed up behind it. The velocity is then again calculated according to Equation 1, but with the perimeter length exchanged for a straight reaction front.

RESULTS

CHEMILUMINESCENSE

The correlation between pressure information and chemiluminescence images has been used for engine research for a long time [14]. Later findings have shown good agreement between average chemiluminescence intensity and rate of heat release (RoHR) also for HCCI combustion [15, 16]. For the present setup this relation is investigated to validate the measurement technique and to compare the fully resolved single cycle information with previous information based on ensemble averaging. This is performed for HCCI without the usage of spark assistance. Figure 4 illustrates the relation of intensity and RoHR from start of combustion until the reacting zones are mainly outside of the visible area of the combustion chamber.

HCCI combustion at close to stoichiometric conditions diluted with trapped residuals is seen to burn rather stratified when looking at the chemiluminescence images. The late combustion near the perimeter of the combustion chamber will then not correlate with chemiluminescence since it can not be seen by the camera. However the early part of combustion correlates well with chemiluminescence intensity. This is good enough since it is the ignition process and the early combustion that is of interest in this study.

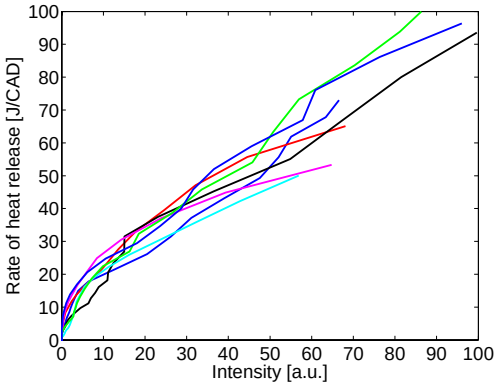

Figure 4. Rate of heat release versus mean chemiluminescence intensity for several individual cycles. Graph showing pure HCCI combustion.

INITIAL SLOW HEAT RELEASE (ISHR)

Close to and also past the normal dilution limit for SI combustion in terms of residual dilution, it is possible to achieve an effect from the spark and thereby run the engine in SACI mode. One attempt to explain the effect is that the locally raised temperature from the spark kernel forms a hot spot that provokes the charge to auto ignite. By looking at a pressure trace from SACI operation it is obvious that there is more to it. Figure 5 shows an initial slower heat release related to the spark that is set off at -25 CAD ATDC. Later the well known fast heat release related to HCCI combustion takes over. This suggests an initial SI flame propagation and heat release with an elevated temperature that triggers auto-ignition and the subsequent combustion in HCCI mode.

Hyvönen et al. [17] defined the initial slow heat release (ISHR) as shown in Equation 2.

Equation 2. Initial slow heat release.

$$ISHR = \frac{Q_{threshold}}{Q_{\max}} \cdot 100[\%]$$

Since HCCI combustion is generally much faster than SI combustion a break point is calculated by finding the maximum difference of the derivative (2nd derivative) of the rate of heat release (RoHR) for individual cycles. This is done by fitting a moving first order polynomial of a finite length to the derivative. This way noise can be excluded to get more reliable results. The break point therefore indicates the point where combustion speed changes the most. By using a first order polynomial to fit the derivative the calculated breakpoint appears slightly later (less than 0.4 CAD). Although a higher order polynomial can increase the accuracy in some points, it will increase the high frequency content making it more

difficult to separate the wanted second derivative from noise.

By applying this to the calculated RoHR in Figure 5, a break point (black dashed line) is added where auto-ignition is calculated to have occurred. This gives slightly more than 30% of the total heat released as ISHR at this particular operating point (160 CAD NVO). However, since the early auto-ignition process is also relatively slow if not initiated by the spark, this estimation will still show some percent of ISHR even for pure HCCI.

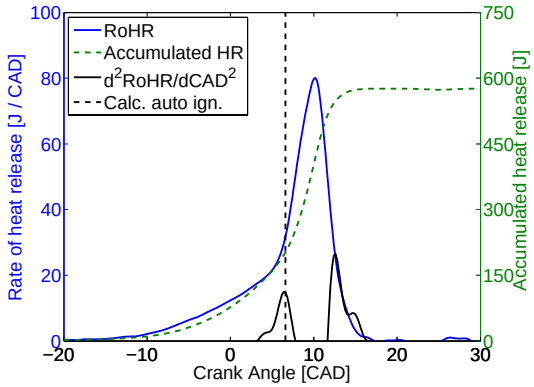

Figure 5. Rate of heat release, accumulated heat release, calculated second derivative of RoHR used to find the estimated CAD where auto-ignition occurs.

1. NVO SWEEP

To see the influence of the two different heat release modes (ISHR and fast heat release) a sweep is performed ranging from 0 CAD NVO to an NVO of 200 CAD with increments of 40 CAD, trapping more and more residuals with increased NVO. The engine is run at stoichiometric conditions with a constant fueling of 680 Joule / cycle corresponding to a load of approximately 3.5 bar $IMEP_{net}$ at 200 CAD NVO. At low NVO the engine is run throttled with a lower $IMEP_{net}$ due to pumping losses and as the NVO is increased the intake pressure also increases as more residuals are trapped. For all spark assisted measurement points in the sweep the spark timing is kept constant at -19 CAD ATDC. The constant spark timing will give a variation in combustion timing for the different NVOs. The definition of combustion timing in this work is crank angle for 50 % heat released (CA50). However, the spark timing is though as more important than combustion timing for the study of the early heat release originating from the spark. CA50 is in-between 8-10 CAD ATDC for 0, 40, 80 and 200 CAD NVO and around 15 CAD ATDC for the cases at 120 and 160 CAD NVO.

Figure 6 shows the amount of ISHR when increasing the NVO. Since the engine has to be run with rather low cooling water temperature and has low CR the engine has to be run with a rather low octane fuel. Therefore the engine exhibits auto-ignition provoked by the ISHR also for low NVO. As the NVO is increased the amount of ISHR drops due to increasing residual rates. At 200 CAD NVO the intake pressure is close to ambient (0.97 bar). A last operating point was run by opening the throttle fully without increasing the NVO further. HCCI combustion was achieved without the need of the spark at slightly lean conditions. This measurement point is used to be able to do a later comparison between SACI and HCCI combustion at almost similar conditions. For all the operating points, shown in Figure 6, the coefficient of variation (COV) in IMEP is below 1.4 %.

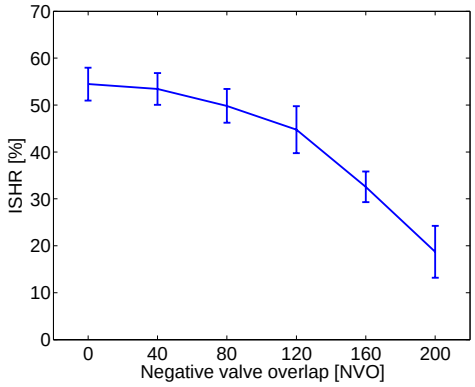

Figure 6. Amount of mean ISHR and standard deviation of 1000 cycles for increasing NVO.

From the chemiluminescence images obtained it is clear that we have a flame propagation followed by auto-ignition in the outer rims of the combustion chamber at low NVO. This is expected since the in cylinder conditions are then typically as for an SI engine with insufficient fuel octane rating. However, when the residuals are increased by higher NVO the amount of flame propagation is lowered due to higher charge temperature and thus, a greater part of the charge burns in HCCI mode. In appendix A and B the combustion event of two SACI cycles at an NVO of 200 CAD can be followed, starting with the early flame development originating from the spark, provoking the later auto-ignition followed by faster HCCI combustion. Appendix A with spark timing at -19 corresponds to one of the cycles used for the expansion speed calculation in the NVO sweep at 200CAD.

To see how the flame development is affected by the increasing NVO, flame expansion speed calculations are performed as explained in the image processing section. Figure 7 shows the calculated averaged mean expansion speed of twenty cycles when increasing the NVO from 40 to 200 CAD. The 0 NVO case

unfortunately had to be removed due to errors during image acquisition.

The flame calculations are started a few CADs after spark ignition. The bright light from the spark break through will affect the calculation result if starting earlier. The length of the calculations is limited by auto-ignition or if the flame is moves outside the visible part of the combustion chamber making it impossible to obtain the flame area. To cancel out cycle by cycle differences in the early flame propagation the mean of 20 cycles is shown. The cycle individual expansion speeds for the 200 CAD NVO case is shown in Figure 8 to get a better understanding for the variations.

What can be seen is that the flame expansion speed decreases as the residuals increase. However at an NVO of 200 CAD the flame expansion speed close to TDC is still approximately 2/3 of the flame expansion speed at low residual rates.

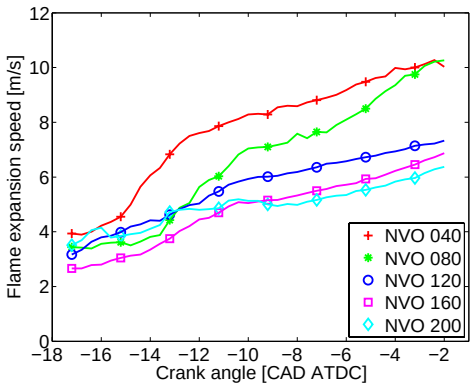

Figure 7.Mean flame expansion speed for increasing NVO, average of twenty cycles.

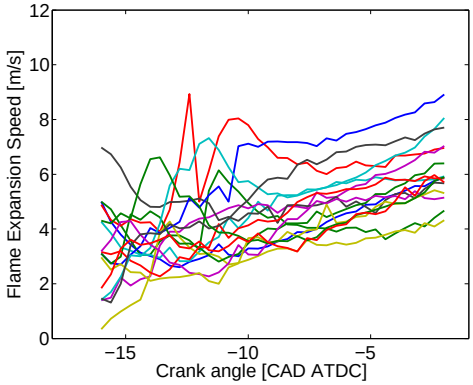

Figure 8. Mean expansion speed for single cycles. 200 CAD NVO.

2. SPARK TIMING SWEEP

To further understand the effect of the early flame on HCCI combustion a spark timing sweep is performed at an NVO of 215 CAD and constant fueling of 490 Joule / cycle corresponding to approximately 2.4 bar $IMEP_{net}$ at stoichiometric conditions.

By phasing the spark timing from -30 to -60 CAD ATDC the combustion timing is advanced from 14.6 to 7.3 CAD ATDC. Combustion timing and coefficient of variation of IMEP (COV_{IMEP}) are illustrated in Figure 9. COV_{IMEP} maintains a stable value of slightly less than 4 % until the spark timing is further advanced to –60 CAD ATDC where it increases to an unacceptable level, the mean combustion timing is also slightly retarded. As indicated by the COV, misfire occurred during measurements and therefore no chemiluminescence data are available. It is not possible to phase combustion any earlier due to the in–cylinder conditions at the very early spark timing. In case of very early spark timing the turbulence levels and the temperature conditions are thought to prohibit flame propagation. One more unknown factor is how well the fresh charge of fuel and air is mixed with the trapped residuals. If the main tumble flow in the cylinder consists of a slightly stratified charge it is possible that the mixture at the spark plug position changes in both equivalence ratio and temperature during the compression, affecting the ignitability of the charge. For retarded spark timing and thereby late combustion timing cycle to cycle variation is known to increase again. This will then influence the early flame by changing the charge conditions. In [6] the presence of optimum spark timing could be found, and in Figure 10 a slightly lower standard deviation of the amount of ISHR can bee seen closer to a spark timing of -40CAD ATDC. The effect is not very significant in this case though.

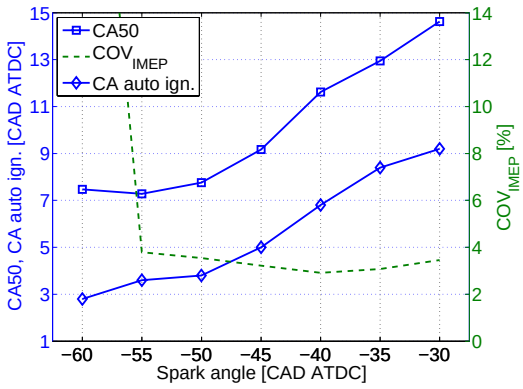

Figure 9. CA50, calculated auto-ignition timing and COV as a function of advanced spark timing.

The amount of ISHR and the standard deviation of ISHR when advancing the spark timing is shown in Figure 10.

The standard deviation of the amount of ISHR is high compared to the trend that can be seen. Still it is possible to distinguish that as the spark timing is advanced the amount of ISHR increases slightly. An increased amount of ISHR means that more heat is released by the early SI flame compared to the later HCCI combustion. The change in combustion timing could then be due to a change in ratio between SI and HCCI. However, the increase in ISHR for earlier spark timing was small and when looking at the calculated auto-ignition timing obtained from the ISHR calculations auto-ignition is seen to be advanced. So the earlier combustion timing is mainly due to phasing of the auto-ignition timing. Both CA50 and calculated auto-ignition timing are shown in Figure 9. The auto-ignition timing is advanced almost as much as CA50. For the case with spark timing at -60 CAD ATDC the cycle to cycle variations are very high and the curves for CA50 and auto-ignition move in opposite direction.

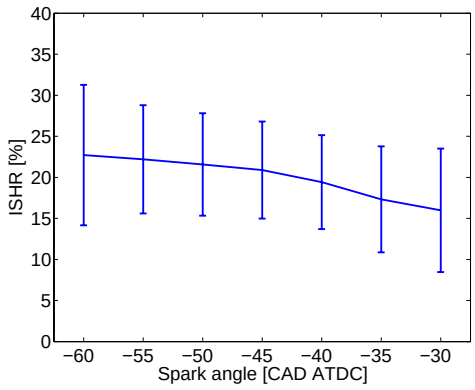

Figure 10. Amount of ISHR and standard deviation for increased spark advance, average of 1000 cycles. Spark timing at -60 CAD ATDC is on the limit to misfire.

The calculated flame expansion speeds for the spark timing sweep is illustrated in Figure 11. As the spark timing is advanced the start of the flame propagation also advances. However the ignition delay, or the time from the spark until it is possible to detect an initial growing flame increases. Also the earliest detected flame expansion speeds are lower for more advanced spark timing. A reason for the lower flame expansion speed at highly advanced spark timing can be the lower charge temperature early in the compression stroke combined with different flow and turbulence conditions.

Although ignition delays differ, the later flame expansion speed increases in an almost similar way for the different cases and reaches a mean expansion speed of slightly less than 5 m/s when some part of the flame starts to expand outside of the visible area and the calculation is terminated.

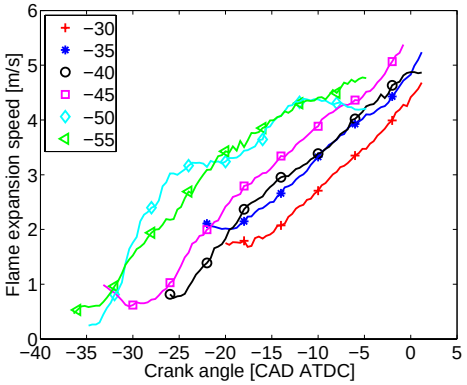

Figure 11. Mean flame expansion speed for increased spark advance, average of twenty cycles.

An increased amount of ISHR is expected to be needed to speed up the auto-ignition process as shown in Figure 10 to reach earlier CA50. Also, earlier combustion phasing will mean a lower exhaust temperature and thereby lower residual temperature for the following cycle again increasing the need for adding more heat to achieve auto-ignition. On the other hand earlier combustion timing means higher heat losses and higher chamber wall temperatures. This is thought to be the reason for a lower amount of ISHR when advancing the spark timing for some of the operating points from the NVO sweep presented earlier when advancing spark timing for them. Also, by earlier heat release due to advanced spark timing, the compression work should increase, raising the temperature at TDC. In those cases combustion timing is phased closer towards TDC compared to what is possible in the spark timing sweep that is conducted at lower load than the NVO sweep. The lower amount of ISHR with the earlier spark timing is illustrated by two single cycles in Appendix A and B, showing flame developments where the only difference is spark timing. It can be seen that the amount of fuel consumed before auto-ignition is significantly lowered at earlier spark timing. By looking at the images for these individual cycles the first sign of auto-ignition in Appendix A is after 20% heat released by the flame compared to less than 4 % in appendix B, with earlier spark timing. In these two single cycle sequences, each image is scaled from zero to maximum intensity to be able to see the early flame with lower intensity. In order not to lose information of RoHR from intensity the calculated amount of heat released (HR) is added above each image.

3. LOAD SWEEP

As the load is lowered the residual rate is increased by increasing the NVO from 197 to 215 CAD, to keep stoichiometric conditions. Increased residual rate should mean increased charge temperature, however as the

load is lowered the residual temperature decays as a direct result of less fuel burned. This decay in residual temperature is here stronger than the effect of higher residual ratio, therefore as the load is lowered the amount of ISHR has to be increased to keep constant CA50. CA50 is kept in-between 8 and 10 CAD ATDC for the load sweep. In Figure 12 the spark timing is shown for the sweep in load. As the load is lowered the spark is set off earlier to increase the ISHR. For the lowest load case the spark timing is advanced as much as possible without increasing the cycle by cycle variations too much. Earlier spark timing can result in misfire due to poor in-cylinder conditions for ignition. A further decrease in load by increasing the residual rate will deteriorate the conditions for spark assistance.

When looking at the calculated flame development speeds in Figure 12 it is difficult to draw any clear conclusions since also spark timing has to be changed when varying the load. It can be seen that closer to TDC the expansion speeds for all the measurement points are reaching similar values although for the higher load cases the flame has much less time to grow. This is also seen above for the spark timing sweep. Closer to TDC and for high loads also at earlier crank angles (BTDC) the temperature in the flame surroundings is increased which improves the conditions for the flame to propagate with less heat losses. However, advanced spark timing of course still increases the amount of heat released by flame development, but at an initially slower pace.

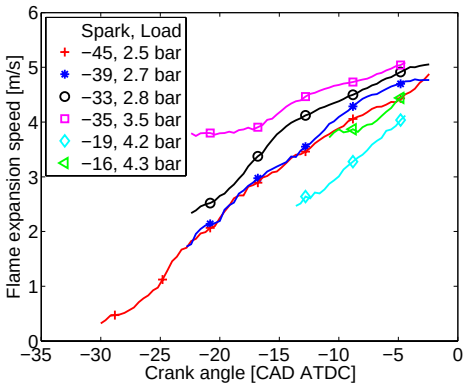

Figure 12. mean flame expansion speed for load sweep at high NVO, average of twenty cycles.

A COMPARISON WITH PURE HCCI

When running 200 CAD NVO with SACI combustion in the NVO sweep presented earlier it was possible to make a transition to full HCCI without the need for the spark. By fully opening the throttle the conditions went from stoichiometric to slightly lean (λ = 1.03) and self sustaining HCCI combustion. The spark can be turned off. For the SACI combustion cases dealt with above the auto-ignition process seemed to be rather stratified, starting at a single location and then advancing through the combustion chamber. Even for pure HCCI this is still the case. Therefore a fictional reaction front spreading velocity can be calculated as described in the image processing section. The ignition processes for three different cycles are shown in Figure 13. It is clear that HCCI reaches very high spreading velocity with high RoHR compared to the ISHR. The peak velocities are around 110 m/s for these cycles. What is also very interesting is that for all cases the initial velocity is rather low, almost comparable to the calculated mean expansion speed of the SI flame. For cycle number 1 it is especially low and lasting for 10 CAD before the RoHR is rapidly increased. It should be noted that the calculation is started when combustion is detected within the visible area, meaning it could have started earlier near the perimeter. The calculations are stopped just before it reaches the end of the visible part of the combustion chamber. Cycles number 1 and 3 are illustrated in Appendix C and D. Since the combustion rate increases during the cycle the time step between the images in the appendix is varied to resolve the interesting parts. For both cycles an initial very stratified slow combustion is seen although they have a different duration, until the faster combustion starts with what seems like new burning islands in front of the combustion zone spreading over the combustion chamber.

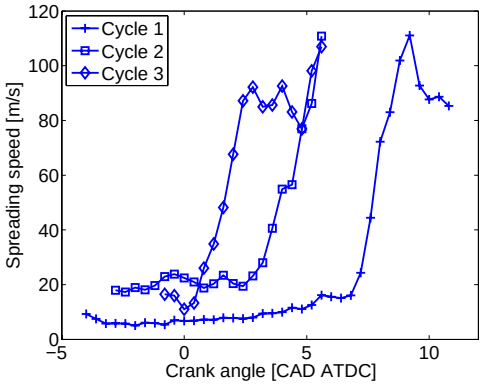

Figure 13. HCCI development speed for three individual cycles, no spark assistance.

The difference in combustion rate for SI, SACI and HCCI is very well reflected by looking at the burning area of the three different combustion modes shown in Figure 14. First for an NVO of 40 CAD the main part of the heat release is in SI mode with a gradually increased enflamed area, increasing in speed as the flame is growing. Secondly, SACI at 200 CAD NVO with the initial SI flame propagation that later is auto ignited with a resulting fast increase in burning chamber area. Last, the pure HCCI case with a steep increase in burning

area. Still the HCCI cycle shows some ISHR in the beginning, burning highly stratified.

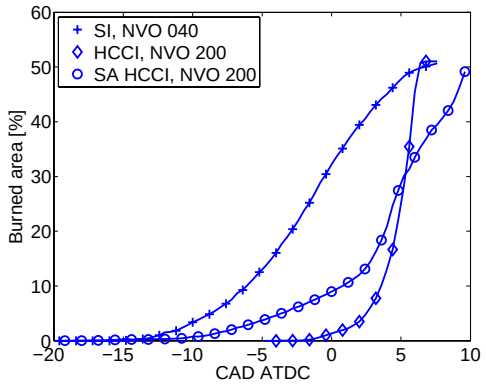

Figure 14. Difference in burning area over CAD for SI, SACI and HCCI.

DISCUSSION

In an SI engine the behaviour of the early flame kernel is of high importance for the ensuing combustion. The turbulence levels in the vicinity of the sparkplug will have a very strong effect on combustion timing and duration. HCCI combustion is normally run very lean or highly diluted with residuals, giving conditions where a flame would be expected to propagate very slowly or not at all.

SACI combustion at these high residual rates past the lean limit of the conventional SI engine is thought to be enabled by the elevated temperature conditions. The early flame development is a balance between the heat released by the flame and the convective heat losses to the surrounding gas. The residuals that dilute the charge will lower the heating value per unit mass, lowering the flame temperature. However, with trapped residuals the initial temperature is higher, thus the effect of heat transfer should be lower.

Also a lower flame speed can be tolerated in SACI compared to in the SI case. For the SI engine, flame speed has to be kept high enough to prevent burn duration from increasing. Too long burn duration means at first, lower efficiency and, in severe cases risk of partial misfire. In SACI the early flame is used only to initiate the greater part of the charge to auto ignite and burn in HCCI mode, therefore slower flame propagation can be accepted in SACI mode.

In the present work shows that it is possible to run a wide variety of operating conditions in the intermediate region between SI and HCCI, here called SACI combustion. For both SACI and pure HCCI combustion the auto-ignition process is seen to be highly stratified and starting between the intake and the exhaust valves, actually closer to one of the intake valves where it would be expected to be colder. These two findings suggest stratification between the hot residuals and the colder fresh charge of fuel and air. The extent and effect of stratification is however difficult to interpret with the measurement technique used in this work.

The flame propagation of SACI combustion and the slow stratified auto-ignition process of pure HCCI show similarities in the behavior in terms of a slow expansion or spreading speed. For the later HCCI combustion the front spreading speed can reach above 100 m/s, but during the early part the velocity is in the range of 5 – 20 m/s which can be compared to the expansion speed of the SACI flame reaching around 6 m/s at very similar conditions.

CONCLUSIONS

A number of conclusions can be drawn from this experimental study:

- Stable combustion is achieved from low to high residual fractions with a fuel blend of ethanol and n-heptane.
- SACI combustion with NVO at close to stoichiometric conditions consists of flame propagation that triggers auto-ignition with following HCCI combustion.
- The propagating flame initiates auto-ignition at the outer rim of the combustion chamber.
- The flame expansion speed deteriorates but the flame prevails also with high residual rates.
- The earlier the spark timing, the longer the ignition delay with initially slower flame expansion.
- Earlier combustion phasing by means of spark advance for SACI combustion also advances the auto-ignition timing in the same order of magnitude.
- When combustion timing is advanced by earlier spark timing the amount of ISHR increases due to more heat needed to force earlier auto-ignition, however advanced auto-ignition can again decrease the amount of ISHR, probably due to higher wall temperatures.
- For low load and high NVO, SACI is limited by too early spark timing resulting in a too low temperature in combination with a very high dilution of residuals extinguishing the early flame.
- The flame expansion speed for SACI combustion and the initial stratified HCCI front spreading speed are of same order of magnitude.

ACKNOWLEDGMENTS

The authors wish to show their great appreciation to the Centre of Competence at Lund University (KCFP) for their financial support, to Cargine for providing the active valve train and to the technicians at the division for their valuable assistance in the lab.

REFERENCES

1. J. Willand, R-G. Nieberding, G. Vent, C. Enderle; ”The knocking Syndrome –Its Cure and its Potential”, SAE Paper 982483
2. J. Lavy, J-C. Dabadie, C. Angelberger, P. Duret, J. Willand, A. Juretzka, J. Schäflein, T. Ma, Y. Lendresse, A. Satre, C. Schulz, H. Krämer, H. Zhao, L. Damiano; ”Innovative Ultra-low NOx Controlled Auto-Ignition Combustion Process for Gasoline Engines: the 4-SPACE Project
3. L. Koopmans, H. Ström, S. Lundgren, O. Backlund, I. Denbratt: ”Demonstrating a SI-HCCI-SI Mode Change on a Volvo 5-Cylinder Electronic Valve control Engine”, SAE Paper 2003-01-0753
4. L. Koopmans, I. Denbratt: ”A Four Stroke Camless Engine, Operated in Homogenous Charge Compression Ignition Mode with Commercial Gasoline”, SAE Paper 2001-01-3610
5. A. Fuhrhapter, W. F. Piock, G. K. Fraidl: ”CSI – Controlled Auto-ignition – The Best Solution for the Fuel Consumption – Versus Emission Trade-Off?”, SAE Paper 2003-01-0754
6. H. Persson, R. Pfeiffer, A. Hultqvist, B. Johansson, H. Ström: ”Cylinder-to-Cylinder and Cycle-to-Cycle Variations at HCCI Operation with Trapped Residuals”, SAE Paper 2005-01-0130
7. T. Urushihara, K. Yamaguchi, K. Yoshizawa, T. Itoh: ”A Study of a Gasoline-fueled Compression Ignition Engine ~ Expansion of HCCI Operation Range Using SI combustion as a Trigger of Compression Ignition”, SAE Paper 2005-01-0180
8. F. Bowditch: ”A New Tool for Combustion Research A Quartz Piston Engine”, SAE Paper 610002
9. B. Johansson: “On Cycle to Cycle Variations in Spark Ignition Engines – The Effect of Fluid Flow and Gas Composition in the Vicinity of the Spark Plug on Early Combustion”, Doctoral Thesis, Lund ISRN LUTMDN/TMKV—1010-SE
10. S. Trajkovic, A. Milosavljevic, P Tunestal, B. Johansson: “FPGA Controlled Pneumatic Variable Valve Actuation”, SAE Paper 2006-01-0041
11. G. Woschni: ”A Universally Applicable Equation for the instantaneous Heat Transfer Coeffficient in the Internal Combustion Engine”, SAE Paper 670931
12. J. Heywood: ”Internal CombustionEngine Fundamentals”, MacGraw-Hill ISBN 0-07-100499-8, 1988
13. A. Hultqvist, M. Christensen, B. Johansson, M. Richter, J. Nygren, J. Hult, M. Aldén: ”The HCCI Combustion Process in a Single Cycle – High-Speed Fuel Tracer LIF and Chemiluminescence Imaging”, SAE Paper 2002-01-0424
14. G. Rassweiler, L. Withrow: ”Motion Pictures of Engine Flames Correlated with Pressure Cards”, SAE Paper 380139
15. A. Hultqvist, M. Christensen, B. Johansson, A. Franke, M. Richter, M. Aldén: “A study of the Homogeneous Charge Compression Ignition Combustion Process by Chemiluminescence Imaging”, SAE Paper 1999-01-3680
16. H. Persson, L. Hildingsson, A. Hultqvist, B. Johansson, J. Ruebel: “Investigation of Boundary Layer Behaviour in HCCI Combustion Using Chemiluminescence Imaging ”, SAE Paper 2005-01-3729
17. J. Hyvönen, G. Haraldsson, B. Johansson: ”Operating Conditions Using Spark Assisted HCCI Combustion During Combustion Mode Transfer to SI in a Multi-Cylinder VCR-HCCI Engine”, SAE Paper 2005-01-0109

CONTACT

Corresponding author:
Håkan Persson

Address
Lund University
Dept. of Energy Sciences
Div. of Combustion Engines
P.O. Box 118
221 00 Lund
Sweden

E-mail
hakan.persson@vok.lth.se

ACRONYMS

ATDC	After Top Dead Center
BTDC	Before Top Dead Center
CAD	Crank Angle Degree
CI	Compression Ignition
EVC	Exhaust Valve Closing
HCCI	Homogeneous Charge Compression Ignition
HR	Heat Release
IMEP	Indicated Mean Effective Pressure
ISHR	Initial Slow Heat Release
IVO	Inlet Valve Opening
LTR	Low Temperature Reaction
NVO	Negative Valve Overlap
PFI	Port Fuel Injection
PPC	Partially Premixed Combustion
RoHR	Rate of Heat Release
SACI	Spark Assisted Compression Ignition
SI	Spark Ignition

Appendix A. SACI combustion 200 CAD NVO, spark timing – 19 CAD ATDC. First image showing valve location

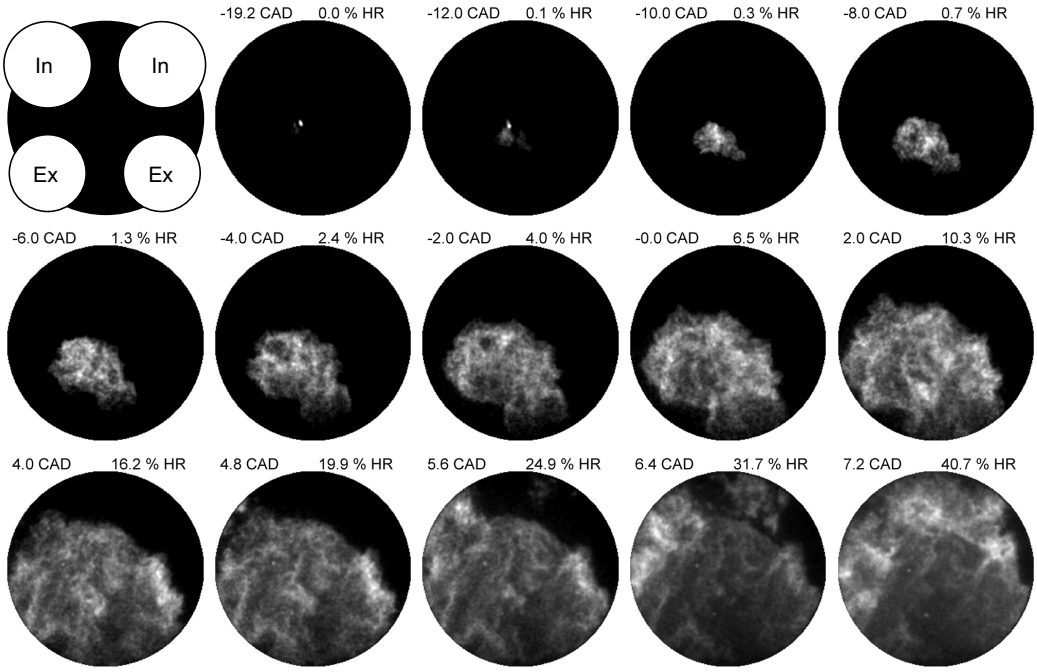

Appendix B. SACI combustion 200 CAD NVO, spark timing – 21 CAD ATDC

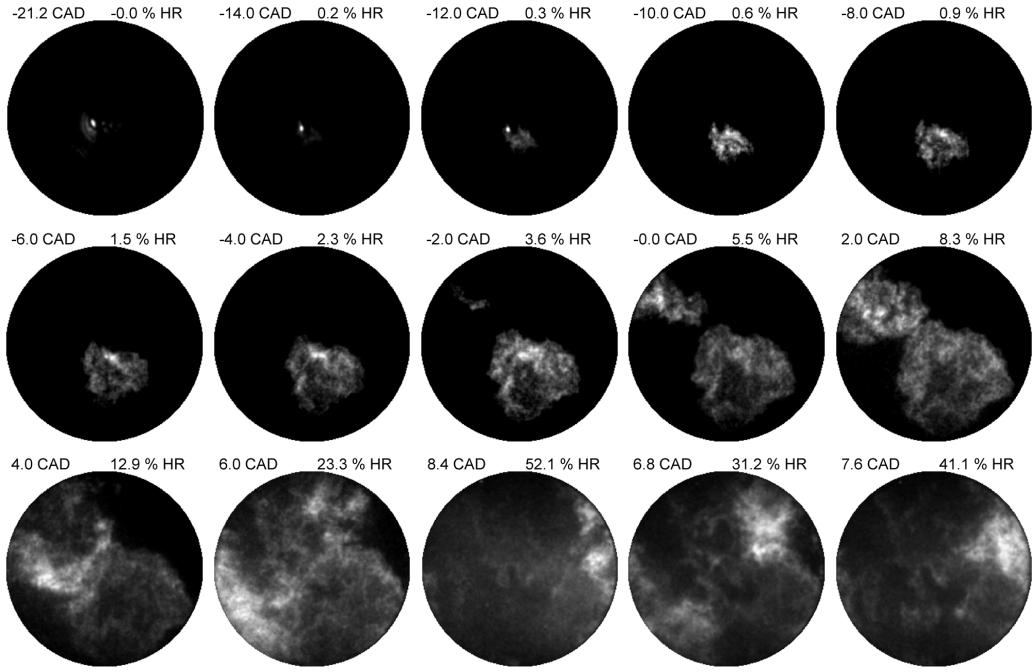

Appendix C. HCCI combustion 200 CAD NVO, cycle number 1 from Figure 13.

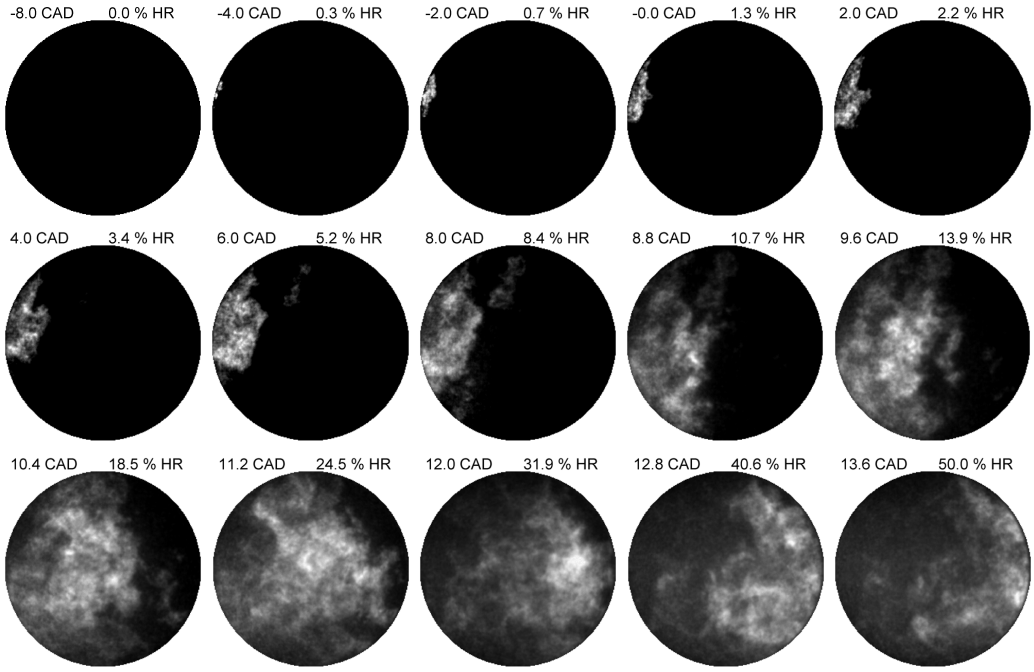

Appendix D. HCCI combustion 200 CAD NVO, cycle number 3 from Figure 13.

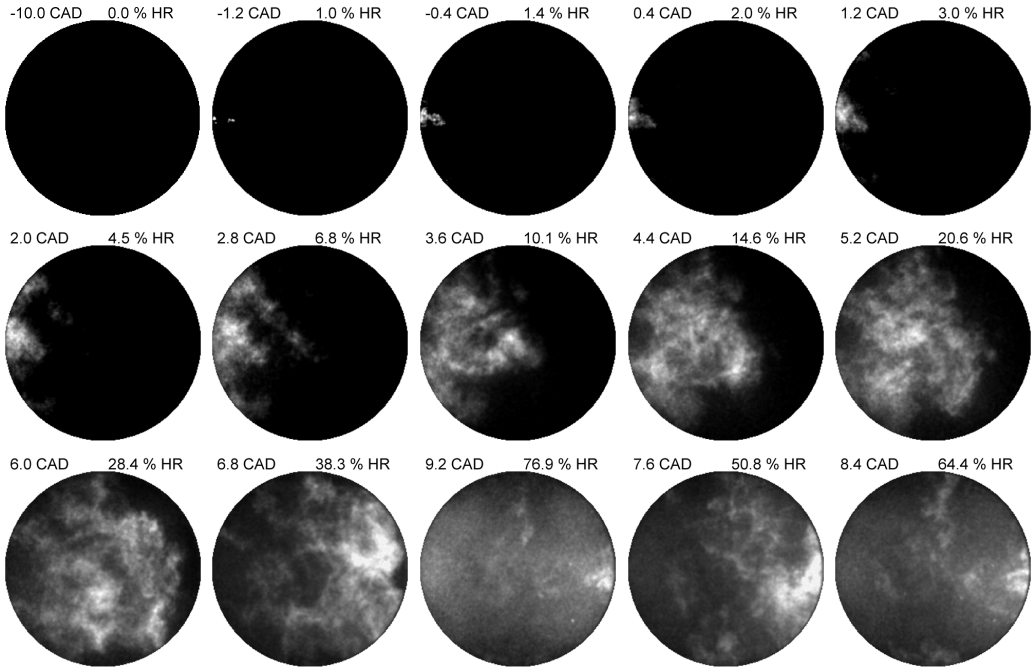

V

JSAE 20077167
SAE 2007-01-1856

The Effect of Swirl on Spark Assisted Compression Ignition (SACI)

Håkan Persson and Bengt Johansson
Lund University

Alfredo Remón
Simon Bolivar University

ABSTRACT

Auto ignition with SI compression ratio can be achieved by retaining hot residuals, replacing some of the fresh charge. In this experimental work it is achieved by running with a negative valve overlap (NVO) trapping hot residuals. The experimental engine is equipped with a pneumatic valve train making it possible to change valve lift, phasing and duration, as well as running with valve deactivation. This makes it possible to start in SI mode, and then by increasing the NVO, thus raising the initial charge temperature it is possible to investigate the intermediate domain between SI and HCCI. The engine is then running in spark assisted HCCI mode, or spark assisted compression ignition (SACI) mode that is an acronym that describes the combustion on the borderline between SI and HCCI.

In this study the effect of changing the in-cylinder flow pattern by increased swirl is studied. This is achieved by deactivating one of the two intake valves. The effect of the increased turbulence is studied both on the initial slow heat release originating from the spark plug and on the following HCCI combustion.

The early SI flame development is highly dependent on the flow field so by increasing the turbulence the flame expansion speed is affected, also at high residual rates. Also, HCCI combustion rate has been shown to slow down as turbulence is increased. As high reaction rate is an issue for HCCI combustion this means that it could be possible to reduce the reaction rate and simultaneously increase the possible usage of SACI combustion by increasing the turbulence.

Synchronized simultaneous pressure and high speed chemiluminescence measurements are conducted making it possible to reproduce fully resolved cycles from the onset of the spark throughout the entire combustion event. From the chemiluminescence images it is possible to calculate a flame expansion speed. The effect on combustion in terms of auto ignition timing, combustion duration and the amount of heat released in the different combustion modes is investigated using heat release analysis. LDV measurements are conducted to support the turbulence effects on SACI combustion.

INTRODUCTION

Throughout the last decades Homogeneous charge compression ignition (HCCI) has been the subject of intensive research that is now branching into two main paths. Diesel HCCI with partially premixed combustion (PPC) and gasoline HCCI with different strategies of residual usage to reach auto ignition temperature, also often refered to as controlled auto ignition (CAI) combustion. In the latter concept the strategy is to run the engine in SI mode when high output power is required and in HCCI mode at low and part load to keep up efficiency. The proposal for using negative valve overlap (NVO) to reach HCCI combustion in an SI engine environment was first published by Willand et al. in 1998 [1]. The first presented results of NVO HCCI combustion by Lavy et al [2] followed in 2000. Cycle to cycle mode switches from SI to HCCI and vice versa has been demonstrated on multi cylinder engines [3] showing the possibility of such a concept.

Recent research has shown the potential of using spark assistance to aid gasoline HCCI combustion at some operating conditions, and even extend the operating regime into regions where unsupported HCCI combustion is impossible. The first reports of combustion stability effects by usage of a spark with NVO HCCI were published by Koopmans et al [4]. Later experiments have shown the possibility to also affect combustion timing [5] and to cancel oscillating behaviour in combustion timing at low temperature conditions [6]. Spark assistance is also investigated when going towards higher possible loads as described by Urushihara et al. [7].

This implies that the usage of spark assisted HCCI or spark assisted compression ignition (SACI) could

help to expand the usable operating regime for NVO HCCI as well as to assist during mode switching events. However more knowledge is needed on the nature of the spark effects and the influence of the ensuing HCCI combustion. This since HCCI combustion normally is run highly diluted with air or residuals, an environment that a normal SI flame would not be expected to endure.

There are ways to increase the performance of SI combustion at unfavourable conditions. Prior SI combustion experiments with the current combustion chamber have shown great improvement in lean burn capability with maintained combustion stability at lean conditions [8]. This has been accomplished by both inlet valve deactivation and late intake valve closing (IVC). The deactivated inlet valve changed the tumbling in-cylinder flow to a swirling motion with increased turbulence intensity and thus faster burn rate. The outcome was even more pronounced with late IVC.

The turbulence is shown in Figure 1 for the case of two inlet valves, and for inlet valve deactivation in Figure 2, both with standard valve timings. The measurements are conducted from one side to the other in the pent-roof, passing the spark plug location. The increase in turbulence is significant. At lean conditions the burn duration of 0 to 10 % heat released could almost be halved.

The above results encourage investigation of SACI combustion at conditions with elevated turbulence levels to further increase the usefulness of SACI combustion.

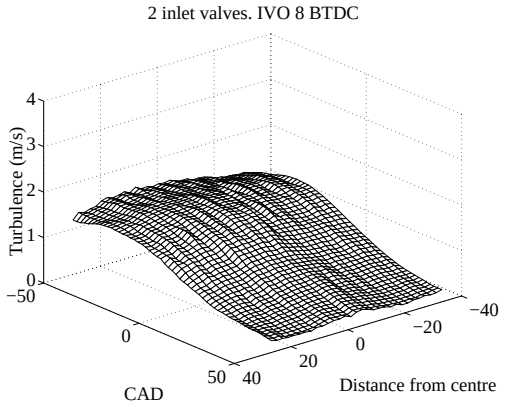

Figure 1. Turbulence for two valve inlet strategy [8].

It is generally accepted that the HCCI combustion process is controlled by chemical kinetics, thereby the effects of turbulent mixing should not affect the chemical reactions and the heat release process since the local chemistry is an order of magnitude faster than turbulence effects.

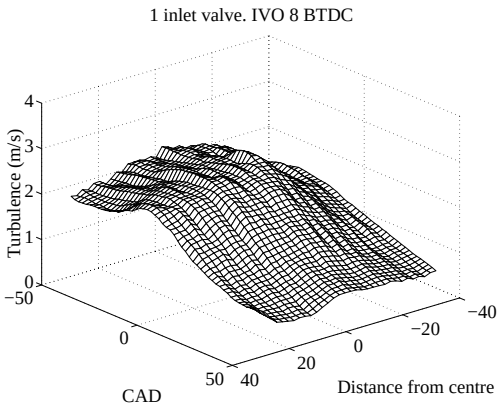

Figure 2. Turbulence for inlet valve deactivation strategy [8].

Earlier experiments have however shown a decreased HCCI combustion burn rate for geometry generated turbulence [9, 10]. For inlet generated turbulence in a lean burn HCCI engine without residuals [11] only minor changes in combustion behaviour could be seen and only small moderations of the intake temperature was needed to maintain the combustion timing.

For HCCI combustion with NVO, some stratification between the trapped hot residuals and the fresh charge can be expected. This means that both temperature and gas composition is inhomogeneous. Thereby the effect of turbulence could be increased. To investigate the role of turbulence for SACI combustion inlet port deactivation is used. Turbulence intensity is measured using Laser Doppler Velocimetry (LDV). The effect on the early flame development is studied with high speed broad band chemiluminescence imaging and the auto ignition timing by pressure and heat release analysis.

EXPERIMENTAL SETUP

ENGINE SETUP

The experimental engine is based on a Volvo D5, which is a passenger car sized five cylinder compression ignition (CI) engine. The engine is converted to single cylinder operation with a bowditch piston extension. The remaining four pistons are motored and are equipped with counter weights to compensate for the extra weight of the piston elongation on the operated piston. A 58 mm diameter quartz glass is fitted in the piston extension resulting in a flat piston crown. The optical access is approximately 51 % of the total combustion chamber area. Also small vertical windows are mounted perpendicularly in the pent-roof giving see-thru access to the vicinity of the sparkplug. The combustion chamber is of SI type with a high pent-roof, four valve design. More engine specifications can be found in Table 1.

Table 1

Displacement	0.48 Liters
Valves per cylinder	4
Bore	81 mm
Stroke	93.15 mm
Combustion chamber	Pent-roof
Compression ratio	9:1
Valve timings	Fully flexible
Speed	1200 rpm

The Engine is fitted with a pneumatic valve train system supplied by Cargine Engineering [12]. The system features fully flexible valve lift, duration and timing as well as deactivation individual for each valve. The engine with the valve actuators mounted on the cylinder head is shown in Figure 3.

In this work a symmetrical NVO is used, meaning exhaust valve closing (EVC) at the same CAD before top dead centre (BTDC) as intake valve opening after top dead centre (ATDC). Intake closing and exhaust opening have been fixed at -160 and 160 CAD ATDC respectively. For all cases a lift height of approximately 8 mm is used with an opening and closing ramp of approximately 25 CAD at 1200 rpm.

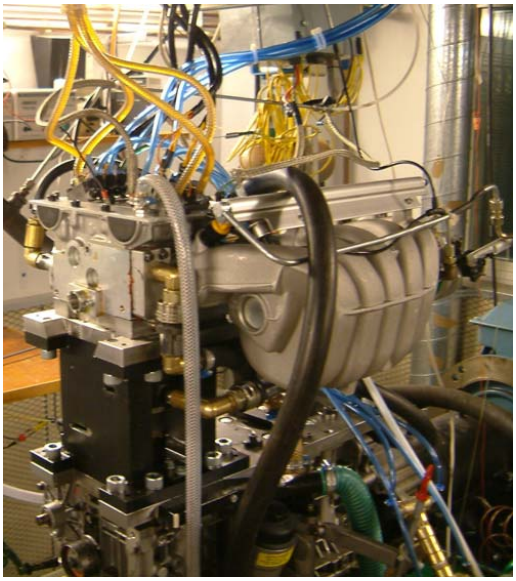

Figure 3. Single cylinder engine with optical access and pneumatic free valve train.

MEASUREMENT SYSTEM

Pressure is monitored with a Kistler 6117B combined sparkplug and pressure sensor with a sample rate of 5 per CAD. The piezo electric pressure sensor is flush mounted in the sparkplug. Emissions are monitored using a Horiba MEXA 8120, measuring NO_x, CO, HC, CO_2 and O_2.

The fluid flow is measured by a 2-component Dantec-fibre flow LDV system at a wavelength of 488 and 512 nm respectively, thus giving two dimensional velocity information. The setup consists of an Ar-ion laser, colour separator and fibre transferring of the laser beams to a probe with a beam expander. An f 310 lens is used to focus the beams near the spark plug through the optical access to the combustion chamber pent-roof. The backscattered light from the seeding particles is collected and transferred back to two photo multiplier (PM) tubes where it is converted to an electric signal. This signal is digitized and analysed with fast Fourier transformation (FFT) by burst spectrum analysers (BSA) to obtain valid velocity data. The BSAs are run with an external frequency generator giving a maximum mean data rate of 150kHz. A polystyrene-latex dispersion with a mean size of 0.46 µm is used as seeding and is added upstream of the intake manifold by a set of Hudson Up-Draft nebulizers.

Combustion is seen by chemiluminescence imaging from below through the piston crown using a Phantom high speed framing camera running synchronised with the engine, taking 2.5 images per CAD. This corresponds to 18000 Hz at 1200 rpm. At this framing rate, image resolution is limited to 304 x 304 pixels, giving a pixel size of 0.2 mm. The camera is used in combination with a Hamamatsu high speed gated image intensifier. This allows short exposure times with less smearing of the images. For all cases an exposure time of 12 µs has been used. A 105 mm f 2.8 macro lens is used and apertures have been kept in the range from 5.6 to 11 depending on operating conditions.

In general both the spark plasma and the main bulk combustion are very bright whereas the early combustion has very low chemiluminescence intensity. Apertures and gains have been balanced to see the early combustion, still not saturating the camera during high rate of heat release (RoHR).

For each operating point in the sweeps simultaneous pressure and image acquisition is conducted. Ten chemiluminescence cycles are captured at each point together with 1000 consecutive pressure cycles.

FUEL

Due to optical constrains the engine is run with a somewhat low compression ratio (CR = 9:1) and a cooling water temperature of 70° C. Because of the usage of seeding particles it was not desired to heat the inlet air, therefore a fuel blend with lower octane number than normal has to be used. A blend of 40 % ethanol and 60 % n-heptane (mass percentage) is used. The choice of ethanol instead of iso-octane is due to that the former seems to cancel the low temperature reactions (LTR) normally associated with n-heptane. The LTR usually occurs at around 20 CAD BTDC and could smear any early reactions originating from the spark plug. No LTR were observed for these operating conditions even during tests with 10 % ethanol and 90 % n-heptane.

IMAGE PROCESSING

The images obtained with the high speed camera have an extremely low noise level. This makes it possible to calculate, with good precision the perimeter of a burning structure from the intensity image. Similarly the projected flame area can be obtained. The process is outlined in [Figure 4].

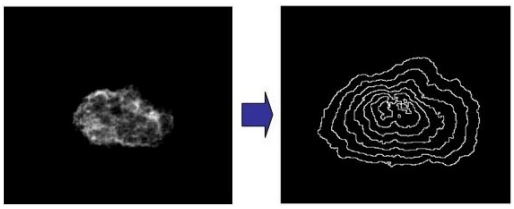

Figure 4. Left: Early flame originating from the spark plug. Right: Obtained perimeter for growing flame, image showing every fifth calculated perimeter (2 CAD separation)

A mean expansion speed is calculated according to Heywood [13] with the assumption that the flame is growing as a sphere, although it is here calculated in two dimensions, thus a circle. Therefore the perimeter of each flame image is calculated as the perimeter of a circle with the same area as the projected area of the flame

By applying Equation 1 using the differential area between two images and calculating the time step, then dividing it with the calculated flame perimeter length (L), a mean expansion speed of the flame is obtained.

Equation 1. Mean expansion speed

$$u_f = \frac{dA/dt}{L}$$

L = Perimeter length

RESULTS

TURBULENCE INFLUENCE

The high influence of turbulence on SI combustion is well known. Increasing turbulence level wrinkles the growing flame, increasing the flame surface, thus the expanding flame area. Further it is well documented that the turbulence level increases with inlet port deactivation with the combustion chamber geometry used in this study. The question that remains is if turbulence plays the same role for residual diluted SACI combustion. For NVO HCCI and SACI combustion the state of the residuals in the current cycle depends highly on the previous cycle both in terms of composition and temperature. This could indeed influence the conditions for the growing flame as it has been seen to give rise to oscillation of the HCCI combustion timing [14].

To investigate the effects of turbulence LDV measurements are conducted 1.5 mm away from the edge of the spark plug gap just upstream of the mean tumble flow. The engine is run at stoichiometric conditions with wide open throttle (WOT) in SACI mode with both inlet valves activated and a NVO of 200 CAD

From the velocity data obtained by the LDV measurements turbulence information are calculated according to Johansson [15]. For each measurement point 120 cycles of velocity data are collected, the calculated position of CA at 1 % heat released is then correlated against the turbulence level using a linear correlation coefficient according to Equation 2.

Equation 2. Linear correlation coefficient

$$R(i,j) = \frac{C(i,j)}{\sqrt{C(i,i) \times C(j,j)}}$$

Figure 5 shows the Correlation coefficient of the relation between CA 1 % heat released and the turbulence level for 120 cycles as a function of crank angle. Three different measurement points are shown all at the same distance (y) from the spark gap (upstream of the mean flow), but at different depth (x). According to statistic theory the correlation is not very high but it does exist. For all three measurement points the trend is the same that the correlation decays closer to TDC.

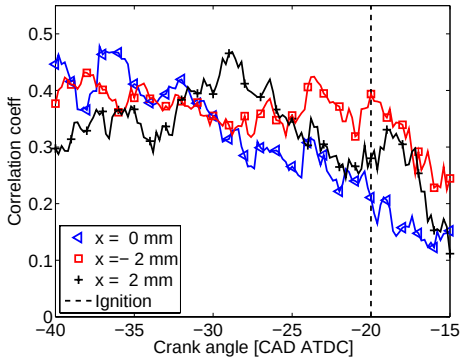

Figure 5. Correlation coefficient of relation between timing of CA 1 % heat released and turbulence over CAD.

The nature of the correlation is presented in Figure 6. This is at the crank angle of spark discharge shown by the black dashed line in Figure 5 for the measurement at x = -2 mm.

When fitting a second order polynomial to the turbulence scatter an earlier position of CA 1 % burned is seen for increased turbulence levels. The correlation coefficient at this position is 0.39. This behaviour is consistent if looking at both different crank angles and measurement points. At higher turbulence levels the effect is the opposite and the flame growth is delayed. This effect is however not as pronounced for all measurement points.

The retarded flame growth for very high turbulence levels could be due to increased heat losses when

the early flame is too heavily wrinkled with high area to volume ratio.

It can be concluded that the turbulence level plays an important role for the early flame propagation in SACI combustion with high residual rates.

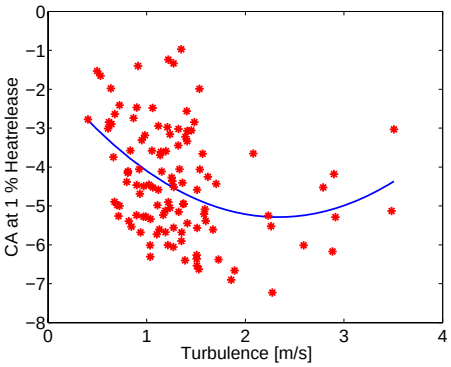

Figure 6. Correlation between CA at 1 % heat released and turbulence at -20 CAD ATDC, corr. coeff = 0.39.

FLAME EXPANSION SPEED

As the residual rate is increased by increasing the NVO the flame speed decays. The calculated flame expansion speed for an increased NVO is shown in Figure 7. The engine is run with constant spark timing at – 19 CAD ATDC. All points are run stoichiometric at constant fueling so for increased NVO, higher residual rates are balanced by reduced throttling i.e. increased intake pressure until 200 CAD NVO where the engine is run practically un-throttled.

Due to the low octane fuel some of the charge burns with HCCI combustion already at low NVO. The HCCI part of the SACI combustion increases with increased NVO, and full HCCI is reached at 200 CAD NVO with a slightly lean charge. The engine load at 202 CAD NVO is 3.3 bar $IMEP_{net}$. As the NVO is decreased also load decreases due to increased pumping losses.

As explained in [16] the possibility to still have flame propagation at these residual diluted conditions is thought to be due to elevated temperature of the residuals pushing the limit of where the heat losses from the early flame to the surroundings is too high. This is combined with the fact that the slower SI combustion with SACI can be accepted since it is followed by the onset of HCCI combustion, keeping down the total burn duration.

The effect of swirl is investigated by inlet valve deactivation while simultaneously recording in-cylinder pressure information and taking high speed videos of broad-band chemiluminescence. To ensure that the results are valid, the measurements are started with a reference case with both inlet ports activated. Then one port at a time is deactivated. Finally the reference case is run again.

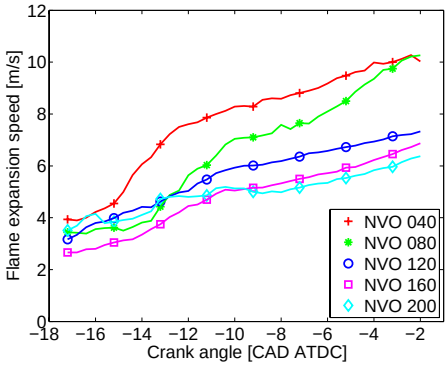

Figure 7. Calculated flame expansion speed for increased NVO.

Figure 8 shows the mean expansion speed for a NVO of 40 CAD. The calculation of flame expansion speed starts some CADs after the spark is set of as soon as a growing flame can be detected, and is terminated before either the flame grows bigger than the quartz glass or auto ignition occurs, whichever comes first. For the 40 CAD NVO a clear effect of increased turbulence by inlet valve deactivation can be seen. When both inlet valves are active and the in cylinder flow consists of a pure tumble flow pattern the same expansions speeds can be seen for both reference cases, reaching around 10 m/s which corresponds well to the calculated speed in the NVO sweep shown in Figure 7. With intake valve deactivation already the early flame development has increased in velocity compared to the reference cases and stays higher all the way reaching around 12 m/s before the calculation has to be terminated. Chemiluminescence images of single cycles for the 40 CAD NVO case can be seen in Appendix A for the reference case and in Appendix B for intake valve deactivation. If looking at TDC approximately 19 % of the heat is released in the reference case whereas 33 % when using valve deactivation.

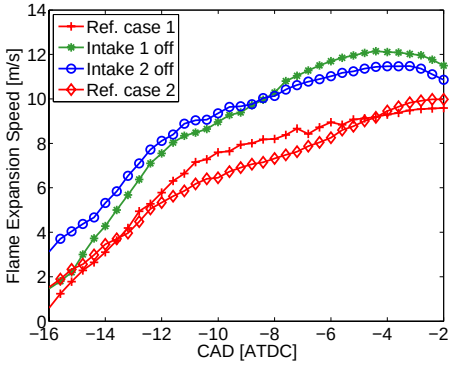

Figure 8. 40 CAD NVO, stoichiometric conditions.

At 202 CAD NVO, WOT and stoichiometric conditions the engine is still run in SACI mode, but with the greater part of the charge burning in HCCI mode. Figure 9 shows the calculated mean expansion speeds from -16 to -2 CAD ATDC. The calculation is

terminated due to auto ignition as opposed to flame size in this case.

Again we can see a strong distinction between the tumble flow and the high turbulent swirling flow. The cases with valve deactivation show a mean expansion speed around 2 m/s greater than for the reference cases. The choice of valve for deactivation has only a minor influence on the flame expansion speed. This comes as no surprise since the inlet ports are symmetric. However when looking directly on the high speed videos the different rotational directions are obvious.

Appendix C shows pictures from one of the high speed videos of the reference cases with both inlet valves active. Appendix D shows snap shots from a move where inlet valve 1 is deactivated. When comparing the images at -2 CAD, the larger flame for the swirl case is obvious. At this point the flame in the valve deactivation case has reached the edge of the visible region and the reference case shows the first signs of auto ignition.

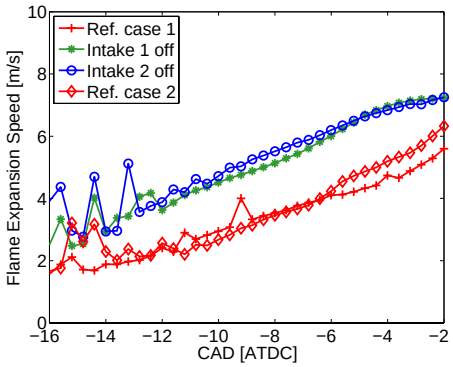

Figure 9. 202 CAD NVO, stoichiometric conditions.

EFFECTS ON AUTO IGNITION

The positive effect on flame growth by valve deactivation and increased turbulence seems straightforward; the remaining question is how does it affect the latter part of SACI combustion i.e. the HCCI combustion.

From the calculated heat release rate it is possible to estimate the auto ignition timing and the ratio of combustion prior to auto ignition. Hyvönen et al. [17] defined the initial slow heat release (ISHR) as shown in Equation 3.

Equation 3. Initial slow heat release

$$ISHR = \frac{Q_{threshold}}{Q_{\max}} \cdot 100[\%]$$

Since HCCI combustion is generally much faster than SI combustion a break point ($Q_{threshold}$) is calculated by finding the maximum difference of the derivative (2nd derivative) of the rate of heat release (RoHR). This is done here by fitting a moving polynomial of a finite length to the derivative. This way any noise can be suppressed to get more reliable results. The break point will indicate the point where combustion speed changes the most. This calculation predict the auto ignition well for SACI combustion, however when the amount of ISHR is low, the initial HCCI combustion can also be rather slow before the reaction rate increases, this can not be detected by the calculation, the amount of the charge burning in SI mode will then be over predicted.

Combustion timing and ISHR

If we apply the ISHR calculation to the calculated heat release information at three different operating conditions as shown in Figure 10 we can distinguish different behaviours depending on which combustion mode is superior.

For low NVO when the ISHR is high (here above 40 %) the faster flame development with valve deactivation will result in an advanced combustion timing towards TDC as shown in Figure 11 with a higher temperature thus slightly faster auto ignition and lower amount of ISHR.

At high residual rates as for the 202 CAD NVO case the ISHR instead increases although the flame expansion speed is increased. At the same time combustion timing is retarded. These trends correspond well with what can be seen from single cycle chemiluminescence information in Appendix C and B from this measurement point.

One explanation of the retarded combustion timing at high residual rates could be that the stratification between the hot inert residuals and the fresh stoichiometric charge is lowered by the increased mixing of the swirling motion thereby lowering the reactivity of the total charge. Auto ignition can be expected to occur in the border between the hot residuals and the fresh charge. Increased mixing with the fresh charge will lower the temperature, delaying auto ignition. This would then also be in agreement with Christensen [18] regarding temperature in-homogeneities.

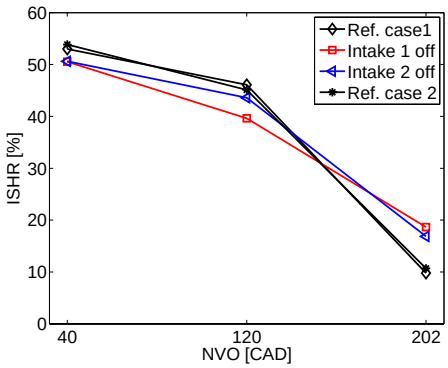

Figure 10. ISHR as a function of NVO for different inlet valve strategies.

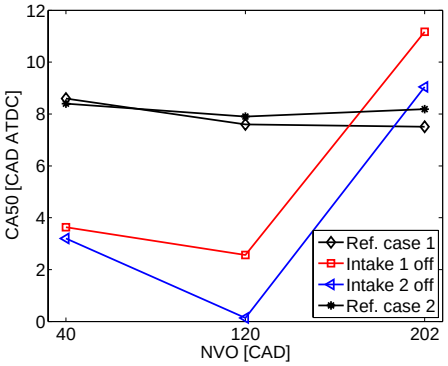

Figure 11. CA50 as a function of NVO for different inlet valve strategies.

Burn duration

Besides the turbulence effect on the auto ignition process the influence on the HCCI combustion duration is of interest. Figure 12 shows the combustion duration from the calculated point of auto ignition to CAD 90 % heat released. For the low NVO case the HCCI combustion duration is decreased, however it should be kept in mind that in this case CA50 is advanced much closer to TDC which in itself would lead to shorter combustion duration.

For the measurement point at 202 CAD NVO the HCCI burn duration is increased by approximately 25 %. At the same time the amount of fuel burned with HCCI is decreased. The calculated amount of ISHR changes from 10 to 20 % and combustion timing is slightly retarded with valve deactivation.

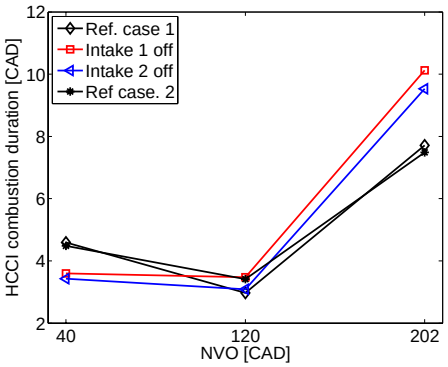

Figure 12. Combustion duration from calculated point of auto ignition to CA 90 % heat released.

Auto ignition location

The turbulence increase from valve deactivation affects not only the auto ignition timing and duration. The auto ignition location is also altered. The early flame growth is faster with the increased turbulence, however the altered flow field also transports the whole burning structure. This can be clearly seen in the chemiluminescence images in appendix E through G. Appendix E shows SACI combustion at 210 CAD NVO at a load of 2.2 Bar $IMEP_{net}$ with both inlet valves active with an air fuel equivalence ratio (λ) of 1.01. Appendix F and G is run with inlet valve deactivation. Unfortunately λ dropped to 0.94 in these cases, therefore comparisons to the reference case regarding flame growth and auto ignition timing should be done with great care. At this low load the first chemiluminescence originating from the spark is more stretched and does not really look like the growing flames shown previously. Since the intensity of these images is very low the reason could be insufficient gain of the acquisition system. As the combustion continues a more flame like structure can again be recognized, clearly following the swirling flow. The auto ignition location can be seen to move from the right side of the combustion chamber in appendix F with inlet valve 1 deactivated to the left side when inlet valve 2 is deactivated in appendix G.

SUMMARY AND CONCLUSIONS

Increased turbulence by inlet valve deactivation has been shown to influence SACI combustion in both of the two combustion modes. The interpretation of the results from the initial SI combustion is relatively straight forward. To fully understand the influence on the auto ignition process requires more knowledge of the residual stratification and its response to the mixing process caused by valve deactivation. Still a number of conclusions can be drawn.

- With valve deactivation an advanced, faster early flame expansion speed at high residual rates is seen to be related to increased turbulence levels.
- Using inlet valve deactivation thus increasing the turbulence levels increases the flame expansion speed at both high and low NVO i.e. high and low residual rates.
- The increase in flame expansion speed at high NVO by increased turbulence suggest the possibility of reaching lower loads in SACI mode by valve deactivation.
- For SACI combustion at high NVO the auto ignition is delayed by increased turbulence.
- The amount of ISHR increases as the turbulence is increased at high residual rates.
- The burn duration from calculated auto ignition until 90 % burned increases with valve deactivation at high NVO, however combustion timing is simultaneously slightly delayed.
- Increased mixing of the fresh charge and the hot residuals by the highly turbulent swirling flow is thought to be responsible for the delayed auto ignition and longer burn duration.
- The induced swirling motion captures the whole burning structure, moving the following auto ignition location in an almost symmetrical manner relative to the inlet ports.

ACKNOWLEDGMENTS

The authors wish to show their great appreciation to the Centre of Competence at Lund University (KCFP) for their financial support, to Cargine for providing the active valve train and to the technicians at the division for their valuable assistance in the lab.

REFERENCES

1. J. Willand, R-G. Nieberding, G. Vent, C. Enderle; "The knocking Syndrome –Its Cure and its Potential", SAE Paper 982483
2. J. Lavy, J-C. Dabadie, C. Angelberger, P. Duret, J. Willand, A. Juretzka, J. Schäflein, T. Ma, Y. Lendresse, A. Satre, C. Schulz, H. Krämer, H. Zhao, L. Damiano; "Innovative Ultra-low NOx Controlled Auto-Ignition Combustion Process for Gasoline Engines: the 4-SPACE Project
3. L. Koopmans, H. Ström, S. Lundgren, O. Backlund, I. Denbratt: "Demonstrating a SI-HCCI-SI Mode Change on a Volvo 5-Cylinder Electronic Valve control Engine", SAE Paper 2003-01-0753
4. L. Koopmans, I. Denbratt: "A Four Stroke Camless Engine, Operated in Homogenous Charge Compression Ignition Mode with Commercial Gasoline", SAE Paper 2001-01-3610
5. A. Fuhrhapter, W. F. Piock, G. K. Fraidl: "CSI – Controlled Auto Ignition – The Best Solution for the Fuel Consumption – Versus Emission Trade-Off?", SAE Paper 2003-01-0754
6. H. Persson, R. Pfeiffer, A. Hultqvist, B. Johansson, H. Ström: "Cylinder-to-Cylinder and Cycle-to-Cycle Variations at HCCI Operation with Trapped Residuals", SAE Paper 2005-01-0130
7. T. Urushihara, K. Yamaguchi, K. Yoshizawa, T. Itoh: "A Study of a Gasoline-fueled Compression Ignition Engine ~ Expansion of HCCI Operation Range Using SI Combustion as a Trigger of Compression Ignition ~", SAE Paper 2005-01-0180
8. B. Johansson, F. Söderberg: "The Effect of Valve Strategy on In-Cylinder Flow and Combustion", SAE Paper 960582
9. M. Christensen, B. Johansson, A. Hultqvist; "The Effect of Combustion Chamber Geometry on HCCI Operation" SAE Paper 2002-01-0425
10. S.M. Aceves, D.L. Flowers, J. Martinez-Frias, F. Espinosa-Losa, M. Christensen, B. Johansson, R.P. Hessel; "Analysis of the Effect of Geometry Generated Turbulence on HCCI Combustion by Multi-Zone Modeling", SAE 2005-01-2134
11. H. Persson, J. Rübel, L. Hildingsson, A. Hultqvist, B. Johansson: "Investigation of Boundary Layer Behaviour in HCCI Combustion using Chemiluminescence Imaging", SAE Paper 2005-01-3729
12. S. Trajkovic, A. Milosavljevic, P Tunestal, B. Johansson: "FPGA Controlled Pneumatic Variable Valve Actuation", SAE Paper 2006-01-0041
13. J. Heywood: "Internal Combustion Engine Fundamentals", MacGraw-Hill ISBN 0-07-100499-8, 1988
14. L. Koopmans, O. Backlund, I. Denbratt: "Cycle to Cycle Variations: Their influence on Cycle Resolved Gas Temperature and Unburned Hydrocarbons from a Camless Gasoline Compression Ignition Engine", SAE Paper 2002-01-0110
15. B. Johansson: "On Cycle to Cycle Variations in Spark Ignition Engines – The Effect of Fluid Flow and Gas Composition in the Vicinity of the Spark Plug on Early Combustion", Doctoral Thesis, Lund, ISRN LUTMDN/TMKV—1010-SE
16. H. Persson, A. Remón, A. Hultqvist, B. Johansson: "Investigation of the Early Flame Development in Spark Assisted HCCI Combustion using high Speed Chemiluminescence Imaging", Submitted to SAE WC 2007
17. J. Hyvönen, G. Haraldsson, B. Johansson: "Operating Conditions Using Spark Assisted HCCI Combustion During Combustion Mode Transfer to SI in a Multi-Cylinder VCR-HCCI Engine", SAE Paper 2005-01-0109
18. M. Christensen: "HCCI Combustion - Engine Operation and Emission Characteristics", Doctoral Thesis, Lund, ISRN LUTMDN / TMHP--02/1006--SE

CONTACT

Corresponding author:
Håkan Persson

Address
Lund University
Dept. of Energy Sciences
Div. of Combustion Engines
P.O. Box 118
221 00 Lund
Sweden

E-mail
hakan.persson@vok.lth.se

DEFINITIONS, ACRONYMS, ABBREVIATIONS

CAI	Controlled Auto Ignition
CI	Compression Ignition
EVC	Exhaust Valve Closing
FFT	Fast Fourier Transform
HCCI	Homogenous Charge Compression Ignition
ISHR	Initial Slow Heat Release
IVC	Inlet Valve Closing
IVO	Inlet Valve Opening
LDV	Laser Doppler Velocimetry
NVO	Negative Valve Overlap
RoHR	Rate of Heat Release
SACI	Spark Assisted Compression Ignition
SI	Spark Ignition
TDC	Top Dead Center
WOT	Wide Open Throttle

APPENDIX A
40 CAD NVO, both inlet valves active

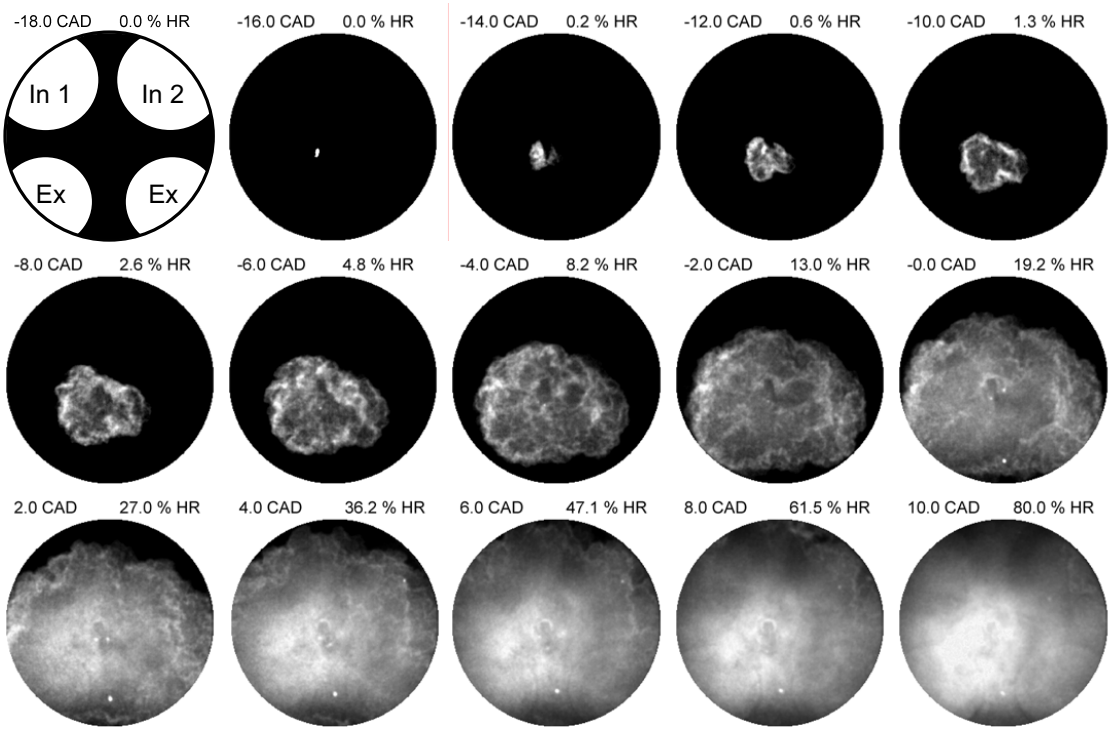

APPENDIX B
40 CAD NVO, inlet valve 1 deactivated

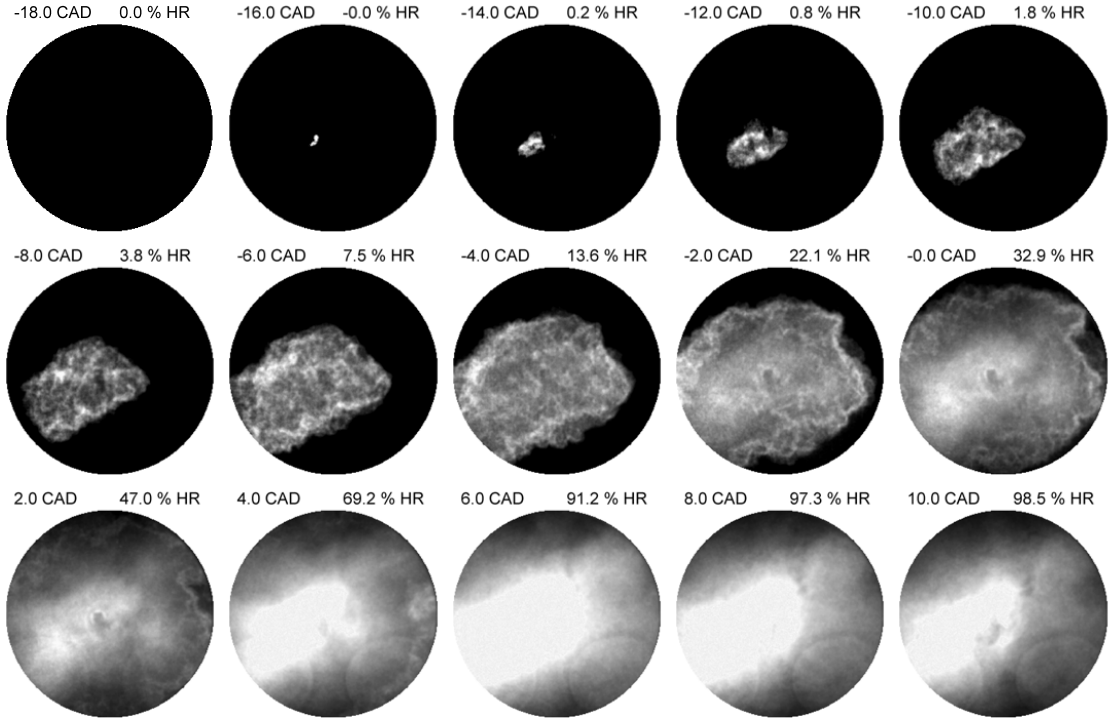

APPENDIX C
202 CAD NVO, both inlet valves active

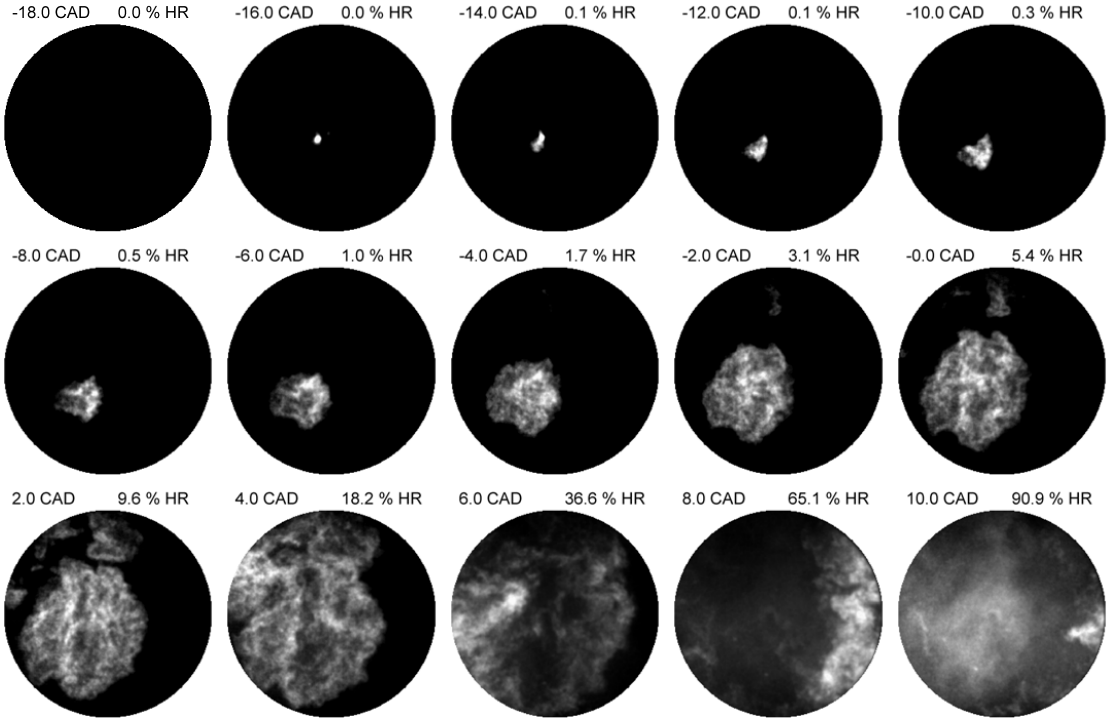

APPENDIX D
202 CAD NVO, one inlet valve deactivated

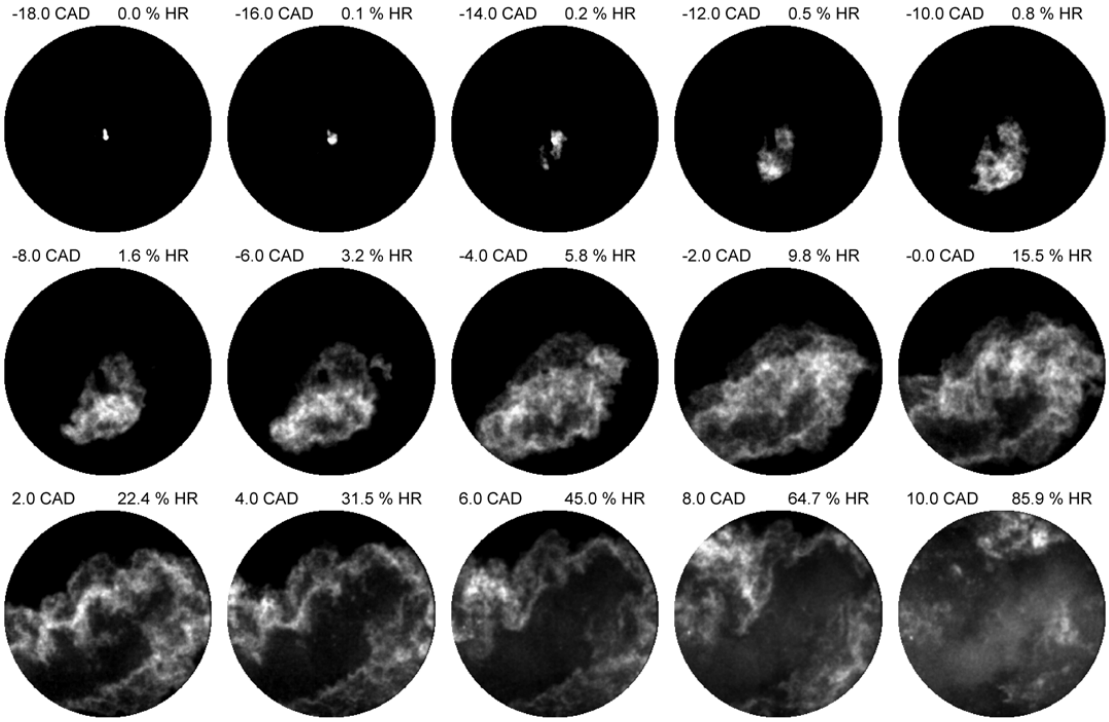

APPENDIX E

210 CAD NVO, both inlet valves active

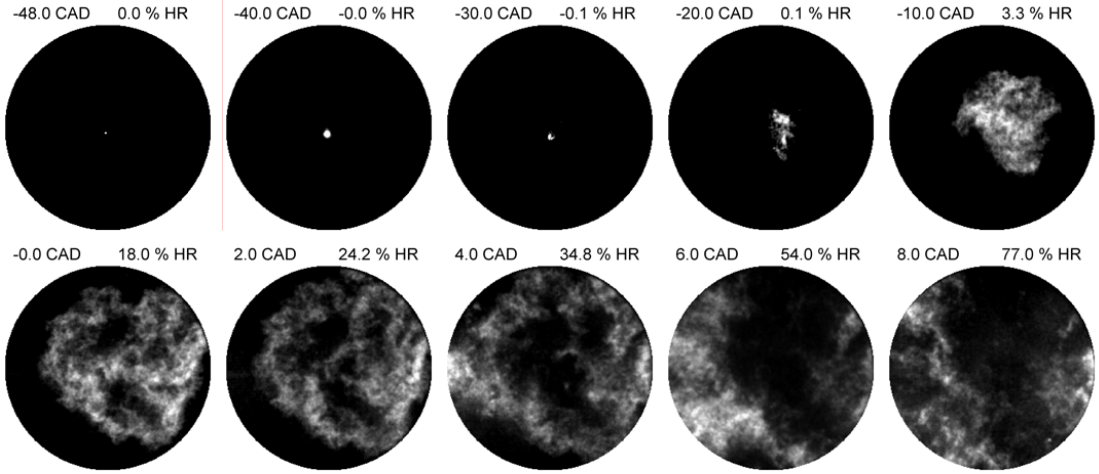

APPENDIX F

210 CAD NVO, Inlet valve 1 deactivated

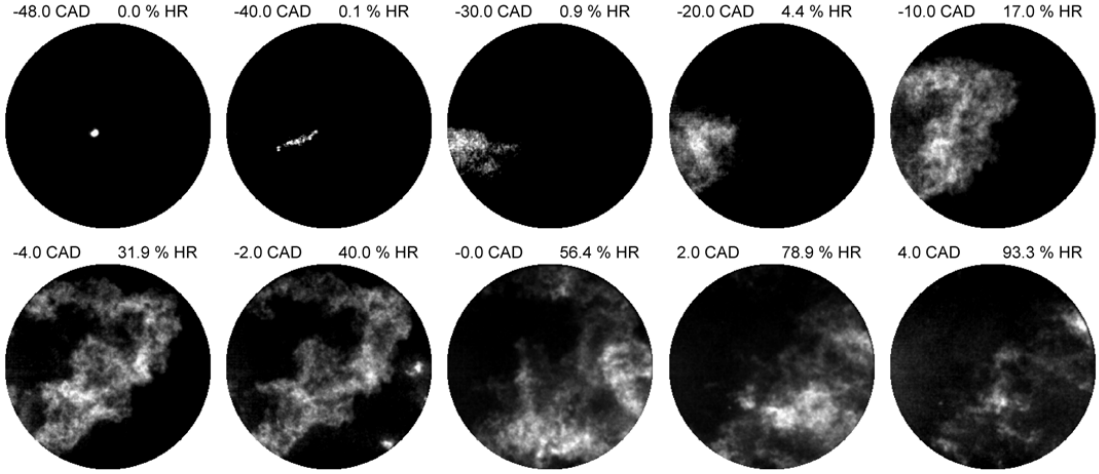

APPENDIX G

210 CAD NVO, Inlet valve 2 deactivated

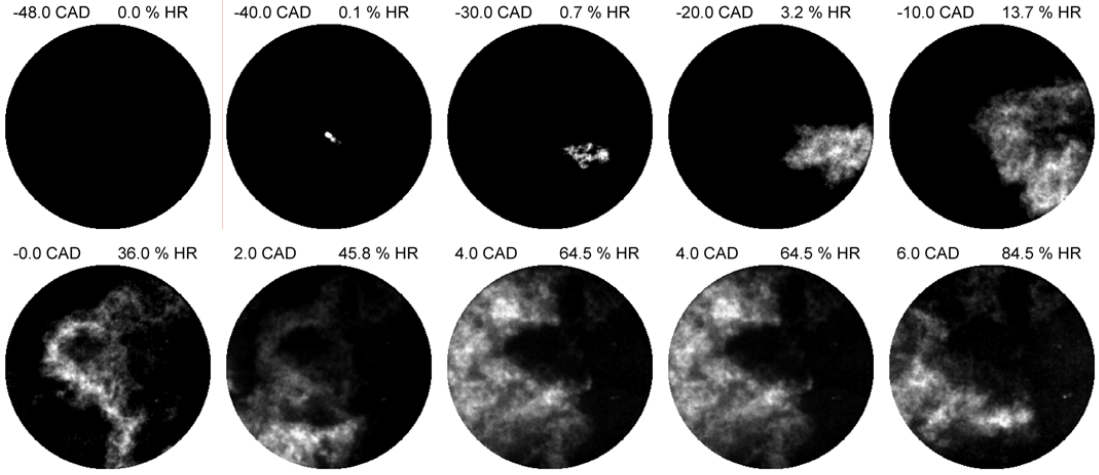

VI

2008-01-2401

Study of Fuel Stratification on Spark Assisted Compression Ignition (SACI) Combustion with Ethanol Using High Speed Fuel PLIF

Håkan Persson, Johan Sjöholm, Elias Kristensson, Bengt Johansson, Mattias Richter, Marcus Aldén
Lund University

ABSTRACT

An engine can be run in Homogenous Charge Compression Ignition (HCCI) mode by applying a negative valve overlap, thus trapping hot residuals so as to achieve an auto-ignition temperature. By employing spark assistance, the engine can be operated in what is here called Spark Assisted Compression Ignition (SACI) with ethanol as fuel. The influence of fuel stratification by means of port fuel injection as well as in combination with direct injection was investigated.

A high-speed multi-YAG laser system and a framing camera were utilized to capture planar laser-induced fluorescence (PLIF) images of the fuel distribution. The charge homogeneity in terms of fuel distribution was evaluated using a homogeneity index calculated from the PLIF images. The homogeneity index showed a higher stratification for increased proportions of direct-injected fuel.

It was found that charge stratification could be achieved through port fuel injection in a swirling combustion system. For the combined port fuel and direct injection strategy, a strong stratification was demonstrated. Although combustion phasing remained constant, a slight increase in the combustion duration was observed. For increased stratification with direct injection in a base of port-injected fuel, an increased amount of ignition sites could be observed. However, the most fuel-rich regions did not necessarily ignite first. Rather, ignition occurred in the mixing zone between the rich and the leaner regions.

INTRODUCTION

The emission legislation is becoming increasingly stringent at the same time as demands for higher fuel efficiency multiply. Both these factors call for a new technology. For Spark Ignition (SI) and Compression Ignition (CI) engines, one alternative under extensive research consists in Homogenous Charge Compression Ignition (HCCI). As far as the SI engine is concerned, this can be achieved by using hot residuals. One way first suggested by Willand et al. [1] is to trap hot residuals during a Negative Valve Overlap (NVO). This increases the charge temperature and dilution, thus rendering it possible to run HCCI at low load with residual dilution and SI combustion at high load with low amounts of residuals. This type of HCCI combustion is also often referred to as Controlled Auto Ignition (CAI) combustion. The combustion can be controlled by moderating the NVO and thereby the charge temperature and dilution. A method of enhancing the control is by spark assistance, and the first report on obtaining a stabilizing effect in this manner was published by Koopmans et al [2]. Later experiments have demonstrated the possibility of also influencing combustion timing [3] and canceling oscillations in combustion timing at low temperature conditions [4]. Spark assistance has furthermore been investigated when going towards higher loads, as described by Urushihara et al. [5].

The present work employs Spark Assisted Compression Ignition (with the acronym SACI) for spark assisted HCCI. Another possible deployment of SACI is for making mode switches between SI and HCCI and vice versa.

The feasibility of SACI combustion is directly connected to the flammability limits. If a turbulent flame kernel is unable to develop and propagate, SACI combustion is not possible. For HCCI combustion, the flammability limit is extended for a number of reasons:

- For higher gas temperatures, the burning velocity of a flame becomes increased [6]. The elevated temperature during the compression for operation with HCCI or SACI combustion is, as compared to traditional SI combustion, expected to lower the heat losses for the early flame originating from the spark plug. The flame speed increases and thereby stretches the flammability limit towards leaner conditions.

- Due to the elevated temperature of the residuals in relation to the fresh charge, the mass-based dilution at a given load is lower for an engine with trapped residuals as compared to an engine running with a high compression ratio in order to achieve auto-ignition. This further increases the possible low load with SACI combustion due to less heat losses for the flame.

- A lower SI flame expansion speed can be tolerated for SACI combustion as compared to that for the SI engine since, in SACI combustion, only part of the charge is consumed by the comparably slow flame development. The later part is auto-ignited and oxidizes rapidly enough to complete the combustion.

The final low load limit is reached as the temperature and local lambda are insufficient with heat losses that are too high for the early flame kernel. This causes a rapid increase in cycle–to-cycle variations that can result in misfire.

For the SI engine, an increased turbulence during the late compression can augment the lean capability of combustion. This trend has also been observed [7] for SACI combustion, thus indicating a further possible lean capability. 2-D velocities were measured in the vicinity of the spark plug and a correlation between higher turbulence and earlier / faster flame growth could be detected. This was also supported by high speed chemiluminescence measurements. As the flame expansion speed increased due to the higher turbulence levels, the following HCCI combustion was found to slow down. This occurred at the same time as the auto ignition timing was slightly retarded.

Fuel stratification has been suggested in order to further expand the operating regime for HCCI. Significant effects have been reported for fuels exhibiting Low Temperature Reactions (LTR), e.g. two-stage auto-ignition [8 - 10]. For fuels exhibiting LTR, a more staged combustion event is reported with slower RoHR thus enabling a higher load. Dec et al. showed that the effect becomes more modest with single-stage ignition fuels [11]. For single stage ignition fuels, fuel stratification has been used to improve the combustion efficiency and decrease the low load limit by a reduction of over lean zones [13].

The focus of the present study has been directed to how fuel stratification affects combustion, and especially to the interaction between the flame development and auto-ignition of an ethanol fueled engine run in SACI mode. Ethanol exhibits single-stage ignition, a common behavior for most fuels related to the SI engine environment.

Fuel PLIF is a useful technique for investigating fuel distribution in addition to the ignition behavior [12]. Earlier studies have been conducted for HCCI combustion with lean burn and preheating in order to reach auto-ignition temperatures [13].

For a better understanding of the interaction between the initial SI flame and the following auto-ignition in combination with fuel stratification, Planar Laser Induced Fluorescence (PLIF) measurements were performed and the results were analyzed in combination with in-cylinder pressure information.

EXPERIMENTAL SETUP

ENGINE CONFIGURATION

The test engine was based on a passenger car sized diesel engine, modified for single cylinder operation. The operating cylinder was equipped with a Bowditch piston extension as seen in Figure 1. The upper part of the cylinder liner was replaced by a quartz liner for optical access to the combustion chamber, combined with the flat quartz piston crown, thus allowing a 3-D access to the combustion chamber. Engine specifications can be found in Table 1. The engine was connected to a 30 kW A/C dynamometer with the capability of both motoring and braking at a desired speed.

To attain the trapped residuals required for auto-ignition as well as for combustion control, the engine was equipped with a fully variable valve train [14]. This pneumatic valve train could be controlled from a PC with an FPGA-card (Field Programmable Gate Array). The valve lift was obtained by pneumatics and stabilized by hydraulics, and it was possible to separately moderate the valve lift, duration and timing for each valve. The engine was equipped with both a direct injection (DI) system as well as port fuel injection (PFI), with one injector for each of the two intake ports. The glow plug was replaced by a modified NGK ER8EH 8-mm thread spark plug. In combination with the variable valve train, this enabled SI, SACI as well as the transition to pure HCCI operation.

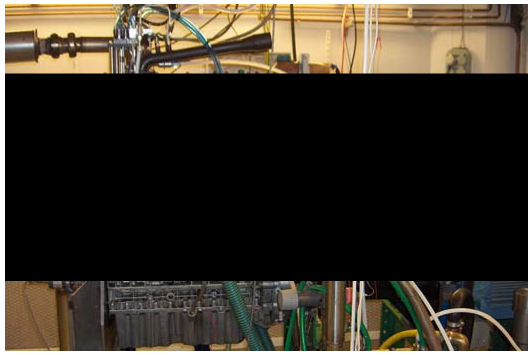

Figure 1. A single cylinder optical engine with a pneumatic variable valve train.

A close to symmetrical NVO was used in the investigation, signifying an Exhaust Valve Closing (EVC) at the same CAD Before Top Dead Centre (BTDC) as the Intake Valve Opening (IVO) After Top Dead Centre (ATDC). The Intake Valve Closing (IVC) and Exhaust Valve Opening (EVO) were fixed at -180 and 160 CAD ATDC, respectively. For all cases, a lift height of approximately 8 mm was used with an opening and closing ramp of approximately 20 CAD at 1200 rpm.

Table 1. Engine specifications

Displacement (one cylinder)	0.48 Liters
Valves per cylinder	4
Bore	81 mm
Stroke	93.2 mm
Combustion chamber	Pancake
Compression ratio	12:1
Valve timings / Lift	Fully flexible
Fuel	90 % Ethanol 10 % Acetone
Speed	1200 rpm

MEASUREMENT SETUP

The pressure was monitored with a Kistler 6053C pressure sensor at a rate of 5 samples per CAD. Emissions were monitored using a Horiba MEXA 8120, measuring NO_x, CO, HC, CO_2 and O_2, and an ETAS LA3 broadband lambda sensor.

The engine was preheated prior to each test and run for several minutes before measurements were started to achieve stabile boundary conditions. Since continuous operation with un-lubricated piston rings and optical components impose a high stress of the optical engine, motored pressure traces were taken before and after each measurement sweep to further ensure comparable conditions.

FUEL TRACER

Planar laser-induced fluorescence, PLIF with an excitation wavelength of 266 nm was used for fuel visualization. The main fuel was ethanol and as this substance is non-fluorescent, acetone was added as a fluorescent tracer. In general, a suitable tracer should display very specific characteristics. The optical absorption and the resulting fluorescence must be spectrally separated and should ideally be independent of temperature, pressure and composition of the surrounding gas. The tracer must also follow the fuel during the entire process and be consumed during the combustion in order to avoid tracer buildup. The tracer should also influence the combustion process itself as little as possible [15].

Acetone (CH_3COCH_3) was selected as a fuel tracer in this work as it has previously shown a number of advantages as a tracer molecule in PLIF imaging measurements [16, 17]. The absorption band of acetone in the UV region is located between 225 and 320 nm rendering it accessible with several common laser systems, e.g. quadrupled Nd:YAG and Excimer lasers. The subsequent fluorescence occurs between 350 and 550 nm.

The differences in evaporation characteristics, e.g. the boiling point and diffusion coefficients, between acetone and ethanol was considered a possible issue since the fuel was partially injected with a direct injection system. However, since the mixing was mainly spray-driven the difference in diffusion coefficient should have a negligible impact. The deviation in boiling point (78 ˚C for ethanol and 56 ˚C for acetone) could however cause a minor over prediction when measuring the fuel spread.

The fluorescence yield of acetone has a dependence on temperature. However, this temperature dependence is correlated to the excitation wavelength and for an excitation wavelength of 266 nm, only a fair sensitivity to temperature changes was observed [18 - 19].

The pyrolysis of acetone was another potential source of error. However, in earlier investigations by the authors, the optically detected start of acetone consumption correlated well with the start of the heat release calculated from the pressure trace for this given fuel/tracer combination. Such a correlation has also been demonstrated through simultaneous PLIF imaging of acetone and chemiluminescence. Here the disappearance of the acetone signal and the increase in the chemiluminescence intensity from the combustion were strongly correlated [20].

OPTICAL SETUP

One of the main goals of the present investigation was to visualize the fuel distribution in the combustion chamber as well as how it changed over a single cycle. For this purpose Planar Laser-Induced Fluorescence (PLIF) was employed. In order to obtain such a cycle-resolved imaging, a very high repetition rate from the laser source was required. For this purpose, a custom-made multi-YAG laser cluster from Thales Laser was used.

The system consisted of four separate Nd:YAG laser channels, each operating with a repetition rate of 10 Hz and with a fundamental laser wavelength of 1064 nm. In order to superimpose the four beam paths, a specially designed beam-combining scheme was used. The setup consisted of a sequential doubling and combination system that also frequency-doubled the laser radiation from all lasers to 532 nm. In a first step, the beam from laser 1 was frequency-doubled to 532 nm using a second harmonic generating crystal, after which the frequency-doubled beam was separated from the fundamental beam by way of a dichroic mirror. A second dichroic mirror then combined the fundamental beam

from laser 2 with the frequency-doubled beam from laser 1. This second mirror had a high reflectance of 532 nm as well as a high transmittance of the fundamental IR beam. The two beams were then sent through a second harmonic generating crystal where the fundamental beam from laser 2 was frequency-doubled. The already doubled beam from laser 1 passed almost unaffected through this crystal as the phase-matching condition could not simultaneously be met for both 1064 and 532 nm. This procedure was repeated for all four lasers in sequence, and the entire laser system thus had a single output path for all pulses at 532 nm. Prior to the output, the combined beam was directed through a fourth harmonic generator crystal that frequency-doubled the green beams to 266 nm, which was used to excite the acetone. The individual lasers in the system also had the option of opening the Q-switch twice during one flash lamp discharge thus extending the number of pulses from four to eight. These eight pulses could be emitted in a very rapid burst. The time separation between two consecutive pulses, when firing the eight pulses with equal time separation, could be set to values as short as 6.25 µs. A more thorough description with regard to the multi-YAG laser system can be found elsewhere [21].

In order to detect the acetone fluorescence generated by each of the laser pulses in the burst from the multi-YAG system, a high-speed framing camera from Hadland was utilized. The framing camera had a single optical input in front of which a Bernard-Halle quarts lens (f = +100 mm, f/2) was mounted. An image intensifier was positioned directly after the optical entrance of the camera to enhance the sensitivity of the detector and enable UV detection. The intensified signal was then split up onto eight individual intensified CCD modules using an eight-facet prism. Each module consisted of a micro-channel plate and a CCD image sensor with 384x576 pixels.

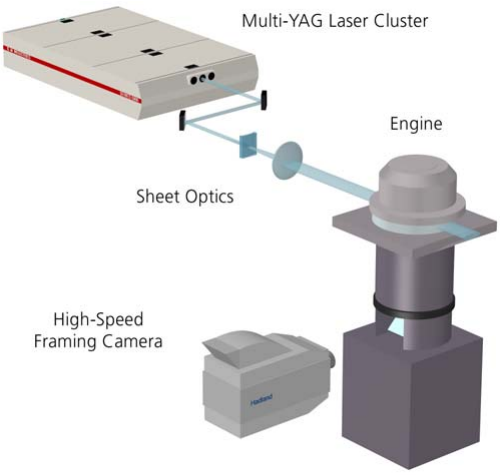

Figure 2. A schematic of the optical setup.

The micro channel plate functioned as an electronic shutter and further intensified the signal. The shutter function ensured that each CCD only detected signals from one laser pulse and they were thus synchronized with the laser pulse train.

Figure 2 shows a schematic sketch of the optical setup. In order to obtain two-dimensional images of the fuel distribution, the laser beam from the multi-YAG laser cluster was formed into a thin horizontal laser sheet using a set of cylindrical and spherical lenses. The laser sheet was directed into the engine through the quartz cylinder liner and focused in the vertical direction in the center of the combustion chamber. The laser sheet was slightly divergent in the horizontal plane before the engine, which compensated for the focusing effect of the outer quartz liner surface and thus enabled a larger part of the combustion chamber to be imaged. The sheet was positioned five millimeters from the cylinder head surface and was 55 mm wide in the center of the combustion chamber.

The fluorescence signal from the acetone was imaged perpendicularly to the sheet down through the quartz window in the piston and via a 45-degree UV-enhanced mirror in the piston extension to the high-speed framing camera. In order to reduce scattered laser light from being detected by the CCD detectors, two optical filters were placed in front of the camera; one long pass filter consisting of a 12 mm optical path length quartz cuvette with liquid N,N-dimethyl-formamide blocking 266 nm, and one short-pass filter with a cut-off wavelength at 500 nm to avoid interference from any remaining 532 nm laser light.

During the measurements, the engine speed was kept at 1200 rpm, thus matching the overall repetition rate of the laser system of 10 Hz. A pulse originating from the engine crank angle encoder was used to fire the laser system at the desired position.

The multi-YAG laser system was operated in double pulse mode, resulting in an energy of approximately 16 mJ per pulse at 266 nm and a total average optical output power of 1.1 W. The time-separation between two consecutive laser pulses and thus images was 139 µs corresponding to 1 CAD. In order to suppress the background radiation from the combustion process, the exposure time of the camera was set to 50 ns for each image acquisition.

The images that were recorded with this system were analyzed in order to produce accurate results of the fuel concentration in the cylinder. First, a background was subtracted. This was recorded late in the cycle, well after all of the fuel had been consumed by the combustion. This removes unwanted reflections from the laser in the cylinder head. A compensation for the inhomogeneous laser profile of the images was then carried out by dividing them with a profile acquired from an image recorded well before the onset of combustion.

HOMOGENEITY INDEX

In order to evaluate the homogeneity of the fuel distribution for various operating conditions, such as different DI-duration, the images were analyzed with a homogeneity evaluation process that is described in detail elsewhere [22-23]. This process required each evaluated image to be digitalized and the charge was considered homogeneous if the pixels containing no signal were randomly distributed throughout this digitalized image I_D. To evaluate this, the number of shifts between no signal and signal was calculated when traversing I_D in rows and columns. As a comparison to the digitalized image, a homogeneous image was generated, with the same surface fraction covered with signal as the original image. The number of shifts from the digitalized image was then divided with the number of shifts found in the randomly generated one, giving the homogeneity index for the original image. By using this approach, an image with a homogeneous, random spatial distribution of the fuel would be given a high index value (close to unity), whereas a non-homogeneous distribution would result in a low value. Since the images had to be digitalized, the signal strength could not be accounted for when using this approach. An example of the procedure is given in Figure 3, where I_D (to the left) and the randomly generated image (to the right) are shown. Indicated below each image is the number of shifts, providing a measure of the homogeneity (also indicated) of the charge distribution.

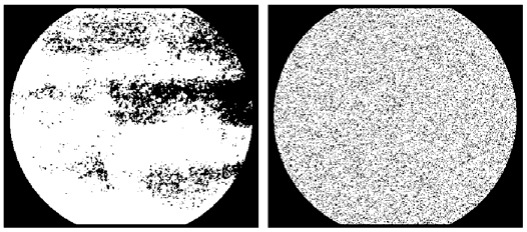

9926 30615

Homogeneity index = 0.32

Figure 3. Examples of the homogeneity index procedure.

RESULTS

SACI / HCCI

For an initial characterization of the SACI ignition process a comparison to pure HCCI, based on the same initial boundary conditions, was in place. The engine was run at a lambda of 1.3 with an NVO of 160 CAD. The charge temperature was increased by the early EVC to the point that auto-ignition was achieved at the end of the compression stroke. The engine was run auto-ignited with Crank Angle for 50 % burned (CA50) at 5.5 CAD ATDC. A pressure trace and the Rate of Heat Release (RoHR) are shown in Figure 4, HCCI solid lines. Spark assistance was applied at -40 CAD ATDC, and hence the engine was run in SACI mode. Combustion timing (CA50) advanced approximately 4 CAD at the same time as a characteristic Initial Slower rate of Heat Release (ISHR) [24] was observed from the RoHR (dashed lines). The slow RoHR observed for SACI started earlier and had a longer duration before the increase in reaction rate as compared to for the HCCI case. By observations from PLIF information as well as with the support from a previous study using chemiluminescence [25], the ISHR originated from a growing premixed flame initiated by the spark plug. Depending on the flame development speed and spark advance in relation to the auto-ignition timing, the effect on RoHR could differ.

When only a small portion of the charge is consumed by an SI flame, caution should be taken when interpreting the RoHR since also the early stages of auto-ignition is slow as compared to the later characteristic rapid HCCI combustion.

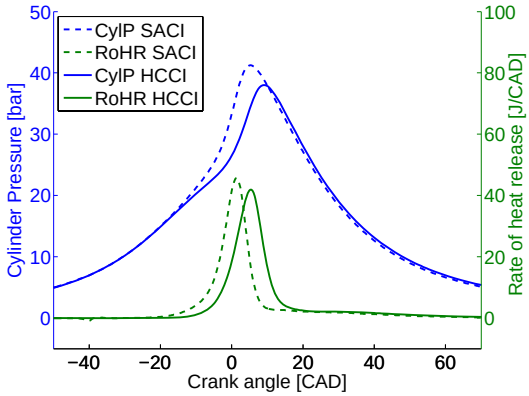

Figure 4. The average cylinder pressure and the RoHR for 400 cycles, SACI (dashed) and HCCI (solid), both with PFI.

Figure 5 presents some of the single-cycle PLIF images that correspond to the pressure traces and RoHR curves in Figure 4. _The bright areas in these images are indicative of high signals and correspondingly regions with high fuel concentrations. The black areas, on the other hand, signify that the fuel has been consumed by combustion.

The three PLIF images in the top row are from a single cycle as the engine is run in HCCI mode. The images were taken -10, -7 and -4 CAD ATDC. The corresponding images for the SACI case are shown in the bottom row. The large black patch in the center of the combustion chamber for the SACI case indicates where the flame that was initiated by the spark earlier in the cycle had consumed the fuel. This propagating flame was the cause for the ISHR. In the HCCI case, auto-ignition can be seen in the top-right corner of the last

image as indicated by the dark patches where the fuel had been consumed. When performing optical observations of SACI combustion, it is crucial to utilize high-speed imaging with several images per cycle so as to separate the slowly growing SI flame from the fast reaction zone of HCCI combustion.

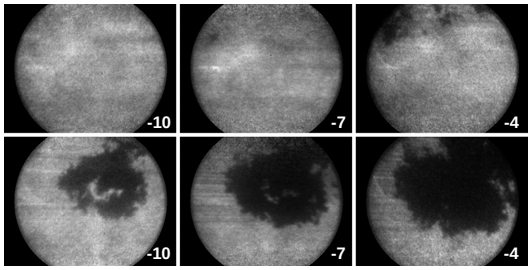

Figure 5. Single-cycle PLIF images of the fuel distribution during the early combustion with PFI. Top row: the engine is operated in HCCI mode. Bottom row: the engine is operated in SACI mode. The images are taken -10, -7 and -4 CAD ATCD as indicated in the lower right corner of each image.

The engine can be run with pure PFI with one injector for each port thus rendering it possible to stratify fuel during the gas exchange process by injector deactivation. In-cylinder fuel stratification was also feasible by adding fuel from the DI system. Figure 6 (left) displays the part of the combustion chamber that was visible from below. The spark plug was located between the intake valves and the DI injector can be seen just below in the center of the image. The right part of the figure shows a PLIF image taken 6 CAD after the spark was discharged. Only a small portion of the fuel was direct injected. The rest was added by PFI and can be seen as a smooth grey region behind the five spray plumes of the DI injection. The DI injector was mounted in such a way that one of the five fuel-rich regions passed in the vicinity of the spark plug position.

To quantify the effect of fuel stratification with SACI, combustion tests were conducted by switching from pure PFI to a combined injection strategy where the DI part was increased whilst maintaining constant the total amount of fuel to the engine.

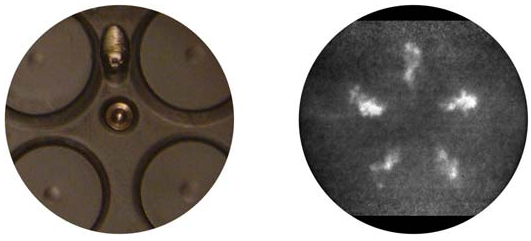

Figure 6. Optical access through piston extension and a PLIF image of combined PFI and DI.

PORT FUEL INJECTION

A first suggestion for achieving fuel stratification would be to utilize PFI and only inject fuel in one of the two ports. A previous study [10], in which a tumble flow combustion chamber was used, demonstrated a large-scale stratification effect of the fuel, whereas the effect on combustion timing, or RoHR was insignificant. In the present case, a swirling combustion system was used, and hence more communication was expected between the flows of the two intake ports. Since the mixing time for the fuel-rich and the pure air flow was long, the charge should either reach the same homogeneity as that of PFI in both ports or present a smaller-scale heterogeneity. This differs in comparison to the large scale stratification effect that can be achieved when using a tumble flow.

Tests were first conducted with fuel injection in both intake ports after which one injector was deactivated and the injection duration of the other was increased in order to maintain a constant fuel mass to the engine. The engine was run at a load of approximately 2.7 bar IMEPnet and lambda 1.4. Figure 7 shows an insignificant change in timing for the early heat release (CA10). However, the change in combustion duration in terms of CA90-CA10 was found to be considerable. The single point injection cases had much longer burn durations. Unfortunately, a deviation in the injector calibration resulted in a slightly increased amount of fuel for the double port injection entraining an augmentation in IMEP by 4 % and a drop in lambda by approximately 0.03. The increased fuel mass was expected to augment the reaction rate and thus, decrease the combustion duration.

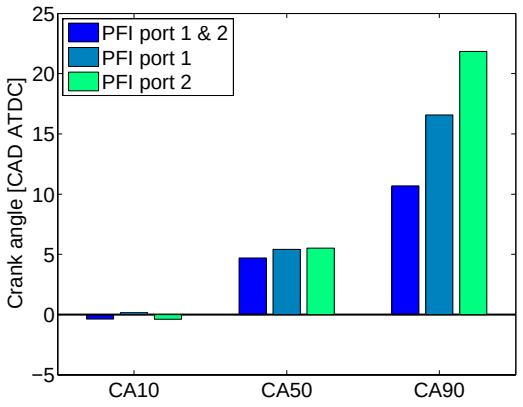

Figure 7. The combustion timing for PFI SACI combustion with port fuel stratification.

Figure 8 shows the homogeneity index for the three PFI strategies under analysis. Each homogeneity index was calculated from a set of at least 20 PLIF images taken between -38 and -32 CAD ATDC recorded from three different cycles. This was approximately the same time

as the spark was set off and thus the homogeneity values represent the conditions for the early SI flame in the combustion chamber. The figure also contains the 95% confidence levels for the mean values. It can be seen in Figure 8 that the injection strategy where both ports were used provided a more homogeneous fuel distribution as compared to the cases where the entire amount of fuel was delivered through a single port. Despite this, the start of combustion in terms of CA10, remained unchanged whereas the end of combustion was retarded.

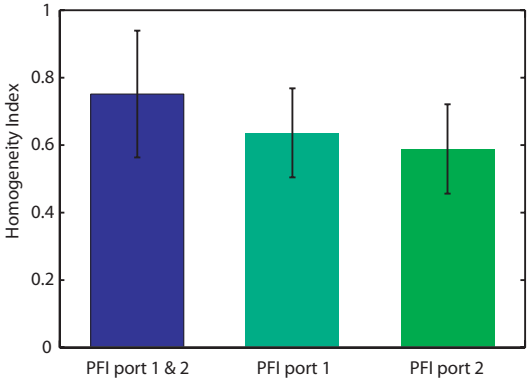

Figure 8 The homogeneity index for three PFI strategies. The bars indicate the 95% confidence level for the mean values.

SACI WITH COMBINED PFI AND DI

The use of direct injection renders it possible to reach a higher level of stratification in the cylinder in relation to what is possible with PFI. Tests were started employing only DI with an injection pressure of 400 bars at -180 CAD ATDC for both pure HCCI and SACI combustion. As the injection event was phased later into the compression, a higher level of stratification could be seen prior to ignition. At this load, the injection timing could not be advanced closer to TDC than -70 CAD ATDC while maintaining proper combustion for either SACI or HCCI combustion. The pancake-shaped combustion chamber in combination with the high momentum of the spray forced a large part of the fuel to the outer rim of the combustion chamber, thus leaving very lean conditions in the vicinity of the spark. It was considered a possibility that light stratification could lead to better conditions for running SACI combustion with shorter penetration of the stratified areas.

Another approach was adapted starting with pure PFI and then shifting towards an increased percentage of DI at –70 CAD ATDC while maintaining the same total injected fuel mass. In order to decrease the drag of the spray in the vicinity of the spark plug, the injection pressure was decreased and finely set to 130 bars. The spark timing was –40 ATDC.

Figure 9 shows the combustion event in terms of RoHR and accumulated heat release as the DI/PFI ratio was increased. Due to difficulties in the calibration, the proportions of DI to PFI should be considered as approximate values, although the total amount of fuel per cycle was kept stable.

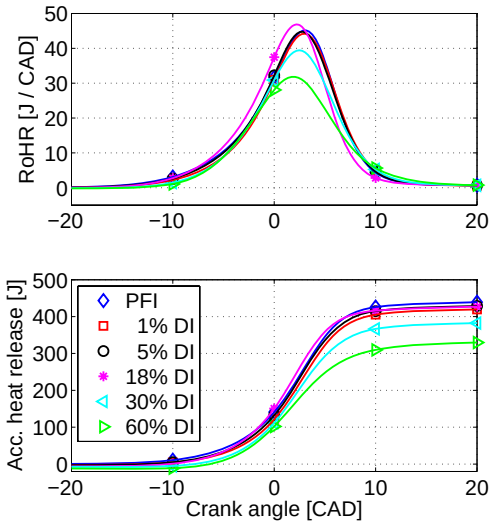

Figure 9. RoHR and accumulated heat release for an increased amount of DI at -70 CAD ATDC.

Earlier studies with a two-stage ignition fuel have demonstrated both an advanced combustion timing as well as a slower RoHR when applying fuel stratification [8, 26]. For fuels exhibiting single stage injection, the effect was not as pronounced [10]. It was suggested that the effect of the charge stratification was counteracted by the reduced temperature caused by the heat of vaporization of the fuel. When considering Figure 9, it can be seen from both the RoHR and the accumulated Heat Release (HR) that the combustion timing was maintained almost constant. For the cases with a DI ratio of 30 and 60 %, a clear decrease can be seen in RoHR as well as in accumulated HR. This was thought to be the result of high stratification in the combustion chamber perimeter with possible wall-wetting as well as overly rich mixtures giving rise to partial burn. Such a high stratification in the outer rim would then result in too lean conditions at the spark plug position. The early RoHR for these cases shows an absence of ISHR related to SACI. Since the spark was thought to have a reduced effect, two main reasons remain for explaining the maintained combustion timing.

- Increased fuel stratifications provoking advanced auto-ignition on multiple sites.

- An increased charge temperature for the high stratification case due to partial burn, leaving reactive species in the cylinder during the NVO.

The idea of a presence of reactive species was supported by pressure data displaying an increased expansion work during the NVO for the high DI ratio. The incomplete combustion during the NVO resulted in both an increased temperature during the compression stroke as well as an ignition affected by the remaining radicals.

Although the combustion timing was kept fairly constant, also for the high levels of stratification as shown in the left-hand side of Figure 10, the Coefficient of Variation of IMEP was drastically increased due to the incomplete combustion. The lower reaction rate, displayed to the right in the figure, was decreased from 50 to 40 J / CAD, which corresponds to the decreased load due to partial burn.

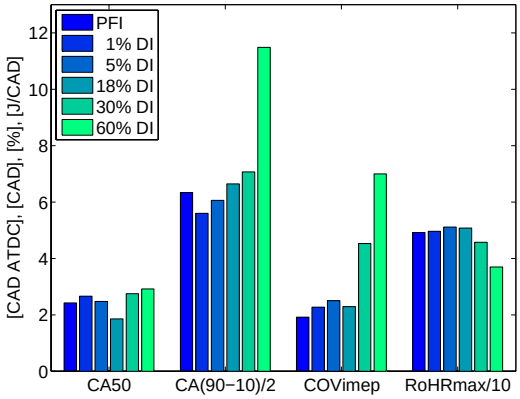

Figure 10. The combustion timing CA50 [CAD ATDC], combustion duration CA(90 – 10)/2 [CAD], combustion stability COV_{IMEP} [%] and RoHRmax/10 [J / CAD] for various percentages of DI.

Figure 10 presents the combustion duration in terms of CA10 to CA90. As the amount of direct injected fuel was increased, the combustion duration was lengthened; the point with the highest percentage of DI demonstrated a substantially increased combustion duration. This was due to partial burn and a poor combustion stability as indicated by the elevated value of COV_{IMEP} for this point, also evidenced in Figure 10. The trend in combustion duration with increasing stratification was found to be contradicted by the PFI point. However, the PFI point was run at a slightly lower load thus giving rise to a longer burn duration.

The homogeneity index as a function of the percentage of DI is displayed in Figure 11. Each value represents an average over four to five sets of eight images and the bars indicate the 95% confidence level of each value. Figure 12 provides examples of the images that underlie this curve, which were taken around -40 CAD ATDC and thus well before the start of combustion. This timing also coincided with the spark when the engine was run in SACI mode and the effect of the homogeneity on the ISHR could thereby be studied. It was observed that a higher amount of DI led to an increased deviation in fuel concentration. A larger part of the fuel ended up in the periphery of the visual part of the combustion chamber.

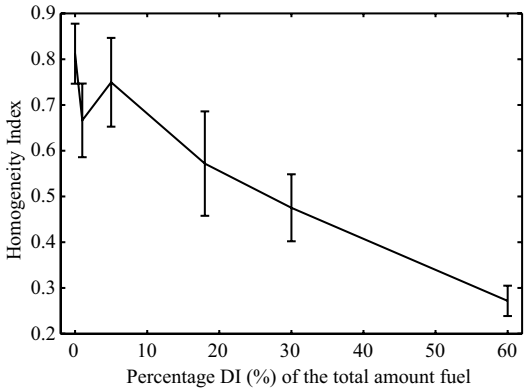

Figure 11. The homogeneity index as a function of the percentage of DI. The bars indicate the 95% confidence level for the mean values.

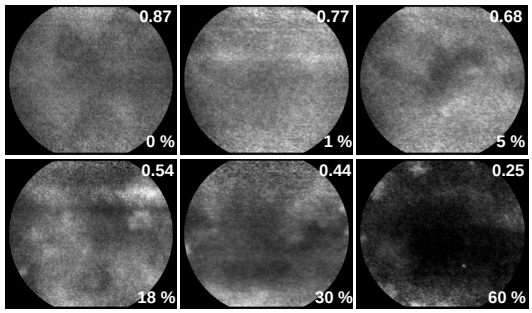

Figure 12. PLIF images of the fuel concentration around -40 CAD ATDC for various percentages of DI (0, 1, 5, 18, 30 and 60 %). The evaluated homogeneity index for each image is indicated in the top right corner.

PLIF IMAGES

The image matrixes in Figure 13 and Figure 14 show the PLIF signal for two DI timings, i.e. when the DI injector was triggered. Figure 13 includes representative images for the DI timing of -70 CAD ATDC and Figure 14 presents similar images for the DI timing of -50 CAD ATDC.

The images in each column of these matrixes were recorded during a single cycle of the engine. The images were taken with 1 CAD (139 μs) separation within one cycle. The different columns and thus cycles represent the various percentages of DI. The columns display, from left to right, 1, 5, 18, 30 and 60 percent direct-injected fuel, of the total amount l. It should be noted that the total amount of fuel to the engine was kept constant for all these cases by simultaneously varying the PFI and the DI. It is thus the relative amount of DI that increases when going from left to right in the figures. The increase in DI also led to a corresponding augmentation of the stratification.

The flame that was ignited by the spark plug earlier in the cycle can be seen in the top right quadrant of each image. The reason that the SI combustion was not centered was, first of all, that the spark plug was positioned between the intake valves somewhat above the center of the images (see Figure 6). The flame was then moved to the right in the images by the swirling motion of the gas in the cylinder. The auto-ignition, of which the start can be seen in the images, took place at random locations in the combustion camber.

One can conclude from these images that the stratification, as shown in Figure 11, caused by the direct injection at -70 CAD ATDC, was still present at -8 CAD ATDC and certainly changed the combustion behavior. This effect was even stronger as the direct injection was triggered later in the cycle (-50 CAD ATDC) as the time for mixing was decreased.Furthermore, one can observe that the number of ignition kernels in the auto-ignition process increased at the same time. It can also be seen, especially for the -50 CAD ATDC DI timing in Figure 14, that the area containing burned gas was increased for a given timing when going from a low to higher DI durations (from left to right in the matrix).

As shown in Figure 12 the fuel concentration in the centre of the combustion chamber was lowered with an increasing amount of DI. According to Figure 13 and Figure 14, the effect of the lower fuel concentration was found to decrease the flame expansion speed while the auto-ignition seemed to be advanced at multiple sites. Although the peripheries of the images were initially more fuel-rich, these bright zones can be seen to endure for several crank angels before becoming consumed as combustion occurred at other locations. The reason for this was probably the higher temperature of the lean mixture containing partially burned species from the trapped residuals. The regions with high fuel concentrations suffered from the heat of vaporization of the direct injected ethanol. Therefore, ignition could take place in the mixing area between the regions with a high temperature and those with an increased fuel concentration.

However, the geometry of the combustion chamber had been optimized for optical access and not the combustion performance. The pancake geometry did not hinder the fuel spray from reaching the outer walls of the combustion chamber that are well beyond the field of view. This means that, as the DI duration was increased, more and more of the fuel was positioned outside the measurement volume. This rendered comparisons between images slightly more difficult. It was also a problem when considering the effect of the DI on the early development of the SI flame. If the fuel spray was transported towards the periphery of the combustion chamber it would not increase the amount of fuel in the local region around the spark. Instead, the lower PFI levels would render the region leaner and thus inhibit the development of the SI flame.

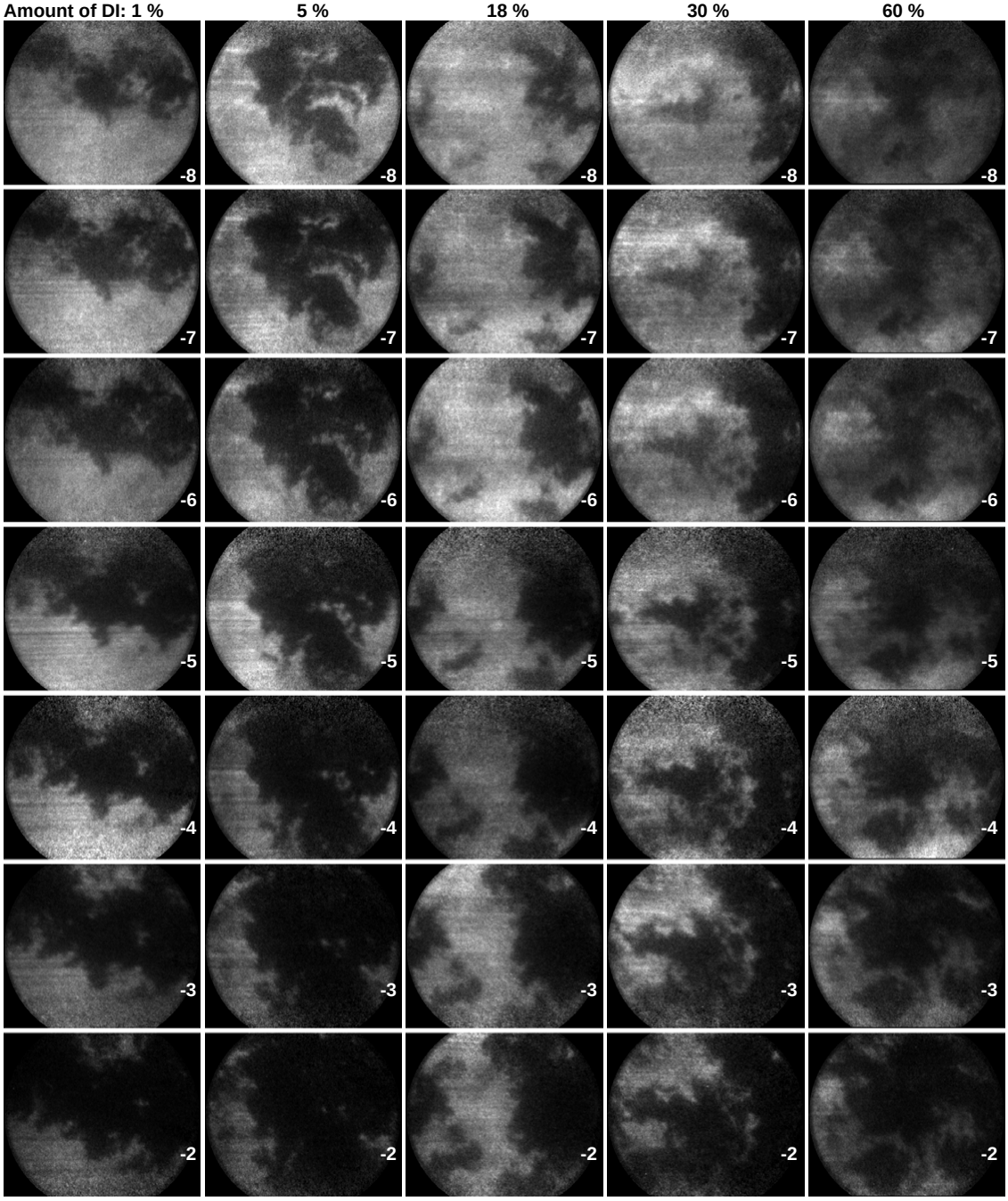

Figure 13. PLIF images taken between -8 and -2 CAD ATDC with 1 CAD separation as indicated by the number in the lower right corner of each image. Each column was taken in one cycle for a specific DI duration. The DI duration was 1, 5, 18, 30 and 60 % from left to right. The DI timing was -70 CAD ATDC. In each column, the gray scale was set between minimum and maximum values.

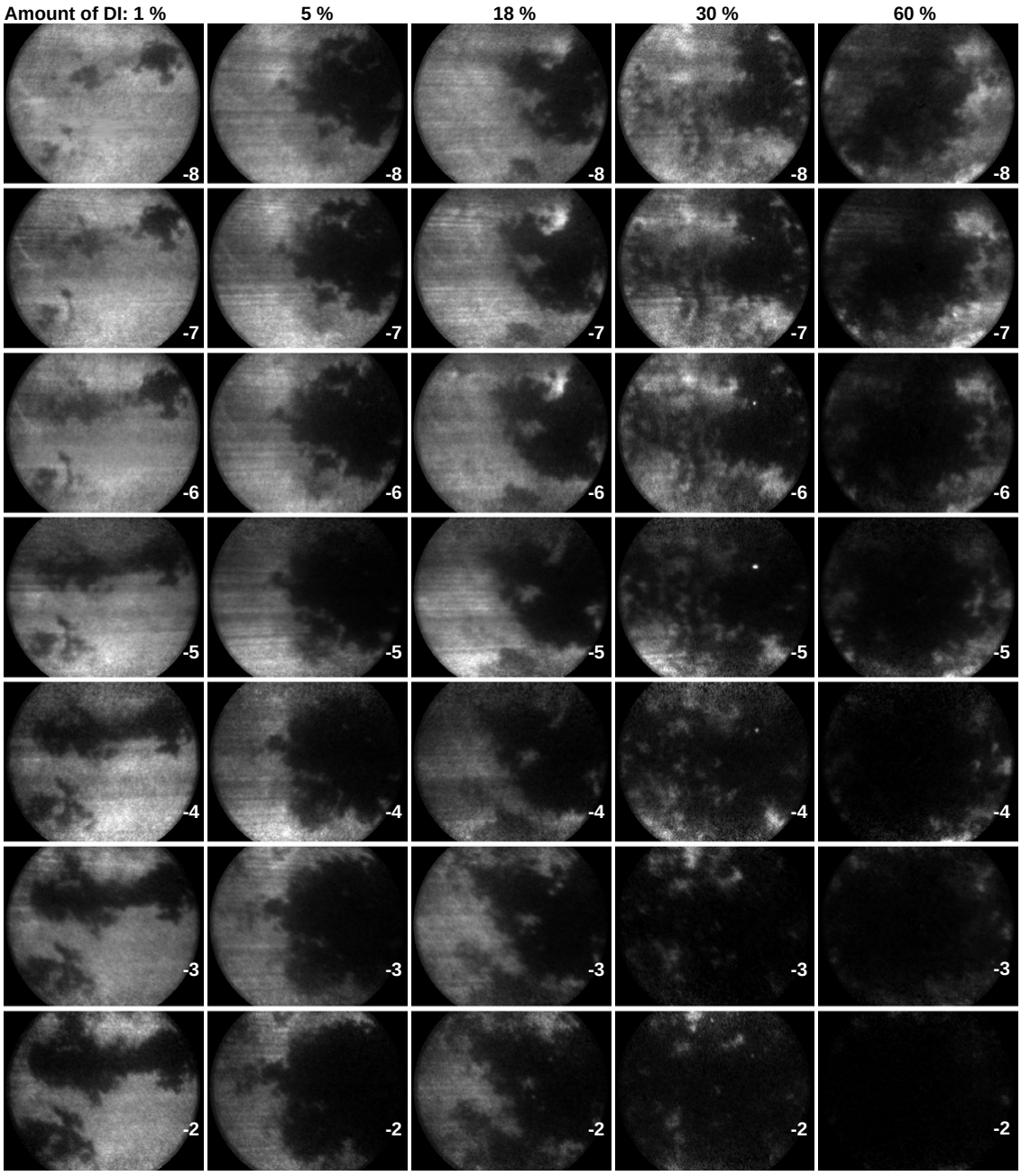

Figure 14. PLIF images taken between -8 and -2 CAD ATDC with 1 CAD separation as indicated by the number in the lower right corner of each image. Each column was taken in one cycle for a specific DI duration. The DI duration was 1, 5, 18, 30 and 60 % from left to right. The DI timing was -50 CAD ATDC. In each column, the gray scale was set between minimum and maximum values.

CONCLUSIONS

Spark Assisted Compression Ignition, SACI, was studied with ethanol as fuel in order to understand the effect of fuel stratification when using high speed fuel PLIF.

- A homogeneity index was defined and employed to evaluate the level of stratification for both PFI and DI. The homogeneity index expectedly showed a higher stratification for an increased DI percentage.

- By using PFI, it was demonstrated that moderate charge stratification could be achieved for a swirling combustion system with ethanol. The charge stratification seemed to decrease the reaction rate, although the combustion timing in terms of CA50 was not significantly affected. Instead, the end of combustion was delayed.

- For the combined PFI / DI strategy, a strong stratification was displayed. Combustion phasing remained constant, also for a high percentage of DI. For an increased stratification with DI, an augmentation in combustion duration was observed. The highest percentages of DI resulted in partial burn, and the partially burned fuel was further oxidized during the NVO thereby increasing the charge temperature during the compression.

- For an increased stratification with DI in a base of PFI fuel, a higher amount of ignition sites were found to occur. However, it was not necessarily the most fuel-rich zones that ignited first. The high heat of vaporization lowered the temperature of the rich zones. Ignition could therefore occur in the mixing region between the colder rich zones and the hotter lean zones containing a higher amount of port-injected fuel, residuals and radicals at a higher temperature.

ACKNOWLEDGMENTS

The authors wish to show their appreciation to the Competence Centre Combustion Processes (KCFP) at Lund University for their financial support. Also the Swedish Foundation for Strategic Research (SSF) is acknowledged for partly financing this work. Special thanks are directed to the technicians at the division for their valuable assistance in the lab.

REFERENCES

1. J. Willand, R-G. Nieberding, G. Vent, C. Enderle; ”The knocking Syndrome – Its Cure and its Potential”, SAE Paper 982483
2. L. Koopmans, I. Denbratt: ”A Four Stroke Camless Engine, Operated in Homogeneous Charge Compression Ignition Mode with Commercial Gasoline”, SAE Paper 2001-01-3610
3. A. Fuerhapter, W. F. Piock, G. K. Fraidl: ”CSI – Controlled Auto Ignition – The Best Solution for the Fuel Consumption – Versus Emission Trade-Off?”, SAE Paper 2003-01-0754
4. H. Persson, R. Pfeiffer, A. Hultqvist, B. Johansson, H. Ström: ”Cylinder-to-Cylinder and Cycle-to-Cycle Variations at HCCI Operation with Trapped Residuals”, SAE Paper 2005-01-0130
5. T. Urushihara, K. Yamaguchi, K. Yoshizawa, T. Itoh: ”A Study of a Gasoline-fueled Compression Ignition Engine ~ Expansion of HCCI Operation Range Using SI Combustion as a Trigger of Compression Ignition ~”, SAE Paper 2005-01-0180
6. G. E. Andrews, D. Bradley: “The Burning Velocity of Methane-Air Mixtures“, Combustion & Flame, 19: 275-288 (1972)
7. H. Persson, A. Rémon, B. Johansson: "The Effect of Swirl on Spark Assisted Compression Ignition (SACI)”, JSAE 20077167, SAE Paper 2007-01-1856
8. K. Kumano, N. Iida: “Analysis of the Effect of Charge Inhomogeneity on HCCI Combustion by Chemiluminescence Measurement”, SAE Paper 2004-01-1902
9. M. Sjöberg, J. E. Dec: “Smoothing HCCI Heat-Release Rates Using Partial Fuel Stratification with Two-Stage Ignition Fuels”, SAE Paper 2006-01-0629
10. B. Thirouard, J. Cherel, V. Knop: “Investigation of Mixture Quality Effect on CAI Combustion”, SAE Paper 2005-01-0141
11. J. E. Dec, M. Sjöberg: “Isolating the Effects of Fuel Chemistry on Combustion Phasing in an HCCI Engine and the Potential of Fuel Stratification for Ignition Control”, SAE Paper 2004-01-1900
12. M. Richter, J. Engström, A. Franke, M. Aldén, A. Hultqvist, B. Johansson: ”The influence of charge inhomogeneity on the HCCI combustion process”, SAE Paper 2000-01-2868
13. W. Hwang, J. E. Dec, M. Sjöberg: “Fuel Stratification for Low-Load HCCI Combustion: Performance & Fuel-PLIF Measurements”, SAE Paper 2007-01-4130
14. S. Trajkovic, A. Milosavljevic, P Tunestål, B. Johansson: “FPGA Controlled Pneumatic Variable Valve Actuation”, SAE Paper 2006-01-0041
15. Schulz, C., Sick, V., “Tracer-LIF diagnostics: quantitative measurement of fuel concentration, temperature and fuel/air ratio in practical combustion systems”, *Progress in Energy and Combustion Science*, Vol. 31, No. 1, pp. 75-121, 2005.
16. Thurber, M. C., Grisch, F., Hanson, R. K., “Temperature imaging with single- and dual-wavelength acetone planar laser-induced fluorescence”, *Optics Letters*, Vol. 22, No. 4, pp. 251-253, 1997.
17. Thurber, M. C., Grisch, F., Kirby, B. J., Votsmeier, M., Hanson, R. K., “Measurements and modeling of acetone laser-induced fluorescence with implications for temperature-imaging diagnostics“, *Applied Optics*, Vol. 37, No. 21, pp. 4963-4978, 1998.
18. Thurber, M. C., Hanson, R. K., “Pressure and composition dependences of acetone laser-induced fluorescence with excitation at 248, 266, and 308

nm", *Applied Physics B*, Vol. 69, No. 3, pp. 229-240, 1999.
19. Grossman, F., Monkhouse, P. B., Ridder, M., Sick, V., Wolfrum, J., "Temperature and pressure dependence of the laser induced fluorescence of gas-phase acetone and 3-pentanone", *Applied Physics B*, Vol. 62, No. 3, pp. 249-253, 1996.
20. Hultqvist, A., Christensen, M., Johansson, B., Richter, M., Nygren, J., Hult, J., Aldén, M., "The HCCI Combustion Process in a Single Cycle- High-Speed Fuel Tracer LIF and Chemiluminescence Imaging", SAE 2002-01-0424, 2002.
21. Hult, J., Richter, M., Nygren, J., Aldén, M., Hultqvist, A., Christensen, M., Johansson, B., "Application of a high-repetition-rate laser diagnostic system for single-cycle-resolved imaging in internal combustion engines", *Applied Optics*, Vol. 41, No. 24, pp. 5002-5014, 2002.
22. R. Collin, J. Nygren, M. Richter, M. Aldén, L. Hildingsson, B. Johansson: "The Effect of Fuel Volatility on HCCI using Simultaneous Formaldehyde and OH PLIF", SAE Paper 2004-01-2948
23. M. Richter, R. Collin, J. Nygren, M. Aldén, L. Hildingsson, B. Johansson: "Studies of the Combustion Process with Simultaneous Formaldehyde and OH PLIF in a Direct-Injected HCCI Enging", JSME International Journal, vol. 18, 701-707 (2005)
24. J. Hyvönen, G. Haraldsson, B. Johansson: "Operating Conditions Using Spark Assisted HCCI Combustion During Combustion Mode Transfer to SI in a Multi-Cylinder VCR-HCCI Engine", SAE Paper 2005-01-0109
25. H. Persson, A. Rémon, A Hultqvist, B. Johansson: "Investigation of the Early Flame Development in Spark Assisted HCCI Combustion Using high Speed Chemiluminescence Imaging", SAE Paper 2007-01-0212
26. A. Berntsson, I. Denbratt: "HCCI Combustion Using Charge Stratification for Combustion Control", SAE Paper 2007-01-0210

CONTACT

Corresponding author:
Håkan Persson

Address
Lund University
Dept. of Energy Sciences
Div. of Combustion Engines
P.O. Box 118
221 00 Lund
Sweden

E-mail
hakan.persson@energy.lth.se

DEFINITIONS, ACRONYMS, ABBREVIATIONS

ATDC	After Top Dead Centre
BTDC	Before Top Dead Centre
CA10	Crank Angle for 10% Burned Mass Fraction
CA50	Crank Angle for 50% Burned Mass Fraction
CA90	Crank Angle for 90% Burned Mass Fraction
CAD	Crank Angle Degree
CAI	Controled Auto Ignition
CI	Compression Ignition
COV	Coeficcient of Variation
DI	Direct Injection
EVC	Exhaust Valve Closing
EVO	Exhaust Valve Opening
FPGA	Field Programmable Gate Array
HCCI	Homogeneous Charge Compression Ignition
HR	Heat Release
IMEP	Indicated Mean Effective Pressure
ISHR	Initial Slow Heat Release
IVC	Inlet Valve Closing
IVO	Inlet Valve Opening
LTR	Low Temperature Reaction
NVO	Negative Valve Overlap
PFI	Port Fuel Injection
PLIF	Planar Laser-Induced Fluorescence
RoHR	Rate of Heat Release
SACI	Spark Assisted Compression Ignition
SI	Spark Ignition